NASA Contractor Report 145313

Design and Fabrication of Metallic Thermal Protection Systems for Aerospace Vehicles

(NASA-CR-145313) DESIGN AND FABRICATION OF METALLIC THERMAL PROTECTION SYSTEMS FOR AEROSPACE VEHICLES (Grumman Aerospace Corp.) 188 p HC A09/MF A01 CSCL 11F

N78-22204

Unclas

G3/26 15693

Angelo Varisco
Paul Bell
Willy Wolter

GRUMMAN AEROSPACE CORPORATION
Bethpage, N.Y. 11714

CONTRACT NAS 1-14112
February 1978

National Aeronautics and
Space Administration

Langley Research Center
Hampton, Virginia 23665

1. Report No.	2. Government Accession No.	3. Recipient's Catalog No.
NASA CR 145313		

4. Title and Subtitle
DESIGN & FABRICATION OF METALLIC THERMAL PROTECTION SYSTEMS FOR AEROSPACE VEHICLES

5. Report Date
February 1978

6. Performing Organization Code

7. Author(s)
Angelo Varisco, Paul Bell, Willy Wolter

8. Performing Organization Report No.

9. Performing Organization Name and Address
Grumman Aerospace Corporation
Bethpage, New York 11714

10. Work Unit No.

11. Contract or Grant No.
NAS 1-14112

12. Sponsoring Agency Name and Address
National Aeronautics and Space Administration
Langley Research Center
Hampton, Virginia 23665

13. Type of Report and Period Covered
Contractor Report

14. Sponsoring Agency Code

15. Supplementary Notes
NASA Technical Monitor, John L. Shideler

16. Abstract
A program was conducted to develop a lightweight, efficient metallic thermal protection system (TPS) for application to future shuttle-type reentry vehicles, advanced space transports, and hypersonic cruise vehicles. Technical requirements were generally derived from the space shuttle. A corrugation-stiffened beaded-skin TPS design developed by Grumman was used as a baseline. The system was updated and modified to incorporate the latest technology developments and design criteria. The primary objective was to minimize mass for the total system.

One basic design concept was developed under the program. The concept consisted of a corrugation-stiffened beaded-skin surface panel, a specially designed support system, and an insulation package. Using the one basic design concept, two TPS were developed and optimized under the program: René 41, a nickel-base alloy for use to 1144 K (1600°F), and Haynes 188, a cobalt-base alloy, for use to 1255 K (1800°F). One full-scale panel 61 cm (24 in.) wide by 91 cm (36 in.) long was fabricated from each material. Each panel represented one and one-half bays, and included a longitudinal expansion joint.

The primary objective of reducing TPS mass was achieved. The Haynes 188 design is 35% lower in mass than the baseline Haynes 25 design. Similar reductions were achieved with the René 41 system. Both test articles, which were instrumented to measure temperature and deflection, were delivered to NASA/Langley for evaluation of cyclic life characteristics.

17. Key Words (Suggested by Author(s))		18. Distribution Statement
Corrugation-Stiffened Panel	Hypersonic Vehicle	Unclassified - Unlimited
Haynes 188	Rene 41	Subject Category 26
Heat Shield	Thermal Protection System	

19. Security Classif. (of this report)	20. Security Classif. (of this page)	21. No. of Pages	22. Price*
Unclassified	Unclassified		

* For sale by the National Technical Information Service, Springfield, Virginia 22161

FOREWORD

This report describes the work performed between November 1975 and November 1977 under Contract NAS 1-14112. Technical direction of the contract was performed by Mr. J. L. Shideler, NASA/Langley Thermal Structures Branch, Structures and Dynamics Division.

The program was managed by A. Varisco under the cognizance of F. Berger, Manager, Advanced Development System Engineering. Major contributions were made to the program by W. Wolter, Structural Temperatures; P. Beli, Structures; A. Borysewicz, Design; E. Leszak, Manufacturing; and H. Patterson, Instrumentation.

CONTENTS

CONTENTS (continued)

CONTENTS (continued)

ILLUSTRATIONS

ILLUSTRATIONS (continued)

ILLUSTRATIONS (continued)

TABLES

Section 1

SUMMARY & INTRODUCTION

1.1 SUMMARY

A program was undertaken to develop a lightweight, efficient, metallic thermal protection system (TPS) applicable to future shuttle-type reentry vehicles, advanced space transports, and hypersonic cruise vehicles. Technical requirements and criteria were derived generally from the space shuttle.

Grumman's corrugation-stiffened TPS design was used as the baseline starting point. The system was updated and modified to incorporate the latest technology developments and design criteria. Emphasis was placed on minimizing weight for the overall system.

One basic design concept was developed during the program, and this concept was optimized for operation at two different temperatures using two different materials: René 41, a nickel-base alloy for use to 1144 K (1600°F), and Haynes 188, a cobalt-base alloy for use to 1255 K (1800°F). Significant weight reductions were achieved over existing metallic systems. Moreover, the advanced TPS developed under this program are mass-competitive with the directly bonded RSI system presently used on the space shuttle.

Two, extensively instrumented, full-scale test panels were fabricated, one from each material. Each panel represented one and one-half bays and included an expansion joint. Both test articles were delivered to NASA/Langley for evaluation of cyclic life characteristics in the Langley Thermal Protection System Test Facility, which is capable of test conditions representative of entry flight.

1.2 INTRODUCTION

The development of high-temperature, metallic heat shield TPS for entry vehicles has been a general subject of attention for many years. (See, for example, ref. 1-1 and 1-2.) Recently, a greater interest in this area has been motivated by the space shuttle and its related technology requirements. As a result of this increased interest, NASA/Langley initiated a broad-based program to develop TPS over the temperature range of 811-1589 K (1000-2400°F) and similar work was begun by many aerospace companies. (See ref. 1-3 through 1-11.) As an extension to the NASA program, a contract was awarded to Grumman Aerospace Corporation to advance technology for metallic TPS in the temperature range of 1144-1255 K (1600-1800°F) by incorporating the latest technology developments and design criteria. The results of this effort are presented herein.

In general, technical requirements and design criteria were derived from the space shuttle orbiter, although the systems developed are applicable to advanced space transports and hypersonic cruise vehicles. A state-of-the-art assessment and review was undertaken to identify promising design features of existing systems, including current analytical techniques for predicting TPS performance. The review reaffirmed that a corrugation-stiffened beaded-skin concept offered the most promise for a reliable minimum-mass TPS, and this system was used as the baseline starting point. Primary emphasis was placed on minimizing mass for the overall system.

One basic design concept was developed under the program. The concept consisted of a corrugation-stiffened beaded-skin surface panel, a specially designed support system, and an insulation package. Using the one basic design concept, two TPS were developed and optimized under the program: René 41, a nickel-base alloy for use to 1144 K (1600°F), and Haynes 188, a cobalt-base alloy, for use to 1255 K (1800°F). One full-scale panel 61 cm (24 in.) wide by 91 cm (36 in.) long was fabricated from each material. Each panel represented one and one-half bays, and included a longitudinal expansion joint. Both test articles, which were instrumented to measure temperature and deflection, were delivered to NASA/Langley for evaluation of cyclic life characteristics.

1.3 SYMBOLS & UNITS

Although calculations were made in U.S. Customary Units, they are presented in this report in the International System of Units (SI) also. Factors relating to the two systems are given in reference 1-12. Symbols throughout this report are defined as they are introduced.

The appropriate quantities for the SI units used in this report are:

Quantity	Unit	SI Symbol
length	meter	m
force	newton	N
pressure	pascal	Pa
mass	kilogram	kg
temperature	kelvin	K

Abbreviations for the following prefixes have been employed for multiples of units in this report:

Prefix	Multiplication Factor	Abbreviation
centi	10^{-2}	c
milli	10^{-3}	m
kilo	10^{3}	k
mega	10^{6}	M
giga	10^{9}	G

1.4 REFERENCES

1-1 Anderson, Roger A; and Brooks, William A. Jr.: Effectiveness of Radiation as a Structural Cooling Technique for Hypersonic Vehicles. Journal of Aero/Space Sciences, January 1960.

1-2 Anderson, Melvin S.; and Stroud, C. W.: Experimental Observation of Aerodynamic and Heating Tests on Insulating Heat Shields. NASA TN D-1237, March 1962.

1-3 Stein, B. A.; Bohon, H. L.; and Rummler, D. R.: An Assessment of Radiative Metallic Thermal Protection Systems for Space Shuttle. NASA TMX-2570, July 1972.

1-4 Black, W. E.: Evaluation of Coated Columbium Alloy Heat Shields for Space Shuttle Thermal Protection System Application. NASA CR-112119-2, 1973.

1-5 Eidenoff, H. L.; and Rose, L.: Thermal-Structural Evaluation of TD Ni-20Cr Thermal Protection System Panels. NASA CR-132487, June 1974.

1-6 Deveikis, W. D.; Miserentino, R.; Weinstein, I.; and Shideler, J. L.: Aerothermal Performance and Structural Integrity of a René 41 Thermal Protection System in a Mach 6.6 Stream. NASA TN D-7943, November 1975.

1-7 Brandon, H. J.; and Masek, R. V.: Measurement and Correlations of Aerodymanic Heating to Surface Corrugation Stiffened Structures in Thick Turbulent Boundary Layers. NASA CR-132503, 1975.

1-8 Bohon, H. L.; Sawyer, J. Wayne; Hunt, L. R.; and Weinstein, I.: Performance of Thermal Protection Systems in a Mach 7 Environment. Journal of Spacecraft and Rockets, vol. 12, no. 12, December 1975.

1-9 Rummler, F. R.; and Black, W. E.: Evaluation of Coated Columbium for Thermal Protection Systems Application. AIAA Paper 75-817, Denver, Colorado, 1975.

1-10 Johnson, R., Jr.; and Killpatrick, D. H.: Evaluation of Dispersion Strengthened Nickel-Base Alloy Heat Shields for Space Shuttle Application. NASA CR-2614, March 1976.

1-11 Davis, J. W.; and Cramer, B. A.: Prediction and Verification of Creep Behavior in Metallic Materials and Components for the Space Shuttle Thermal Protection System. NASA CR-2685, July 1976.

1-12 Metric Practice Guide. E380-72, Amer. Soc. Testing & Materials. June 1972.

Section 2

DESIGN CRITERIA & ENVIRONMENT DEFINITION

2.1 DESIGN CRITERIA

The following thermal and mechanical loading conditions were developed for design of the metallic TPS test specimen. Also discussed are other necessary design requirements to make the TPS compatible with the operating characteristics of a functional reentry vehicle such as a space shuttle orbiter. In general, technical requirements were derived from the space shuttle system; where deviations have been made, they are noted. The design requirements and critical loading conditions are summarized in table 2-1.

Table 2-1. – Lower surface (mid-fuselage) design conditions.

Condition	Pa	psf	Fig.
Continuous surface press. at T_{max} (entry)	862-2490	18-52	2-3
Max maneuver surface press. at T_{max} (entry)	8618	180	2-3
Max temp level during entry – Haynes	1255 K	1800°F	2-3
Max temp level during entry – René	1144 K	1600°F	
Max dynamic press – entry	11 490	240	2-3
Max dynamic press. – boost	33 516	700	2-4
Max surface press differential – boost	+13 885 -20 588	+290 -430	
Max surface press. differential – postentry (subsonic flight)	+16 758 -12 448	+350 -260	
Acoustic environment			
Liftoff			
• Overall sound press. level	161 db		
• Critical 1/3-octave band level	150 db		
Max qα (ascent)			
• Overall sound press. level	158 db		
• Critical 1/3-octave band level	146 db		
Allowable permanent deflection between Panel supports	$\delta = 0.1 + 0.1L$		
Factors of safety			
Mechanical loads	1.0 limit 1.15 yield 1.4 ultimate 1.0 creep deflection		
Thermal effects	1.0 limit 1.4 ultimate		
Max primary structure temp rise ($T_{max} - T_{initial}$ = 350°F – 120 = 230°F)	383 K	230°F	
Flutter	Reference 4-2		

2217 86W

The mission profile and environmental parameters considered in the TPS design requirements are:

- Launch/boost - acoustic vibration, maximum aerodynamic pressures
- Orbit - initial TPS temperature at start of entry
- Entry - maximum aerodynamic heating, aerodynamic loads
- Postentry flight - maneuver loads, touchdown loads
- Ground handling - weather, inspection, refurbishment, storage

Specific design requirements are discussed in the following paragraphs.

2.2 DESIGN GOALS

In addition to the loading and thermal criteria, the test specimen was designed to meet the following goals:

- Reuse capability of 100 missions
- Minimum leakage at expansion joints
- Simple removal of panels
- Surface emittance of 0.80 or higher
- Moisture - In contrast to the current orbiter design, no special design requirements were included in this design to control TPS moisture absorption. It was assumed that during ground storage, prelaunch, and ferrying the vehicle will be protected from exposure to direct water impingement and high humidity conditions of ground support equipment. Immediately after entry and up to one hour after landing, the insulation will not absorb moisture because the residual heat stored in it during entry is sufficient to dry the insulation. This built-in protection would be effective in situations short of heavy rainstorms. If the vehicle is inadvertently exposed to rain or high-humidity condensing cycles, a drying cycle will be required before vehicle launch. The most significant concern in relation to water absorption for fibrous insulation is the associated increase in mass.
- Surface contour - The allowable panel surface normal permanent deflection between supports was $y = 0.254 + 0.01L$, where y is maximum deflection in cm and L is panel span. (This deflection criterion was taken from ref. 2-2, vol. II, p. 7-4.) This requirement will limit the total amount of creep deformation over 100 mission cycles.
- Surface roughness - To avoid uncontrolled ingestion of high-energy boundary-layer air in the panel expansion joints, all such potential gaps were aft facing in relation to the general flow direction. Also, the height of surface steps, beads, and protruding fasteners was such that local interference-heating effects will not be excessive.

2.3 THERMAL CONDITIONS

The primary thermal requirement ıĸ ‘he TPS is entry heating from orbit, with a 100-mission reusability goal. Space shuι..e orbiter entry trajectory 14040 was used as a design requirement for this program. Its salient features are shown in figure 2-1. The typical, external, heat-flux history for most of the vehicle's lower surface is shown. Maximum-temperature isotherms for the lower surface are shown in figure 2-2. The specific area of concern for the test specimen is the 1144-1255 K (1600 to 1800°F) temperature range. The surface-temperature history is shown in figure 2-3.

The thermal condition which determines the insulating requirement for the TPS is that in which the maximum TPS/primary structure temperature exists at the beginning of entry. Space shuttle mission 3, which is a launch into orbit and return to the launch site within a single revolution, creates a condition in which the residual effects of launch aerodynamic heating are still present when the vehicle starts its entry maneuver. The temperature on the lower surface structure at the start of entry for mission 3 is 322 K (120°F). This temperature was used as the initial TPS/structure temperature in conjunction with the 14040 entry trajectory heating.

The insulation was sized to limit the temperature of the primary structure to a maximum of 450 K (350°F) during entry and subsequent postlanding soak-out. Ground soak-out assumed a 311 K (100°F) ambient environment. The primary structure had the equivalent thermal heat-sink capacity of a .51-cm (0.2-in.) thick aluminum plate with an adiabatic back face.

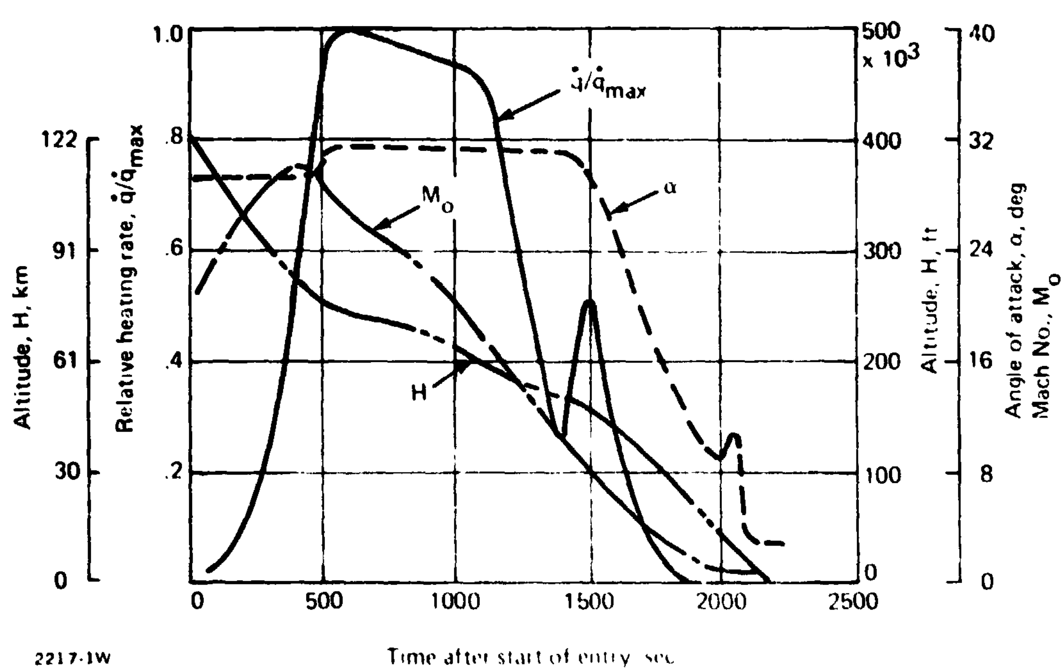

Figure 2-1. – Design entry trajectory.

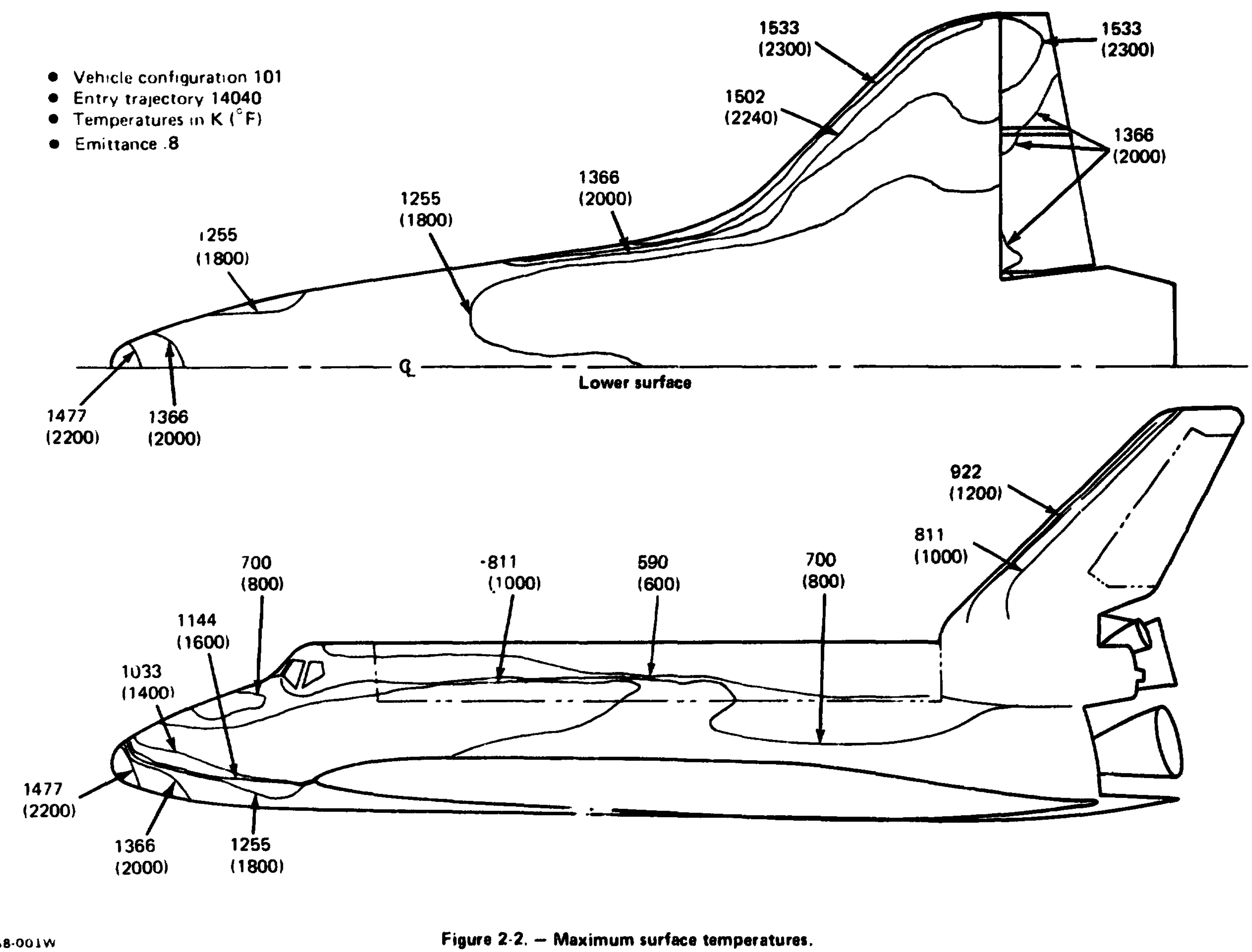

Figure 2-2. – Maximum surface temperatures.

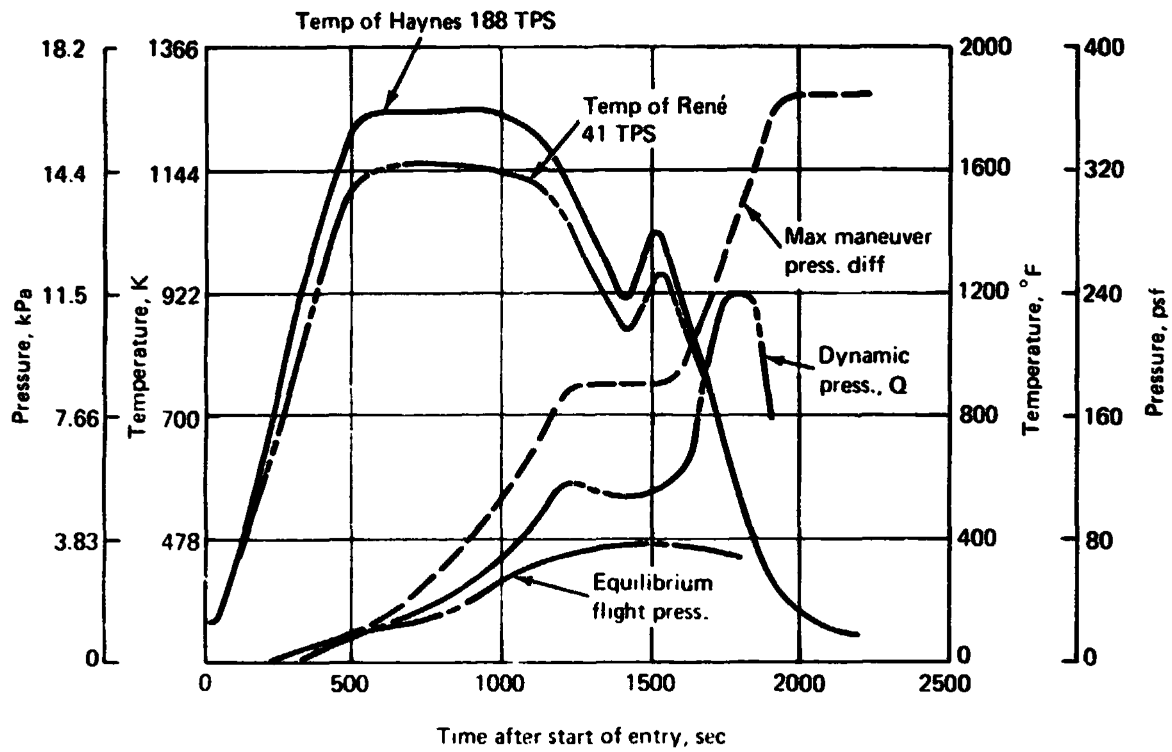

Figure 2-3. – Surface temperature and pressure profile.

Another thermal condition of significance is that which produces the maximum temper ure gradients in the TPS/structure. Shuttle studies have shown that this condition is one in which the minimum TPS/structure temperature exists at the start of entry. The minimum starting temperature for the current shuttle orbiter lower surface is the resu'' of mission 2, tail-sun orientation, and results in a 203 K (-95°F) temperature for the lower surface. This temperature was used as the minimum starting temperature in this study, in conjunction with entry trajectory 14040.

2.4 DIFFERENTIAL PRESSURE LOADING

Tw. types of static pressure loadings were considered in the design of the TPS. The first is maximum maneuver load conditions, which are intermittent and of short duration. The static strength of the panel must be sufficient to withstand these loads. The maximum maneuver load factor for the current orbiter is 2.5g during entry and subsonic flight. However, there is insufficient aerodynamic force to produce 2.5g maneuver until about 1200 sec after the start of entry, which is near the end of maximum heating (see fig. 2-3). The maximum maneuver line in figure 2-3 represents the maximum intermittent pressure differential on the lower surface for the entry maneuver.

The second type of static pressure loading considered is the continuous-loading level at high temperature, which was used to determine the amount of creep that occurs in the panel. This is the equilibrium flight pressure loading line shown in figure 2-3.

The maximum pressure differentials during boost and postentry subsonic flight are shown in table 2-2; they occur at low temperatures. The boost trajectory is shown in figure 2-4.

Table 2-2. – Orbiter lower surface maximum differential pressures for boost and postentry flight.

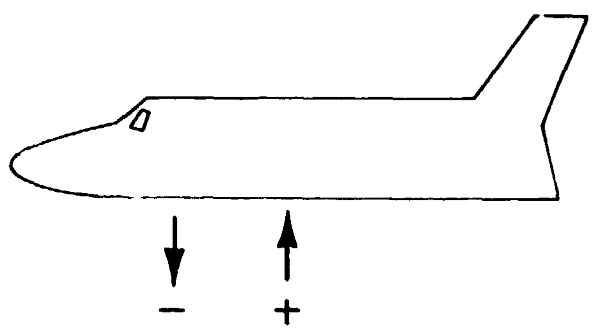

Condition	Max negative kPa (psf) Limit	Max negative kPa (psf) Ultimate	Max positive kPa (psf) Limit	Max positive kPa (psf) Ultimate
High Q boost	-20.6 (-430)	28.8 (-602)	+13.9 (+290)	+19.4 (+406)
Postentry	-12.6 (-260)	17.4 (-364)	+16.8 (+350)	+23.4 (+490)

2217-4W

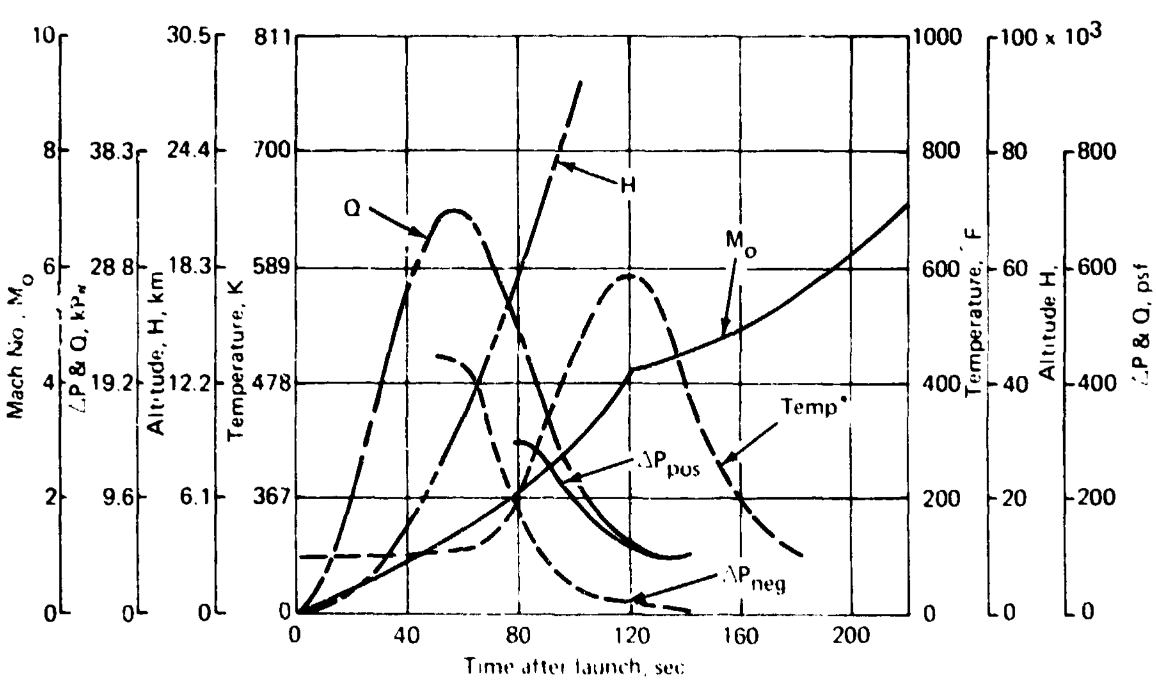

*Temperature on lower surface approximately 508 cm (200 in.) aft

1368-002W

Figure 2-4. – Design boost trajectory.

The pressure-loading conditions used here were derived from critical design conditions supplied by Rockwell International and postprocessed by Grumman in the course of the shuttle orbiter wing design effort.

2.5 ACOUSTIC ENVIRONMENT

Liftoff and ascent overall sound pressure levels are given in table 2-1. These levels are approximately the same ones used to test a corrugation-stiffened, beaded-skin TPS test panel similar to the panel designed for this program. The test, which was performed in the Grumman Sonic Test Facility, is documented in reference 2-1. The test panel endured the 100-mission equivalent of 5100 sec of high-intensity acoustic pressures, without failure. Because of this successful test, an acoustic analysis was not performed on the new design.

2.6 REFERENCES

2-1 Development of a Reusable Metallic TPS for Lifting Reentry Vehicles. ADR 02-04-70.1, Grumman Aerospace Corporation, April 1970.

2-2 Prediction and Verification of Creep Behavior in Metallic Materials and Components for the Space Shuttle Thermal Protection System. NASA CR-132605, vol. I and II, June 1975.

Section 3

MATERIAL PROPERTIES

3.1 CANDIDATE MATERIALS - METALLIC TPS

Candidate metallic TPS materials underwent considerable experimental evaluation during the early phases of the space shuttle program. At that time, studies were performed to determine which of the commercially available high-temperature metal alloys appeared most attractive for use in the surface panel and support structure. Consideration was given to the availability, fabricability, oxidation resistance, thermal stability at peak temperature, and availability of sufficient mechanical-properties data at temperature. The candidate alloys were Ti-6Al-25n-4Zn-2Mo, duplex annealed; René 41 solution heat treated and aged; Haynes 25 or 188; Inconel 718; TD Ni-20Cr; and Cb 752 coated with R512C.

A conceptual panel design was used as the focal point of a design analysis to determine comparative weights of metal panels utilizing the candidate alloys over the temperature range of 589-1588 K (600-2400°F). The results of the study (ref. 3-1) indicated that to minimize TPS weight for a given vehicle requires the use of more than one alloy for panel construction. A vehicle such as a shuttle orbiter will require the use of at least three different alloys for the "acreage" lower-surface TPS. To minimize the weight of a panel using a given alloy requires a careful design optimization, which results in a specific cross-section geometry and material gauge. Panels so designed of different materials must interface with one another over a large lineal footage. To minimize the need for special interface panels and to reduce development costs, it seems desirable to arrive at a common design concept for all metal panels which cover this large "acreage." A common design concept requires some tradeoffs, since the early study indicated that minimum-weight panel cross sections for all the candidate materials are not identical. The study showed that René 41 is lightest in the range of 755-1144 K (900-1600°F). Haynes 25 or 188 was lightest in the range of 1144-1255 K (1600-1800°F).

The program reported herein was limited to optimizing a TPS in both René 41 and Haynes 188 since the range of temperatures covered by these materials would encompass the major portion of TPS requirements for a typical vehicle. No materials testing was performed under the program since adequate data on René 41 and Haynes 188 were already available.

There were, however, two areas of concern with these materials: establishing allowable design stresses under creep conditions and determining a thickness allowance for emittance treatment and oxidation losses. These areas were investigated in the program, and design allowables were established. These areas will be discussed later in this section.

3.2 HAYNES 188 PROPERTIES

Haynes 188 alloy is a cobalt-base alloy possessing excellent high-temperature strength and oxidation resistance to 1367 K (2000°F). Its excellent oxidation resistance results from minute additions of lanthanum to the alloy system. The lanthanum modifies the protective oxide scale in such a manner that the oxide becomes extremely tenacious and impervious to diffusion when exposed to temperatures through 1367 K (2000°F). All properties which follow for Haynes 188 are for the solution-heat-treated condition - heating to 1450 K (2150°F) followed by either a rapid air-cool or water quench.

3.2.1 Chemical Composition

- Chromium: 20-24%
- Nickel: 20-24
- Tungsten: 13-16
- Iron: 3, maximum
- Carbon: .05-.15
- Silicon: .20-.50
- Manganese: 1.25, maximum
- Lanthanum: .03-.15
- Cobalt: balance

3.2.2 Physical & Mechanical Properties

- Density (RT): 9.13 g/cu cm (.330 lb/cu in.)
- Incipient fusion temperature: 1603 K (2425°F)
- Electrical resistivity (RT): 92.2 microhm/cm
- Poisson's ratio: M .29 (RT, ref. 3-2)
- Mean coefficient of thermal expansion vs temperature: figure 3-1
- Thermal conductivity vs temperature: figure 3-1
- Specific heat vs temperature: figure 3-1
- Oxidation resistance: The outstanding oxidation resistance of Haynes 188 is illustrated in figure 3-2, where it is compared to Haynes 25 and Hastelloy X, two alloys known for their resistance to oxidation
- Mechanical properties: The design mechanical properties were assumed to be the same as for Haynes 25, and were taken from reference 3-3. Table 3-1 gives the properties used in the program.

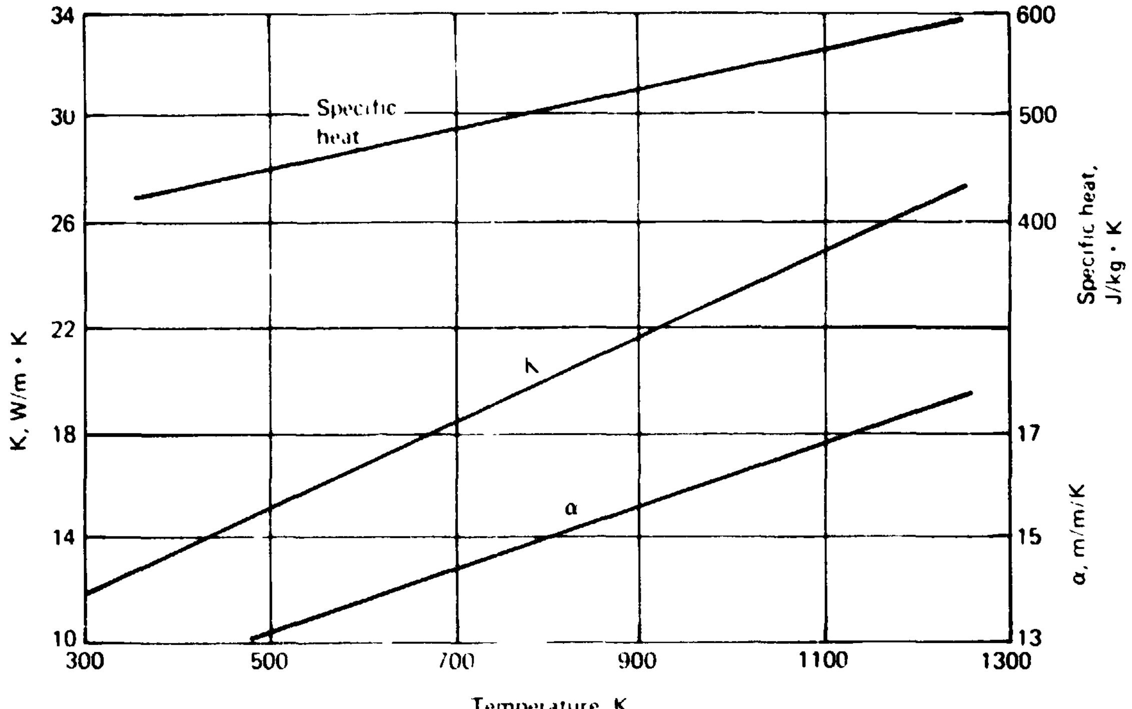

2217 6W

Figure 3-1 – Thermal expansion coefficient (α), thermal conductivity (K), and specific heat vs temperature for Haynes 188.

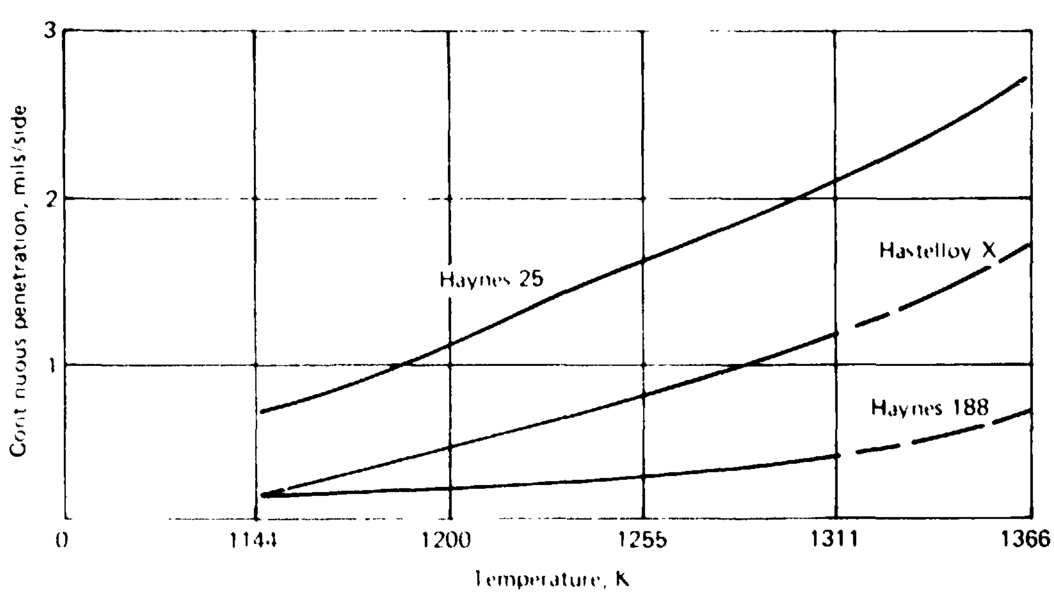

2217 6W

Figure 3-2 - Oxidation resistance in dry air, 100 hr test.

3.2.3 Establishment of Creep Allowable Stress

An analysis was made to determine the allowable stress based on creep strains for a typical corrugation-stiffened Haynes 188 panel cross section subjected to uniform pressure loading. The panel was assumed to be a simply supported beam subjected to a uniformly distributed load. The maximum allowable permanent center deflection, taken from reference 2-2, is:

$$y = .254 + .01L$$

where L is the span, in cm. (3-1)

Creep deformations cause nonelastic strain distributions in a beam cross section, but the elastic beam relationship was used as a first approximation to obtain an allowable strain. For the simply supported beam, the center deflection is:

$$y_{max} = \frac{5}{384}\frac{wL^4}{EI} \qquad (3\text{-}2)$$

where w is the unit load.

If it is assumed that an optimum panel cross section is one with the neutral axis at the mid-depth, so that tension and compression strains are equal, the outer fiber strain is:

$$\epsilon = \pm\frac{MC_{max}}{EI} \text{ and } M_{max} = \frac{wL^2}{8} \qquad (3\text{-}3)$$

therefore,

$$\epsilon = \pm\frac{wL^2C_{max}}{8EI} \qquad (3\text{-}4)$$

If creep stress-strain relationships are assumed to be identical for tension and compression, equations (3-2) and (3-4) combine to obtain strain in terms of center deflection:

$$\epsilon_{allow.} = \frac{9.6\, y_{max}\, C_{max}}{L^2} \qquad (3\text{-}5)$$

Using equation (3-1) to define y_{max},

$$\epsilon_{allow.} = \frac{2.44\, C_{max} + .096\, C_{max} L}{L^2} \qquad (3\text{-}5)$$

From reference 2-2, Vol II, equation 7-1, page 7-4, the following equation for creep strain in Haynes 188 is obtained:

$$\ln \epsilon = -2.89413 - .01743t + .54892 \ln t + 1.31015 \ln \sigma$$
$$-6.66548\,(1/T) + .19131\,\sigma \ln T + .00021\, T\sigma t \qquad (3\text{-}6)$$

where:

t = total accumulated time at T_{max} hours

σ = stress level, in MPa

T = temperature, in K/1000

ϵ strain, in %

A typical configuration for a metallic TPS panel is expected to have a span of 48.3 cm (19.0 in.) with a cross-section depth of 1.52-2.54 cm (.60-1.0 in.). From equation (3-5), $\epsilon_{allow.}$ is a function of cross-section depth, h:

h, cm (in.)	$\epsilon_{allow.}$, %
1.52 (0.6)	.23
2.03 (0.8)	.31
2.54 (1.0)	.39

For the design heating mission,

t = 16.7 hr (time at T_{max} for 100 cycles at 10 min/cycle)

T_{max} = 1255 K (1800°F)

$$T = \frac{1255}{1000} = 1.255$$

Substituting values and rearranging equation (3-6) to solve for stress, σ, that corresponds to $\epsilon_{allow.}$, we obtain the following $\sigma_{allow.}$:

h, cm (in.)	HS-188 $\sigma_{allow.}$, MPa (psi)
1.52 (0.6)	26.4 (3828)
2.03 (0.8)	29.0 (4175)
2.54 (1.0)	31 3 (4539)

The allowable stress, therefore, within the depth range of 1.52-2.54 cm (.6-1.0 in.), can be expressed as:

$$\sigma_{allow.} = 19.1 + 4.8h \text{ (MPa)} \quad \left[2770 + 1770h \text{ (psi)}\right]$$

Note that the allowables shown are based on simple-element creep data. It was assumed that the coefficients of equation 3-6 do not change with time and that strain hardening and the effects of permanent creep deformations have a negligible effect.

3.2.4 Design Allowance for Oxidation Losses

Since thin-gage material, 0.25 cm (.010 in.) or less, was to be employed and because Haynes oxidizes at elevated temperatures, it was necessary to include a design allowance (thickness increase) to provide for losses due to pre-oxidation to increase emittance and due to oxidation during service life.

Table 3-1. – Haynes 188 mechanical properties.

Property	Stress at temperature			
	294 K	70°F	1255 K[a]	1800°F[a]
F_{tu}	896 MPa	130 ksi	145 MPa	21 ksi
F_{ty}	379 MPa	55 ksi	76 MPa	11 ksi
F_{cy}	379 MPa	55 ksi	76 MPa	11 ksi
E	234 GPa	34 000 ksi	94 4 GPa	13 700 ksi

[a]The effect of temperature on F_{TU}, F_{TY}, F_{CY}, and E is given in reference 3-3, based on 1/2 hr exposure, which cannot be used for TPS design. The values listed are based on 25-hr exposure, and were taken from reference 2-1, based on a 0.4% creep strain

2?1-8W

The following design requirements were assumed in preparing the estimat oxidation loss:

- Peak service temperature will be 1255 K (1800°F)
- The mission cycle will include 10 min at peak temperature
- Each panel will have a 100-mission life

The use of an applied surface coating for emittance control was to be avoided. The surface oxide of the HS-188 was to be used, if possible. A total hemispherical emittance of .80, or more, at 1255 K (1800°F) was a goal.

3.2.4.1 Allowance Required for Emittance Treatment

The emittance requirements were to be fulfilled by a preoxidation treatment during final stages of component fabrication. An oxide film thickness of .00025 cm (.0001 in.) was thought sufficient to achieve the required value.

3.2.4.2 Allowance Required for Oxidation Losses

Oxidation under entry conditions is dependent on peak temperature, number of exposure cycles, atmospheric pressure at peak temperature, and airflow rate. Two experimental oxidation studies have been conducted on HS-188 under conditions that simulated space shuttle entry conditions.

The first of these activities, reference 3-4, involved the cyclic self-resistance heating of sheet specimens in a reduced-pressure air environment. The thermal cycle involved heating to 1477 K (2200°F), holding for 30 min, and then cooling to room temperature. The specimens underwent 100 thermal cycles. The test atmosphere, air, was maintained at a pressure of 1333 Pa (10 torr). The test specimens underwent a metal thickness loss of .00089 cm (0.00035 in.) per side.

The second effort in this area, reference 3-5, utilized an arc-jet to simulate space shuttle entry conditions. Sheet specimens were inserted into a Mach 6 test stream for 30 min and then allowed to cool. The test temperature was 1378 K (2020°F), surface pressure was 1013 Pa (7.6 torr). After 50 30-min cycles, the test specimens had lost .0019 cm (.00075 in.) of thickness per side.

Obviously, the most conservative approach would be utilization of the arc-jet test data. However, the oxidation which occurred at 1378 K (2020°F) was a result of a significantly higher oxidation rate than that which occurred at temperatures of 1255 K (1800°F) or below. References 3-2 and 3-6 show that the oxidation rate at 1366 K (2000°F) is double the rate at 1255 K (1800°F). Therefore, an oxidation loss allowance of .0010 cm (.0004 in.) was used for the external surfaces of the TPS panel.

3.2.1.3 Total Allowance Required for Emittance & Oxidation

In summary, the allowances provided are:

- External air-passage surface (beaded skin)

– Emittance allowance (.00025 cm side):	.00051 cm	.0002 in.
– Oxidation allowance (.0010 cm, exterior):	.00100	.0004
– Total allowance:	.00151 cm	.0006 in.

- Internal surfaces (corrugation)*

– Emittance allowance (.00025 cm/side):	.00051 cm	.0002 in.

3.3 RENÉ 41 PROPERTIES

René 41 is a vacuum-melted, nickel-base alloy possessing exceptionally high strength in the temperature range of 920-1255 K (1200-1800°F). It is a precipitation-hardening alloy, and its strength is developed by various solutioning and aging heat treatments. All properties which follow for René 41 are for forging at 1450 K (2150°F), age hardening at 1172 K (1650°F) for 4 hr, and air cooling.

3.3.1 Chemical Composition

• Chromium:	18.00-20.00	• Titanium:	3.00-3.30
• Iron:	5.00	• Molybdenum:	9.00-10.50
• Carbon:	0.05-0.12	• Aluminum:	1.40-1.60
• Silicon:	0.50	• Boron:	0.003-0.010
• Cobalt:	10.00-12.00	• Sulphur:	0.015
• Manganese:	0.10	• Nickel:	balance

*Internally, no allowance beyond the emittance allowance was required because of the low-pressure quiescent condition of the internal air.

3.3.2 Physical & Mechanical Properties

- Density: 8.25 g/cu cm (.298 lb/cu in.)
- Melting temperature: 1580 K ($2385^{o}F$)
- Specific heat: .108 cal/$g^{o}C$ (.108 Btu/$lb^{o}F$)
- Poisson's ratio (μ): .31 at 300 K, .35 at 1150 K
- Mean coefficient of thermal expansion vs temperature: figure 3-3
- Thermal conductivity vs temperature: figure 3-3
- Specific heat vs temperature: figure 3-3
- Mechanical properties: The design mechanical properties were taken from reference 3-3. Table 3-2 gives the properties used in the program

3.3.3 Establishment of Creep Allowable Stress

The procedure for determining the René 41 allowable stress based on creep strains is identical to the one developed for Haynes, which is given in para 3.2.3. Equations (3-1) through (3-5) are applicable to René 41 with identical results. From reference 2-2, Vol II, equation 7-3, page 7-4, the following equation for creep strain in Rene 41 is obtained;

$$\begin{aligned}\ln \epsilon = {} & -39.55860 + 29.13646T + .71922 \ln t \\ & + .32125 (\ln \sigma - 1.931) - .000016 \sigma^2 \\ & + .08183 (\ln \sigma - 1.931)^3 - .000125\, t\, \sigma\, T + .0000105\, T^3\end{aligned}$$

where:

t = total accumulated time at T_{max} (16.7 hr)

T = temperature, in K/1000 = 1144/10000 - 1.144

ϵ = strain, in %

σ = stress level, in MPa

From equation (3-5), we obtain

Cross-Section Depth, h, cm (in.)	$\epsilon_{allow.}$, %
1.52 (0.6)	.23
2.03 (0.8)	.31
2.54 (1.0)	.39

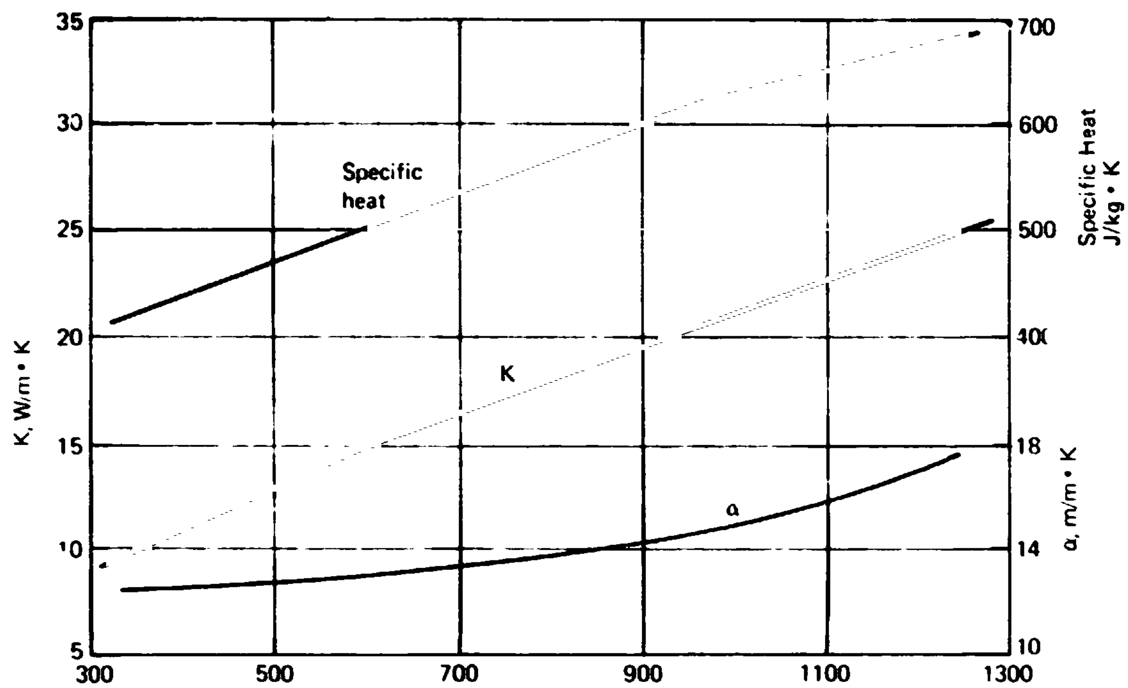

2217-10W

Figure 3-3. – Thermal expansion coefficient (α), thermal conductivity (K), and specific heat vs temperature for René 41.

Table 3-2. – René 41 mechanical properties.

Property	Stress at temperature			
	249 K	70°F	1144 K	1600°F
F_{tu}	1158 MPA	168 ksi	603 MPa	87.4 ksi
F_{ty}	876 MPa	127 ksi	524 MPa	76.0 ksi
F_{cy}	931 MPa	135 ksi	400 MPa	58 ksi
E	218 GPa	31 600 ksi	122 GPa	17 700 ksi

2217-9W

Substituting values and rearranging equation (3-6) to solve for stress, σ, that corresponds to $\epsilon_{allow.}$ we obtain:

Cross-Section Depth, h, cm (in.)	$\sigma_{allow.}$, MPa (psi)
1.52 (0.6)	62.50 (9063)
2.03 (0.8)	72.06 (10 456)
2.54 (1.0)	81.60 (11 832)

The allowable stress, therefore, within the depth range of 1.52-2.54 cm (.60-1.0 in.), can be expressed as:

$$\sigma_{allow.} = 33.9 + 18.8\,h\ (MPa)\ \left[4910 + 6920\,h\ (psi)\right]$$

3.3.4 Design Allowance for Oxidation Losses

The oxidation resistance of René 41 is good up to 1255 K (1800°F). Therefore, the allowances required for emittance treatment were assumed to be the same as for Haynes 188. The allowances (thickness increase) required are:

- External air-passage surfaces
  - Emittance allowance (.00025 cm/side): .00051 cm .0002 in.
  - Oxidation allowance (.0010 cm, exterior): .00100 .0004
  - Total allowance: .00151 cm .0006 in.
- Internal surfaces
  - Emittance allowance (.00025/side): .00051 cm (.0002 in.)

3.4 REFERENCES

3-1 Material Choice for Lightest Metallic Heat Shield. Grumman Memorandum B35-197-MO-11, revision A, December 1970.

3-2 Aerospace Structural Metals Handbook, AFML-TR-68-115. 1974.

3-3 MIL-HDBK-5, Metallic Materials and Elements for Flight Vehicle Structures.

3-4 Sanders, W. A; and Barrett, C. A.; Oxidation Screening at 1204°C (2200°F) of Candidate Alloys for the Space Shuttle Thermal Protection System. NASA Technical Memorandum TM X-67864, Lewis Research Center, Cleveland, Ohio, October 1971.

3-5 Centolanzi, F. J.; Probst, H. B.; Lowell, C. E.; and Zimmerman, N. D.: Arc Jet Tests of Metallic TPS Materials. NASA Technical Memorandum TM X-62092, Ames and Lewis Research Centers, October 1971.

3-6 Lund, C. H.; and Wagner, H. V.: Oxidation of Nickel and Cobalt Base Super Alloys. DMIC Report 214, Battelle, Columbus, March 1, 1965.

Section 4

TPS CONCEPT SELECTION & DESIGN

4.1 STATE-OF-THE-ART ASSESSMENT & REVIEW

A review of existing panel design concepts and TPS-related work was conducted at the start of the program. The objective was to identify promising design features of existing radiative TPSs, including current analytical techniques for predicting TPS performance. The reports studied were references 1-1 through 1-11, 2-1, 2-2, 3-1, and 4-1.

4.1.1 Skin Panel Concept

The review reaffirmed that the corrugation-stiffened beaded-skin concept offered the most promise for a reliable, minimum-weight metallic heat shield. This concept, for example, was selected by the McDonnell Douglas Company for their full-size TD Ni-20Cr test panel after evaluating various alternate concepts (ref. 1-10). The unstiffened beaded-skin concept (ref. 1-6) appears attractive because of its simplicity and low mass. However, this concept requires a large number of supports to limit creep deflections. Additionally, the large bead depth provides a less desirable aerodynamic surface, which causes increased heating under crossflow conditions, and the unstiffened skin is more prone to flutter than a stiffened skin.

The review also substantiated the danger of ending the skin beads short of the panel edge. The two concepts which ended the beads in this manner developed cracks at the bead closeouts after thermal cycling.

Overall, the corrugation-stiffened beaded-skin concept offered the most potential for a minimum-weight, reliable heat shield. The advantages and performance of the beaded-skin approach have been well established in many panel tests. The beads absorb lateral expansion, thereby eliminating lateral expansion joints, and serve to stiffen the skin for increased flutter and bending strength. The corrugations provide an efficient transfer of surface panel loads to the support ribs.

4.1.2 Expansion Joint

The review of expansion joints confirmed that separate edge closure retention members like those employed in the TD Ni-20Cr panel (ref. 1-10) or the columbium panel (ref. 1-4) are undesirable. They add complexity, produce forward-facing steps, and impose unpredictable pressure and restraint to panel edges.

The shingle concept offers the most promise for meeting joint requirements. Specifically:

- Maximum simplicity - no extra parts required
- Unrestrained panel edges

- No forward-facing steps
- Each panel is individually removable

Additionally, because the skin beads run out to the panel edge, no lateral expansion joints are required.

4.2 TPS CONCEPT

The TPS considered in this program is a shingled, radiative system. Heat-rejection rate, therefore, dependes on the fourth power of the surface temperature, and becomes large if high temperatures can be tolerated. Thus, the intensity of heating which can be accommodated is limited by the temperature capability of the panel material.

An existing Grumman-developed TPS designed for operation at 125 K ($1800^{o}F$) was selected as a baseline design in the program. The concept, shown in figure 4-1, consists of a corrugation-stiffened beaded skin, insulation, and beaded support ribs. The corrugations are welded to the beaded skin to form an efficient panel with high longitudinal bending stiffeners. Applied surface-pressure loading is transferred by beam action to the rib supports. The supports are located on 51-cm (20.0-in.) centers, with an expansion joint every 102 cm (40.0 in.) to permit longitudinal growth of the panel. Although the panel is considered to be 102 cm (40.0 in.) long, it is fixed at the center support so that a 51-cm (20.0-in.) span expands in each direction. The center support rib includes a drag support to react longitudinal (drag) loads. The panel lateral expansion is absorbed by flexing of the beads in the skin. The corrugations have little effective stiffness in the lateral direction.

The advantage of this concept is that the panels are not size-limited in the lateral direction, and an expansion joint is required only in the longitudinal direction. The design also eliminates forward-facing steps and incorporates a simple splice of adjacent panels, thus facilitating panel removal and inspection. A mass breakdown for the baseline system is also shown in figure 4-1.

4.3 SURFACE PANEL DESIGN

Several surface panel configurations were considered, including trapezoidal and semicircular corrugation-stiffened skin, double-faced corrugation, integrally stiffened plate, and honeycomb sandwich. Double-faced corrugations and honeycomb sandwich designs were eliminated due to thermal stresses induced by the temperature gradient from outer to inner face sheets. Integrally stiffened plate designs were eliminated because this approach is not mass-competitive. Another disadvantage of those designs which have flat skins is the requirement for expansion joints at four edges. The semicircular corrugation was eliminated because it is not as mass-efficient as the trapezoidal. (para 4.3.8). Examination of the baseline design indicated that the corrugation sidewalls were operating at low stress levels. This resulted from the use of one material thickness for the entire corrugation.

To minimize corrugation mass, two approaches were considered: first, the use of one thickness as before but with the addition of lighting holes; and second, the use of chem-milling. A weight estimate showed that holes would not significantly reduce mass. Moreover, punching holes in thin-gage material and the subsequent deburring would be very costly. Chem-milling, however, permitted the maximum elimination

FOLDOUT FRAME 1

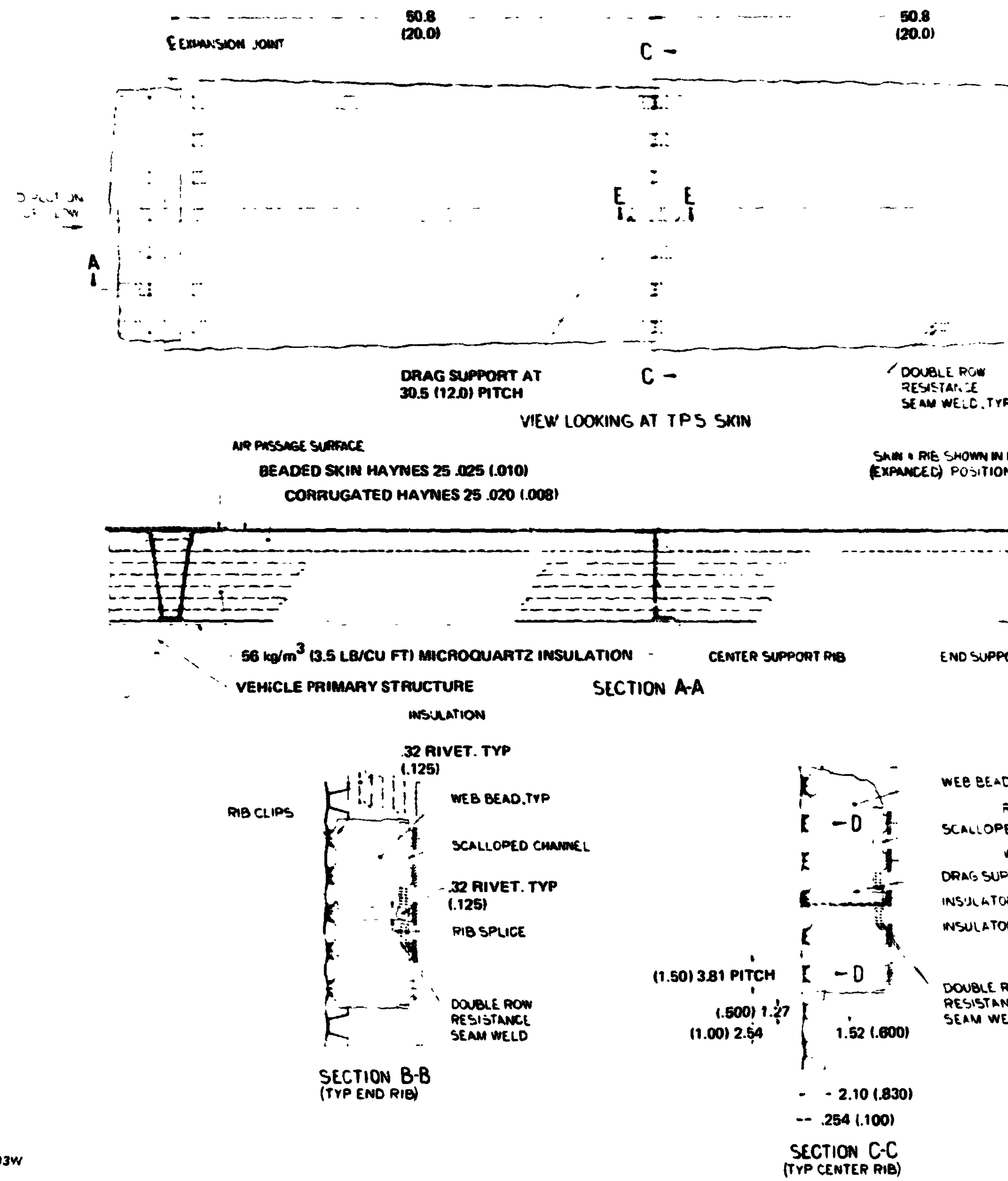

1368-003W

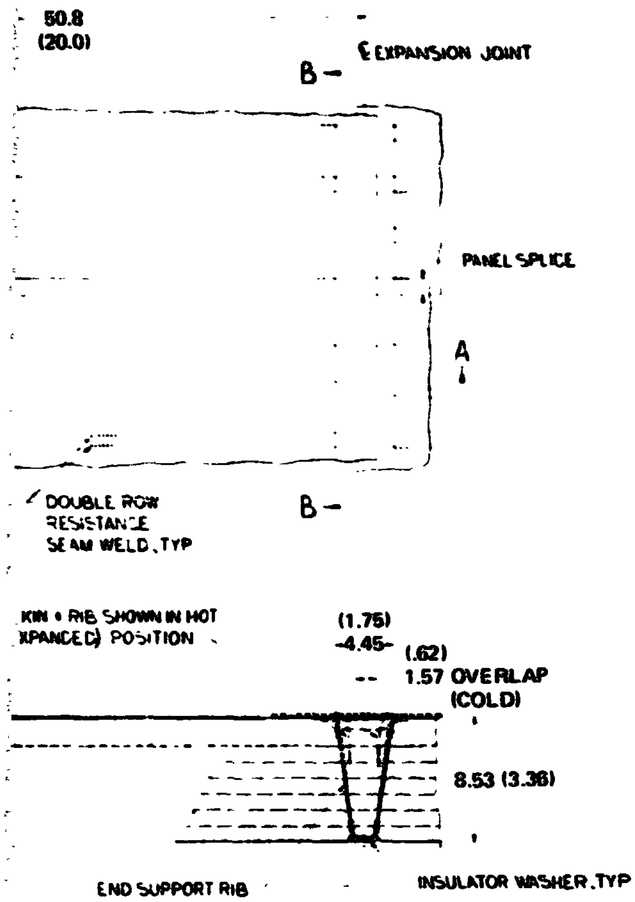

Mass Breakdown					
Item	Total mass, lbm, 40 x 41 panel	Lbm/ft^2 (11.3889)	% of item	Sub elem % of item	Item % of TPS
Expansion rib	(2.1584)	(0.1895)			7.7
Upper clip	.4978	.0437	23.1	55.9 (clips)	
Lower clip/angle	.7085	.0622	32.8		
Web	.8389	.0737	38.9		
Rivets	.1132	.0099	5.2		
Center rib	(2.8841)	(0.2532)			10.3
Upper clip	1.3463	.1182	46.7	83.6 (clips)	
Lower clip	1.0633	.0934	36.9		
Web	.3613	.0317	12.5		
Rivets	.1132	.0099	3.9		
Drag Bracket (4 per 41-in. panel)	0.3888	0.0341			1.4
Skin assembly	(13.1002)	(1.1503)			46.7
Skin	5.6622	.4972	43.2	20, total	
Corrugation	7.4380	.6531	56.8	26, total	
Attaching hardware	(0.8635)	(0.0758)			3.1
Skin rivets (blind)	.2278	.0200	26.4		
Primary bolts	.3360	.0295	38.9		
Insulating washers	.2997	.0263	34.7		
Insulation system	8.6366	0.7583			30.8
Total	28.0316	2.4612			100.0

DIMENSIONS: CM (INCHES)

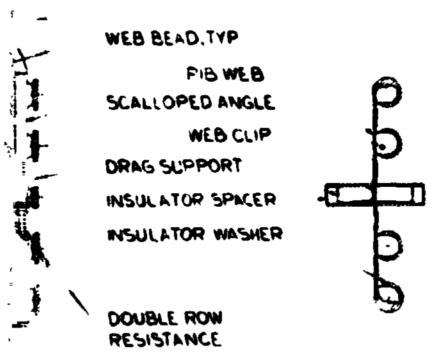

SECTION D-D

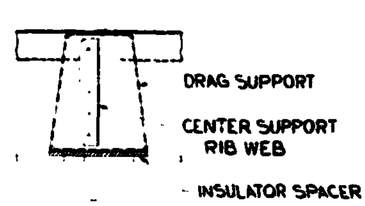

SECTION E-E

Figure 4-1. – Grumman baseline TPS concept.

of unnecessary material. Moreover, since the skin/corrugations are sized to meet the maximum bending moment at the span center, additional weight could be saved by profiling the chem-mill at the span edges. Additionally, with the use of chem-milling, the thickness of each element of the cross section could be permitted to vary for maximum efficiency. It was decided, therefore, to chem-mill the test specimen.

4.3.1 Skin/Corrugation Optimization

A digital computer program was written to optimize the 51 cm (20 in.) panel. The program accounted for creep due to bending between supports, buckling of the various elements of the skin/corrugation, and flutter of the outer skin. All design variables such as pitch, various element thicknesses, and lengths were initially not constrained. Thus, designs which were developed within specified constraints could be compared with designs developed under other constraints or with designs developed under strength constraints only. Attachment hardware such as clips and rivets were not included in the computer program. This program, which is presented in Appendix A, should not be considered as a true optimization program, since some of the steps necessary to determine the panel cross-section with the least mass are graphical and require the user to interface with the program. Furthermore, thermal stresses which occur due to lateral thermal expansion were not accounted for in the optimization program. Instead, the optimum design was checked against thickness constraints determined from analysis of lateral thermal expansion. (See Section 4.3.3.)

4.3.1.1 Design Loads

The critical airload design conditions selected are listed in table 4-1.

4.3.1.2 Safety Factors

Design allowable stress ($F_{allow.}$) is any of the following:

- $F_{tu}/1.4$
- $F_{cy}/1.15$
- $F_{ty}/1.15$
- $F_{creep}/1.15$
- $F_{crel}/1.4$

Each denominator is the appropriate factor of safety and F_{crel} is the local elastic buckling stress.

Table 4-1. – Critical airload design conditions.

Condition	Description	Differential pressure		Temperature			
				Haynes 188		René 41	
		kPa	psf	K	°F	K	°F
A	Boost	-20.59	-430	294	70	294	70
B	Postentry	16.76	350	294	70	294	70
C	Max maneuver	4.78	100	1255	1800	1144	1600
D	Equil flight	2.39	50	1255	1800	1144	1600

2217-12W

4.3.1.3 Critical Conditions

A preliminary analysis determined the elements critical for the designated conditions. These elements are listed in table 4-2.

4.3.1.4 Fabrication Constraints

Section definition and properties are shown in figure 4-2. Two fabrication constraints which were imposed on the optimization of the surface panel (skin/corrugation) are:

- The minimum face sheet thicknesses, t_1 and t_2, must be .0127 cm (.005 in.) for handling considerations

- The minimum flat between beads, P-b, must be at least 1.016 cm (.40 in.) to permit attachment of the support clips

4.3.1.5 Optimization Considerations

It is generally accepted that for a nonredundant structure, such as these panels, the least-mass design is obtained when the applied stress in each element is equal to the allowable stress for as many of the design conditions as possible. For example, element 1 of the section definition shown in figure 4-2 should be buckling-critical under condition B, creep-critical under condition D, flutter-critical under the design dynamic pressure, and yield-critical under conditions of lateral thermal expansion. It is, however, usually not possible to satisfy all conditions.

Additionally, design constraints, such as minimum-gage considerations, may constrain the optimum design even further. Figure 4-3 illustrates such a situation. It also shows that if the thickness and flat-width design constraints were neglected, the least-mass section occurs when the neutral axis is at the midheight of the section. In this case, both the upper and lower fibers would be creep-critical, as well as buckling-critical, for the appropriate conditions. Addition of the design constraints, however, increases the mass by a significant amount. For example, by modifying the neutral-axis location to 55% of the total section height (central curve), the section is less efficient from a strength standpoint than the previous design, but when the design constraints are considered, the acceptable section is lighter than its companion in the first case.

Table 4-2. – Critical conditions.

Element	Condition				
	A	B	C	D	Other
1		Buckle		Creep	(a)
2-3		Buckle			
4	Buckle			Creep	
5	Buckle			Creep	

[a]Lateral thermal expansion and bead flutter

`17-14W

Section definition

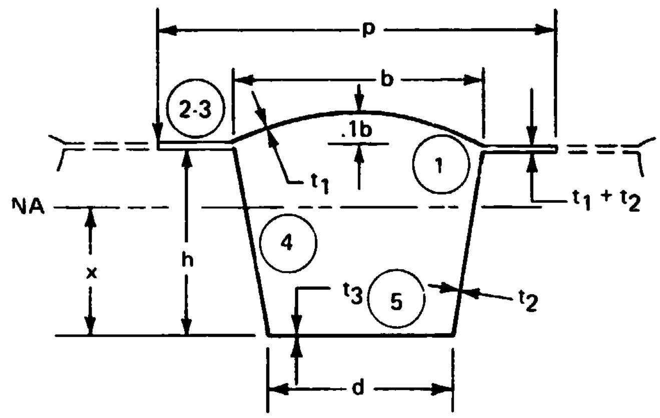

Section properties

$$\Sigma A = 1.02646bt_1 + (p - b)(t_1 + t_2) + 2ht_2 + dt_3$$

$$\Sigma Ax = 1.02646bt_1[h + b(.00649)] + (p - b)(t_1 + t_2)(h) + 2ht_2(h/2)$$

$$\Sigma Ax^2 = 1.02646bt_1[h + b(.00649)]^2 + (p - b)(t_1 + t_2)(h)^2 + 2ht_2(h/2)^2$$

$$\Sigma I_{oo} \cong 2t_3h^3/12$$

$$\bar{x} = \Sigma Ax/\Sigma A$$

$$I_{NA} = \Sigma Ax^2 + \Sigma I_{oo} - (\Sigma A)(\bar{x})^2$$

2217-13W **Figure 4-2. — Section definition and properties.**

It can, therefore, be concluded that the least-weight, strength-constrained section will not necessarily be the least-weight acceptable design.

The skin/corrugation design equations and optimization procedure are given in appendix A. Also given is a listing of the computer program, HAYNES, developed to simplify selection of the optimum configuration. The optimized Haynes 188 section as determined by the computer program is illustrated in Figure 4-4. The section shown and the thickness indicated include no allowance for emittance treatment and oxidation losses expected during the life of the system. The production section which includes these allowances is given later in Figure 4-10.

The René 41 section as determined by the computer program is illustrated in Figure 4-5. The production René 41 section is given later in Figure 4-10.

4.3.2 Skin Bead Flutter

Previous experience with similar designs indicated that flutter requirements could determine the skin thickness. The minimum required face-sheet thickness to prevent local flutter of the skin bead was determined using the analysis procedure given in reference 4-2. The procedure is summarized as follows:

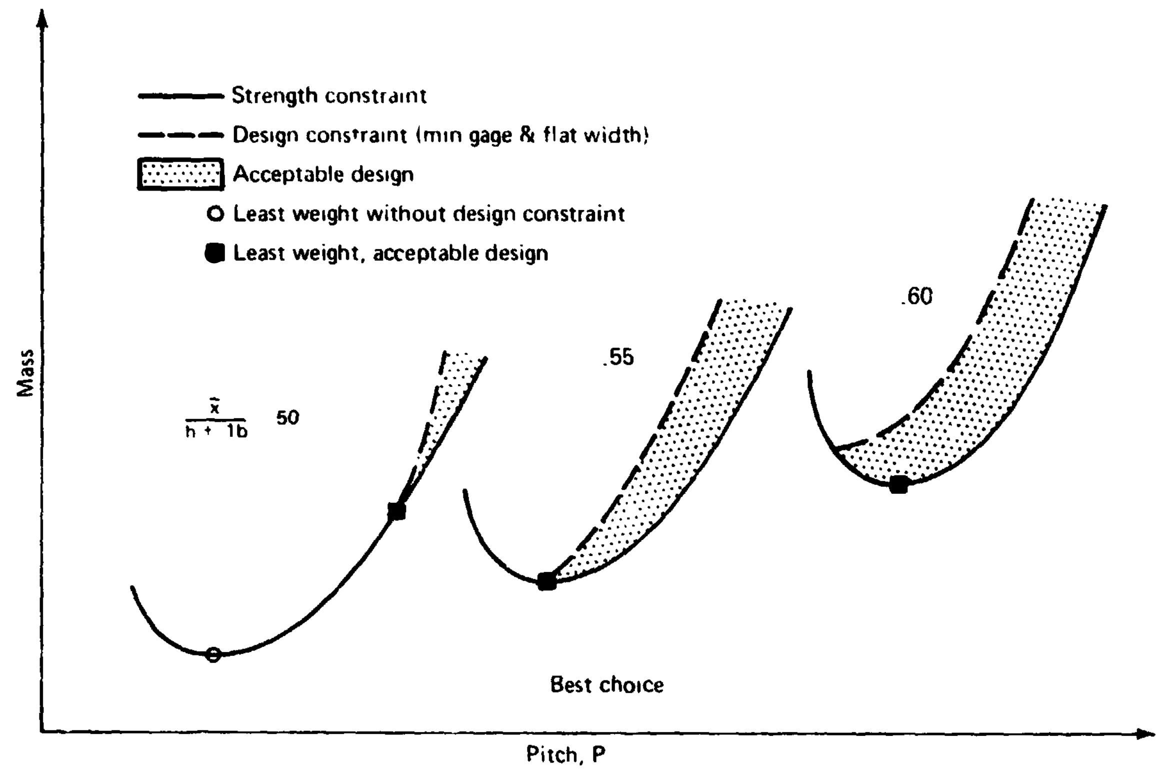

1368-004W

Figure 4-3. – Schematic of least mass designs vs pitch for three neutral axis locations.

$$t_1 = \emptyset_B \, L \left[\frac{q}{f(m) \; E}\right]^{1/3} \qquad (4\text{-}1)$$

where q_{max} = 3418 kg/m^2 (700 psf) at M = 1.3, H = ~~914~~ 9144 m (30 000 ft)

$q/f_{(m)}$ = 7080 kg/m^2 (1450 psf) (ref. 4-2, figure 2)

FS = 1.5 (ref. 4-3, para 4.5.1.3)

L = 48.5 cm (19.1 in.)

$$\emptyset_B = \frac{1.284}{2.924 + \frac{L}{b+2b'}} - .019 \qquad (4\text{-}2)$$

Note that equation (4-2) is an empirical fit to $\emptyset_B$ vs L/W in ref. 4-2, where W = b + 2b'.

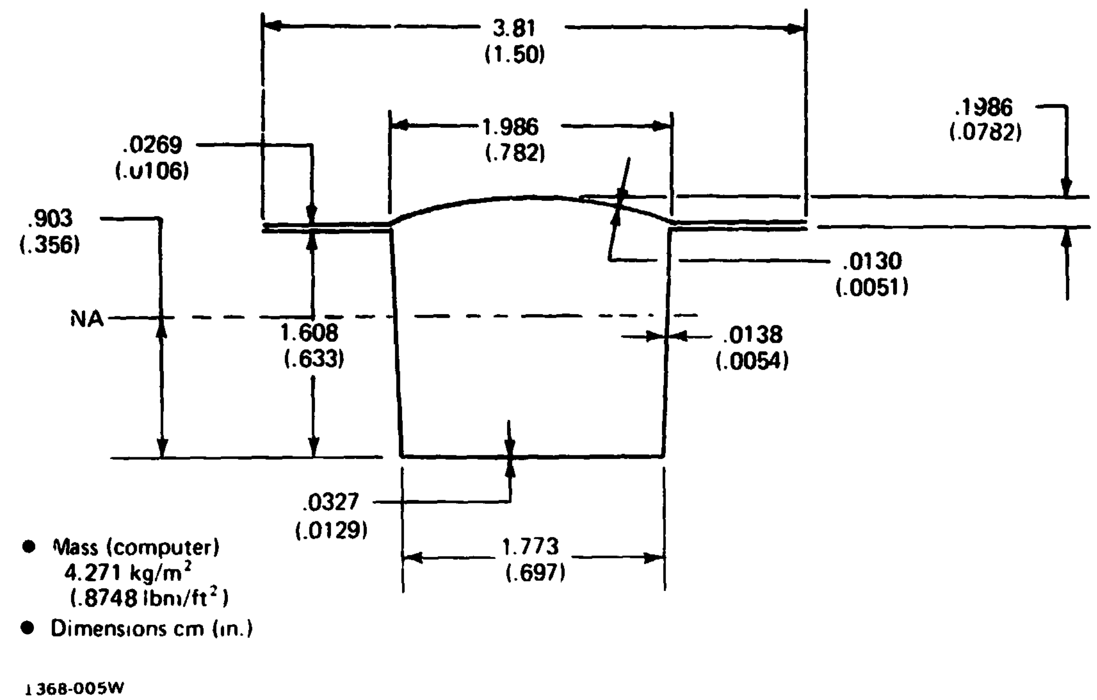

Figure 4-4. – Haynes 188 optimum computer section.

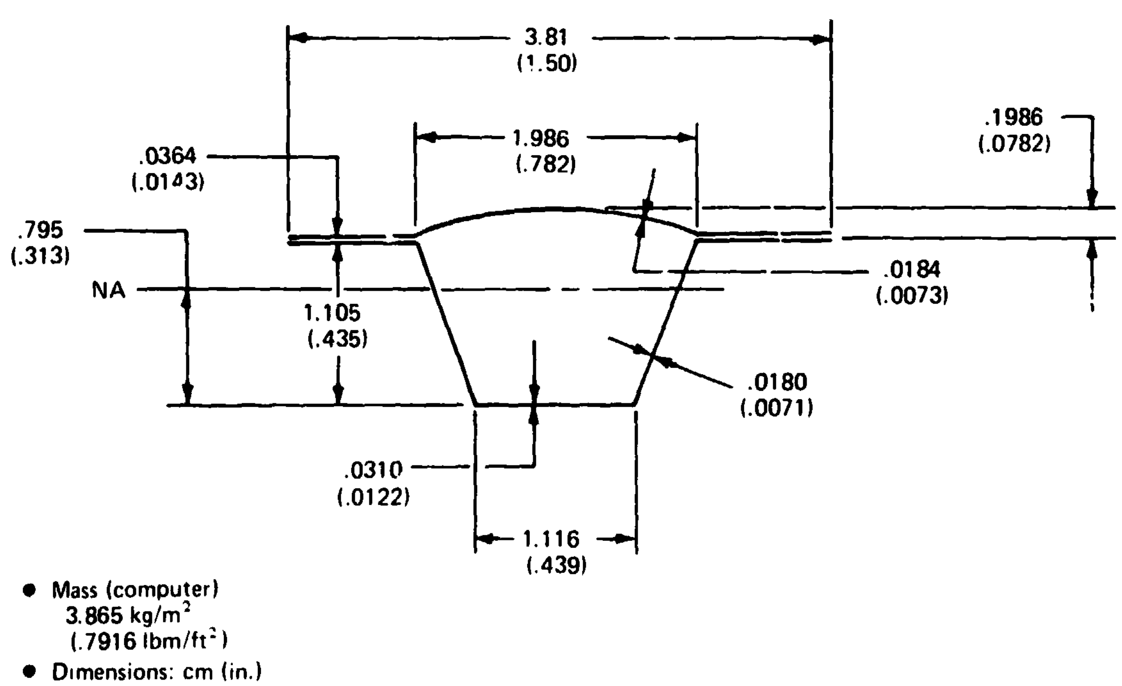

Figure 4-5. – René 41 optimum computer section.

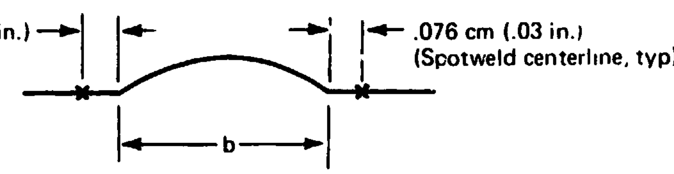

1368-024W

Equation (4-1) was solved for both materials to provide a minimum thickness (or lower bound) for t_1. The results are presented in figure 4-6 for Haynes 188 and figure 4-7 for Rene 41. The curves were fitted to the empirical equations for use in the computer program, and are:

- $t_1 = .0155\ (b+.152)$ cm ($t_1 = .0061\ (b + .06)$ in.) for Haynes 188
- $t_1 = .0198\ (b+.152)$ cm ($t_1 = .0078\ (b + .06)$ in.) for René 41

4.3.3 Lateral Thermal Expansion

The lateral thermal expansion is constrained by the adjacent panel, which prohibits lateral growth, and the support ribs, which prevent normal displacements. Thermal strains are absorbed by the face sheet beads in bending. The value b/10 is sufficiently large to avoid thermal buckling of the circular arc (ref. 2-1).

The edge load, P, and moment, M (per unit length, ℓ) are (from ref. 2-1) given by:

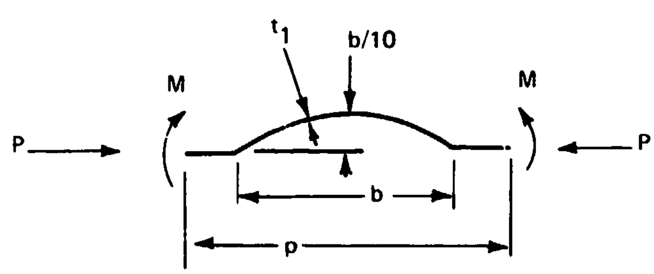

$$P = \frac{2\,EI\Delta}{\frac{b^3}{100}N}\left\{\frac{p-b+\pi bN}{\pi(p-b)+bN\left(\frac{2}{\pi}-8\right)}\right\}\frac{1}{\ell}$$

$$M = \frac{4\,EI\Delta}{\frac{b}{10}}\left\{\frac{1}{\pi(p-b)+bN\left(\frac{2}{\pi}-8\right)}\right\}\frac{1}{\ell}$$

where

$$N = \frac{1}{\pi\left[1-\frac{\pi}{2}\left(\frac{\pi}{10}\right)^2\right]} = .37671$$

Δ α p ΔT

ℓ unit length 1

The analysis is nonlinear and considers only bending energy. The thermal and mechanical properties employed are given in table 4-3.

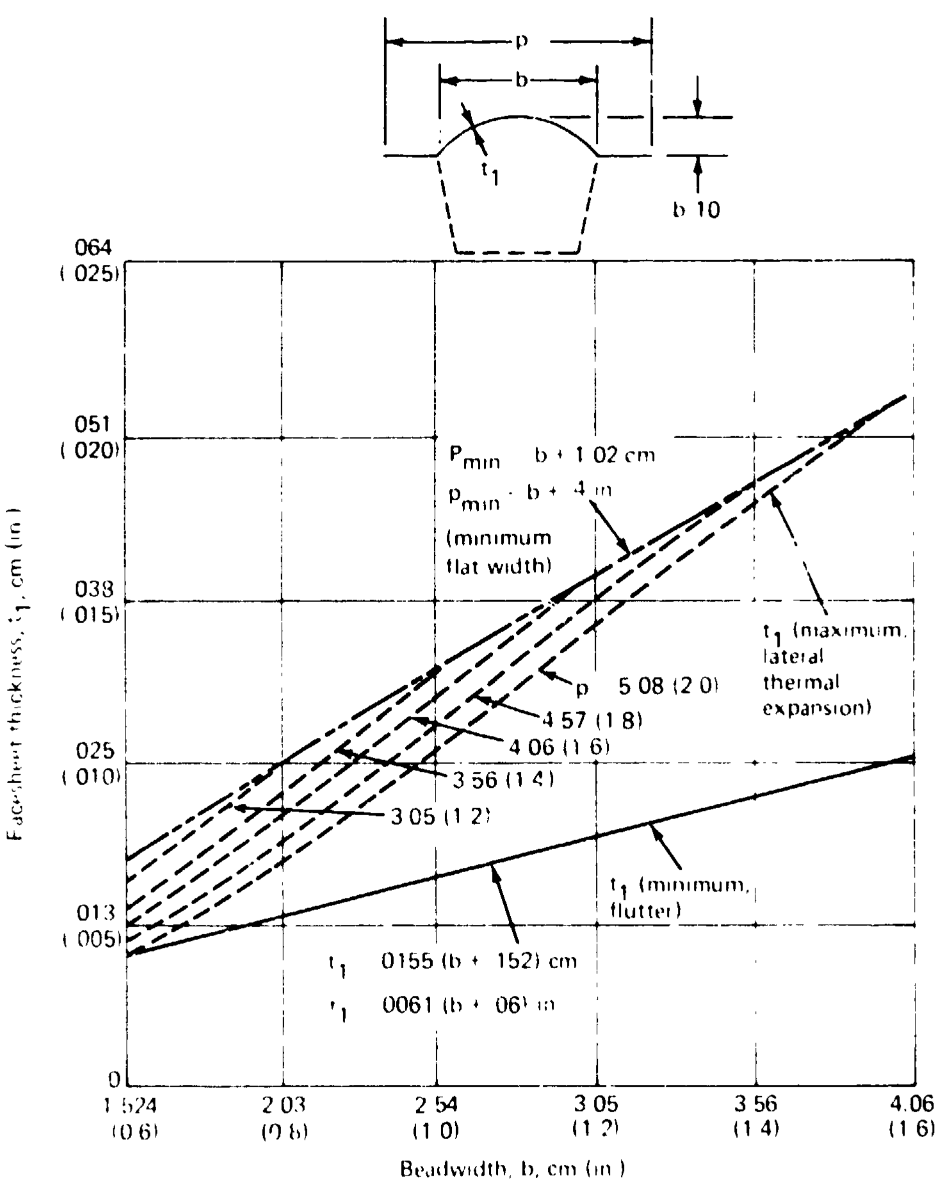

Figure 4-6. – Haynes 188 flutter and thermal constraints.

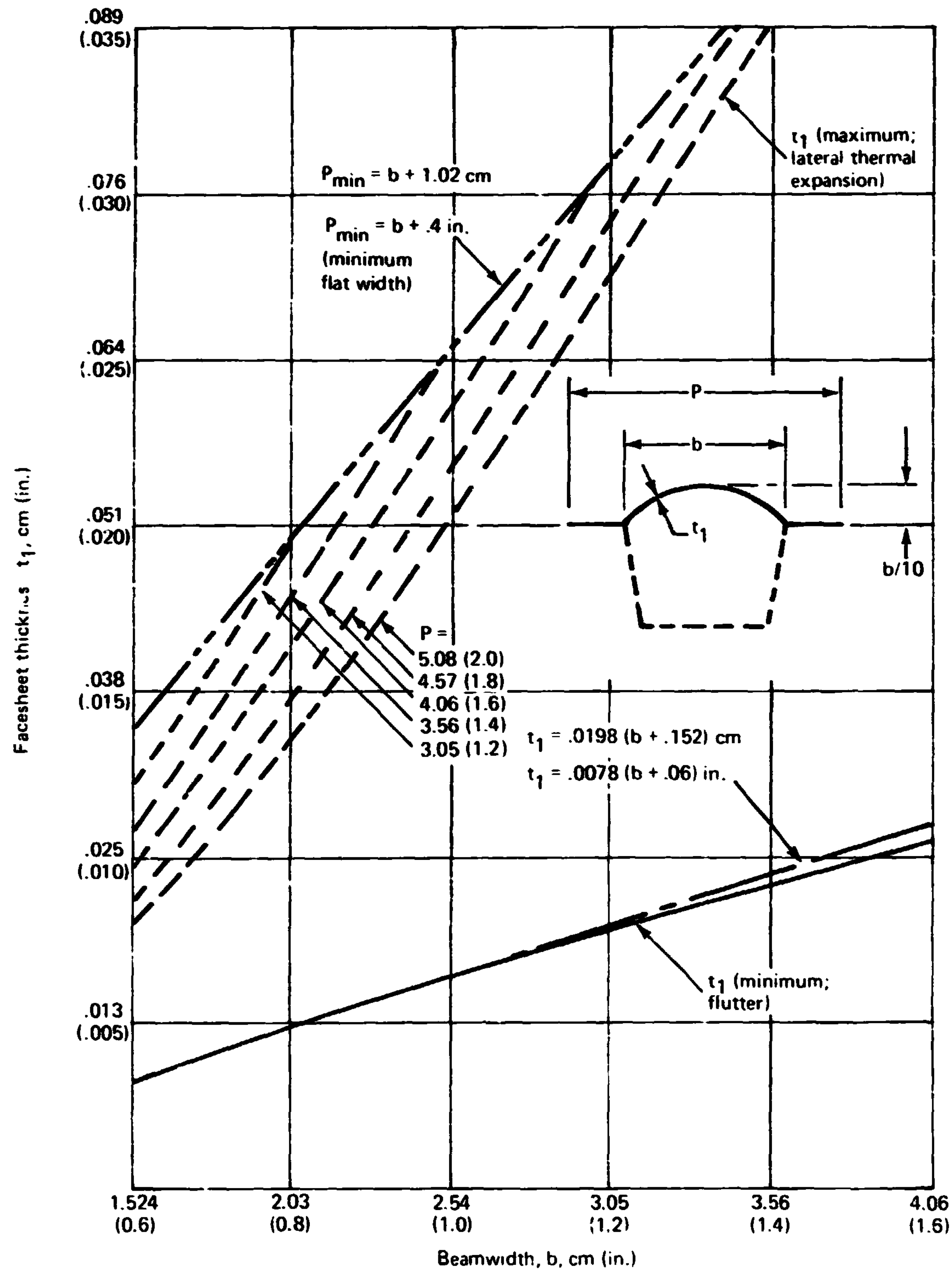

1368 007W

Figure 4-7. – René 41 flutter and thermal constraints.

Table 4-3. – Thermal and mechanical properties.

Property	Haynes 188		René 41	
	SI	Customary	SI	Customary
Max temperature	1255 K	1800° F	1144 K	1600° F
Δ temperature	1217 K	1730° F	1105 K	1530° F
α	17.7 m/m/K	9.7×10^{-6} in./in./°F	15.7 m/m/K	8.5×10^{-6} in./in./°F
E	94.4 GPa	13.7×10^6 psi	122 GPa	17.7×10^6 psi

2217-18W

The maximum fiber stress was limited to yield (0.2% permanent deformation) at peak temperature, resulting in an allowable total strain, ϵ_T, and comensurate allowable elastic stress $F_{allow.}$ (figure 4-8). (The factor of safety was taken as 1.0.) Thus:

$$F_{allow.} = E \epsilon_T$$

$$= 13.7 \times 10^6 (.0034) = 331 \text{ MPa } (46\ 600 \text{ psi}) - \text{Haynes}$$

$$= 17.7 \times 10^6 (.0052) \quad 634 \text{ MPa } (92\ 000 \text{ psi}) - \text{René}$$

It can be shown that the maximum bending moment, M, occurs at the top of the bead, so that:

$$\overline{M} = P \frac{b}{10} - M$$

and

$$f_b = \frac{6M}{t_1^2}$$

taking

$$I = \frac{t_1^3}{12}$$

and setting

$$f_b = F_{allow.}$$

The maximum allowable t_1 can be obtained for given values of p and b.

$$t_{1_{max}} = \frac{b\left[\pi(p-b) + b(.7043)\right] F_{allow.}}{10p\left[\frac{p-b}{b(.3767)} + \pi - 2\right] E \alpha \Delta T}$$

The solution of this equation is plotted as the family of dashed curves in figure 4-6 for Haynes 188 material and figure 4-7 for René 41. These curves define an upper bound for the face-sheet thickness.

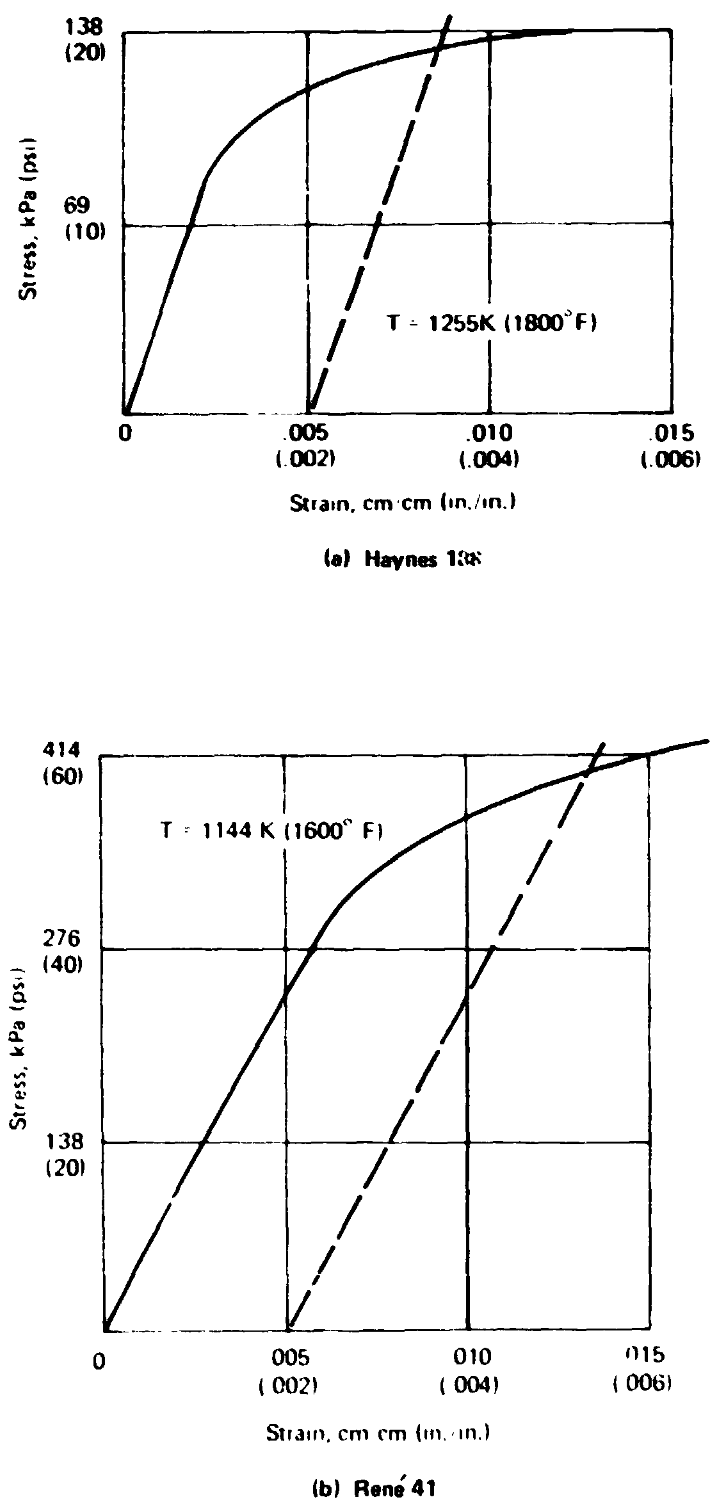

1368 030W

Figure 4-8. – Haynes 188 and René 41 Stress-strain curves at elevated temperature.

4.3.4 Selection of Optimum Haynes 188 Section

The results of the optimization program for the minimum-mass section are illustrated in figure 4-9. It can be seen that the optimum design occurred at a pitch of 3.73 cm (1.47 in.). For convenience and simplicity, a panel with a pitch of 3.81 cm (1.50 in.) was selected for the final design. Dimensions of the selected section, which define the midspan cross section, are also shown in figure 4-9. This section produced a surface panel with a mass of 4.27 kg/m^2 (0.875 lbm/ft^2). This section, however, was modified to accommodate surface emittance treatment and material oxidation losses during the 100-mission life. Additionally, the corrugation lower cap pad was sculptured to minimize mass and provide uniformity of stress. The modified section, which was the section that was fabricated, is shown in Figure 4-10(a). The mass of this section, including doublers, attachment rivets, and mass reduction resulting from sculpturing, is 4.536 kg/m^2 (.929 lbm/ft^2). This new design indicated a 22% reduction in mass from the baseline panel. (See figure 4-1.)

4.3.5 Selection of Optimum René 41 Section

The principal differences between René 41 and Haynes 188 is that Rene 41 has superior mechanical properties at room temperature and suffers less degradation in mechanical properties at elevated temperature because its service temperature is lower - 1144 K (1600°F) vs 1255 K (1800°F). Although the moduli of elasticity are similar, the creep strength of René 41 at service temperature is typically, 69 MPa (10 000 psi) vs 27.6 MPa (4000 psi) for Haynes 188. The increased creep strength produced two effects on the optimum René 41 section relative to the Haynes section: the overall section height (and associated dimensions) decreased, and the width-to-thickness ratio for the various elements decreased. The latter effect resulted from satisfying buckling criteria for conditions A, B, or C, while also satisfying creep criteria for condition D. As an illustration of this effect, consider element 5. For a given moment of inertia and neutral axis location, condition A yields

$$f = \frac{Mc}{I} = M_A\left(\frac{\bar{x}}{I_{na}}\right) = \frac{F_{crel}}{1.4} = \frac{K_{cr}E\left(\frac{t_3}{d}\right)^2}{1.4} \tag{4-3}$$

and condition D yields

$$f = \frac{Mc}{I} = M_D\left(\frac{\bar{x}}{I_{na}}\right) = \frac{F_{creep}}{1.15} \tag{4-4}$$

where

M_A - moment from applied pressure, condition A

M_D - moment from applied pressure, condition D

1.4 and 1.15 - factors of safety

K_{cr} - buckling coefficient

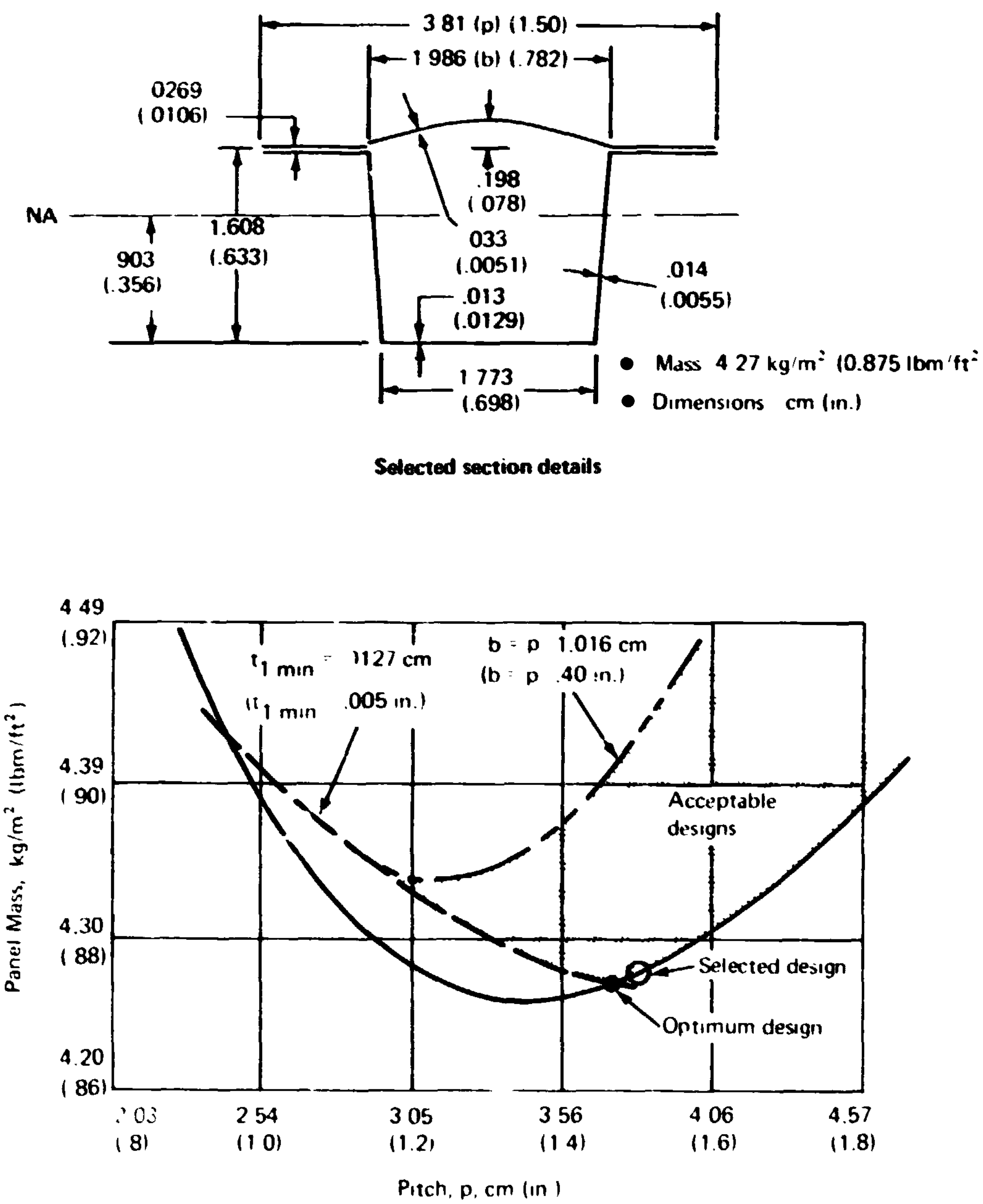

1368 008W

Figure 4-9. – Haynes 188 skin/corrugation optimization.

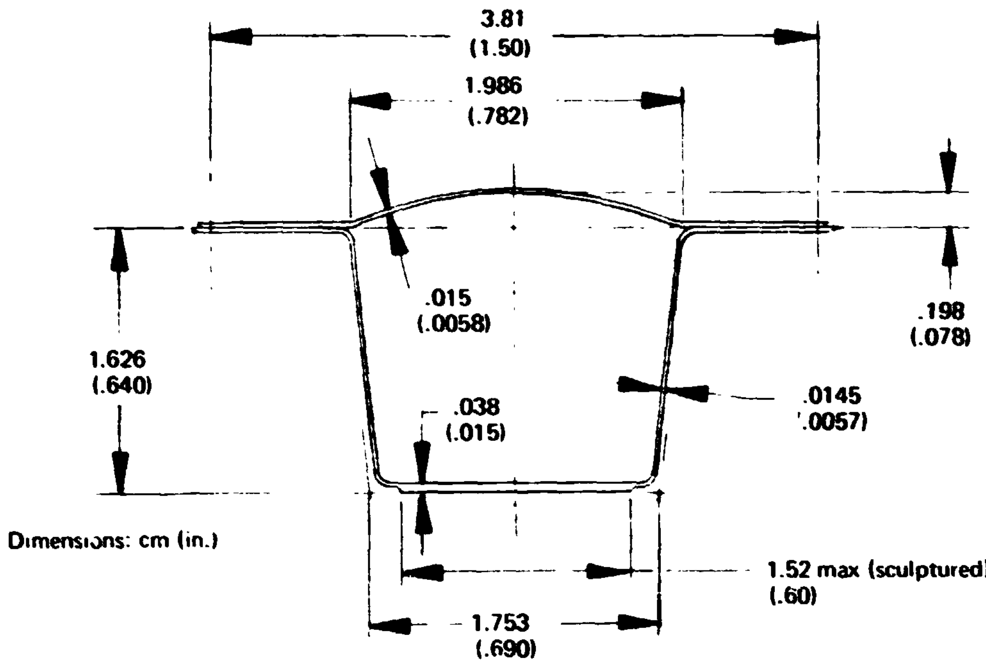

(a) Haynes 188 Production Section

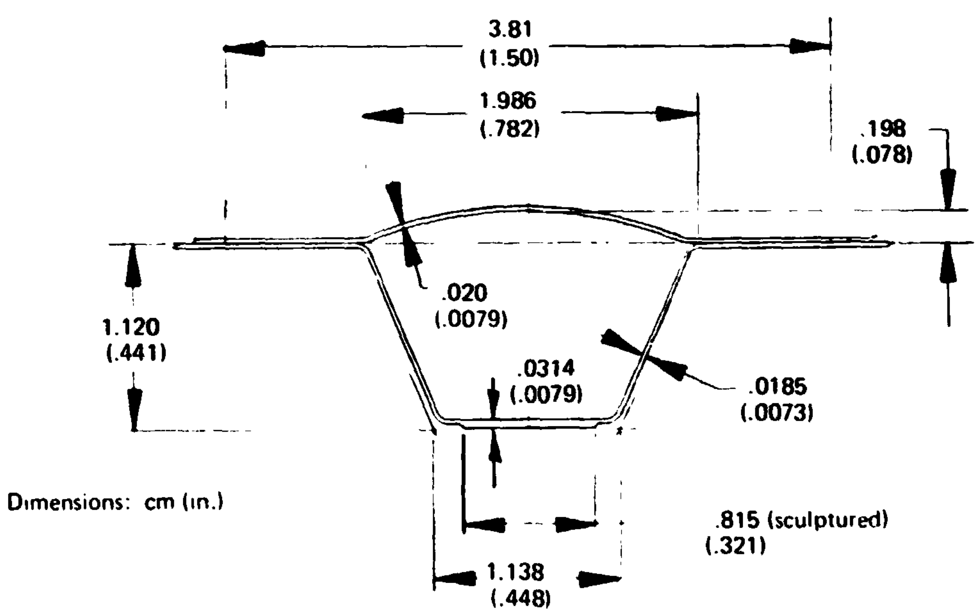

(b) René 41 Production Section

1368-009W

Figure 4-10. – Production TPS sections.

Solving each equation for $\bar{x}/I_{na}$ and equating the results yields

$$\frac{t_3}{d} = \left[\frac{F_{creep}}{E}\left(\frac{M_A}{M_D}\right)\left(\frac{1.4}{1.15}\right)\frac{1}{K_{cr}}\right]^{.5}$$

The only significant variable is F_{creep}, which is about 2.5 times greater for René 41 than for Haynes 188, so that for a given value of x/I_{na} (t_3/d) for René is about 1.6 times greater than for an equivalent Haynes panel. In addition, equation (4-4) shows that if the creep allowable is increased by a factor of 2.5, the value of x/I_{na} can increase by the same amount. All of these effects tend to reduce the overall dimensions of the René 41 cross section relative to the Haynes.

The René optimization results are presented in figure 4-11. Several values were assumed for beta. (Beta is the ratio of neutral-axis location to overall section height.) Design constraints limiting the face-sheet thickness to .013 cm (0.005 in.), minimum, and the flat between beads to at least 1.02 cm (0.4 in.) are also shown. It can be seen that the optimum René panel has a pitch of 1.98 cm (0.78 in.) and an average weight of 3.58 kg/m^2 (0.734 lbm/ft^2). Details of this section are presented in figure 4-12(a). The computer-designed section possesses acute angles at the bend lines, making the section difficult to fabricate. As a result, the section was modified to that shown in figure 4-12(b). Both sections are the same except that the width and thickness of the bottom element were altered as shown. As a result, while the area of the elements and moment of inertia of the sections are identical, the buckling stress of the bottom element is now higher and, therefore, has a positive margin of safety. The computer program sized the dimensions of the element based on buckling with zero margin of safety.

4.3.6 Compromise Haynes/René Optimum Section

One objective of the program was to address the problem of "interface" between metallic TPS optimized and fabricated from different metals. It was decided, therefore, that a compromise section geometry would be selected for the skin panel so that the Haynes and René systems could be used as adjacent panels. Moreover, the use of one skin geometry could significantly lower fabrication and tooling costs for a flight vehicle.

Since only the skin of each system interfaces at the expansion joint, the corrugation of each configuration can still be optimized independently. It can be seen from figure 4-9 that the pitch of the Haynes section cannot be smaller than 2.95 cm (1.16 in.). This is somewhat above the optimum René 41 pitch of 1.98 cm (.78 in.) From a cost and mass standpoint, it is desirable to increase section pitch to reduce the number of clips and attaching rivets on the rib support. To identify a compromise pitch, a simplified study was conducted; it included the effects of pitch on panel mass, and accounted for upper and lower clip mass for both the center and end support ribs. Items not included in the study because their mass remains relatively constant with respect to pitch include support rib webs, drag brackets, miscellaneous fasteners, and insulation.

The results of the study are shown in figure 4-13. It can be seen that the Haynes 188 total mass (panel plus clips) is minimized at a pitch of 3.91 cm (1.54 in.). The minimum-mass René 41 panel occurs at a pitch of 2.39 cm (0.94 in.). The middle curve shows a mass-pitch curve for a 50% Haynes 188/50% René 41 panel mix. The

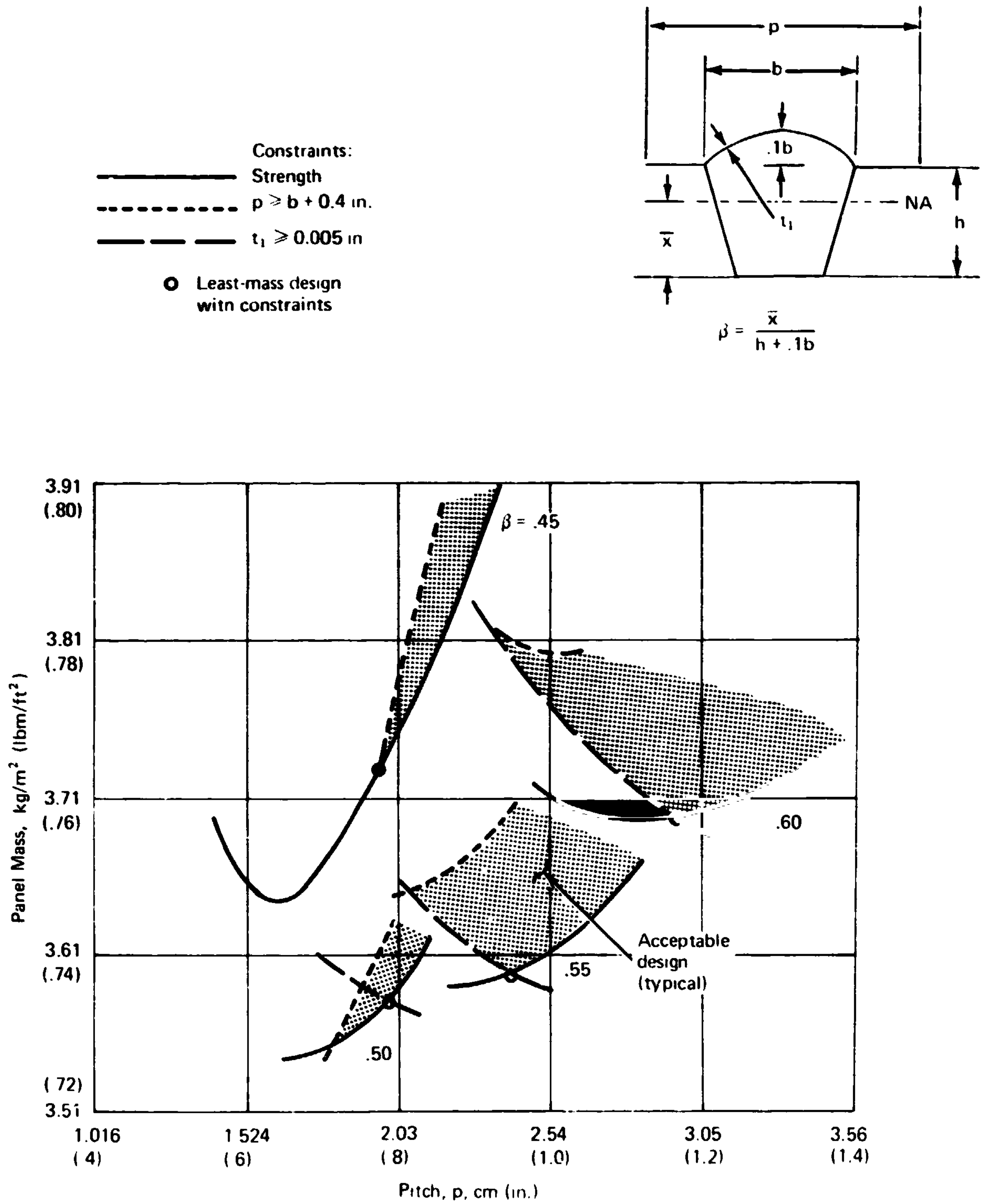

1368 010W

Figure 4-11. – René 41 skin/corrugation optimization.

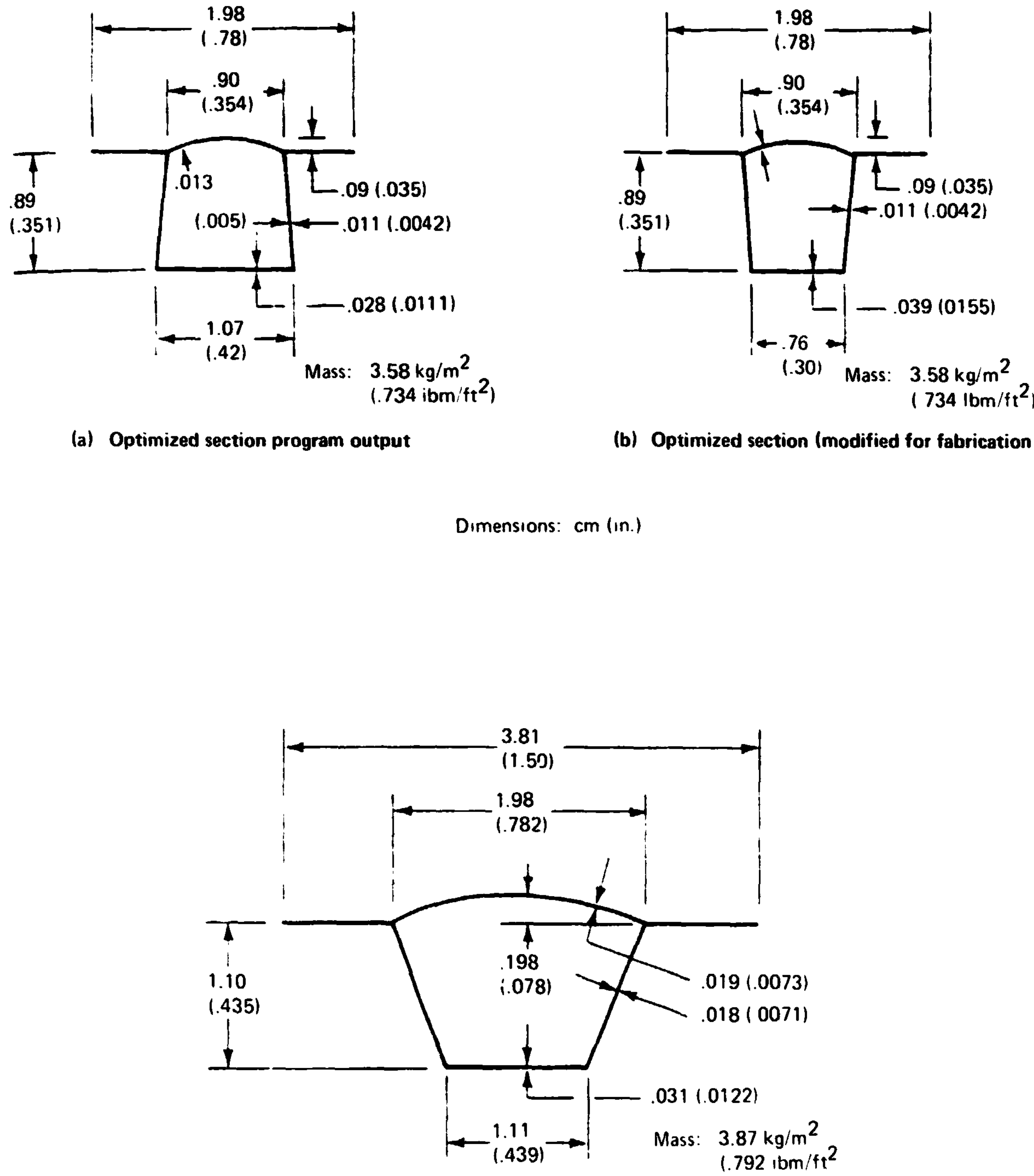

(a) Optimized section program output

(b) Optimized section (modified for fabrication)

(c) Optimized section matched to 3.81 cm (1.5 in.) pitch

1368-011W

Figure 4-12. – René 41 section dimensions.

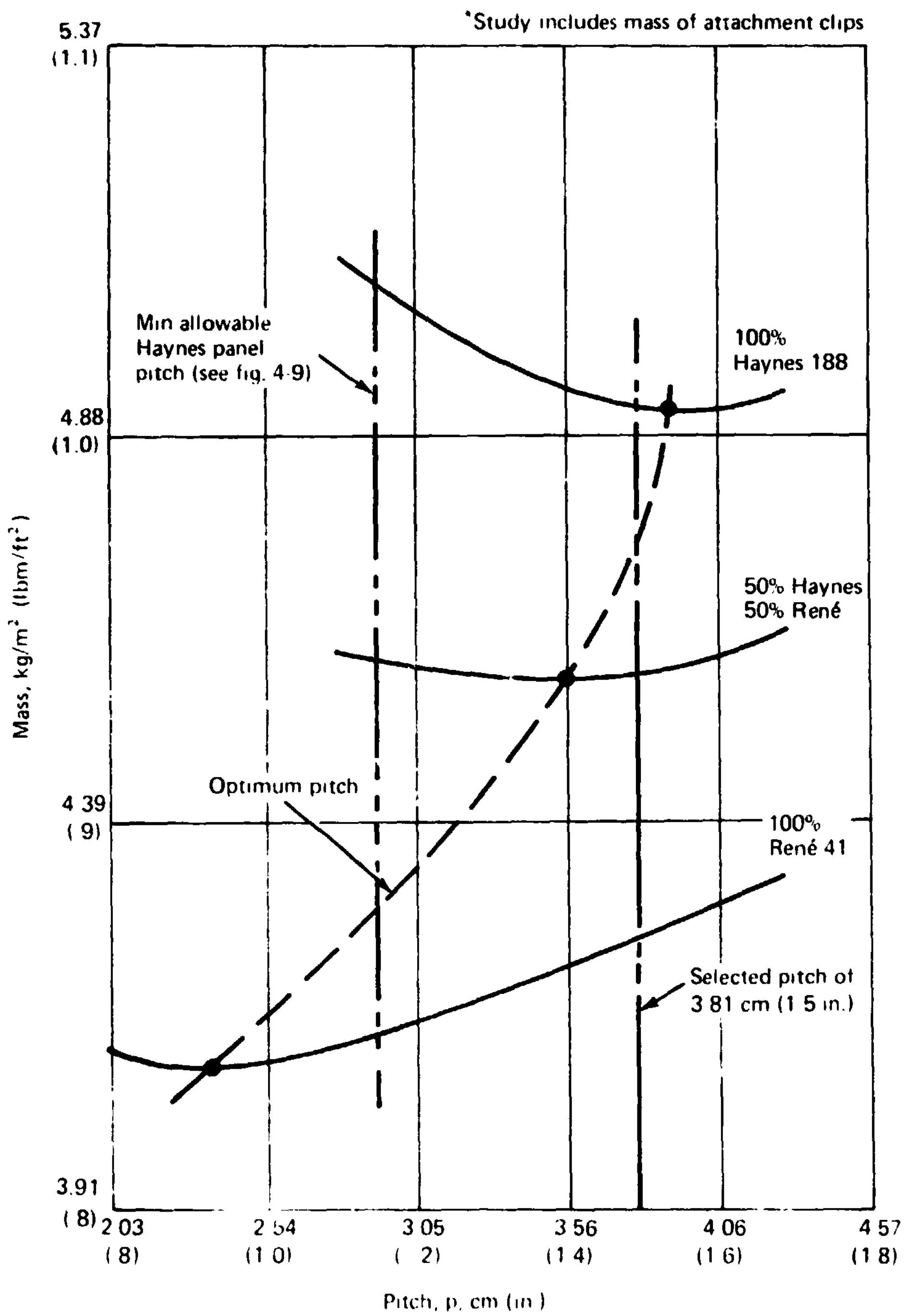

2217-26W

Figure 4-13. – Mass study results.*

minimum composite mass occurs at a pitch of 3.58 cm (1.41 in.). The dashed line connects the three calculated points and is an estimated relationship between optimum pitch and surface panel mass. Based on these curves, the greater density of Haynes 188, and the desire to space an even number of corrugations across a 61-cm (24-in.) span, it was decided to use a common pitch of 3.81 cm (1.50 in.) for Haynes 188 and René 41.

The mass penalty to the Haynes 188 design is less than .005 kg/m^2 (.001 lbm/ft^2), or, about 0.1%. The mass penalty to the René 41 design is 0.166 kg/m^2 (0.03 lbm/ft^2), or, about 4.0%. The René 41 section was reanalyzed to determine the optimum section with a pitch of 3.81 cm (1.50 in.) and a bead width of 1.99 cm (.782 in.). The analysis indicated the optimum beta to be .61, which was used to determine a section with these two constraints. (See appendix A, figure A-2). The resulting René 41 section is shown in figure 4-12(c). The production section is shown in figure 4-10(b). This section includes thickness increases for oxidation and emittance allowance and slight geometry changes to accommodate lower-cap sculpturing.

4.3.7 Corrugation Sculpturing

To minimize corrugation mass, the lower horizontal flat of the corrugation was sculptured to match the bending moment. Since the corrugation already included chem-milling, the addition of a profiled chem-mill line did not significantly increase fabrication costs. The profile was selected such that the area and buckling allowable stress remained the same. (The analysis by which the profile was selected is given in appendix B. The profile geometry is given in appendix B, table B-1.)

The values for d' (appendix B) are minimums required, and these values generate a curved profile. The mass which could have been saved by sculpturing the curved profile was .168 kg/m^2 (.0344 lbm/ft^2) for the Haynes 188 panel and .092 kg/m^2 (.0188 lbm/ft^2) for the René 41. However, a straight-line profile was used to facilitate fabrication and thereby lower the costs of chem-milling. The actual masses saved using a straight profile are .145 kg/m^2 (.0299 lbm/ft^2) for the Haynes 188 and .080 kg/m^2 (.0163 lbm/ft^2) for the René 41 panel.

4.3.8 Circular Corrugation Study

A circular corrugation-stiffened panel was examined as part of the panel optimization effort. The circular corrugations were considered because they possess many of the beneficial characteristics of a trapezoidal corrugation, particularly flexibility transverse to the corrugations, which relieves transverse in-plane thermal stresses. The circular corrugations also offer a high resistance to local buckling. The results of the study, in which a constant-thickness corrugation was assumed, are shown in figure 4-14. The minimum-mass design at 5.57 kg/m^2 (1.14 lbm/ft^2) is 1.29 kg/m^2 (.265 lbm/ft^2) more than the chem-milled trapezoidal corrugation.

By chem-milling portions of the circular corrugation, some reduction in weight could probably have been achieved. However, chem-milling would have degraded the buckling resistance of the unchem-milled portions of the arc.

A constant-thickness trapezoidal corrugation was also investigated in an effort to provide a direct comparison between the circular and trapezoidal corrugations. Figure 4-15 illustrates that the minimum weight of this design is 4.91 kg/m^2 (1.005 lbm/ft^2), or about 12% lighter than the circular corrugation.

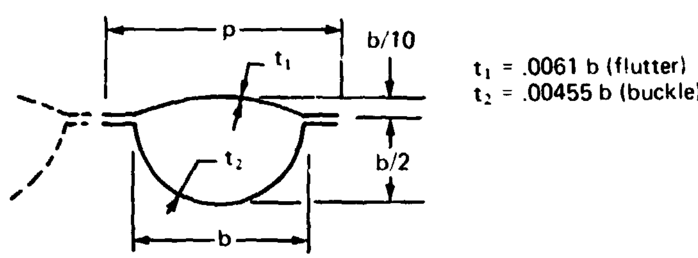

Section Geometry

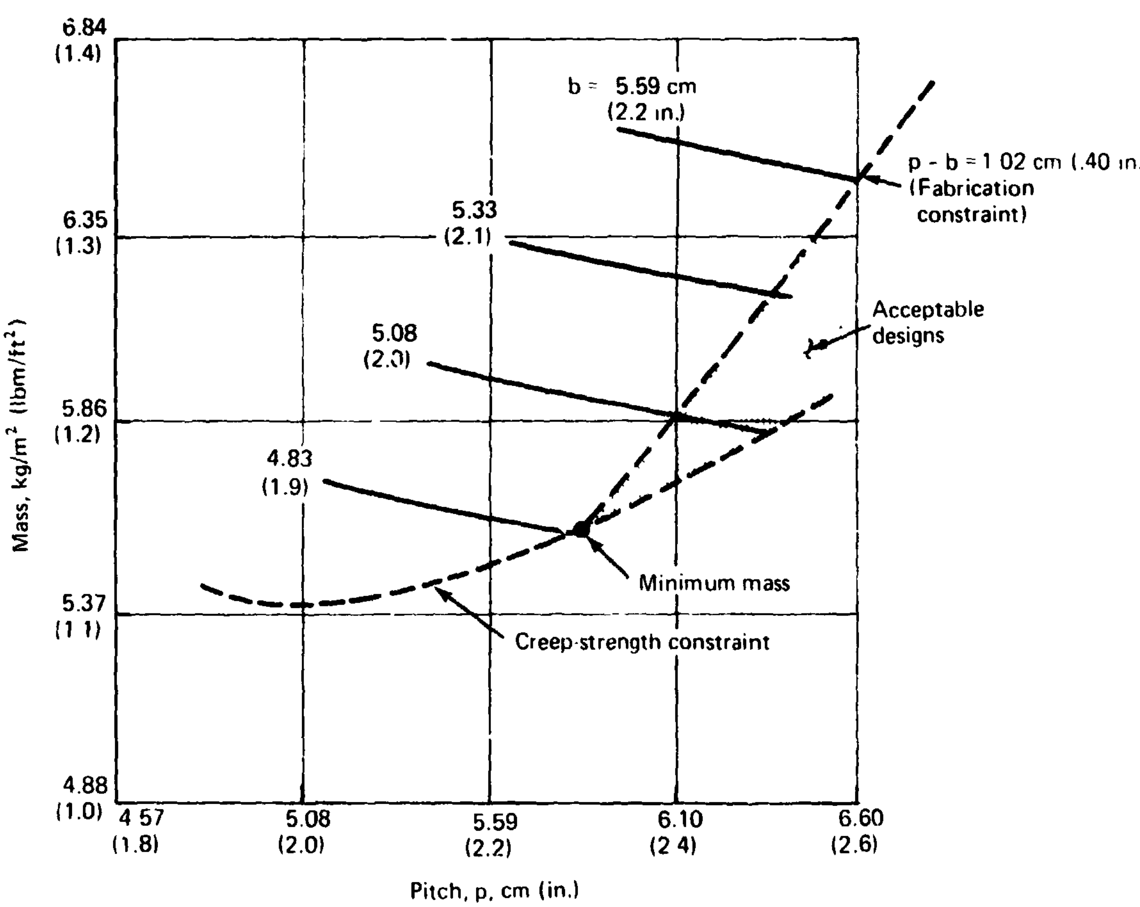

Figure 4-14. – Circular corrugation panel optimization.

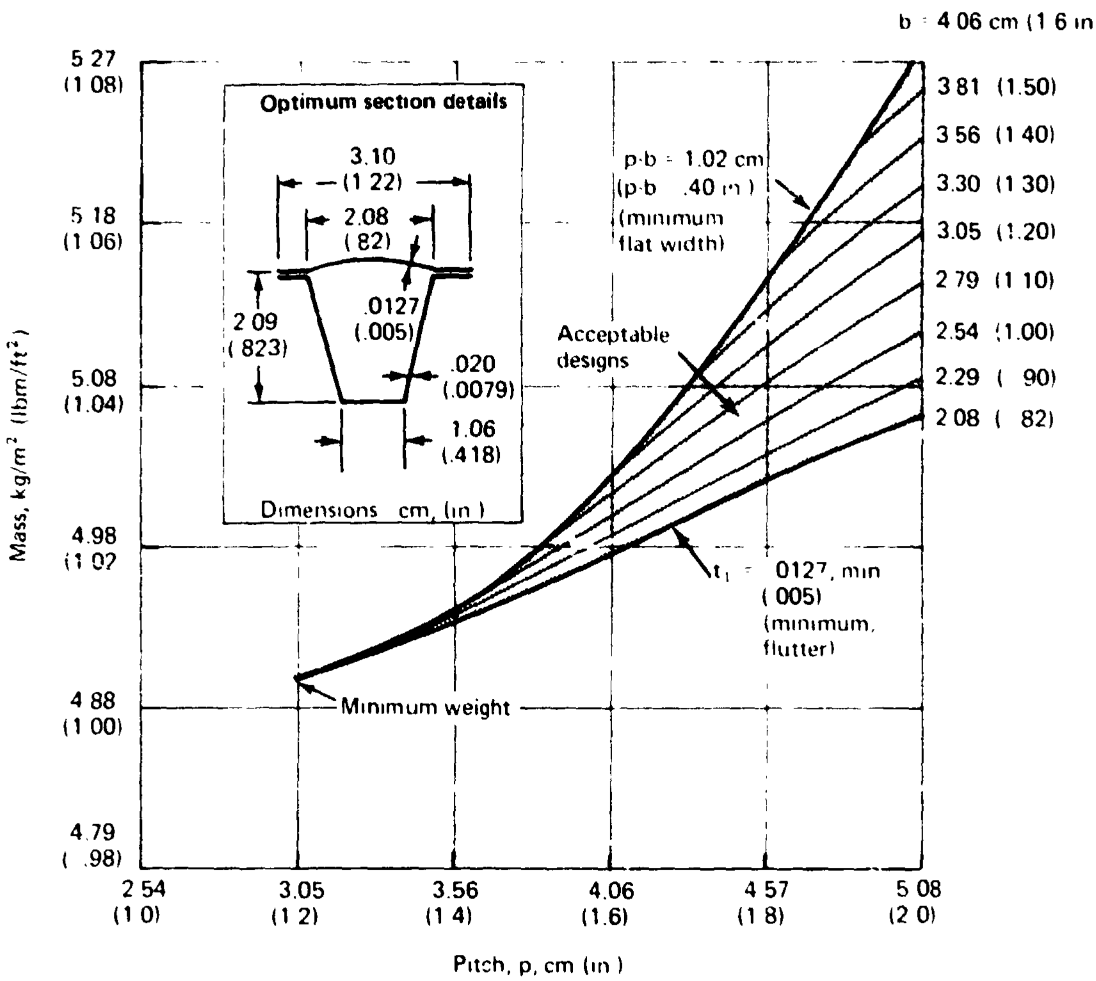

1368 013W

Figure 4-15. – Constant-thickness trapezoidal corrugation-panel optimization.

The trapezoidal section is lighter because the design loads are exclusively bending. Whether the sections are chem-milled or not, the trapezoidal section provides more bending material about the neutral axis than the circular section. The circular corrugation, therefore, was eliminated from further study.

4.3.9 Flutter Check for TPSTF Test Environment

Analysis has shown that the current Haynes 188 heat shield panel design is flutter-free for the required shuttle orbiter design flight environment. The following analysis was performed to determine if the TPSTF testing environment is likely to impose a more severe flutter requirement on the panel.

Figure 4-16 shows the operating envelope of the NASA Langley Thermal Protection System Test Facility (TPSTF); the dashed line indicates a typical space shuttle entry trajectory (ref. 4-1). Maximum dynamic pressure, q, for the portion of the trajectory within the operating envelope occurs at the left boundary, where the following conditions exist:

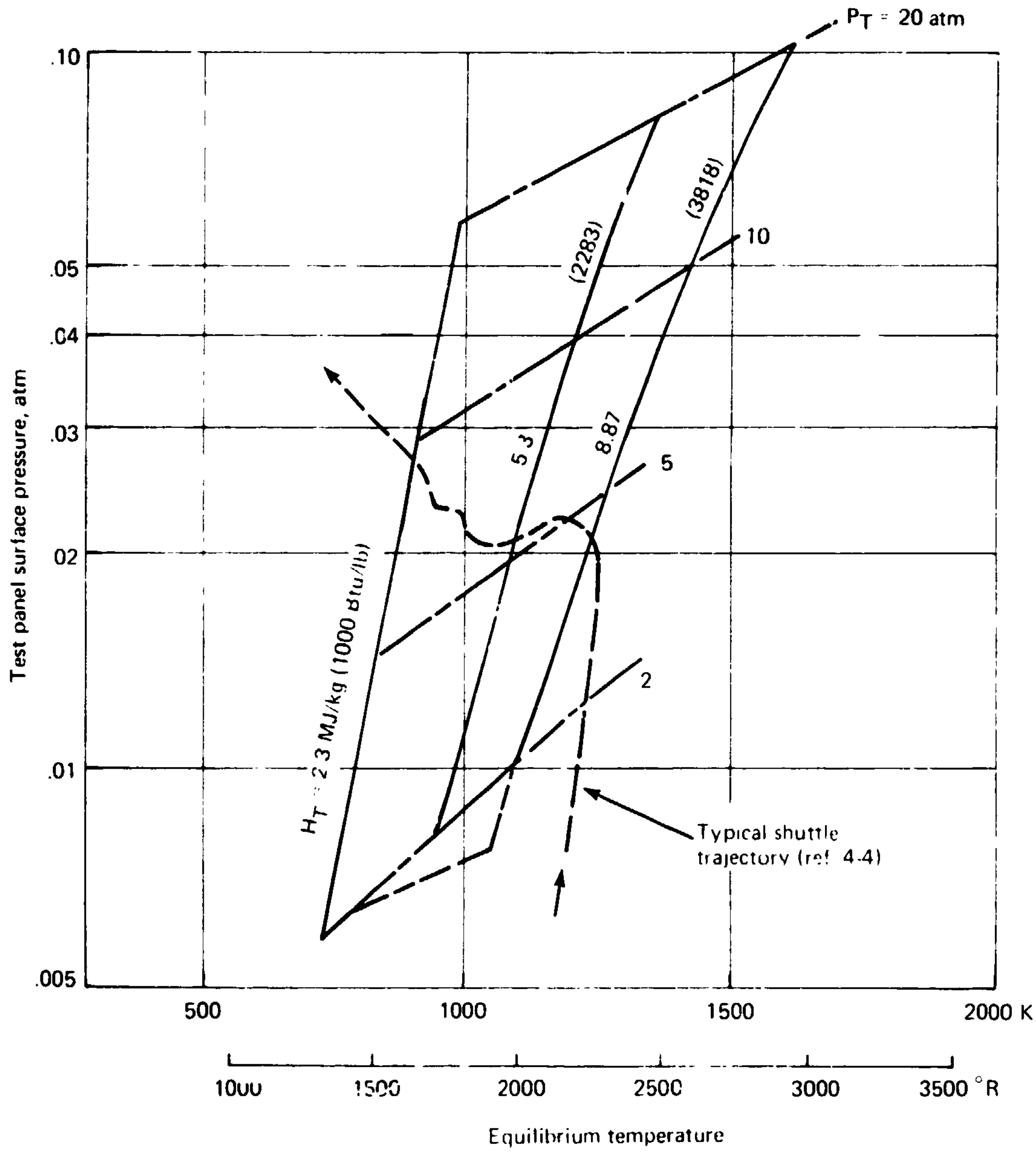

2217-29W

Figure 4-16. – TPSTF operating envelope.

$H_T = 2.3$ MJ/kg (1000 Btu/lbm)

$P_T = 9.5$ atm

and, from reference 4-5, for the TPSTF area ratio $A/A^* = 25$:

$$M = 4.06$$

$$q/P_T = 0.035$$

Thus,

$$q = (q/P_T)\, P_T = 33.7 \text{ kPa (704 psf)}$$

$$\beta = (M^2 - 1)^{\frac{1}{2}} = 3.93$$

and

$$q/\beta = 8.6 \text{ kPa (179 psf)}$$

The outer skin over the width of one corrugation was treated as a simply supported flat panel. The thickness required to prevent flutter was calculated using reference 4-6:

$$GP = \frac{a}{b}\sqrt{\frac{D_{12}}{D_1}} = \frac{a}{b} = 20 \text{ (geometry parameter)}$$

$$FP = \frac{0.0593}{(5+GP^2)\ \sqrt{4+2\,GP^2}} = 5.163 \times 10^{-6} \text{ (flutter parameter)}$$

$$FP = \frac{D_1\ f(M)}{q\ a^3}$$

For

$$D_1 = \frac{Et^3}{12(1-\mu^2)} \quad \text{and } f(M) = \beta$$

$$t = \left[\frac{12(1-\mu^2)\ (FP)\ a^3}{E}\ \frac{q}{\beta}\right]^{1/3}$$

where

$a = 50.8$ cm (20.0 in.)

$\mu = .29$

For conservatism, the modulus for the Haynes 188 panel was selected at 1256 K (2260°R), which is the maximum temperature the panel would experience at the right boundary in figure 4-16: $E = 93.7$ GPa (13.6×10^6 psi). Thus, for the Haynes 188 panel, $t = 0.01$ cm (.00347 in.).

This thickness is 60% of the .010-cm (.0058-in.) design thickness. Conversely, the value of q/beta required in the TPSTF to cause the panel to flutter was calculated to be 40.1 kPa (838 psf). Therefore, the panel should be flutter-free when tested at the selected conditions in the TPSTF.

The René 41 panel is exposed to a lower q beta in the TPSTF, and the modulus at temperature is greater than that for Haynes 188. Therefore, the René 41 panel, which has the same aspect ratio and greater thickness, should be less susceptible to flutter in the TPSTF than the Haynes panel.

4.3.10 Surface Panel Thermal-Structural Analysis

An analysis was performed on the Haynes 188 panel to determine if the combination of thermally induced stresses and stresses due to aerodynamic loadings would exceed allowable stresses in the surface panel. Six load conditions were identified and examined. Five of the conditions, designated design conditions A through E, were obtained from the shuttle orbiter boost and entry trajectories. The sixth condition represented a predicted test environment in the TPSTF.

4.3.10.1 Mission Trajectories

A typical shuttle orbiter mission is divided into four phases: boost, orbit, entry, and postentry. Significant heating effects which could cause temperature gradients and resultant thermal stresses can occur only during boost, entry, and postentry, when the panel surface experiences aerodynamic heat inputs. During orbit, only solar heat inputs, which are not significant, are experienced. The only impact of the on-orbit condition is to determine the initial temperature at the start of entry. Similarly, the panel experiences significant aerodynamic loadings only during boost, entry, and postentry. (Figures 2-4 and 2-1 show the boost and entry trajectories used for panel design.)

4.3.10.2 Heat Inputs

Figures 4-17 and 4-18 show the aerodynamic heat inputs to the panel surface during boost and entry, respectively, resulting from these trajectories. The heating is defined on the basis of an effective boundary-layer temperature (recovery temperature) and a convective heat-transfer coefficient. The convection coefficient was obtained using a modified Van Driest method for turbulent flow over a flat plate. The heat flux is calculated as

$$q = H_c (T_{BL} - T_W)$$

where

q = heat flux

H_c = convection coefficient

T_{BL} = effective boundary-layer temperature

T_W = panel surface temperature

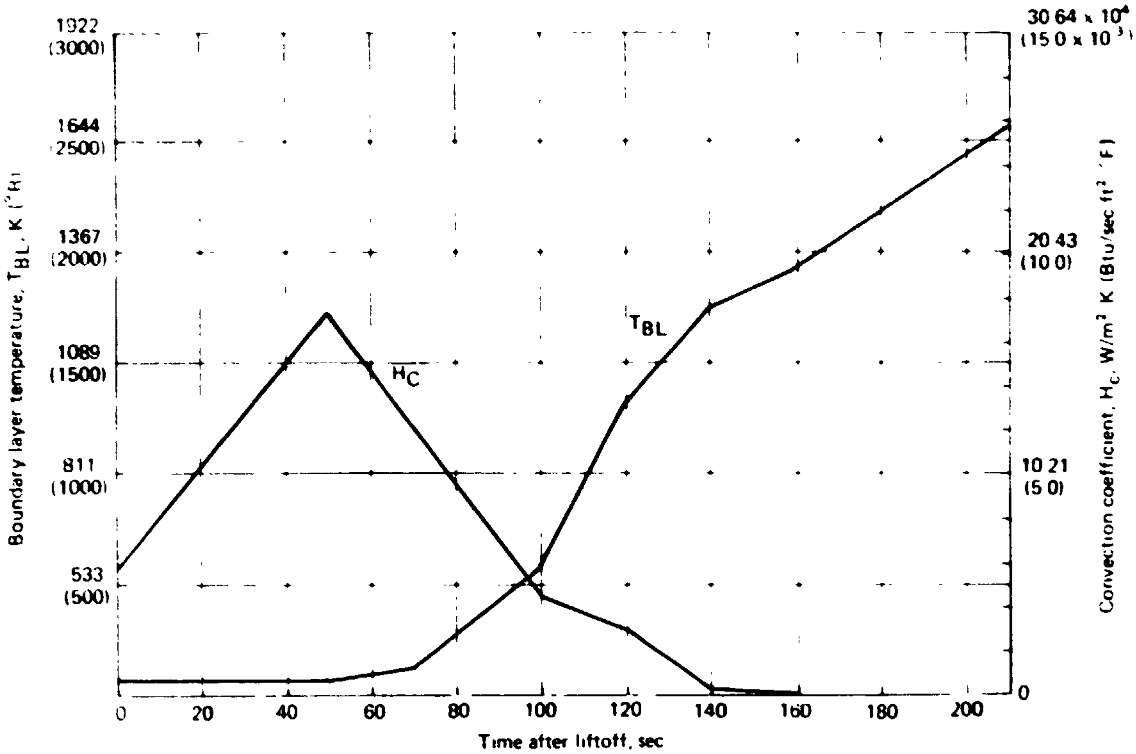

Figure 4-17. – Boost heating profile.

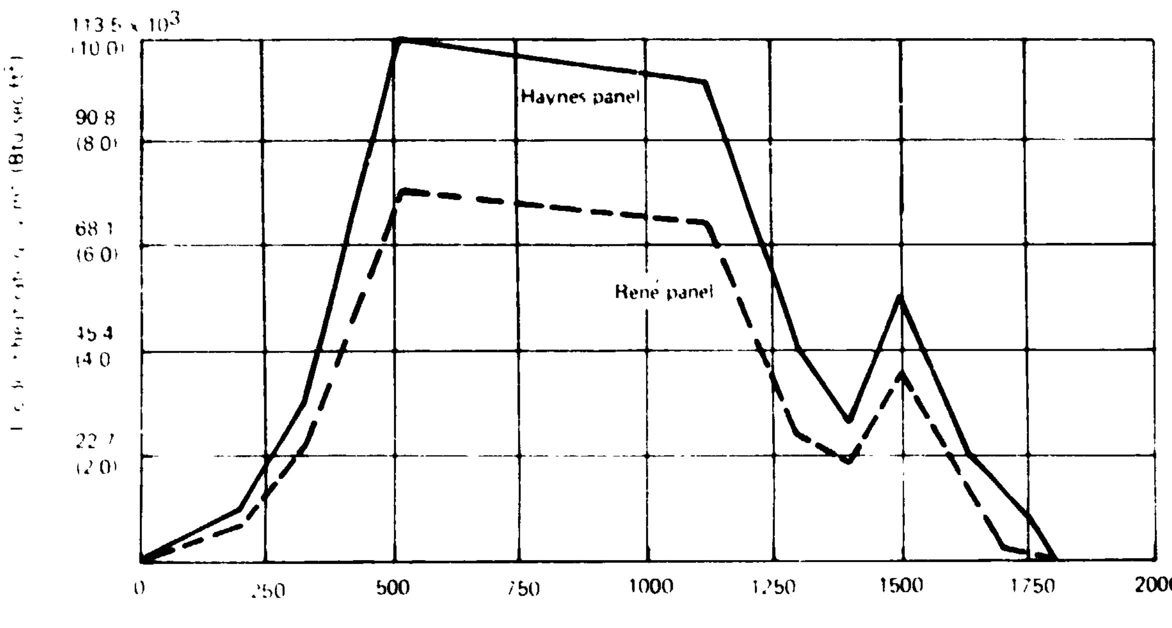

Figure 4-18 – Entry heating profile.

4.3.10.3 Temperature Analysis

A thermal model of the structure was made to determine temperature distributions in the surface-panel structure. This model consisted of four elements, as shown in the insert of figure 4-19. Conduction, convection, and radiation between the elements was considered. The in-house transient temperature analysis program using finite-difference techniques was employed to evaluate the differential equations which represent the thermal model. The output of the computer program is shown in the transient temperature response of the surface-panel elements to the boost and entry heating inputs in figures 4-19 and 4-20 for the Haynes 188 design shown in figure 4-10. A panel surface emissivity of 0.8 was assumed in these analyses. The entry maneuver was assumed to start with an initial temperature of 200 K (-100°F), which is the temperature resulting from an on-orbit cold-soak. Shuttle orbiter studies have identified this as the initial condition that produces the most severe thermal stresses during entry. Figures 4-19 and 4-20 contain all the temperature gradients of significance to the Haynes 188 panel during an orbiter mission.

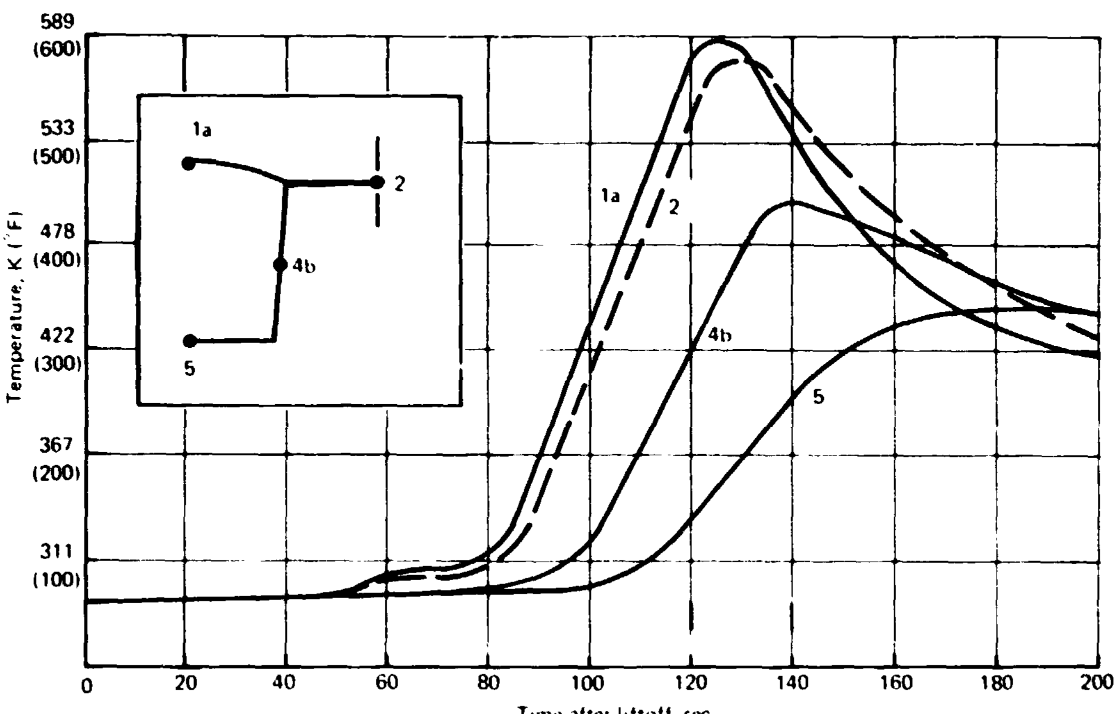

2217-32W

Figure 4-19. – Panel temperature response, boost heating.

4.3.10.4 TPSTF Test Conditions

The test article was also checked for the heating and pressure environment of the TPSTF. The TPSTF heating inputs assumed a three-step simulation of the initial portion of the entry trajectory. It was assumed that the minimum heating at startup of the TPSTF is the lower-left corner of the operating envelope for the TPSTF, which is shown in figure 4-16. This condition gives a heating rate consistent with a radiation equilibrium temperature of 711 K (820°F) and a surface emissivity of 0.8, and results in an initial heating rate of 11 349 W/m^2 (1.0 Btu/sec ft^2). The three-step heat input variation assumed for the TPSTF test condition is shown in figure 4-21. The temperature response of the surface panel to the TPSTF heating was computed using the heating input and the same four-element thermal model employed previously. The results for the Haynes 188 panel are shown in figure 4-22.

4.3.10.5 Selection of Critical Co[illegible]tions

The next step in the analysis was to determine at which times during the trajectories the maximum thermal stresses occur. Only thermal stresses resulting from gradients within the surface panel were considered. The thermal stress analysis performed used simple bending theory and assumed that the panel was free to expand in the direction parallel to the corrugations. The panel was also free to bow up between end supports without incurring any significant bending moments at the end supports. Thermal stresses, therefore, are produced only when the temperature gradient through the depth of the panel cross section is nonlinear. The thermal stresses

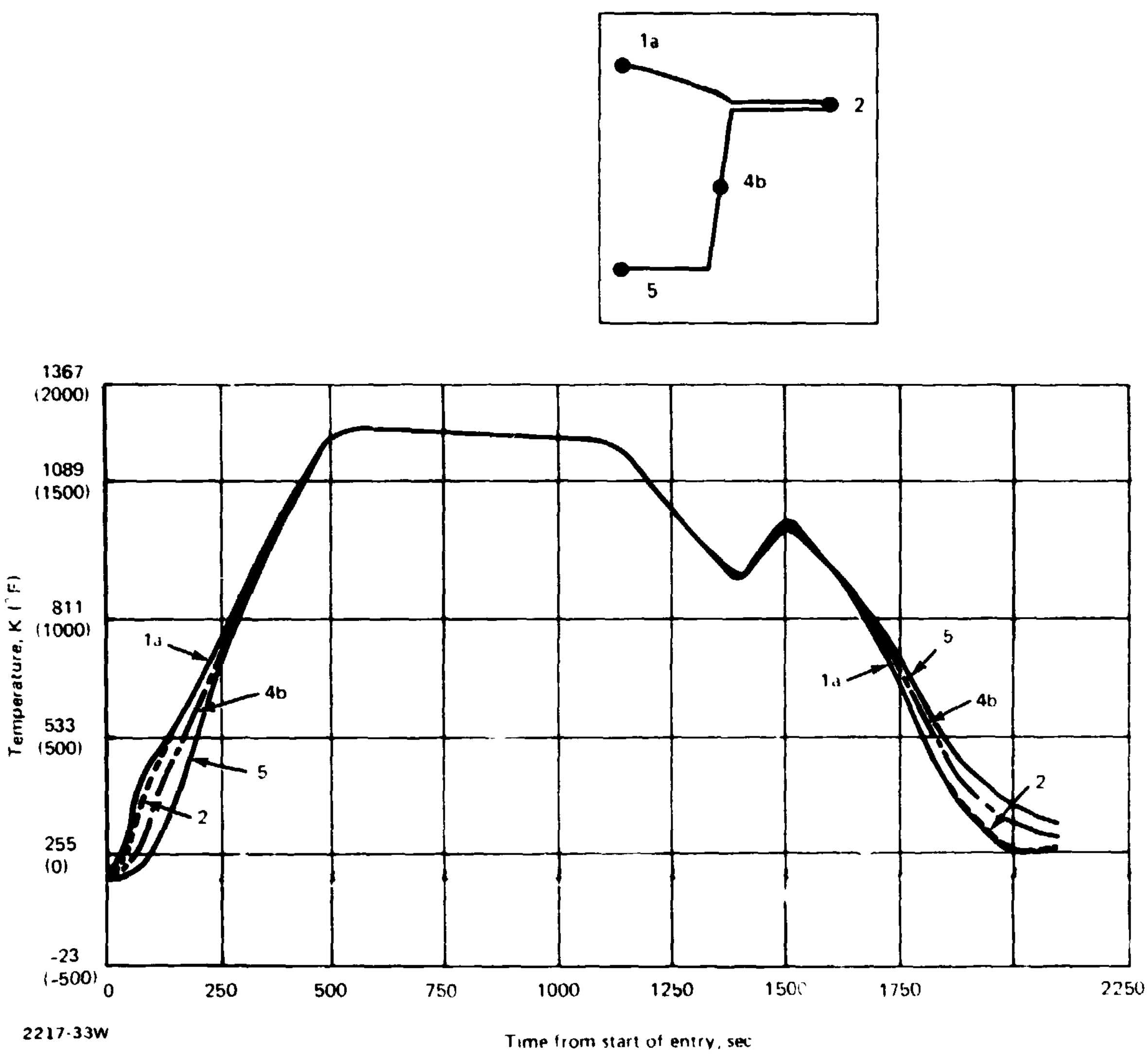

Figure 4-20. – Panel temperature response, entry heating, cold start.

produced will be in a direction parallel to the corrugations. Therefore, they are coincident with the bending stresses produced by surface pressure on the panel. It can be seen by examining figures 4-19 and 4-20 that significant gradients exist only during the following time intervals:

- Boost phase (condition A): 90 through 160 sec
- Entry phase (condition E): 60 through 170 sec
- Postentry phase (condition B): 1700 through 2100 sec

During the other times, the temperature gradients within the surface panel are considerably smaller and are, therefore, not of interest.

4.3.10.6 Determination of Element Stresses

The thermal-stress model consisted of a simple finite-element representation of the panel cross section, as shown in the insert in table 4-4. The appropriate coefficient of expansion, Young's modulus, areas, and temperatures were determined for each element, and were inputted to a transient-temperature structural analysis computer program which determined the stress level in each element. This analysis

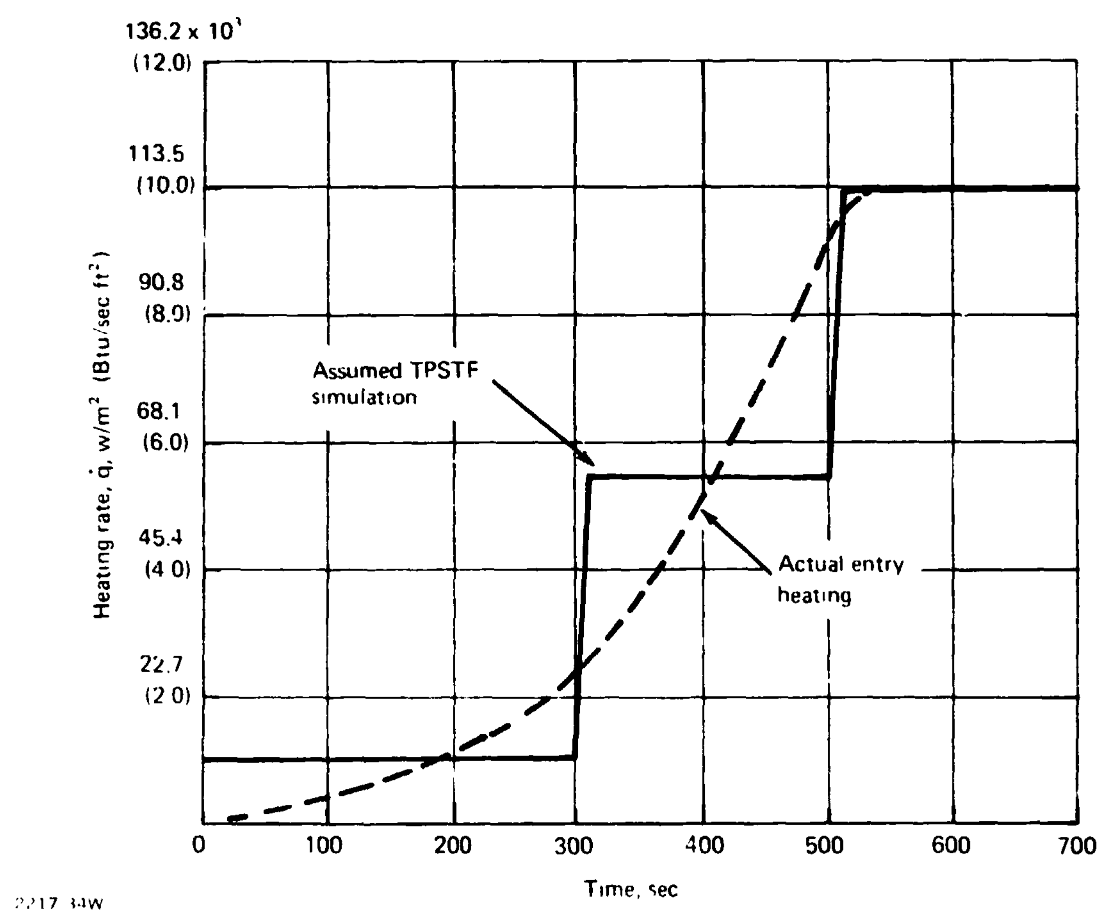

Figure 4-21. – TPSTF heatup simulation.

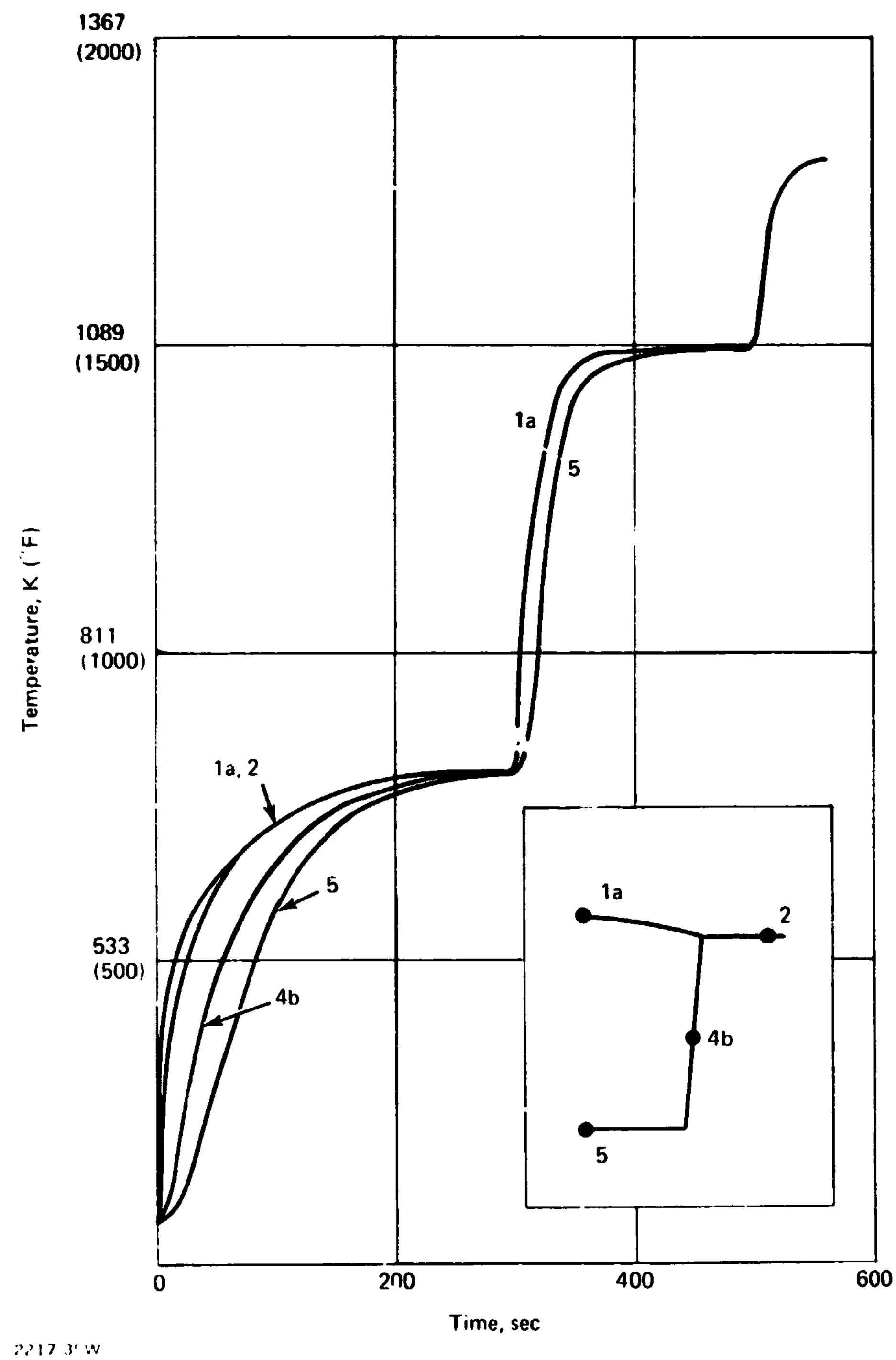

Figure 4-22. -- Panel temperature response, TPSTF heating.

REPRODUCIBILITY OF THE ORIGINAL PAGE IS POOR

Table 4-4. – Thermal stress summary, cold start on entry.

Cond	Description			Limit thermal stress											
				1a		1b		1c		2-3		4b		5	
				MPa, K	ksi, °F	MPa, K	ksi, °F	MPa, K	ksi, °F	MPa, K	ksi, pF	MPa, K	ksi, °F	MPa, K	ksi, °F
A	Boost	90 sec	Stress	-2 8	-.400	-8.96	-1.30	-20 0	-2 90	-20 7	-3.00	23.4	3.40	-17.9	-2.60
			Temp	361	190	361	190	361	190	342	155	303	35	297	75
		100 sec	Stress	-5 5	-.800	-19.3	-2 80	-39 3	-5 70	-39.3	-5.70	68.9	10.00	-33.7	-4.90
			Temp	436	325	436	325	436	325	400	260	322	120	297	75
		110 sec	Stress	-10 3	-1 50	-33 1	-4 80	-60 0	-8 70	-46.2	-6.70	89.6	13.00	-40.7	-5.90
			Temp	514	465	514	465	514	405	469	385	369	205	308	95
		120 sec	Stress	-16 5	-2 40	-44 1	-6 40	-73 8	-10 70	-1 4	-.200	64.1	9 30	-12.4	-1.80
			Temp	581	585	581	585	581	585	550	530	422	300	333	140
B	Post-entry	1850 sec	Stress	10.3	-1 50	4 8	.70	13 8	2 00	3 4	.500	-12 1	-1.75	-2.1	-.300
			Temp	422	300	422	300	422	300	422	300	483	410	533	500
		1900 sec	Stress	-12 4	-1 80	8 96	1 30	24 1	3 50	4 1	.600	-16 5	-2 40	2.1	.300
			Temp	345	161	345	161	345	161	356	180	417	291	461	369
		2000 sec	Stress	-13 1	-.90	2 1	.30	16 5	2 40	9 0	1.300	-15.2	-2.20	-2.8	-.400
			Temp	255	-1	255	-1	255	-1	261	9	324	123	371	207
C	Max temp max man.	550-1000	Stress	0	0	0	0	0	0	0	0	0	0	0	0
			Temp	1255	1800	1255	1800	1255	1800	1255	1800	1255	1800	1255	1800
D	Max temp equilib	550-1000	Stress	0	0	0	0	0	0	0	0	0	0	0	0
			Temp	1255	1200	1255	1800	1255	1800	1255	1800	1255	1800	1255	1800
E	Start entry	78 sec	Stress	-26 9	-3.90	-44 9	-6 51	-63 0	-9 13	35 1	5 10	45.5	6.61	-35.2	-5.10
			Temp	422	300	422	300	422	300	347	165	269	24	291	-63
TPSTF	Test	10 sec	Stress	-77 8	-11 28	-97.0	-14.07	-116 2	-16 86	68 7	9.97	93.8	13.61	78.0	11.31
			Temp	478	400	478	400	478	400	406	270	317	110	299	78

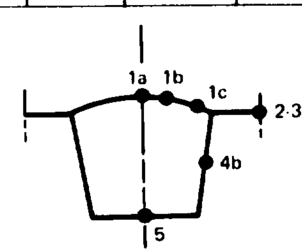

2217-36

was performed for the times during the boost and entry trajecto es that were previously identified as having significant temperature gradients. The results of this analysis are shown in figure 4-23 for 90 through 160 sec for boost, figure 4-24 for 60 through 170 sec for entry, and figure 4-25 for 1800 through 2100 sec for postentry. Figures 4-23, 4-24, and 4-25 show the stress in each element of the cross-section vs time.

Examination of these figure indicates a fluctuation of stress as the transient temperature gradients change wit me. From each figure, times which produced the largest thermal stress and which would combine with the stresses due to aero-

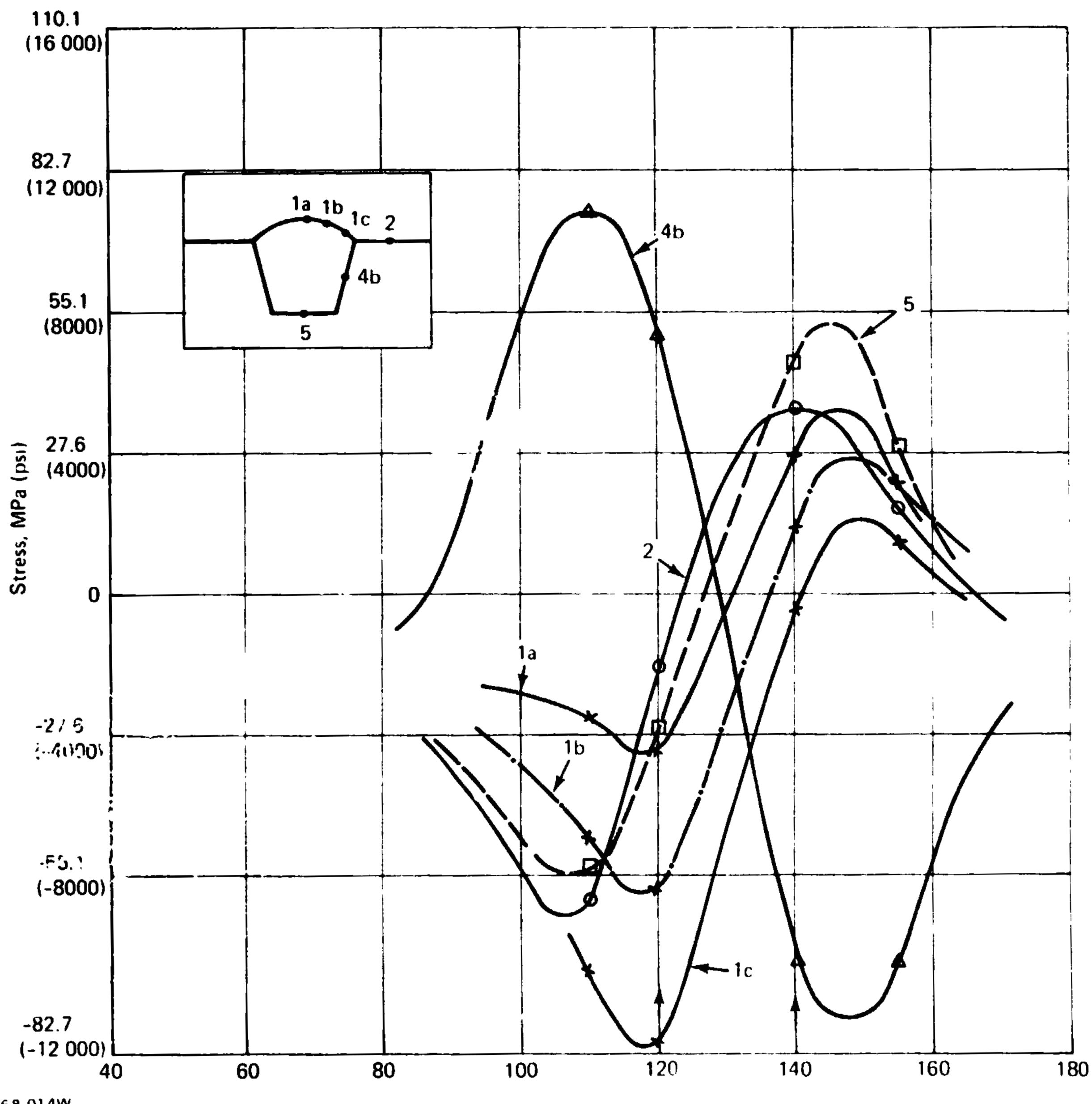

Figure 4-23. Boost, condition A.

dynamic pressure loadings (conditions A through E) were selected. These times are listed in table 4-4. As can be seen, conditions C and D do not have thermal stresses because they are maximum-temperature conditions. At maximum temperature, the thermal gradients in the panel are very small because almost constant heating conditions exist, and the strong radiant heat interchange between the panel elements reduces temperature differences to small values.

The maximum gradient during the TPSTF heating occurred at 10 sec after the start of heating. This condition produced the largest thermal stress in the panel for the test condition. The thermal stresses are shown in table 4-4.

4.3.10.7 Combination of Aero & Thermal Stresses

The stresses due to aerodynamic loadings were determined for the main bending elements of the surface panel, that is, the skin bead and the lower flange. Examination of table 4-4 shows that significant thermal stresses occurred only during conditions A, B, E, and TPSTF. Conditions C and D were not considered because the thermal stresses are essentially zero. The loads for condition A, B, E, and TPSTF are tabulated in table 4-5 for the time periods during which thermal stresses are significant.

4.3.10.8 Check of Skin Bead Stresses

The critical loading condition for the skin bead is compression. The method of analysis is shown in the following example for condition B. Only the Haynes 188 panel was checked. It was felt that checking the René 41 panel was not necessary since the René 41 panel section has lower b/t's, greater modulus, and greater creep allowables.

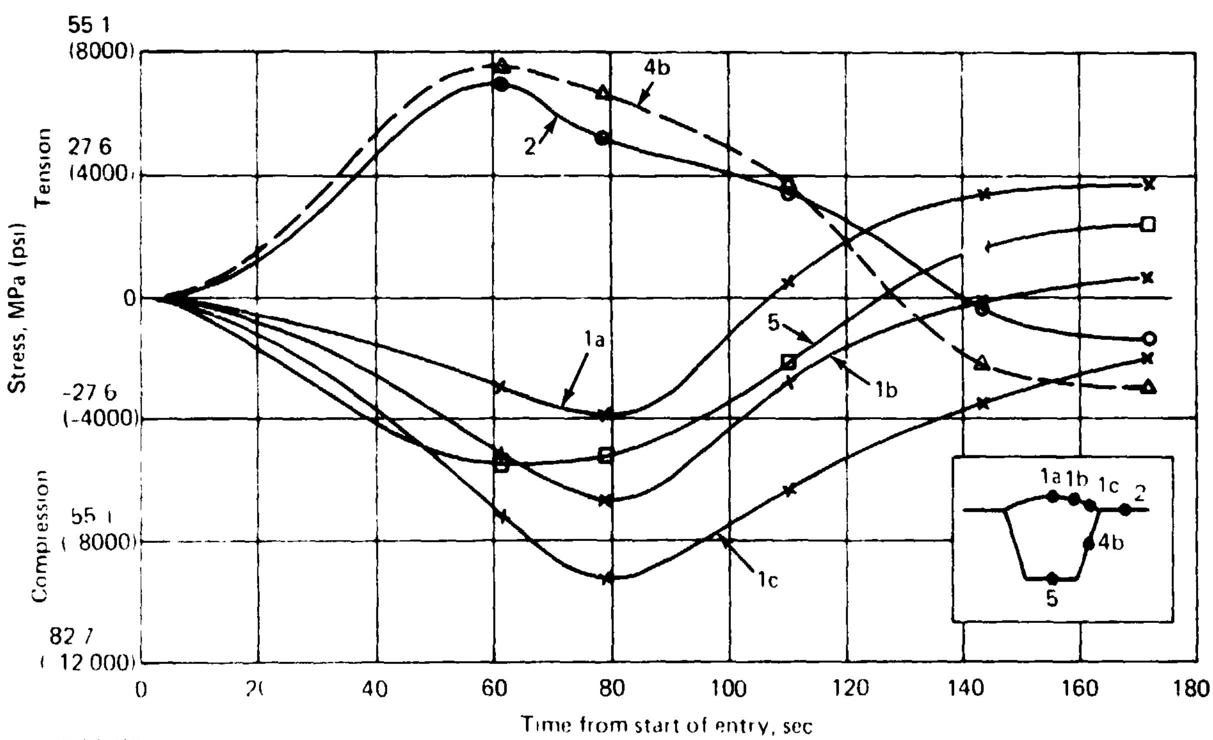

Figure 4-24 – Start of entry, condition E.

4.3.10.8.1 Check of Skin Bead, Condition B

$\bar{x}$ = .903 cm (.3556 in.)

I_{NA} = .100 cm^4 (.0024 $in.^4$)

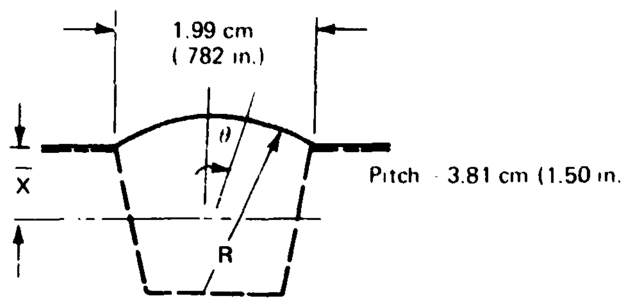

For P_R = 14.8 kPa (310 psf) at 1850 sec

= 16.2 kPa (338 psf) at 1900 sec

= 16.8 kPa (350 psf) at 2000 sec

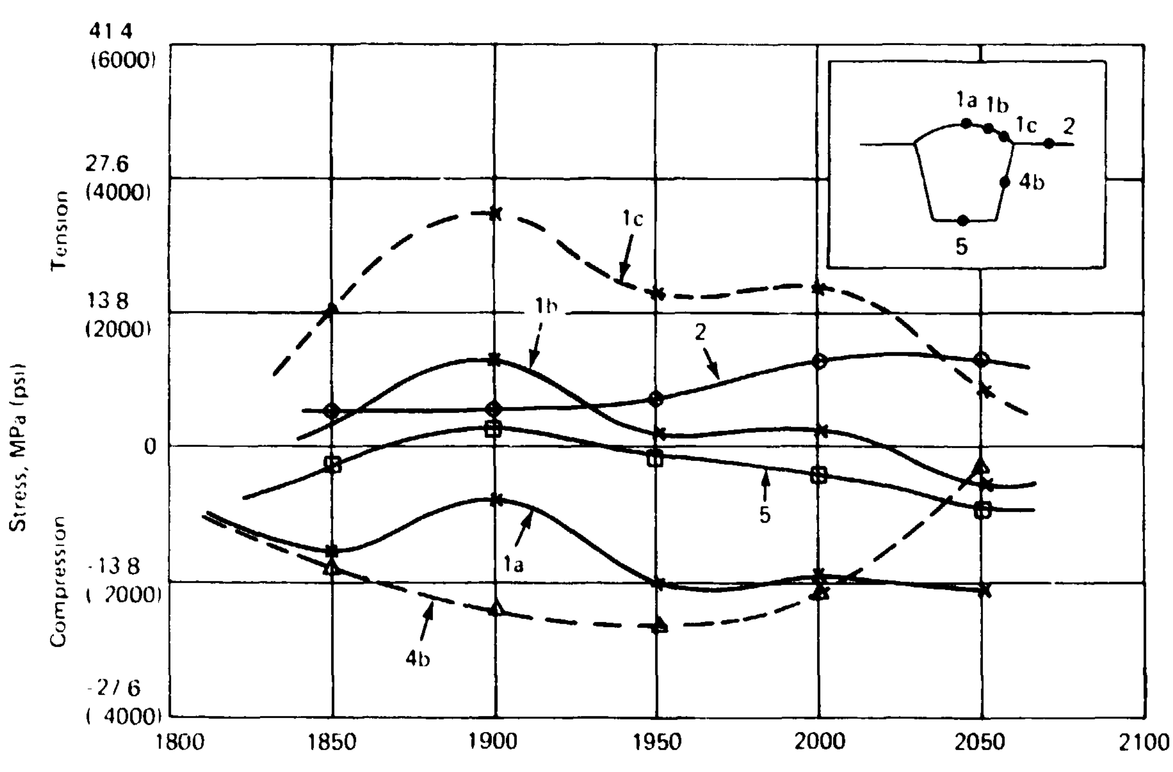

2217-90W

Figure 4-25. – Postentry, condition B.

The bending moment at midspan is:

$$M = 16.6\ \text{N·m}\ (147.3\ \text{in.-lb})\ \text{at 1850 sec}$$

$$= 18.1\ \text{N·m}\ (160.6\ \text{in.-lb})\ \text{at 1900 sec}$$

$$= 18.8\ \text{N·m}\ (166.3\ \text{in.-lb})\ \text{at 2000 sec}$$ (see Appendix A, page A-1)

and the bending stress is:

$$f_b = \frac{Mx}{I_{NA}} = 421\ \text{MPa}\ (61\ 120\ \text{psi})\ \text{at 1850 sec}$$

$$= 459\ \text{MPa}\ (66\ 620\ \text{psi})\ \text{at 1900 sec}$$

$$= 476\ \text{MPa}\ (68\ 990\ \text{psi})\ \text{at 2000 sec}$$

The stresses due to aerodynamic and thermal loads are each plotted in figure 4-26(b) for 1850, 1900, and 2000 sec. The total of these stresses are also plotted. Using 2-1/2-deg increments for θ (except the last increment, which is 2.6 deg), the average total stress at 2000 sec for the skin is:

$$\bar{f} = \left\{ 2.5\left[\frac{26.5 + 26.0}{2} + \frac{26. + 25.4}{2} + \frac{25.4 + 24.4}{2} + \frac{24.4 + 23.2}{2} + \frac{23.2 + 21.9}{2} + \frac{21.9 + 20.5}{2} + \frac{20.5 + 18.9}{2} + \frac{18.9 + 17.3}{2} \right] + 2.6\left[\frac{17.3 + 15.6}{2}\right] \right\} \frac{1}{22.6}$$

$$\bar{f}\ \text{at 2000 sec} = 152.3\ \text{MPa}\ (22\ 100\ \text{psi})$$

Similarly,

$$\bar{f}\ \text{at 1900 sec} = 137.2\ \text{MPa}\ (19\ 900\ \text{psi})$$

$$\bar{f}\ \text{at 1850 sec} = 133\ \text{MPa}\ (19\ 300\ \text{psi})$$

4.3.10.8.2 Check of Buckling, Condition B

$$F_{crel} = .22E \left[\frac{t}{1.3\ (b - z)}\right]$$ (Appendix A, page A-1)

$$F_{allow.} = \frac{F_{crel}}{1.4}$$

where

$t = .013$ cm (.0051 in)

$b = 1.98$ cm (.782 in.)

$z = .152$ cm (.06 in.)

$$E = 1.05 \quad 235.8\ \text{GPa} \quad \text{at 2000 sec,} \quad T \cong 255\ \text{K}\ (0^{\circ}\text{F})$$

$$= .96 \quad 235.8\ \text{GPa} \quad \text{at 1900 sec,} \quad T \cong 333\ \text{K}\ (140^{\circ}\text{F})$$

$$= .88 \quad 235.8\ \text{GPa} \quad \text{at 1850 sec,} \quad T \cong 422\ \text{K}\ (300^{\circ}\text{F})$$

Therefore,

$$\text{at 2000 sec,} \quad F_{allow.} = 181.2\ \text{MPa,} \quad MS = \frac{181.2}{152.3} - 1 = .18$$

$$\text{at 1900 sec,} \quad F_{allow.} = 165.7\ \text{MPa,} \quad MS = \frac{165.7}{137.2} - 1 = .20$$

$$\text{at 1850 sec,} \quad F_{allow.} = 151.9\ \text{MPa,} \quad MS = \frac{151.9}{133.0} - 1 = .14$$

4.3.10.8.3 Check of Skin Bead, Condition A - Figure 4-26(a) shows similar results for the loadings of condition A, obtained by the same method of analysis used for condition B. Combined stresses are examined between 90 and 120 sec for this case, since it can be seen by examining figures 2-4, 4-19, and 4-23 that prior to 90 sec the thermal stresses in the skin bead are small, and that after 120 sec (when the maximum compressive thermal stress exists in the skin bead), the thermal stresses, aerodynamic pressures, and temperatures are decreasing. The average total stresses, allowables, and margins for condition A are given in table 4-6.

Table 4-5. – Aerodynamic pressures at appropriate times compared with design values.

Cond	Time, sec	Design pressure for condition		Pressure at time[a]	
		kPa	psf	kPa	psf
A	90 100 110 120	13 9	290	260, 90 190, 40 140, 25 110, 20	12 5, 4 3 9 1, 1 9 6 7, 1 2 5 3, 96
B	1850 1900 2000	16 8	350	310, 60 338, 95 350, 260	14 8, 2 9 16 2, 4 5 16.8, 12 4
C D	Thermal stresses are negligible				
E	78	4.79	100	0	0
TPSTF	10	2.53[b]	52 9[b]	8	6 5[c]

[a] Figure 2 4 and 2 1
[b] 025 atm (fig. 4 16)
[c] 0078 atm (fig. 4 16)

1 368 015W

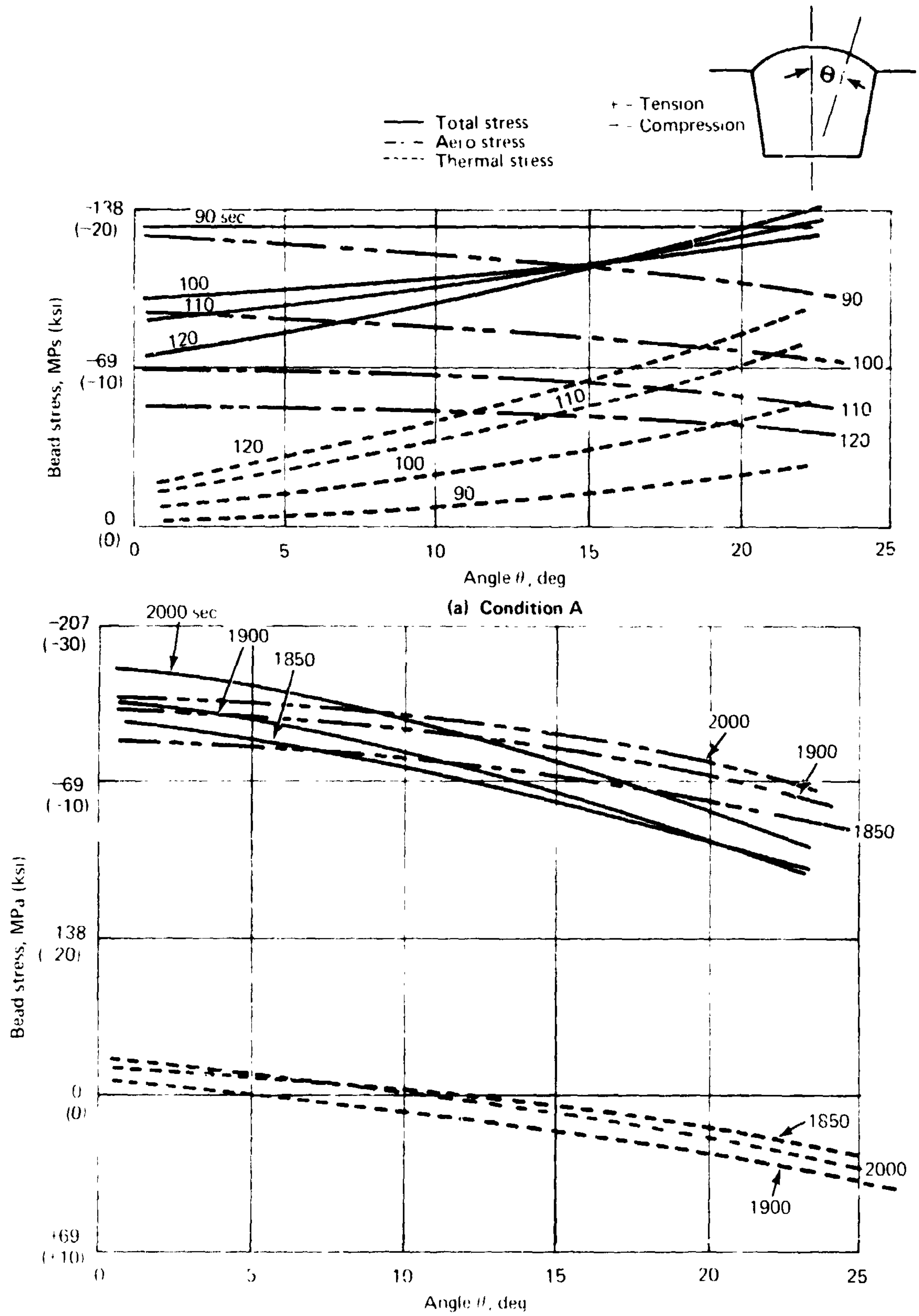

Figure 4-26. – Bead aerodynamic and thermal stresses.

1.3.10.8.4 Check of TPSTF Condition

P_R = 790 Pa (16.5 psf)

p = 0.0381 m (1.50 in.)

M = .885 N·m (7.8 in.-lb) (See Appendix A, page A-1)

$$f_{bmax} = \frac{M\bar{x}}{I} = \frac{.885\,(.903)}{.100} = 8.0 \text{ MPa } (1160 \text{ psi})$$

Combining with the maximum thermal stress of -11.6 MPa (-16 860 psi):

f_{total} = 124 MPa (18,020 psi)

at 477 K (400°F), E = .83 (235.8 GPa) = 196 GPa (28.4 x 10^6 psi)

$$F_{allow.} = .22\ \frac{(196{,}000 \text{ MPa})}{1.4} \left[\frac{.013}{1.3\,(1.98 - .152)}\right] = 144 \text{ MPa } (20\,7[illegible]0 \text{ psi})$$

$$MS = \frac{144}{124} - 1 = .16 \text{ (ample)}$$

1.3.10.9 Check of Lower Flange Stresses

The lower flange is also critical in compression, when combined thermal and aerodynamic loadings are considered. Compressive stresses in the lower flange occur when reversed (negative) aerodynamic pressures are applied, which can only occur during conditions A and B. Condition B has negligible thermal compressive stresses in the lower flange; therefore, only condition A was examined for combined loadings.

1.3.10.9.1 Check of Stresses, Condition A

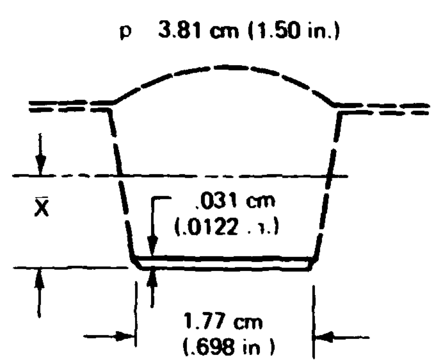

at 100 sec, P_R = -1.92 kPa (-40 psf)

at 110 sec, P_R = -1.20 kPa (-25 psf)

Table 4-6. – Total stresses, allowables, and margins for condition A.

Time, sec	Temperature		Avg stress in bead		Allowable stress		MS
	K	°F	MPa	psi	MPa	psi	
90	361	190	−131	−19 000	162	−23 540	.24
100	436	325	−114	−16 500	−149	−21 660	.31
110	514	465	−113	−16 400	−136	−19 780	.21
120	581	585	−105	−15 250	−124	−18 028	.18

2217-39W

$M = -2.15$ N·m (−19 in.-lb) at 100 sec (see Appendix A, page A-1)

$M = -1.34$ N·m (−11.9 in.-lb) at 110 sec

$$f_b = \frac{M\bar{x}}{I_{NA}} = \frac{-2.15\ (9.03)}{.100} = -19.41 \text{ MPa (2815 psi) at 100 sec}$$

$$= -12.10 \text{ MPa (1755 psi) at 110 sec}$$

Adding maximum thermal compressive stresses:

at 100 sec = −33.78 MPa at 297 K (−4900 psi at 75°F) (table 4-4)

at 110 sec = −40.67 MPa at 308 K (−5900 psi at 95°F)

$$f_{total} = 33.78 + 19.41 = 53.19 \text{ MPa (7715 psi) at 100 sec}$$

$$= 40.67 + 12.10 = 52.77 \text{ MPa (7655 psi) at 110 sec}$$

$$F_{allow.} = \frac{3.62E\left(\frac{t}{d}\right)^2}{1.4} \quad \text{(appendix A, page A-2, element 5)}$$

$$F_{allow.} = \frac{3.62}{1.4}\left[(.99)\ (235.8\ \text{GPa})\right]\left[\frac{.031}{1.77}\right]^2 \quad E = 99\% \text{ at 380 K } (95^\circ F)$$

$$F_{allow.} = .185 \text{ GPa (26 835 psi)}$$

$$MS = \frac{185 \text{ MPa}}{53.19 \text{ MPa}} - 1 = \text{ample}$$

4.3.10.9.2 Check of Stresses – Condition E - For condition E, the maximum compressive thermal stress in the lower flange was 35.1 MPa (5100 psi) at near-room temperature with no aerodynamic load, which gave an ample margin. Temperatures which would have reduced the allowable stress significantly in the lower flange were not reached until after 150 sec in condition E. By this time, the thermal stress in the lower flange had become tension.

4.3.10.9.3 Check of Stresses, TPSTF Condition - No reverse pressure condition was specified for the TPSTF. The thermal stress in the lower flange is well within the allowable since the temperature was low at the time of maximum stress, which occurred at 10 sec.

4.4 EXPANSION JOINT/SPLICE JOINT DESIGNS

4.4.1 Panel Expansion Joint

Because the surface panel expands during heating, an expansion joint is required at the panel edge to permit relative motion of adjacent panels without allowing leakage of boundary layer air. Leakage of high-enthalpy air is undesirable for two reasons: it reduces the effectiveness of the insulation system in protecting the primary structure, and it can cause severe local overheating where the leakage occurs. Each 50.8-cm (20.0-in.) section of the Haynes 188 panel expands about .84 cm (.33 in.) at 1255 K (1800°F). The René panel expands about .71 cm (.28 in.) at 1144 K 1600°F). This amount of motion must be accommodated in the presence of some amount of overall panel bowing due to temperature gradients during heating transients.

After reviewing various concepts (subsection 4.2) the overlapping-shingle concept was selected for the expansion joint, using a 1.60-cm (.63-in.) overlap. Because adjacent skins are mounted at the same height, a one-skin-thickness interference was developed at the faying surface to minimize leakage. Additional thermal protection was provided by packing the expansion cavity with microquartz insulation. (The expansion joint is shown in appendix E, drawing AD1001-100.) The design offers: maximum simplicity (few parts), unrestrained panel edges, and no forward-facing steps. Finally, each panel is individually removable.

4.4.2 Panel Center Joint

Both 51-cm (20-in.) panels meet at the center support rib. A simple lap joint was used because no expansion occurs at this point. The forward panel overlaps the aft panel by .65 cm (.25 in.), producing an aft-facing step. Attachment rivets clamp each panel firmly down, providing a simple and effective seal.

4.4.3 Panel Edge Splice Joint

Since all lateral expansion is absorbed by the skin beads and corrugation, panel width is limited only by fabrication and assembly considerations. The splice joint consists of a simple lap of adjacent panels at the flat between beads. A longitudinal row of rivets is employed to connect adjacent panels.

4.5 SUPPORT RIB DESIGN

The support rib must transfer aerodynamic pressure and panel inertial loads to the vehicle primary structure, while causing a minimum heat short. Two types of supports are used: a flexible one at the expansion joint, and a fixed type where two adjacent panels butt, which is called a center support rib. (See figure 4-1).

Several of the support rib concepts shown in figures 4-27 through 4-31 were considered. To simply mass comparisons between these designs, the following parameters were fixed: standoff height, 9.22 cm (3.63 in.); web thickness, 0.25 cm (.010 in.); and upper and lower clip thickness, .111 cm (.044 in.).

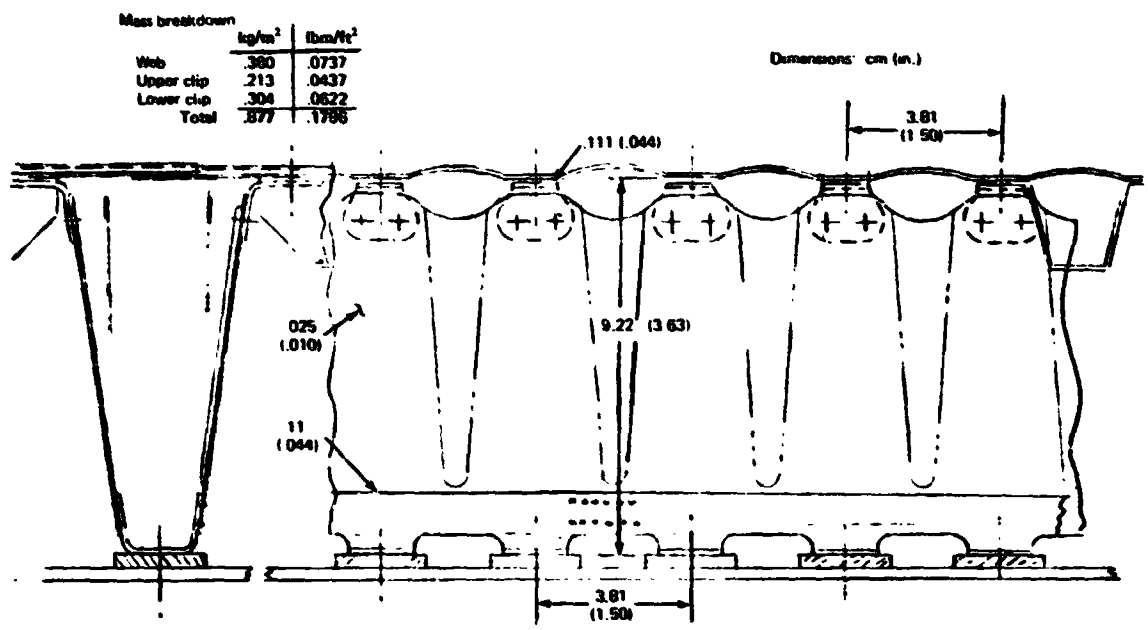

2217-40W

Figure 4-27. – Baseline rib concept.

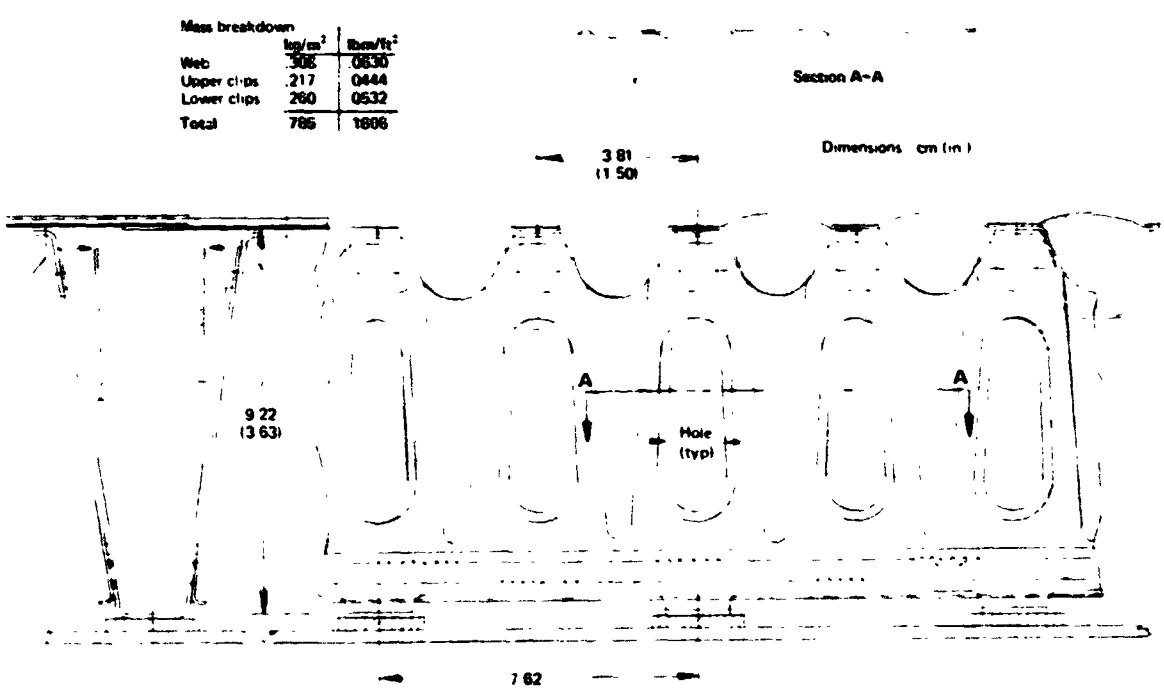

2217-41W

Figure 4-28. – Modified baseline rib concept.

REPRODUCIBILITY OF THE ORIGINAL PAGE IS POOR

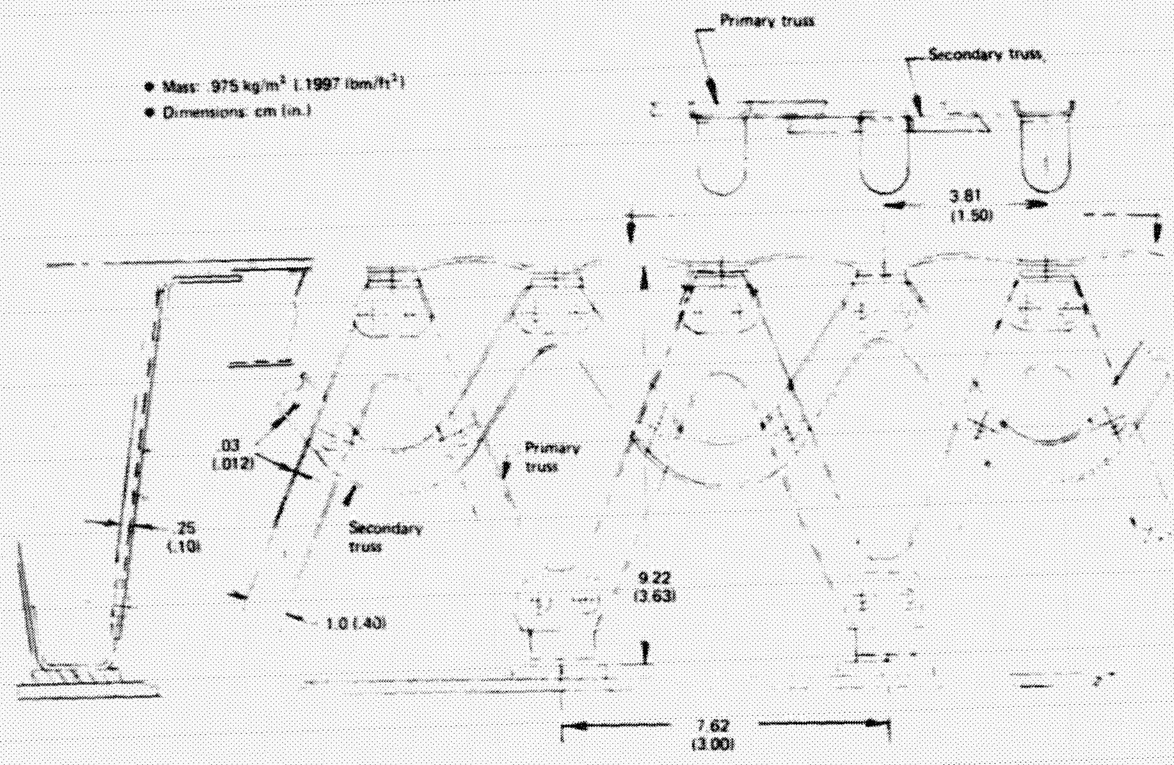

1368-027W

Figure 4-29. – Truss concept.

Mass breakdown:

	kg/m²	lbm/ft²
Web	.228	.0466
Upper clips	.217	.0444
Lower clips	.163	.0334
Total	**.608**	**.1244**

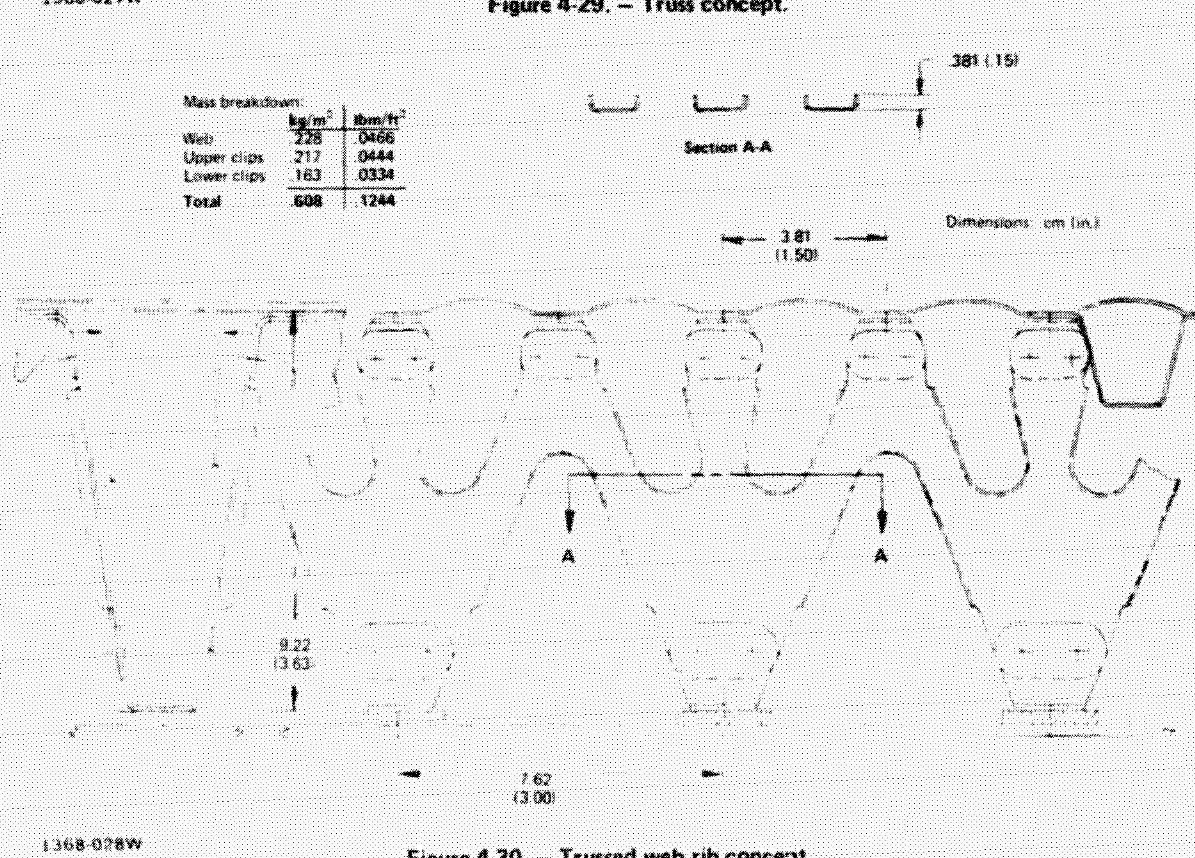

1368-028W

Figure 4-30. – Trussed web rib concept.

The baseline support rib design is shown in figure 4-27. The design is heavy with a mass of .877 kg/m^2 (.1796 lbm/ft^2). Additionally, undesirable heat shorts to the primary structure result from the large number of fasteners required. A modified concept, with half the number of fasteners to the primary structure, is shown in figure 4-28. The design employs lightening holes, and shows a mass reduction of .093 kg/m^2 (.019 lbm/ft^2). Figure 4-29 illustrates a truss concept, which was not pursued because the mass was not promising. Figure 4-30 illustrates a trussed-rib concept with a relatively low mass. Forming of the tight radii, however, would be difficult without cracking the flanges. Additionally, the thin sections are prone to buckle during flexing.

These potential difficulties led to the selection of the concept shown in figure 4-31. The configuration is something between a full web and a truss. The lower arches have adequate radii so that flange cracking is eliminated. The beads serve to eliminate thermal stresses and provide vertical stiffness. Heat shorting is reduced from that of the baseline desing since lower attachments occur at a 7.62-cm (3.0-in.) pitch instead of 3.81 cm (1.50 in.). To further minimize heat shorting, .32-cm (.125-in.) thick insulating washers, fabricated from a glass-reinforced silicone laminate, insulate the lower clip from the aluminum primary structure.

With a mass of .657 kg/m^2 (.135 lbm/ft^2(, this design provides a 25% weight reduction from the baseline design. Detail analyses of the Haynes 188 and René 41 support ribs are given in appendices C and D, respectively. Production drawings are given in appendices E and F.

Mass breakdown:

	kg/m^2	lbm/ft^2
Web	.278	.0569
Upper clip	.217	.0444
Lower clip	.163	.0334
Total	.658	.1347

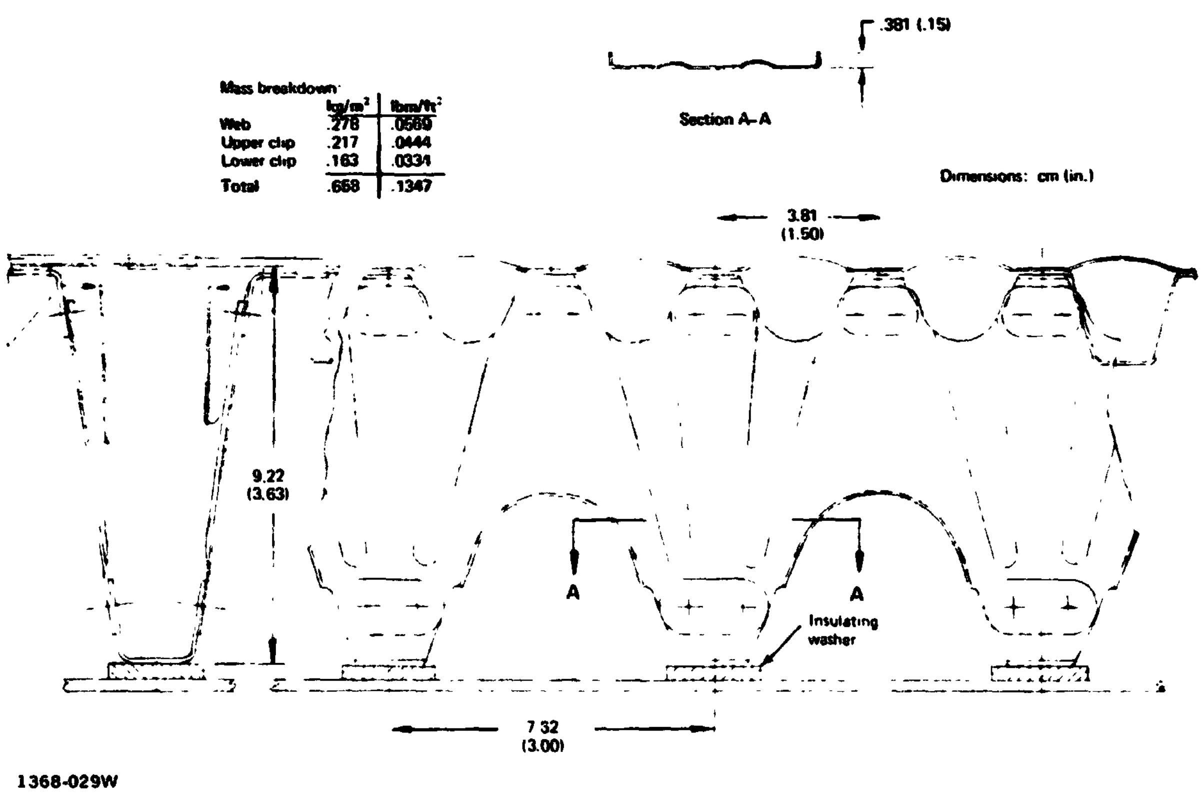

1368-029W

Figure 4-31. – Modified web concept.

4.6 DRAG SUPPORT DESIGN

Because the support-rib standoffs cannot react loads parallel to the skin corrugations (in the longitudinal or drag direction), a drag support is employed at 30.48-cm (12-in.) intervals along the center support to react these loads. The drag support consists of two bent-up channels riveted to each side of the center support rib which stabilizes the channels. The channels pick up the surface-panel screws in their normal location. The drag load is transferred to the primary structure by four screws at the bottom of the channels. Insulating washers are used under the lower clip to minimize heat shorting. (The detail analyses of the supports is given in appendices C and D. Detail dimensions are given in appendices E and F.)

4.7 THERMAL INSULATION SYSTEM DESIGN & ANALYSIS

The insulation system provides the main barrier to radiative heat transfer from the hot surface panel to the vehicle primary structure. The primary objective of the insulation design program was to develop the lowest-mass system which would withstand the thermal, cold-soak, and vibration environments associated with the design entry trajectory.

Only commercially available nonexotic materials were considered. The insulation for the baseline system used for comparison in this study is a homogeneous blanket of 56-kg/m^3 (3.5-lbm/ft^3) Microquartz enclosed in a bag of resistance-welded Inconel foil. The purpose of the bag was to protect the blanket from excessive moisture absorption and damage during handling. However, since the foil bags must be vented, their use seems questionable. The bags are costly to fabricate and add 1.56 kg/m^3 (0.32 lbm/ft^3) to the total TPS mass. For these reasons, and those outlined in subsection 2.5, protective foil bags were not included in the insulation system design. Further modifications to the baseline system which were considered are:

- The use of lower-density high-temperature insulation: 17.6-kg/m^3 (1.1-lbm/ft^3)
- A composite of low-density insulation (TG 15000) and Microquartz
- The use of metal foil radiation barriers in fibrous insulation

4.7.1 Insulation System Comparisons

The initial comparison of the efficiencies of the insulation candidates was made by comparing the density-condutivity (ρ k) product. For the transient heating of an insulated structure, it can be shown that the insulation weight required for a given heat input is proportional to the square root of the product of ρ k for the insulation.

The materials chosen as candidates for comparison with 56-kg/m^3 (3.51 bm/ft^3) Microquartz, manufactured by the Johns Manville Corp., are:

- Astroquartz - 17.6 kg/m^3 (1.1 lbm/ft^3) density, a high-purity silica fibrous felt, fiber diameter = 7 microns, maximum temperature of 1644 k (2500°F), manufactured by J. P. Stevens and Co., New York, N.Y., thermal properties obtained from reference 4-7

- TG 15000 16 kg/m^3 (1.0 lbm/ft^3) density, a silicone-resin-bonded fibrous felt, fiber diameter = 1.0 micron, maximum temperature of 644 K (700°F), manufactured by HITCO-Defense Products Division, Gardena, Cal., thermal properties obtained from reference 4-8. This material was chosen to be used in conjunction with a high-temperature insulation in a composite

- Radiation barriers - The use of thin metal foils inserted in 56-kg/m^3 (3.5-lbm/ft^3) Microquartz and 17.6-kg/m^3 (1.1-lbm/ft^3) Astroquartz was investigated. Aluminum, nickel, and platinum foils .0006 cm (.00025 in.) thick were considered. This gage was the thinnest commercially available and could be readily handled. The foil density was two foils per cm (five per inch), and the emissivity of the foils varied from .05 to .80. The methods used to analyze the performance of the foils are presented in appendix G

Figure 4-32 shows the ρk product of the candidate insulations without radiation foils at 1.0 atmosphere. From this comparison it can be seen that Microquartz is the most efficient at temperatures above 644 k (700°F). At temperatures below 644 K (700°F) TG 15000 is most efficient. This suggests that a composite composed of TG 15000 on the cool side and Microquartz on the hot side would result in a weight reduction when compared to a homogenous Microquartz or Astroquartz package.

Figure 4-33 shows the ρk product for Microquartz and Astroquartz with metal foils inserted as radiation barriers. The results reveal two significant facts: the emissivity of the foils must be kept low ($\approx$ .05) to effect a significant reduction in ρk, and the foils are advantageous, in insulations of this density, only above 644 k (700°F).

The oxidizing environment to which the TPS insulation would be exposed results in the nickel foils having an emissivity of 0.5 or higher (ref 4-9). Examination of figures 4-32 and 4-33 indicates that emissivities of 0.5 or higher result in no reduction in ρk; therefore, the use of nickel foils is not advantageous. Aluminum foil can be eliminated since it has a maximum temperature capability of only 700 K (768°F). Platinum foils appear effective; however this material is considered too exotic and expensive. The conclusion drawn from this investigation is that for the applications considered herein, the use of metal-foil radiation barriers is not a cost-effective way to improve insulation performance.

Design heating trajectory 14040 (subsection 2.2) was used to estimate the amount of insulation required for the Haynes 188 panel with an equilibrium temperature of 1255 K (1800°F). The heat input and pressure vs time for this trajectory are presented in table 4-7. The thermal criteria requirements specified a 322 K (120°F) initial temperature at the start of entry and a 450 K (350°F) maximum temperature on a structural mass equivalent to a 0.5-cm (0.2-in.) thick aluminum plate with an adiabatic backface. The heating rates shown in table 4-7 were used as the boundary conditions of a thermal model which included the metallic surface panel, the insulation layer, and the structural heat-sink mass. These heating rates produce a maximum surface temperature of 1255 K (1800°F) for the Haynes 188 panel.

The properties of the insulation materials used are shown in figures 4-34, 4-35, and 4-36 for Microquartz, Astroquartz, and TG 15000, respectively. The data were obtained from references 4-7, 4-8, and 4-10.

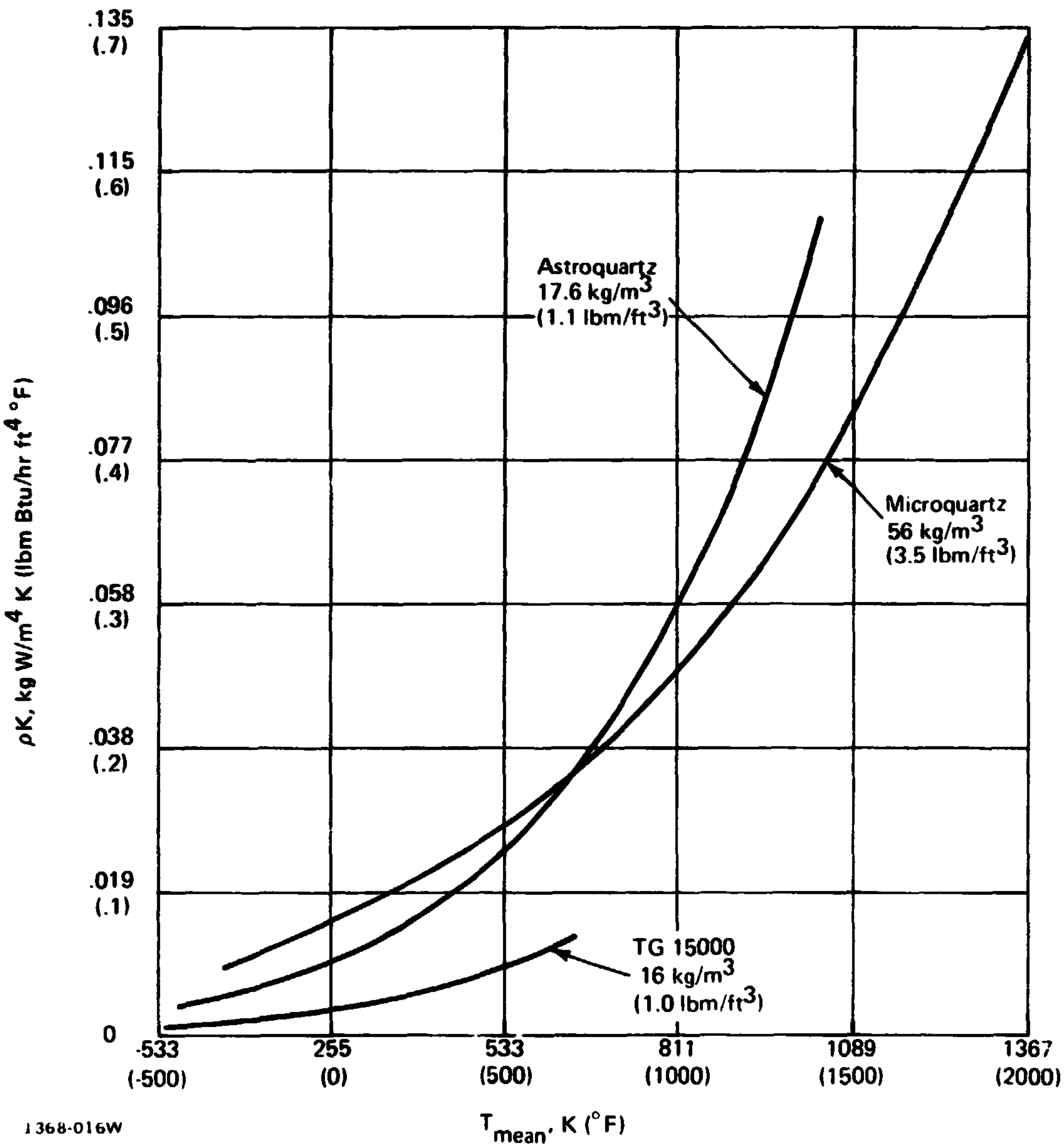

Figı re 4-32.—Density-conductivity product vs temperature at 1.0 atm.

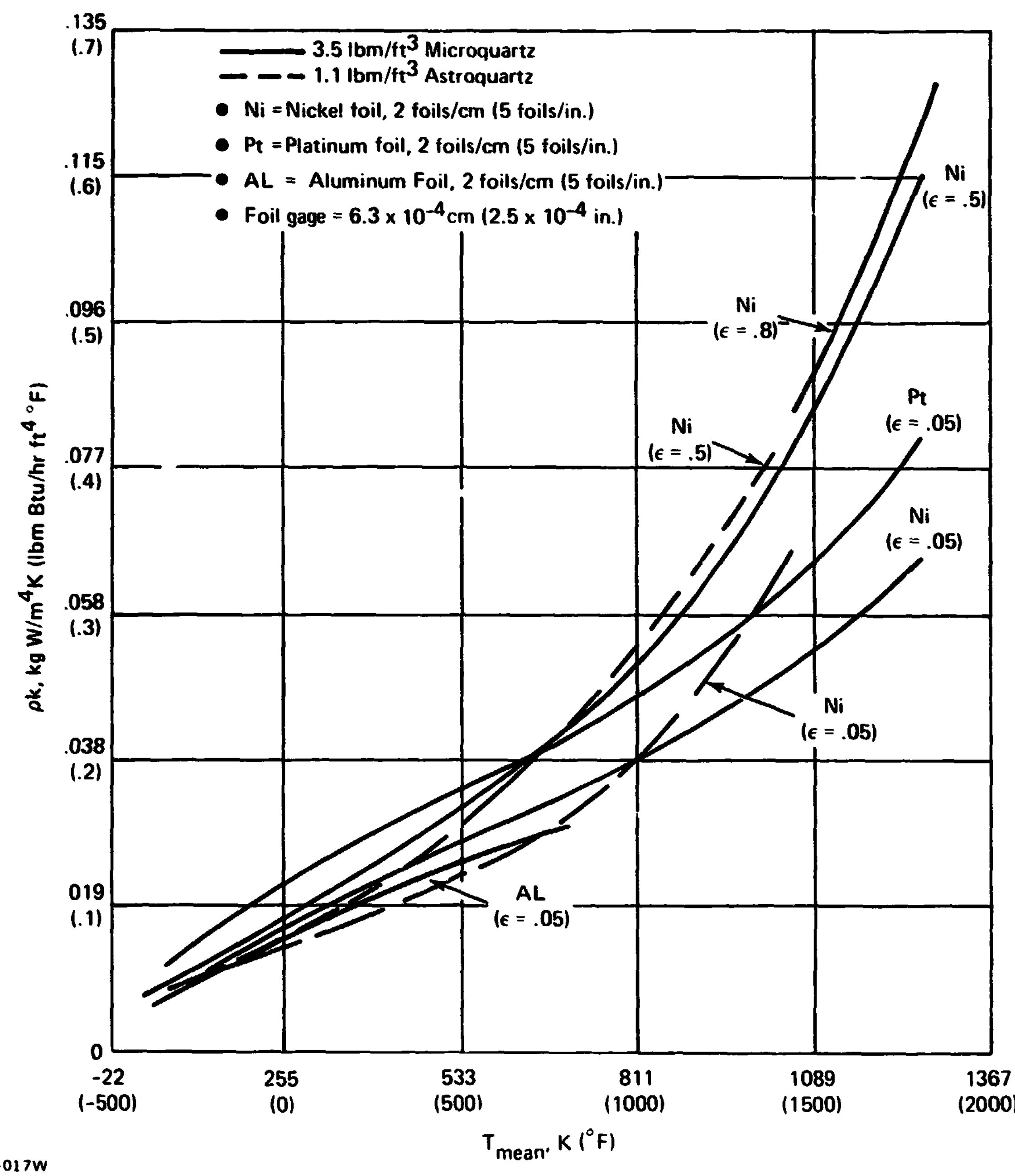

1368-017W

Figure 4-33. – Effect of radiation foils on density conductivity product vs temperature at 1.0 atmosphere.

Table 4-7. – Haynes 188 and René 41 TPS design trajectory heating and pressure history.

Time, sec	Pressure		Haynes heating rate		René heating rate	
	Pa	Torr	W/m^2	$Btu/sec\ ft^2$	W/m^2	$Btu/sec\ ft^2$
0	0.002	1.5×10^{-5}	0	0	0	0
200	.024	1.8×10^{-4}	11 349	1.0	7944	.7
400	667	5	62 419	5.5	45 396	4.0
600	933	7	113 489	10.0	78 308	6.9
800	1466	11	111 219	9.8	76 038	6.7
1000	2533	19	106 679	9.4	73 698	6.5
1200	3333	25	74 902	6.6	52 205	4.6
1400	3466	26	29 507	2.6	20 428	1.8
1500	3600	27	57 879	5.1	40 856	3.6
1600	3866	29	27 237	2.4	21 563	1.9
1800	4266	32	3404	.3	2269	.2
2000	8666	65	0	0	0	0
2200	101 324	760	0	0	0	0

2217-46W

To simplify comparison, the amount of insulation required for the candidate insulation systems was initially determined without including the effect of the heat leak through the panel support attachments. The results for the baseline Microquartz system and three other candidate insulation systems are shown in table 4-8, items 1 through 4.

4.7.2 Insulation System Selection

Comparison of items 1 through 4 in table 4-8 shows that the composite system of Microquartz and TG 15000 (item 4) is the lightest. The mass of the system is .29 kg/m^2 (.06 lbm/ft^2) less than the baseline system (item 1), and represents a 10% mass reduction. This system, therefore, was selected for use on the test specimens. This system and the baseline system were reanalyzed to correct for the heat-shorting effects resulting from the metal supports. These data are shown as items 5 and 6, table 4-8. The difference in mass remained .29 kg/m^2 (.06 lbm/ft^2). The effects of local hot spots at the panel support attachments and lateral conduction effects in the primary structure were not included in the analysis.

The insulation and support rib dimensions corresponding to item 6 are shown in figure 4-37 for the Haynes 188 panel. Note that the distance between the primary structure and the corrugation bottom is 5.7 cm (2.25 in.), which is .63 cm (.25 in.) or 10% less than the required 6.4 cm (2.5 in.). The 10% compression of the insulation has an insignificant effect on the thermal properties and provides better retention of the insulation blanket. The compression also compensates for the slight shrinkage which occurs after repeated high-temperature exposure.

The heat input and pressure time for the design of the René 41 insulation system is given in table 4-7. The heating rate produces a maximum surface temperature of 1144 K (1600°F). The same insulation concept used on the Haynes 188 panel was used on the René 41 panel, resized to the lower surface temperature/heat load requirements. The dimensions of the René 41 system are shown in figure 4-38.

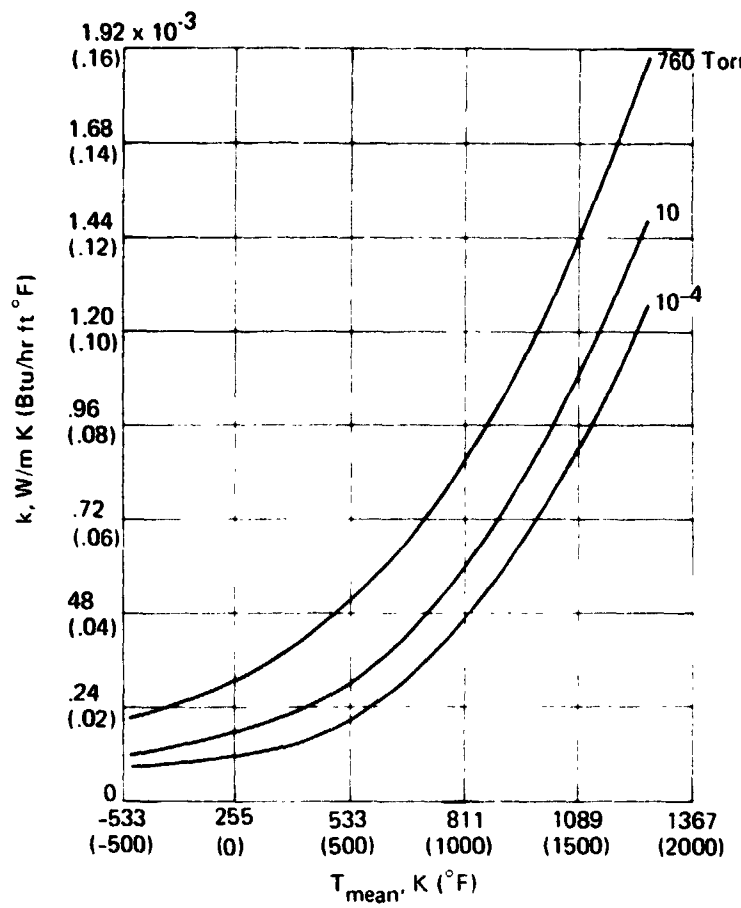

2217-47W

Figure 4-34. – Thermal conductivity vs temperature and pressure of 56-kg/m^3 (3.5-lbm/ft^3) Microquartz.

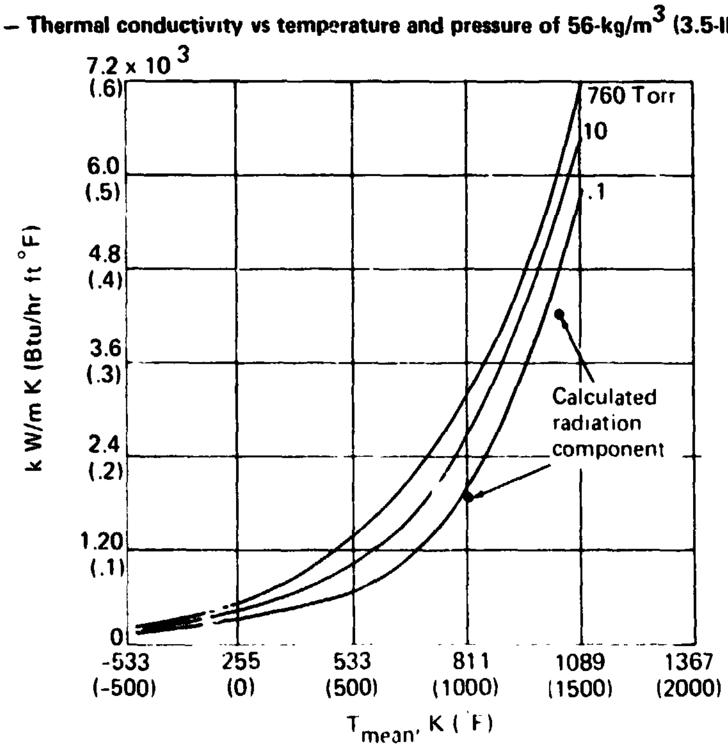

2217-48W

Figure 4-35. – Thermal conductivity vs temperature and pressure of 17.6-kg/m^3 (1.1-lbm/ft^3) Astroquartz (ref. 4-7).

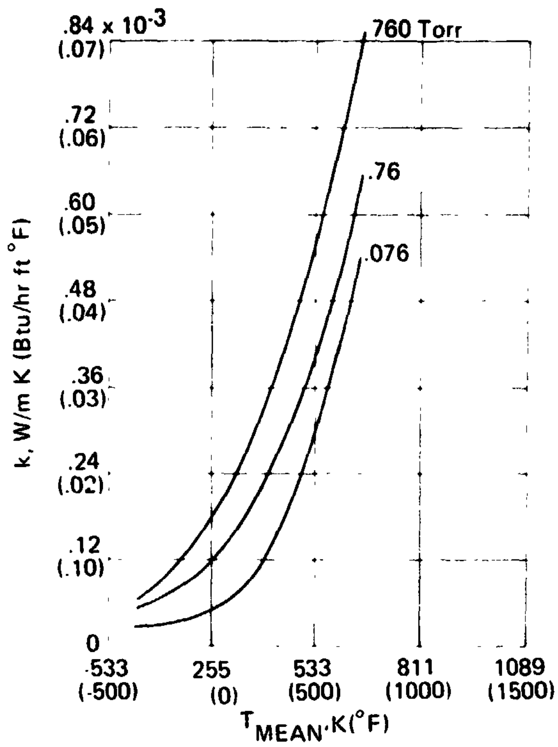

Figure 4-36. – Thermal conductivity vs temperature and pressure of 16-kg/m³ (1.0-lbm/ft³) TG 15000 (ref. 4-8)

4.7.3 Effects of Pressure Environment on Insulation Performance

Since insulation performance is a function of pressure, the effects of operating an all-Microquartz system (item 5, table 4-8) at a pressure of one atmosphere was computed. Item 7 of table 4-4 shows that 7.4 cm (2.92 in.), a 28.6% increase in insulation, is required to maintain a 450 K (350°F) primary structure temperature. Alternately, item 8 shows that if the 5.77-cm (2.27-in.) thickness is maintained, the primary structure would reach 486 K (415°F) at the increased pressure. Thus, the pressure for which an insulation system is designed and the pressure at which the system is tested can have a significant effect on the performance of the system.

Both test specimens were fabricated assuming a reduced-pressure environment.

4.8 CONCEPT MASS BREAKDOWN

The unit mass breakdown of the original baseline design and the new Haynes 188 design is given in table 4-9. The first column gives the estimated mass of the original system. The second column gives the unit mass breakdown of the new design based on nominal material thicknesses. The reductions in mass of the new design are 25% for the surface panel, 50% for the support structure, and 40% for the insulation. This results in an overall 35.4% reduction in mass from the baseline design. The most significant reductions appear for the skin, where the thickness decreased from .025 cm (.010 in.) to .0145 cm (.0057 in.); the support structure, where mass reductions were achieved by reducing the number of lower clips and attaching hardware;

Table 4-8. – Haynes 188 insulation system mass comparisons

Insulation system	Press. Envir	Max struct temperature		Insulation thickness		Insulation mass	
		K	°F	cm	in.	kg/m^2	lbm/ft^2
(1) 3.5-lbm/ft^3 Microquartz w/o supports	14040 Traj	450	350	5.31	2.09	2.98	0.61
(2) 1.1-lbm/ft^3 Astroquartz w/o supports	14040 Traj	450	350	24.7	9.74	3.95	0.81
(3) 3.5-lbm/ft^3 Microquartz +1.0 in. of 1.1-lbm/ft^3 Astro Quartz w/o supports	14040 Traj	450	350	7.04	2.77	2.98	0.61
(4) 3.5-lbm/ft^3 Microquartz + .56 in. of 1.0-lbm/ft^3 TG 15000 w/o supports	14040 Traj	450	350	5.84	2.30	2.68	0.55
(5) 3.5-lbm/ft^3 Microquartz, corrected for structural support heat leak	14040 Traj	450	350	5.77	2.27	3.22	0.66
(6) 3.5-lbm/ft^3 Microquartz + .60 in. of 1.0-lbm/ft^3 TG 15000, corrected for structural support heat leak	14040	450	350	6.35	2.50	2.93	0.60
(7) 3.5-lbm/ft^3 Microquartz, corrected for structural support heat leak	1.0 Atmos	450	350	7.41	2.92	4.15	0.85
(8) 3.5-lbm/ft^3 Microquartz, corrected for structural support heat leak	1.0 Atmos	486	[illegible]15	5.77	2.27	3.22	0.66

- Surface equilibrium temperature = 1255 K (1800° F)
- 3.5 lbm/ft^3 - 56 kg/m^3
- 1.1 lbm/ft^3 - 17.6 kg/m^3
- 1.0 lbm/ft^3 16 kg/m^3

2217 81W

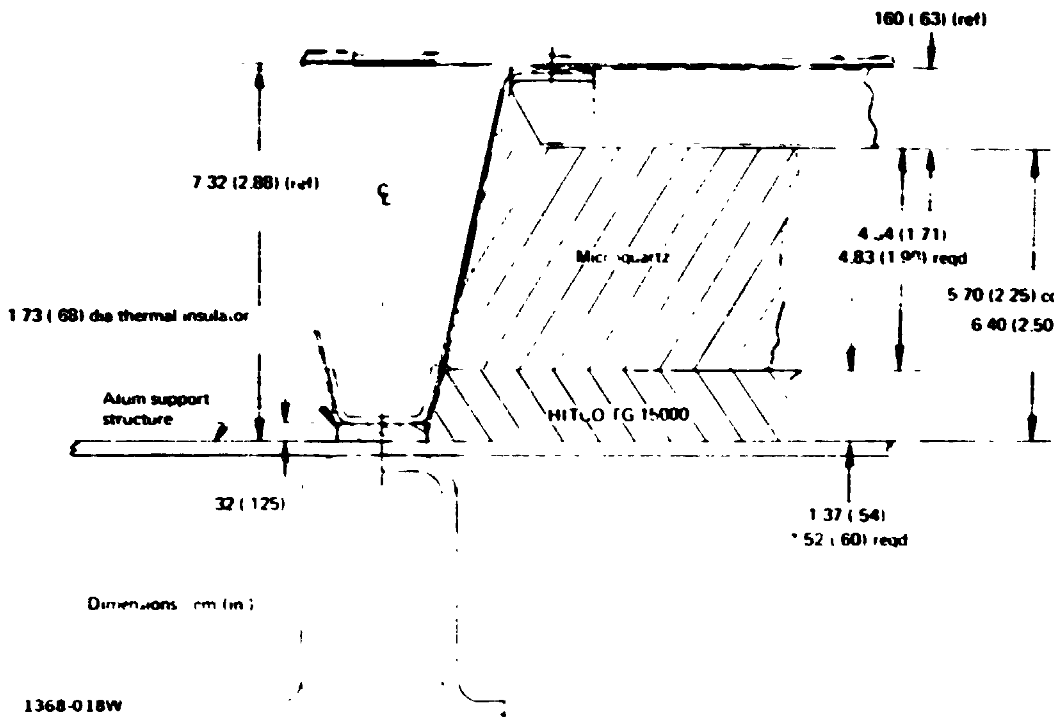

Figure 4-37. – Haynes 188 panel insulation system dimensions.

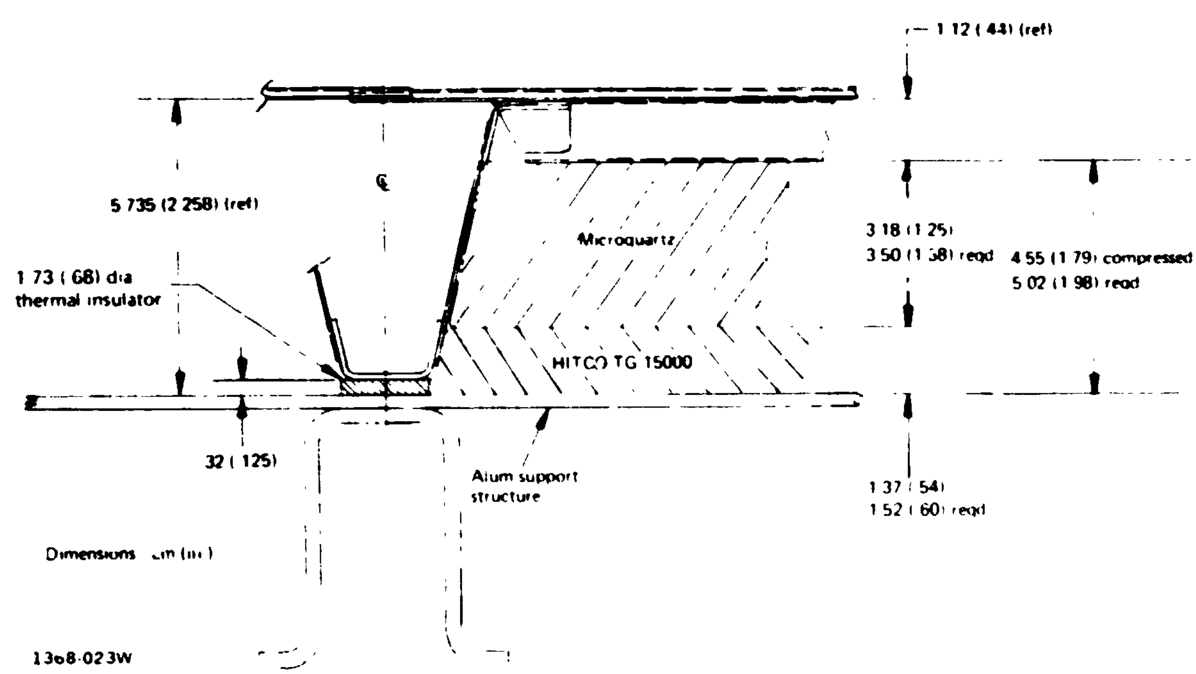

Figure 4-38. – [illegible] 41 panel insulation system dimensions.

Table 4-9. – Mass (estimated nominal weights) comparison of original baseline and new design.

Component	Original baseline		New design	
	lbm/ft^2	kg/m^2	lbm/ft^2	kg/m^2
Surface panel				
Skin	0.523	2.554	0.2866	1.3994
Corrugation	.664	3.242	.5888	2.8749
Doublers	–	–	.0299	.1460
Attach rivets	[a].054	.264	.0240	.1172
Subtotal	1.241	6.060	.9293	4.5375
% change	–		-25.1	
Supports				
Webs	0.090	0.439	0.0539	0.2632
Upper clips	.110	.537	.1064	.5195
Lower clips	.164	.801	.0547	.2671
Drag bracket	.031	.151	.0158	.0771
Attach hardware	.130	.635	.0302	.1475
Subtotal	.525	2.563	.2610	1.2744
% change	–		-50.3	
Insulation				
Microquartz	0.660	3.223	0.5541	2.7055
	[b].350	1.709	[c].0500	.2441
Subtotal	1.010	4.932	.6041	2.9496
% change			-40.2	
Total	2.776	13.555	1.7944	8.7615
% change	–		-35.4	

[a] 8-32 screws and nuts used

[b] Inconel bagging and supports

[c] TG 15000 insulation

2217-52W

and in the insulation system, where reductions were obtained by eliminating foil bagging and support hardware, and the use of low-density TG 15000 insulation.

The actual unit mass of each component was also determined, and is given in the third column of table 4-10. Actual overall mass increased 8.1% from the estimated nominal tolerance system. The largest mass increase (20.7%) occurred in the corrugation, and was the result of thinning at the corrugation bend line. The thinning occurred during the postforming "sizing" operation. Sizing of the corrugation was required to straighten the corrugations after brake-forming. The technique used was to brake-form slightly undersize and subsequently stretch or "size" the corrugation in a form block, machined to the required final dimensions. The sizing was achieved by using pressure plates to size the part to its final dimensions. The plates caused an excessive amount of stretch to occur in the bend area, resulting in significant thinning, approximately .0076 cm (.003 in.) at the bend line. The reduced thickness was used as the base thickness for the chem-milling operation so that the required minimum of .0145 cm (.0057 in.) would be achieved at the bend line. The corruga-

Table 4-10. – Haynes TPS mass breakdown (new design).

Component	Estimated mass (nominal tolerance)		Estimated mass (max tolerance)		Actual mass	
	lbm/ft^2	kb/m^2	lbm/ft^2	kg/m^2	lbm/ft^2	kg/m^2
Surface panel						
Skin	0.2866	1.3994	0.3014	1.4716	0.3090	1.5087
Corrugation	5888	2.8749	.6497	3 1723	.7110	3 4716
Doublers	0299	1460	.0309	1509	[b] .0360	[b] 1758
Attach rivets	0240	.1172	[a] .0240	[a] 1172	[c] .0240	[c] 1172
Subtotal	9293	4.5375	1.0059	4.9120	1.080	5.2733
% change	–		8.2		+16.2	
Supports						
Webs	0.0539	0.2632	0.0573	0 2798	0.0540	0.2637
Upper clips	.1064	.5195	1076	5254	0986	4814
Lower clips	0547	.2671	.0553	.2700	.0548	2676
Drag bracket	0158	.0771	.0163	0796	[b] .0180	[b] .0879
Attach hardware	0302	.1475	.0302	1475	[c] 0302	[c] .1475
Subtotal	2610	1 2744	2667	1 3023	2667	1.2481
% change	-		+2.2		-2 1	
Insulation						
Microquartz	0.5541	2 7055	[a] 0 5541	[a] 2 7055	[c] 0.5541	[c] 2.7055
TG 15000	0500	.2441	[a] .0500	[a] .2441	[c] 0500	[c] .2441
Subtotal	6041	2.9496	.6041	2.9496	6041	2.9496
% change	–		–		–	
Total	1.7944	8.7615	1.8767	9.1639	1 9397	9.4710
% change	–		+4.6		+8.1	

[a] Not available

[b] 044 cm (0175 in) mats used instead of 038 cm (015 in.)

[c] Items not weighed

tion wall thickness averaged .022 cm (.0085 in.) instead of .0145 cm (.0057 in.), which accounts for the 3.47-kg/m^2 (.711-lbm/ft^2) mass. This problem was eliminated during the René 41 forming operations by using a larger bend radius and redesigning the pressure plates used in the sizing operation. Mass increases in the skin doublers and drag bracket resulted from use of .044-cm (.0175-in.) instead of .038-cm (.015-in.) material, which was not available.

The unit mass breakdown of the René 41 TPS is given in table 4-11. As indicated the actual mass of the fabricated panel was only 2.8% higher than estimated.

Table 4-11. – René 41 TPS mass breakdown.

Component	Estimated mass (Nominal tolerance)		Estimated mass (Max tolerance)		Actual mass	
	lbm/ft^2	kg/m^2	lbm/ft^2	kg/m^2	lbm/ft^2	kg/m^2
Surface panel						
Skin	0.3525	1.7211	0.3971	1.9388	0.3600	1.7577
Corrugation	.4447	2.1712	.4751	2.3196	.4800	2.3436
Doublers	.0116	.0566	.0123	.0601	.0103	.0503
Attach rivets	.0240	.1172	[a].0240	[a].1172	[b].0240	[b].1172
Subtotal	.8328	4.0661	.9085	4.4357	.8743	4.2688
% change	–		+9.1		+5.0	
Supports						
Webs	0.0262	0.1279	0.0278	0.1357	0.0324	0.1582
Upper clips	.0655	.3198	.0668	.3261	.0570	.2783
Lower clips	.0337	.1645	.0344	.1680	.0306	1494
Drag bracket	.0103	.0503	.0106	.0518	.0149	.0727
Attach hardware	.0302	.1474	.0302	.1474	[b].0302	[b] 1474
Subtotal	.1659	.8099	.1698	.8290	.1651	.8060
% change	–		+2.3		+0.0	
Insulation						
Microquartz	0.4020	1.9627	[a]0.4020	[a]1.9627	[b]0.4020	[b]1.9627
TG 15000	.0500	.2441	[a] .0500	[a] .2441	[b] .0500	[b] .2441
Subtotal	.4520	2.2068	.4520	2.2068	.4520	2.2068
% change	–				–	
Total	1.4507	7.0828	1.5303	7.471[illegible]	1.4914	7.2816
% change	–		+[illegible].5		+2.8	

[a] Not available
[b] Not weighed

2217-96W

4.9 PANEL STIFFNESS PROPERTIES

Panel stiffness properties were determined for the Haynes 188 and René 41 panels. The properties were calculated for the final production sections, which are illustrated in figures 4-10(a) and 4-10(b). The properties are given in table 4-12.

Table 4-12. – Summary of panel stiffness properties.

Constant	Haynes 188 TPS				René 41 TPS			
	N·m		lb–in.		N·m		lb–in.	
	Room temp	1255 K	Room temp	1800°F	Room temp	1144 K	Room temp	1600°F
D_x	6739	2695	59 643	23 857	2656	1490	23 539	13 185
D_y	.4180	.1695	3.7	1.5	.9830	.5536	8.7	4.9
D_{xy}	2254	902	19 949	7980	1218	682	10 779	6037

2217-97W

4.10 REFERENCES

4-1 Advanced Beaded and Tubular Structural Panels. NASA CR-2514.
Vol 1 - NASA CR-132460
Vol 2 - NASA CR-132482
Vol 3 - NASA CR-132515

4-2 Lemley: Design Criteria for the Prediction and Prevention of Panel Flutter. AFFDL-TR-67-140, Vol. I, 1967.

4-3 Structural Design Criteria Applicable to a Space Shuttle. NASA SP 8057, 1971.

4-4 Klick, George F.: The Langley Thermal Protection System Test Facility: A Description Including Design Operating Boundaries. NASA TMX 73973, November 1976.

4-5 Klick, George F.: Thermodynamic, Transport and Flow Properties of Gaseous Products Resulting From Combustion of Methane-Air-Oxygen Mixtures. NASA TND-8153, June 1976.

4-6 Laurenson, R. M.; and McPherson, J. I.: Design Procedures for Flutter-Free Surface Panels. NASA CR-2801, March 1977.

4-7 High Temperature Insulation Materials For Reradiative Thermal Protection Systems. MDC E0666, 19 July 1972.

4-8 HITCO Materials Specification 20-15.1, July 1972.

4-9 Guboreff, G. G.; Janssen, J. E.; and Torborg, R. H.: Thermal Radiation Properties Survey. Second edition, 1960.

4-10 Lightweight Thermal Protection System Development. ASD-TDR-63-596, Vol. II, June 1963.

Section 5

TEST SPECIMEN FABRICATION

5.1 HAYNES 188 FASTENER DEVELOPMENT

Although conventional, threaded fasteners have been fabricated from Haynes 25 (L-605) alloy, experience has shown that oxide formation after repeated high-temperature exposure makes removal extremely difficult. (Seizure of Haynes 25 screws on a previous test panel is described in reference 5-1, page 13.) Although Haynes 188 is less prone to oxidation than Haynes 25, Haynes 188 threaded fasteners are heavier and more costly to use in blind applications, and should be restricted to areas requiring access to the primary structure. The desirability, therefore, of a low-mass blind rivet for the large areas of the TPS was recognized early in the program, and the development of a blind fastener fabricated from Haynes 188 was undertaken.

The Huck Manufacturing Co., Carson, California, was selected to manufacture the fasteners. The design selected was developed from the existing mechanically locking spindle (MLS) type blind rivet. This type of rivet is used extensively on aerospace-type structures. The fastener developed by Huck is shown in figure 5-1. As illustrated, the fastener employs a forged, brazier-type protruding head. A flush-type head can also be fabricated, if required. The flush-type head was not used on the test specimen so that double dimpling could be avoided. The fastener includes a lock collar for positive retention of the control pin. Both the lock collar and central pin were machined from .317-cm (.125-in.) diameter wire. The head and shank were forged from .396-cm (.156-in.) diameter wire.

5.2 SURFACE-PANEL FABRICATION

5.2.1 Skin Fabrication

The skin was fabricated using conventional rubber-press techniques. The aluminum form block, which includes the bead geometry, is shown in figure 5-2. The finished Haynes 188 skin, formed after chem-milling, is shown in figure 5-3. The René skin was formed on the same block.

5.2.2 Corrugation Fabrication

The corrugation was fabricated using a standard forming brake. The forming sequence is shown in figure 5-4. The corrugation, formed before chem-milling, was predrilled on the edges, using an accurate drill template. The holes were used to locate the upper die by use of an index pin, as shown in figure 5-4(a). Figures 5-4(b) through (g) show the actual brake-forming sequence of the René 41 corrugation. Figure 5-4(h) shows the corrugation being removed from the sizing block, which was used to stretch or size the corrugation to its final dimensions.

"Thinning" at the bend line was experienced with the Haynes 188 corrugation. This was the result of too sharp a radius on the sizing plates, which were used to force and stretch the material into the sizing block. The reduced thickness at the bend lines was identified during chem-milling, and this reduced thickness was used as the base thickness during chem-milling. Consequently, the final wall thickness averaged .022 cm (.0085 in.) instead of the desired .0145 cm (.0057 in.).

The thinning was prevented on the René 41 corrugation by use of a larger bend radius and redesigned sizing blocks. An enlargement of the René 41 corrugation, shown in figure 5-5, indicates essentially no thinning at the upper or lower bend areas.

5.2.3 Surface-Panel Assembly

The skin and corrugation were joined by means of a roll-seam welding technique which produces an overlapping spotweld. Three weld lines were used at each skin/corrugation interface. After seam welding, the edge doublers were added at each end by conventional spotwelding. The fully assembled surface panel is shown in figure 5-6. Also shown is the corrugation chem-mill sculpturing profile employed to minimize mass. (Refer to para 4.3.7.)

5.2.4 Haynes 188 Panel Surface Emittance Treatment

Prior to test specimen final assembly, the Haynes 188 surface panels were preoxidized to increase their surface emittance. The emittance treatment consisted

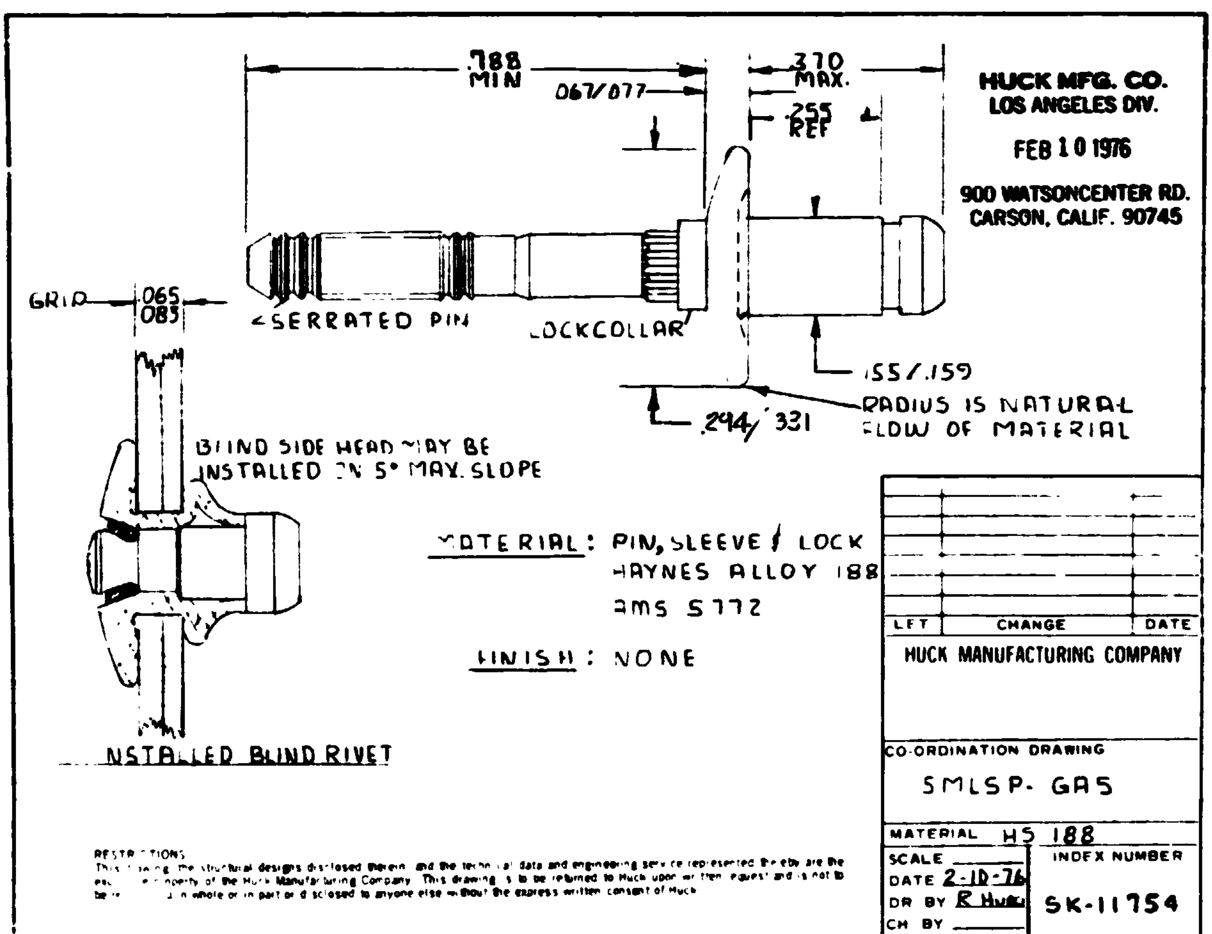

Figure 5 1. – Haynes 188 blind fastener.

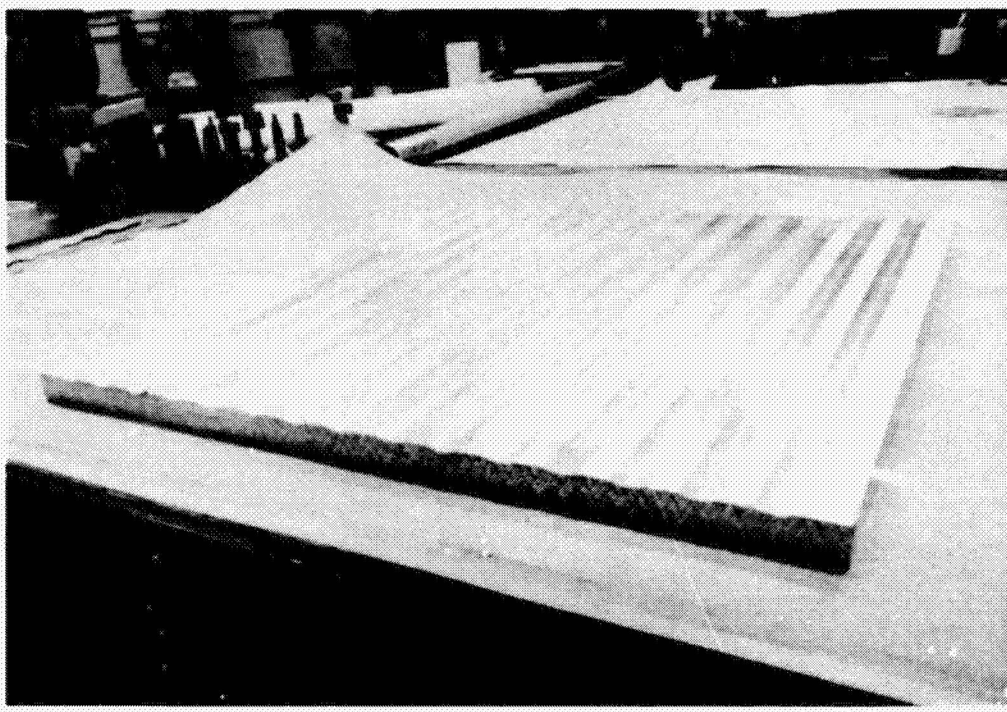

2217-55W

Figure 5-2. — Skin forming tool.

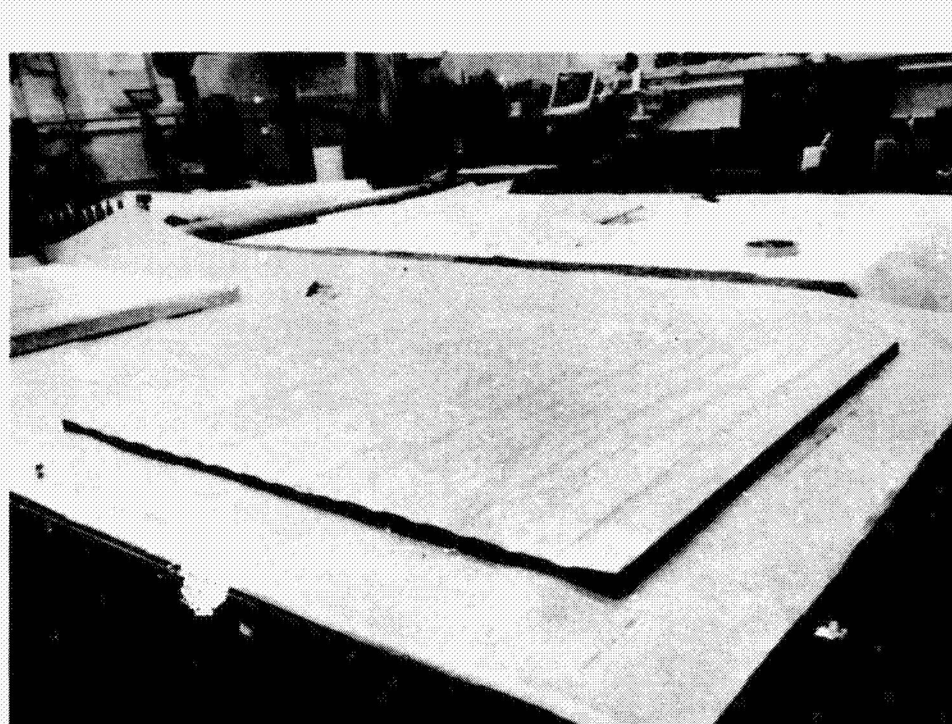

2217-56W

Figure 5-3. — Formed Haynes 188 skin.

2217-57W

Figure 5-4. — Corrugation forming sequence.

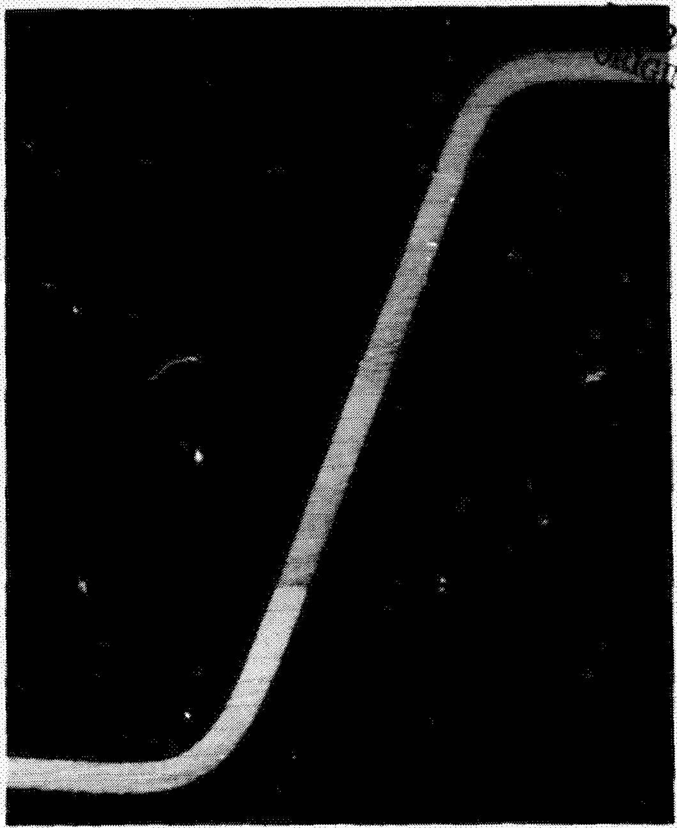

2217-58W

Figure 5-5. – René 41 corrugation bend area enlargement.

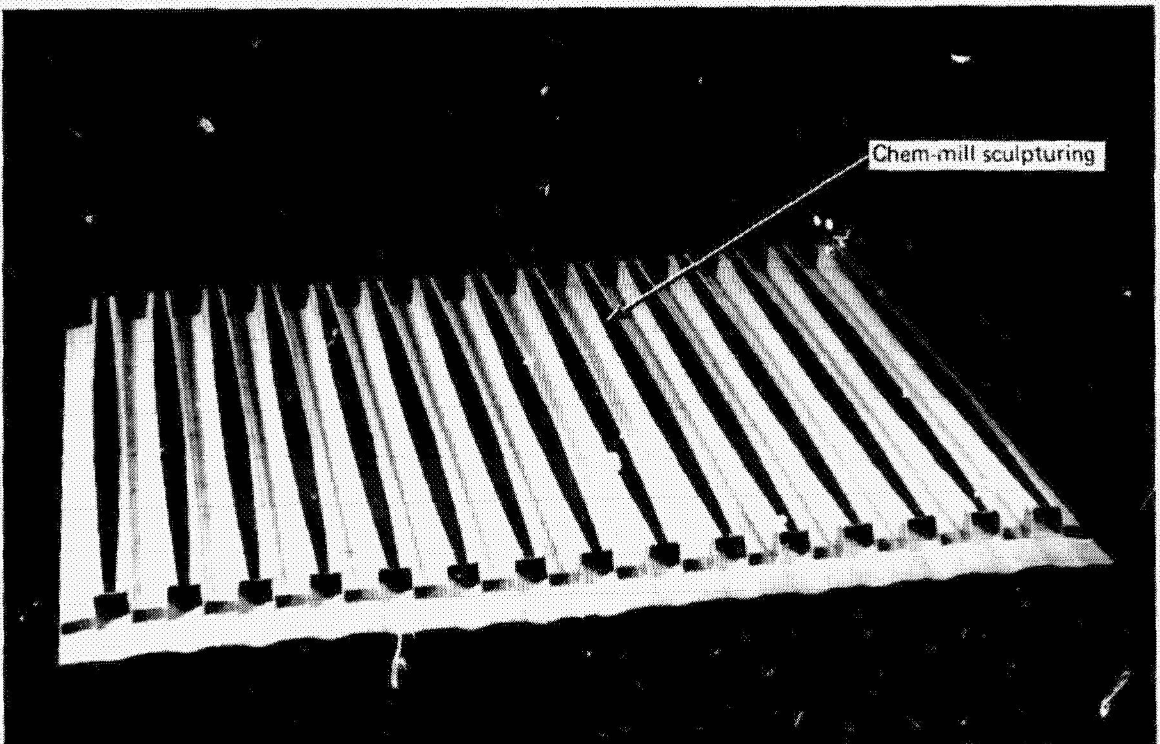

2217-59W

Figure 5-6. – Fully assembled Haynes 188 surface panel.

of cleaning the panels, using a dry vapor hone. Following cleaning, the panels were inserted in an electrically heated oven preheated to 1339 K (1950°F). The panels were exposed at this temperature for 4 hr. A surface emittance of .79 was measured, using a Gier Dunkle Model DB-100 portable reflectometer.

5.2.5 René 41 Panel Surface Emittance Treatment

To obtain a surface emittance of .80 or more on René 41, it is necessary to oxidize the material in air at 1340 K (1950°F) for a minimum of 30 min. Exposure at this temperature reanneals the material, requiring a new solution-treatment cycle. Solution-treatment of René 41 requires heating at 1395 K (2050°F) followed by a rapid quench. Because the René 41 panels were fully assembled, consideration was given to the possibility of warpage and distortion during the quench cycle. It was decided, therefore, to increase the surface emittance of the panel by use of Pyromark, a refractory coating providing high emittance (greater than .80) at a service temperature of 1367 K (2000°F). The coating is a product of Tempil, Inc., Hamilton Blvd., South Plainfield, N.J., and is supplied as a liquid.

The René 41 panels were sprayed with Pyromark and allowed to air-dry for 24 hr. The panels were then baked at 522 K (480°F) for 1 hr. The coating was then vitrified at 1172 K (1650°F) for 4 hr and air-cooled. The vitrification cycle is identical to the material aging cycle, and both were accomplished simultaneously. Following vitrification, a surface emittance of .89 was measured.

It is possible to increase René 41 surface emittance by oxidation rather than use of a coating. The oxidation exposure, however, should be done before solution-treatment and panel fabrication.

5.3 SUPPORT RIBS FABRICATION

Two types of support ribs were used to support the surface panel: a flexible type at the expansion joint, and a fixed type where two adjacent panels butt, which is called the center support rib. Although both ribs are functionally different, a common design was developed for both rib webs to reduce costs. The rib-web stamping die and form block are shown in figure 5-7. Also shown is the Haynes 188 rib-web detail after stamping but before forming. The René 41 rib web was fabricated in an identical manner.

5.3.1 Center Support (Fixed) Rib

The Haynes 188 panel center support rib is shown in figure 5-8. The rib was assembled by locating and spotwelding the upper and lower clips. Two spotwelds were used on the upper clip, three on the lower. The drag supports were also attached by spotwelding. The René 41 support rib is identical to the Haynes 188 rib, except for height.

5.3.2 End Flexing Rib

The Haynes 188 end flexing rib is shown in figure 5-9. Two rib webs were spotwelded to the lower U-shaped clip. The upper clips were then located and spotwelded to the rib web. The lower U clips have a pitch of 7.62 cm (3.0 in.). However, at the left end, the pitch was reduced to 3.81 cm (1.50 in.) to fit within the 51-cm (24-in.) test cavity. The René 41 flexing rib is identical to the one shown, except for height.

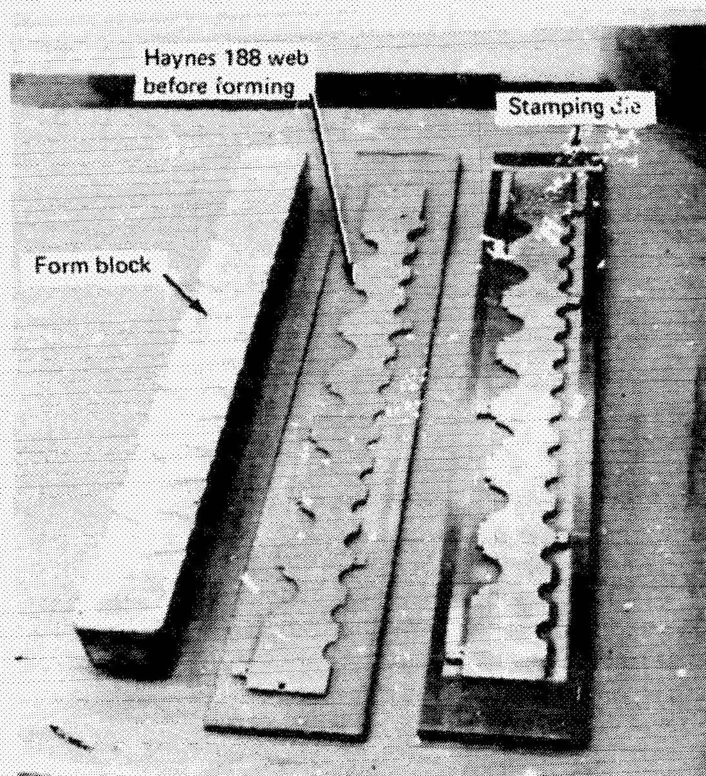

2217-60W

Figure ' - Rib web tools and web detail.

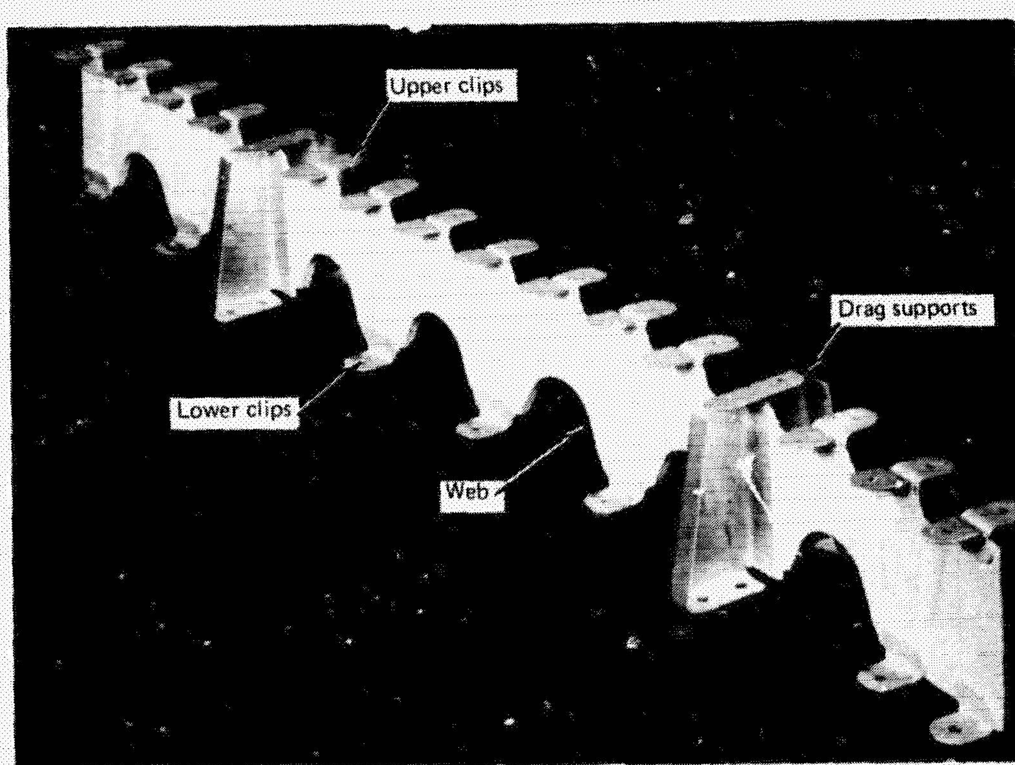

2217-61W

Figure 5-8. — Center support (fixed) rib.

5.4 EDGE FAIRINGS

Edge fairings were designed and fabricated to seal the test specimen within the test cavity and to provide a smooth aerodynamic flow during testing. The fairings are shown in figure 5-10. The forward and aft fairings were rubber-press formed with a bead geometry identical to the skin panels. The beads "close-out" to provide a smooth aerodynamic flow. The side fairings have flat flanges spotwelded to the skin panels. All the edge fairings were formed with a curved (half-circle) lip, which was designed to support a braided rope-type seal made of a silica material. The seal is added during installation of the test specimen in the TPSTF test cavity.

5.5 TEST SPECIMEN FINAL ASSEMBLY

The fully assembled Haynes 188 TPS test specimen is shown in figure 5-11. The 61- x 91-cm (24- x 36-in.) specimen is shown mounted on the aluminum support structure designed to simulate the thermal mass of a typical flight vehicle (subsection 6.5). The first step in final assembly was to attach the support ribs, including insulating washers, to the support structure (appendix E, drawing AD1001-100). The insulation system was then installed between the ribs, as shown. The skin and forward and aft fairings, were then installed on the support ribs and fastened using the Haynes 188 fasteners. The eight holes shown in the support structure side channels are for attaching the test specimen in the TPSTF test cavity. (Dimensions related to the TPSTF test cavity are given on NASA drawings LE-526279, LE-526297, LE-526299, and LE-526464.)

The fully assembled René 41 TPS test specimen is shown in figure 5-12. The specimen was assembled identically to the Haynes 188 specimen. Haynes 188 fasteners were used to attach the skin panels on the René 41 TPS because of their higher temperature capability.

5.6 REFERENCES

5-1 Sawyer, J. W.: Aerothermal and Structural Performance of a Cobalt-Base Superalloy Thermal Protection System at Mach 6.6. NASA TND-3415, May 1977.

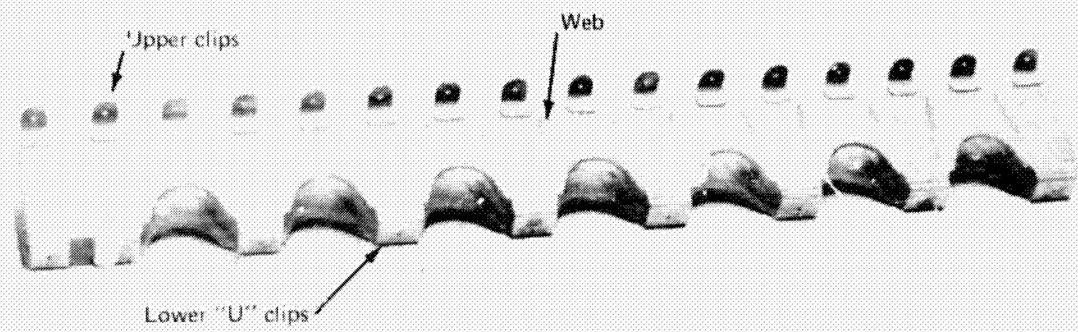

2217-62W

Figure 5-9. — End flexing rib

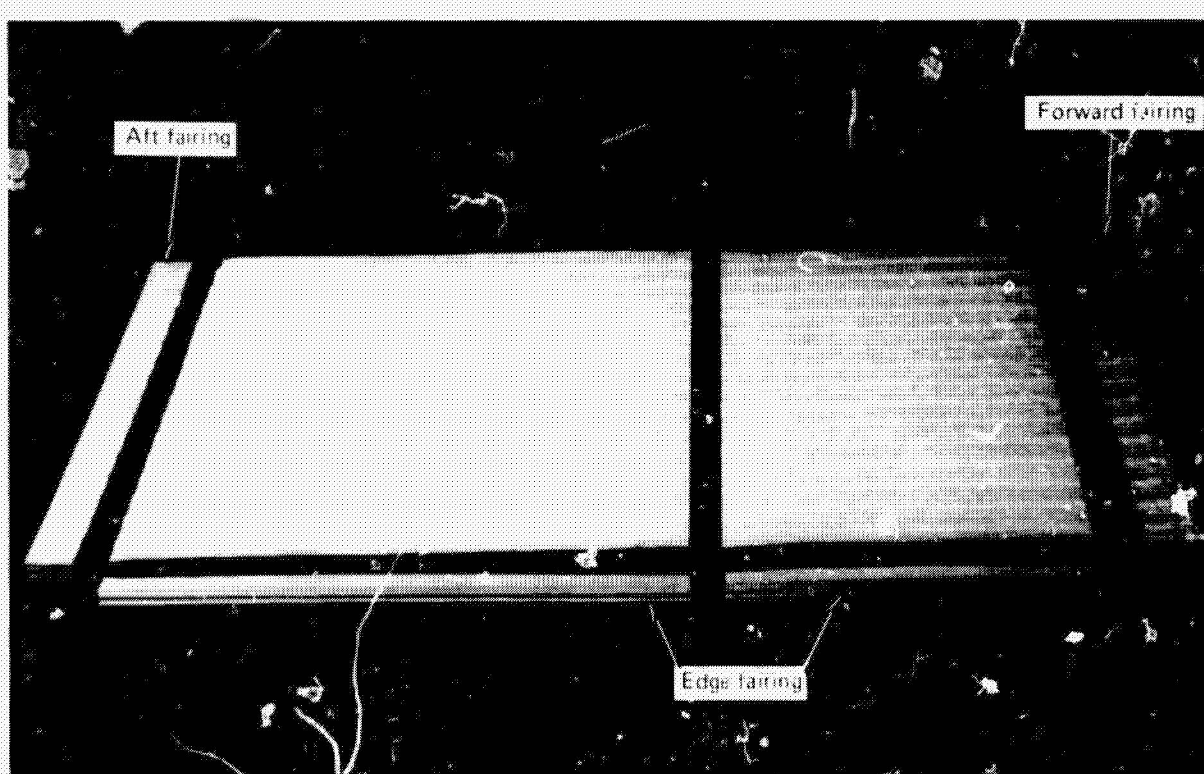

2217-63W

Figure 5-10. — Haynes 188 skin panels and fairings.

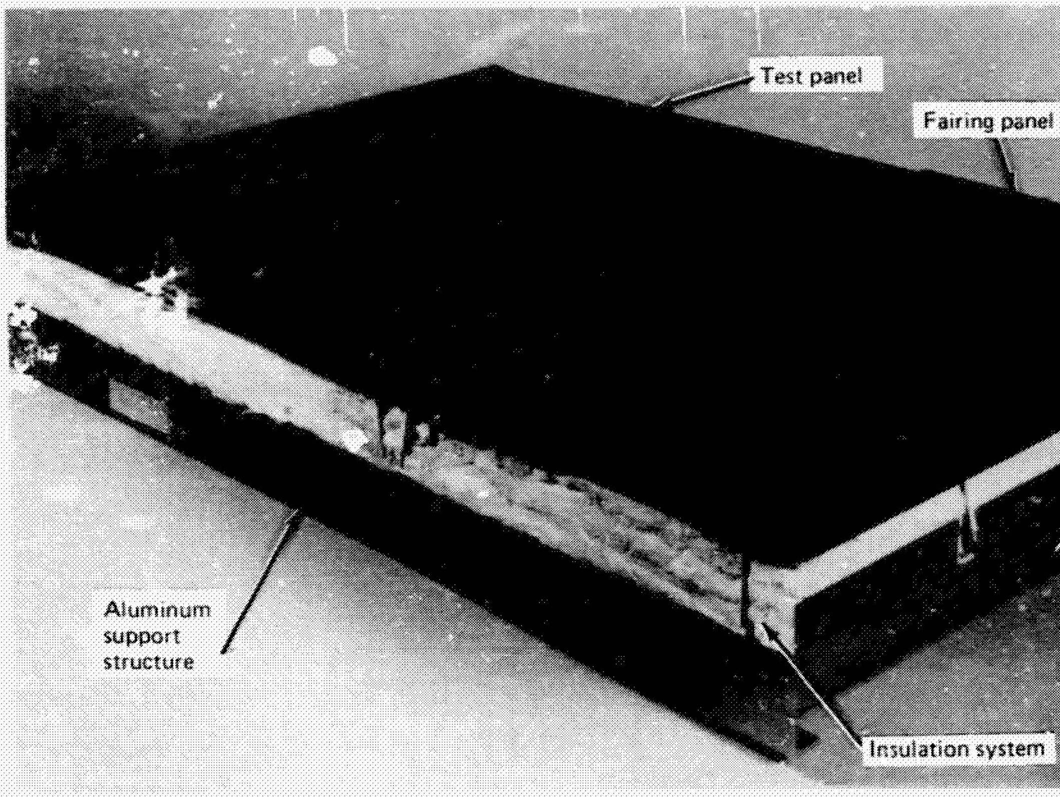

2217-64W

Figure 5-11. – Fully assembled Haynes 188 TPS test specimen.

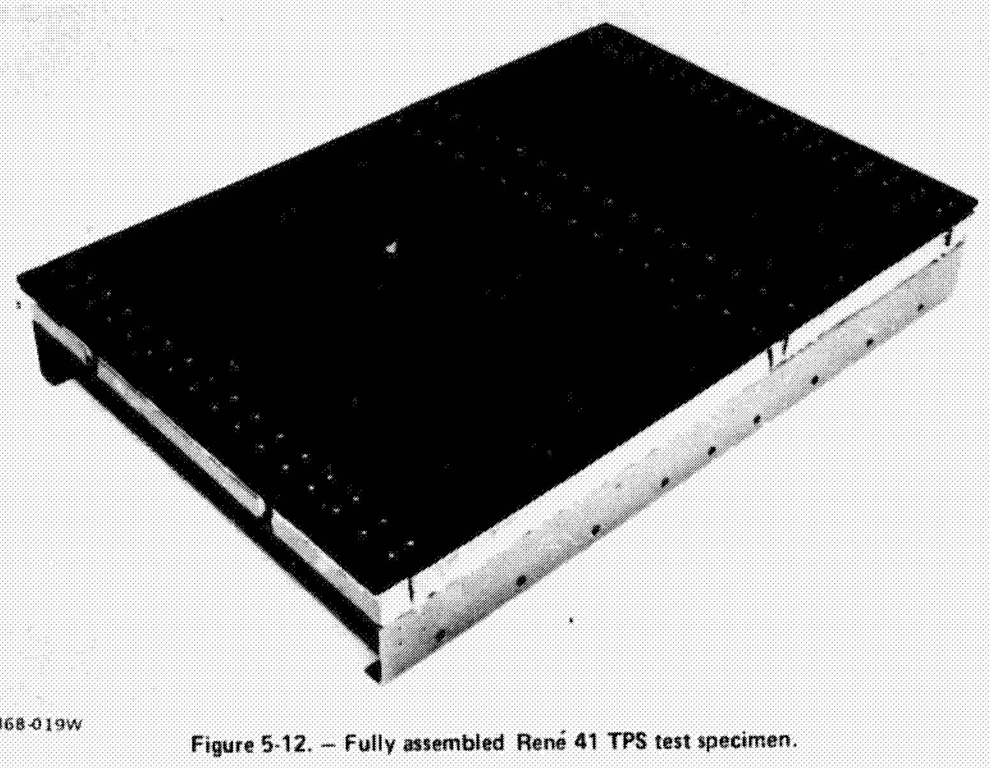

1368-019W

Figure 5-12. – Fully assembled René 41 TPS test specimen.

C.2

Section 6

TEST SPECIMEN INSTRUMENTATION & SUPPORT STRUCTURE

The test specimen instrumentation configuration is shown in figure 6-1. As indicated, 53 thermocouples (T/C) were installed in the locations indicated to monitor test specimen temperatures. The eight T/Cs, which monitored heat-sink temperatures, were fabricated using chromel/alumel fiberglass-insulated 30-gage wire, and attached with a high-temperature adhesive. All other T/Cs are the ceramo type, spotwelded to the test panel. Thermocouples attached to the heat sink are shown in figure 6-2. Transition from 30-gage T/C wire to 24-gage extension wire was made with two-pronged connectors 15.2 cm (6.0 in.) below the structure. The connectors are shown in figure 6-3. Correlation of T/C number and location is given in appendix H.

The Haynes 188 and René 41 test articles were instrumented identically.

6.1 PANEL DEFLECTION MEASUREMENTS

Skin-panel deflections were measured at the center of the 51-cm (20.0-in.) test panel, as indicated in figure 6-1. Measurements were made by a cable-type linear-displacement transducer capable of operation in a 477 K (400°F) environment, with a resolution of .003 cm (0.001 in.). The transducer is, basically, a potentiometer driven by the displacement of the extending cable. The transducer, shown in figure 6-3, was mounted below the heat sink, where the temperature was less than 477 K (400°F).

6.2 INSULATION SYSTEM TEMPERATURES

To evaluate temperature gradients through the insulation thickness, four T/Cs were placed 1.27 cm (0.5 in.) apart on a support plate. Two such arrangements were employed, indicated by the letter "I" in figure 6-1. One is located at the panel center, and one near the flexing rib. The two T/C assemblies are shown in figure 6-2.

6.3 EXPANSION JOINT LEAKAGE

To evaluate expansion joint leakage, three T/Cs were placed in line under the skin, in the expansion joint area. This is illustrated in section A-A of figure 6-1. If leakage were to occur, it was expected that the center T/C would record a higher temperature. This arrangement was employed at three locations in the expansion joint area. The expansion joint T/Cs are shown in figure 6-4.

6.4 EDGE SEAL LEAKAGE

To evaluate leakage around the test specimen edges, four T/Cs were employed, one at each edge, as illustrated in figures 6-1 and 6-4.

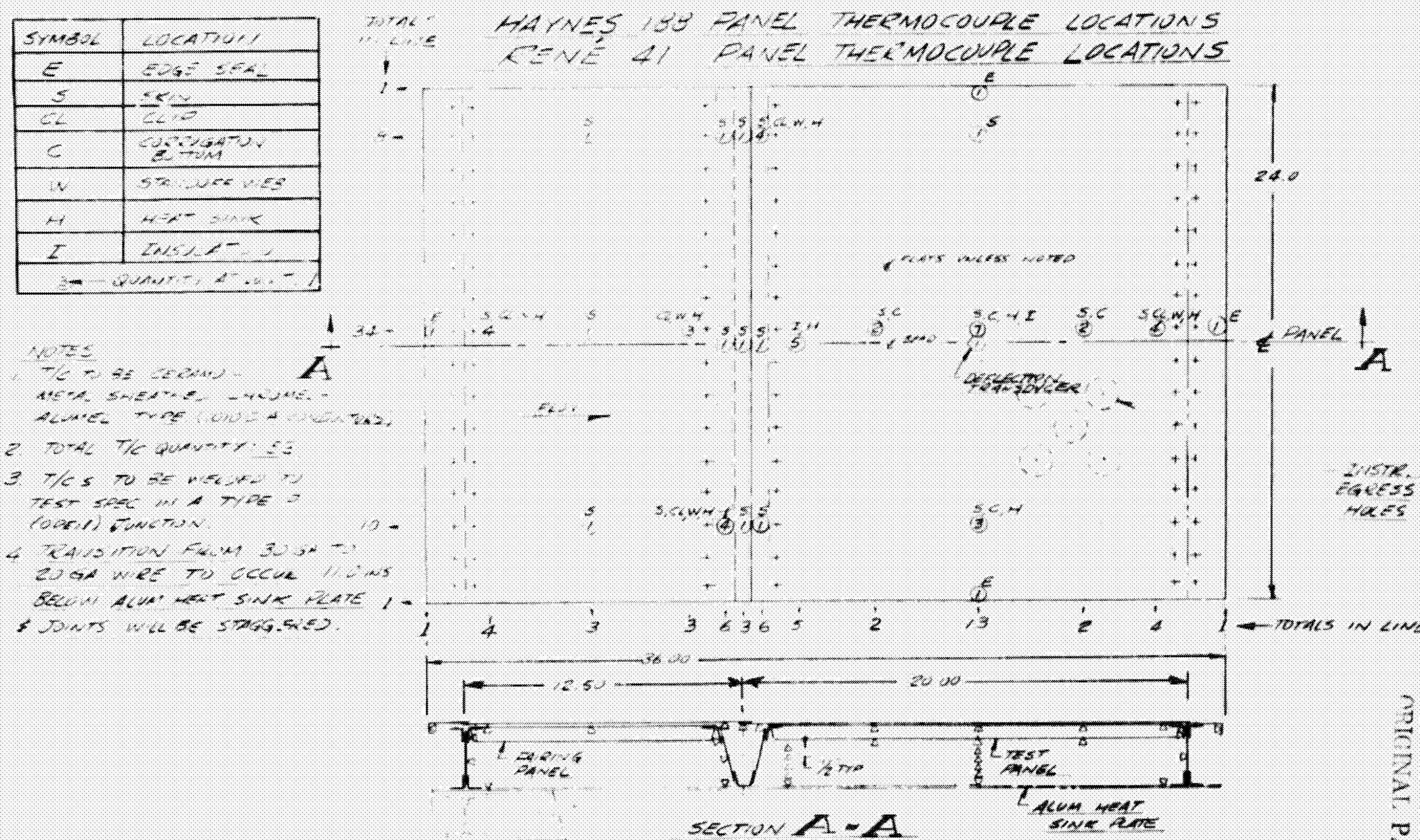

2217-80W

Figure 6-1. — Test specimen instrumentation configuration.

REPRODUCIBILITY OF THE ORIGINAL PAGE IS POOR

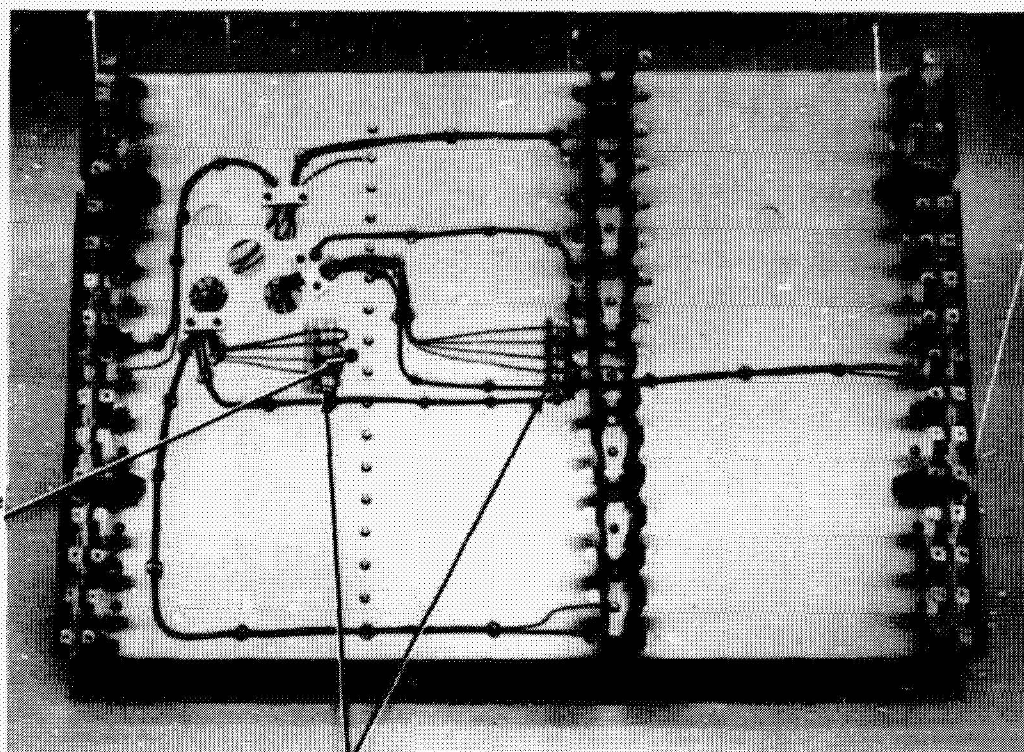

2217-65W

Figure 6-2. – Support structure heat-sink instrumentation – top.

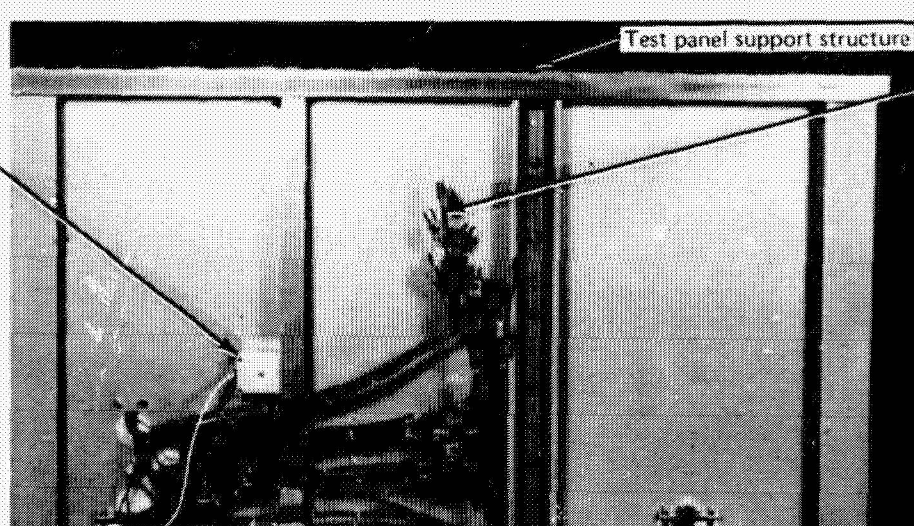

2217-66W

Figure 6-3. – Support structure – bottom.

REPRODUCIBILITY OF THE ORIGINAL PAGE IS POOR

6.5 TEST SPECIMEN SUPPORT STRUCTURE

A structure (figures 6-2 and 6-3) was designed to support the test specimen in the TPSTF. It was to represent the thermal mass of a vehicle substructure equivalent to a .51-cm (0.20-in.) thick aluminum plate. (Detail stress analysis of the support structure is given in appendix I.) Although the maximum pressure in the TPSTF is approximately 2.5 kPa (53 psf), the support structure was designed and checked for a 16.8-kPa (350-psf) limit pressure load. The deflection of the critical beam, under the flexing rib was .005 cm (.002 in.) with the 16.8-kPa (350-psf) loading. (The support structure production drawing (AD1001-104) is given in appendix E.)

The support structures for the Haynes 188 and René 41 panels are identical.

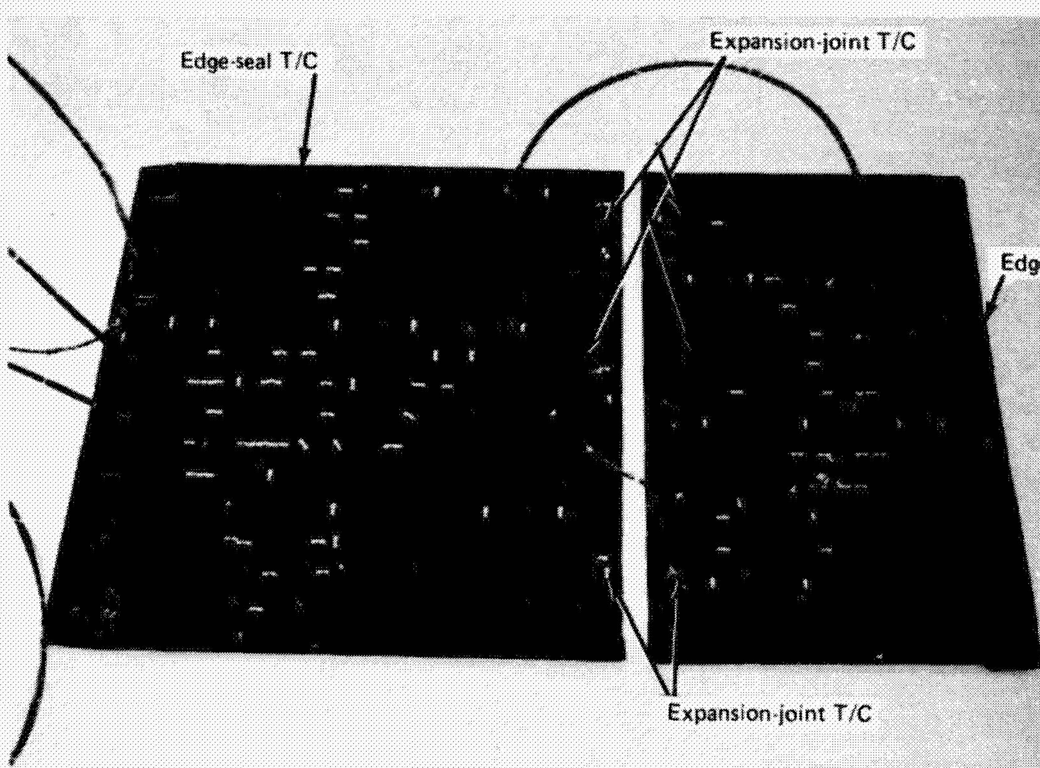

Figure 6-4. – Surface panel instrumentation – lower surface.

Section 7

CONCLUSIONS

A lightweight metallic TPS was designed, and two test articles were fabricated, one from Haynes 188 and one from René 41. A baseline TPS concept, selected at the beginning of the program, consisted of a Haynes 25 corrugation-stiffened beaded skin surface panel, a specially designed support system, and an insulation system. By optimizing the structure for the design loads and by chem-milling to remove material not needed, the mass of the baseline surface panel was reduced 25%, and the mass of the support structure was reduced 50%. The insulation system mass was reduced 40% by using two types of insulation, each suited to its temperature range, and by eliminating a foil bag which encapsulated the baseline insulation system. These reductions resulted in an overall 35% reduction in mass of the Haynes 188 panel from the baseline Haynes 25 design. Similar reductions were achieved with the René 41 system.

The overall program led to the following conclusions:

- René 41 and Haynes 188 heat shields appear to be viable approaches for a thermal protection system for vehicles sustaining temperatures up to 1255 K (1800°F)

- A René 41 TPS with a mass of 7.08 kg/m^2 (1.45 lbm/ft^2) and a Haynes 188 TPS with a mass of 8.7615 kg/m^2 (.794 lbm/ft^2) can be fabricated using state-of-the-art production techniques.

- Two thermal protection systems, optimized for different materials and operating temperatures, can be used as adjacent compatible systems, with only a small decrease in mass efficiency resulting from the compromise.

In view of these results, it is concluded that the basic technology for flat metallic TPS is available.

APPENDIX A

Skin/Corrugation Optimization Procedure

The surface panel (skin/corrugation) optimization procedure is given in the following pages. The design equations and analysis procedure are presented. Also presented is the computer program (HAYNES) which was developed to simplify selection of the optimum Haynes 188 and René 41 configurations.

Design Equations

The bending moment (M) at mid-span is:

$$M = \frac{P_r p L^2}{144 \; 8}$$

$$\therefore M = .31668 \, p P_r$$

Where: P_r = Pressure (PSF)

p = Pitch

L = Span = 19.1 in

E (modulus) is the appropriate value for temp. and material combo.

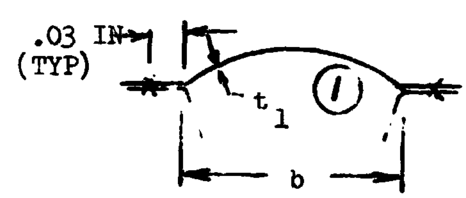

Element 1

(FLUTTER CONSTRAINTS
See Fig. 4-7, 4-8)

(1) $t_1 \geq .0061\,(b+.06)$ (HAYNES)

$t_1 \geq .0078\,(b+.06) - .00192$ (RENE')

BUCKLING

(2) $$.31668p(350)\,\frac{(h+.1b-\bar{x})}{I_{NA}} \leq \frac{.22E\left(\frac{t_1}{R^1}\right)}{1.4}$$ FACTOR OF SAFETY

$R^1 = 1.3\,(b+.06)$ for a 10% aspect ratio bead

CREEP

(3) $$.31668\,p(50)\,\frac{(h+.1b-\bar{x})}{I_{NA}} \leq \frac{F_{creep}}{1.15} = \frac{2770 + 1770\,(h+. \;)}{1.15}$$

(FACTOR OF SAFETY)

ELEMENT (2-3)

(BUCKLING)

(4) $$.31668p\,(350)\,\frac{(h-\bar{x})}{I_{NA}} \le \frac{3.62E\left(\frac{t_1+t_2}{p-b}\right)^2}{1.4}$$

ELEMENT (4)

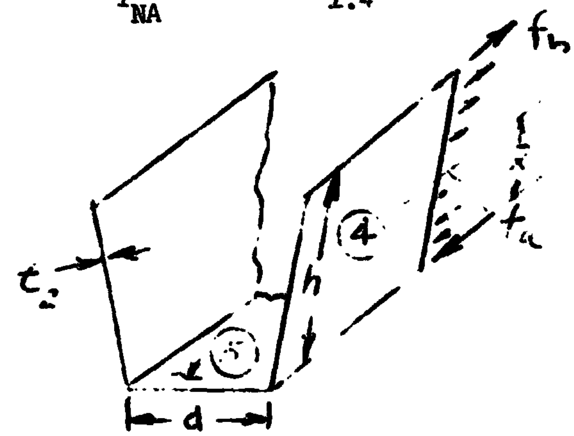

BUCKLING:

COND A

ELEMENT (4) was assumed to be a long plate, simply supported on the long sides, with a bending gradient as shown.

The buckling coefficient was fit to:

(5) $$K_{cr} = e^{[.7355+1.1663\,(\frac{h}{x})]}$$

for the ranges of $\frac{\bar{x}}{h}$ of interest in this study

(6) $$\therefore\ f_a = .31668p\,(430)\left(\frac{\bar{x}}{I_{NA}}\right) \le \frac{K_{cr}E\left(\frac{t_2}{h}\right)^2}{1.4}$$

ELEMENT (5)

(BUCKLING, COND A)

(7) $$.31668p\,(430)\left(\frac{\bar{x}}{I_{NA}}\right) < \frac{3.62E\left(\frac{t_3}{d}\right)^2}{1.4}$$

(CREEP, COND D)

(8) $$.31668p\,(50)\left(\frac{\bar{x}}{I_{NA}}\right) \le \frac{2770+1770\,(h+.1b)}{1.15}$$

ANALYSIS PROCEDURES

		Known Parameters
1.	ASSUME $\beta = \dfrac{\bar{x}}{h+.1b}$	
2.	ASSUME p	p
3.	ASSUME b	b
4.	ASSUME h $\therefore \bar{x}$ is known	h
5.	IF $\bar{x} < (h+.1b)/2$ go to Step 14	
6.	Solve Eq (8) for $(I_{NA})_{REQUIRED}$	$(I_{NA})_{REQ}$
7.	Solve Eq (6) for t_2	t_2
8.	Solve Eq (1) for t_1	t_1
9.	Solve $\dfrac{\Sigma A_x}{\Sigma A} = \bar{x}$ for (dt_3)	
10.	Substitute in Eq (7) and solve for d	d
11.	Solve dt_3 for t_3	t_3
12.	Solve section property equations for $(I_{NA})_{ACTUAL}$	$(I_{NA})_{ACT.}$
13.	IF $\left\lvert \dfrac{(I_{NA})_{ACT}}{(I_{NA})_{REQ}} - 1 \right\rvert >$ TOLERANCE — taken as 0.001. Increment h and return to Step 4, otherwise go to step 15	
14.	Solve Eq (3) for $(I_{NA})_{REQUIRED}$ and go to Step 7.	
15.	Check equations (2) & (4) to see if design is acceptable. If not go to Step 2.	

Known Parameters

16. Calculate Section Weight/Ft^2

$$W = \frac{\Sigma A}{p} \cdot 144 \cdot \text{DENSITY} \left(\frac{lb}{FT^2}\right)$$

WEIGHT

17. Continue varying ρ, b and β to find optimum section.

- Because of the number of arithmetic operations required and the iterative nature of the analysis, a computer program HAYNES, was written. This program can not be considered as the true optimization program, since some of the steps necessary to find the least weight acceptable design section are graphical and require the user to interface with the program.

The program follows the 17 steps outlined above except that the sequence has been altered to improve the program efficiency. A program option allows the margins of safety for each element to be output if desired by the user. The program operates on Grumman's time-share computer.

The computer printout for the optimized HAYNES section is presented in Figure A-1. The face sheet thickness, t_1, was sized to prevent flutter, but it can be seen that it (element 1) has only a 3% margin of safety in buckling under Condition B and a zero margin in creep under Condition D. Elements 4 and 5

```
$ :aynes
EXECUTION BEGINS...

 WHAT ARE P0,DP,PMAX,B0,DB,BMAX,BETA ?

.0,1.5,2.,.0,.782,1.,.5
  0.0     1.50000 2.00000 0.0     0.78200 1.00000 0.50000

         WHAT IS TMIN ?

.005
  0.00500

         WHAT IS IPRT ?

0001
```

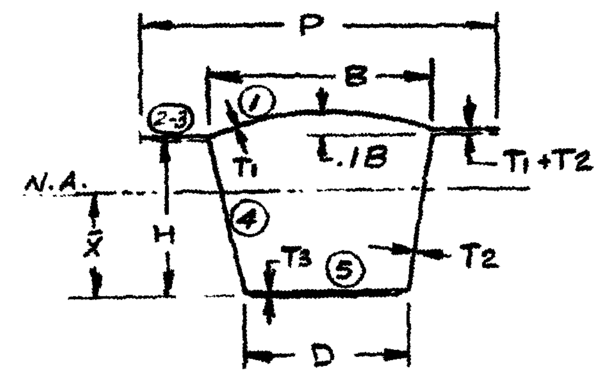


```
   P        B        T1       H        T2       D        T3     AREA     INA     X BAR     A/P    WT/FT2    BEAD

 1.50000 0.78200 0.00514 0.63300 0.00545 0.69788 0.01288 0.02761 0.00241 0.35560 0.01841 0.57473     0

ELEM    A YLD   A BKL    B YLD   B BKL    C YLD    C BKL    D CRP

  1     0.59*********    0.95     0.03    0.36     0.44     -0.00
 23     1.03*********    1.50     0.00    0.75*********      0.28
  4     0.59    -0.00    0.95     1.21    0.36     2.09     -0.00
  5     0.57    -0.00    0.95*********    0.36*********     -0.00
```

Figure A-1 Computer Program Results for Haynes 188 TPS have zero margins under two conditions. Element 2-3 has a zero margin in buckling under condition B. The margin of safety reflects the reserve strength after the appropriate factor of safety has been applied. The results for the optimized Rene' 41 panel are given in Figure A-2.

```
*****RE  41 PANEL OPTIMIZATION*****

WHAT ARE PO,DO,PMAX,BO,DB,BMAX,BETA ?

.0,1.5,2.,.0,.782,1.,.61
 0.0     1.50000 2.00000 0.0      0.78200 1.00000 0.61000

         WHAT IS TMIN ?

.005
 0.00500

         WHAT IS IPRT ?

0001
```

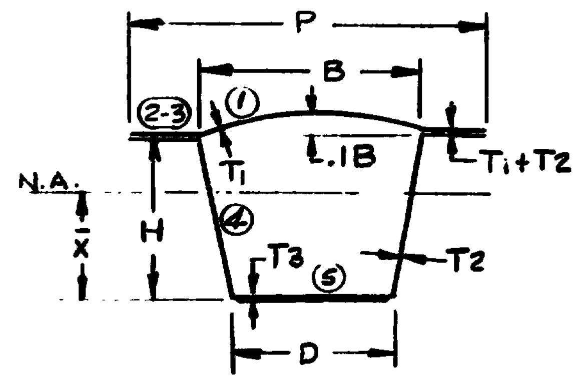


```
    P       B       T1      I       T2      D       T3    AREA     I/A    X BAR    A/P    WT/FT2   BEAD

 1.50000 0.78200 0.00725 0.43510 0.00709 0.43922 0.01222 0.02767 0.00101 0.31311 0.01845 0.79164    1

ELEM     A YLD    A BKL     B YLD   B BKL     C YLD    C BKL     D CRP

 1      1.73*********     2.35    -0.00     4.36     0.96      0.55
23      3.48*********     4.50     0.63     7.79*********      1.56
 4      0.74     -0.00    1.14    14.55     2.42     1.41     -0.00
 5      0.74     -0.00    1.14*********     2.42*********     -0.00
```

$\boxed{\beta = .61}$

Figure A-2 Computer Program Results for René 41 TPS

HAYNES Computer Program for Skin/Corrugation Optimization

```
      REAL MS(7), KCR
      DIMENSION F(7), G(7)
      ERT = 34.2*1000.**2
   99 WRITE(6,4)
    4 FORMAT(2X,//,2X,'WHAT ARE PO, DP, PMAX, BO, DB, BMAX, BETA ?',//)
      READ(5,13) PO,DP,PMAX,BO,DB,BMAX,BETA
      IF (PO .LT. 0.) GO TO 999
   13 FORMAT(6F4.0,I4,F4.0)
      WRITE(6,3)PO,DP,PMAX,BO,DB,BMAX,BETA
      WRITE(6,5)
    5 FORMAT(2X,/10X,'WHAT IS TMIN ?',/)
      READ(5,13) TMIN
      WRITE(6,3) TMIN
      WRITE(6,14)
   14 FORMAT(2X,/10X,'WHAT IS IPRT ?',/)
      READ(5,16) IPRT
   16 FORMAT(I4)
      WRITE(6,1)
    1 FORMAT(2X,///)
      IF( IPRT .EQ. 0 ) WRITE(6,2)
      P = PO
      B = BO
      DO 901 II = 1,5000
      P = P + DP
      IF ( P.GT.PMAX) GO TO 901
      B= BO
      DO 900 JJ = 1,5000
      B = B + DB
      IF(B.GT.P-.0) GO TO 901
      IF(B.GT.BMAX) GO TO 901
      H = 0.
      DH = .1
   50 H = H + DH
      FCREEP = 2770. + 1770.*(H+.1*B)
      XBAR = BETA*(H + 0.1*B)
      ARM = XBAR
      IF (BETA .LT. 0.5) ARM = H+.1*B-XBAR
      RINER = 1.15*.31668*P*50.*ARM/FCREEP
      KCR = EXP(.7355 + 1.1663*H/XBAR)
      T2 = H*SQRT((FCREEP*1.4*450.)/(ERT*1.15*50.*KCR))
      KCR = EXP(.7355 + 1.1663*H/(H-XBAR))
      ARG = .31668*P*350.*(H-XBAR)*1.4/(KCR*ERT*RINER)
      IF (ARG .LE. 0.) GO TO 50
      T2T = H*SQRT(ARG)
      IF (T2T .GT. T2) T2 = T2T
      T1 = .0051*(B + .[illegible])
      T11 = 1.4*1.3*(B+.[illegible])*.31668*P*350.*(H+.1*B-XBAR)
      T11 = T11/(.22*ERT*RINER)
      IDF = 0
```

```
      IF (T11.GT.T1) IRF = 1
      IF (T11.GT.T1) T1 = T11
      DT3 = 1.02345*B*T1*(H+B*.056493) + (P-3)*(T1+T2)*H + T2*H**2
      DT3 = DT3/(DETA*(H+.1*B))
      DT3 = DT3 - (1.02345*B*T1+(P-3)*(T1+T2)+2.*H*T2)
      IF(DT3.LT.0.) GO TO 50
      TEMP = SQRT(FCREEP*1.4*430./(3.62*ERT*1.15*50.))
      D = SQRT(DT3/TEMP)
      T3 = D*TEMP
      A = 1.02345*B*T1 + (P-3)*(T1+T2) + 2.*H*T2 + H*T3
      AX = 1.02545*B*T1*(H+B*.056493) +(P-3)*(T1+T2)*H + T2*H**2
      AX2=1.02345*B*T1*(H+B*.056493)**2 + (P-3)*(T1+T2)*H**2
      AX2 = AX2 + T2*H**3/2.
      XIT = T2*H**3/6.
      XBAR=AX/A
      XINER=AX2 + XIT - A*XBAR**2
      IF(ABS(XINER/RINER-1.) .LE. 0.001) GO TO 50
      IF(XINER .LT. RINER ) GO TO 50
      H = H- DH
      DH = DH/10.
      IF(DH.LE.1./(1000.**2)) GO TO 300
      GO TO 50
   50 CONTINUE
      AW=A/P
      W=AW*144.*0.33
      IF = 0
      F23 = SQRT(1.4*.31558*P*350.*(H-XBAR)/(3.62*ERT*XINER))*(P-3)
      IF (T1+T2 .LT. F23) IF = 1
    2 FORMAT(2X,/,
     1        2X,'  P          B          T1         H          T2         D          T3
     2 AREA       INA       X BAR      A/P       WT/FT2      READ',/)
      IF( IF .EQ. 1) GO TO 300
      IF( IPRT .EQ. 1 ) WRITE(6,2)
      WRITE(6,3)P,B,T1,H,T2,D,T3,A,XINER,XBAR,AW,W,IRF
    3 FORMAT(2X,12F9.5,I3)
      IF (IF .EQ. 1) GO TO 300
      IF ( IPRT .EQ. 1 ) GO TO 333
  333 CONTINUE
      FCREEP = FCREEP
      FTYRT= 55000.
      FTYHOT = 11000.
      EHOT = 13.7*1000.**2
      FAKE = (1.*1000.**2)**2
      CON3 = P*.31558*XBAR/XINER
      CON2 = P*.31558*(H-XBAR)/XINER
      CON1 = P*.31558*(H+.1*B-XBAR)/XINER
      WRITE(6,3)
C         ELEMENT NO. 1
      F(1) = 430.*CON1
      F(2) = F(1)
```

```
      F(3) = 350.*CON1
      F(4) = F(3)
      F(5) = 100.*CON1
      F(6) = F(5)
      F(7) = 50.*CON1
      G(1) = FTYRT/1.15
      G(2) = FAKE
      G(3) = FTYRT/1.15
      G(4) = .22*ERT*T1/1.3/(B+.03)/1.4
      G(5) = FTYHOT/1.15
      G(6) = G(4)*EHOT/ERT
      G(7) = FCREEP/1.15
      IRET = 1
      GO TO 500
  100 CONTINUE
C               ELEMENT NOS. 2 & 3
      F(1) = 430.*CON2
      F(2) = F(1)
      F(3) = 350.*CON2
      F(4) = F(3)
      F(5) = 100.*CON2
      F(6) = F(5)
      F(7) = 50.*CON2
      G(4) = 3.62*ERT*((T1+T2)/(B-D))**2/1.4
      G(6) = G(2)*EHOT/ERT
      IRET = 23
      GO TO 500
  200 CONTINUE
C               ELEMENT NO. 4
      F(1) = 430.*CON3
      F(2) = F(1)
      F(3) = 350.*CON3
      F(4) = F(3)
      F(5) = 100.*CON3
      F(6) = F(5)
      F(7) = 50.* CON3
      KCR = EXP(.7355 + 1.1663*H/XBAR)
      G(2) = KCR*ERT*(T2/D)**2/1.4
      KCR = EXP(.7355 + 1.1663*H/(1-XBAR))
      G(4) = KCR*ERT*(T2/D)**2/1.4
      G(6) = G(4)*EHOT/ERT
      IRET = 4
      GO TO 500
  400 CONTINUE
C               ELEMENT NO. 5
      G(2) = 3.62*ERT*(T3/D)**2/1.4
      G(4) = FAKE
      G(6) = FAKE
      IRET = 5
      GO TO 500
```

```
  490 CONTINUE
      GO TO 300
  500 CONTINUE
      DO 510 I = 1,7
  510 MS(I) = G(I)/F(I) - 1.
    9 FORMAT(2X,/2X,'ELEM     A YLD    A BKL     B YLD    B BKL     C YLD
     1 C BKL     D CRP',/)
      WRITE(6,10)IRET,(MS(I),I=1,7)
   10 FORMAT(I4,7F9.2)
      IF(IRET.EQ.23) GO TO 200
      GO TO (100,100,100,400,490),IRET
  899 CONTINUE
      IF (T1 .GT. TMIN) GO TO 901
  900 CONTINUE
  901 CONTINUE
      GO TO 99
  999 CALL EXIT
      END
 EOF:
```

APPENDIX B

CORRUGATION SCULPTURING PROFILE DETERMINATION

To minimize corrugation mass, the lower horizontal flat of the corrugation was sculptured. The sculpturing profile was designed to match the bending moment and to maintain the area and buckling allowable stress. The design equations and analysis procedure are presented, including the profile for the Haynes 188 and the Rene' 41 panel.

d & t_3 were obtained from optimization procedures

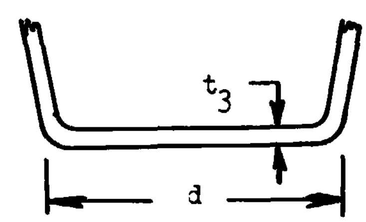

For manufacturing, the lower flange must be altered to this geometry (t_2 from optimization)

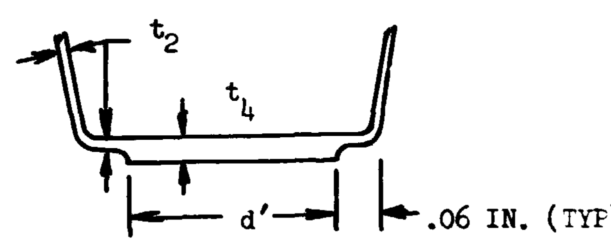

Therefore, select d' & t_4 such that the area and buckling allowable remain the same.

AREA

$$d' \cdot t_4 + 2(.06)(t_2) = d \cdot t_3 \qquad (1)$$

BUCKLING

Since lateral bending stiffness controls the buckling, select d' and t_4 to provide the same, or less, deflection.

LOWER FLANGE (Cont'd)

$$\Delta_1 = \frac{M\left(\frac{d}{2}\right)^2}{2EI}$$

$$I = \frac{1}{12}(t_3)^3$$

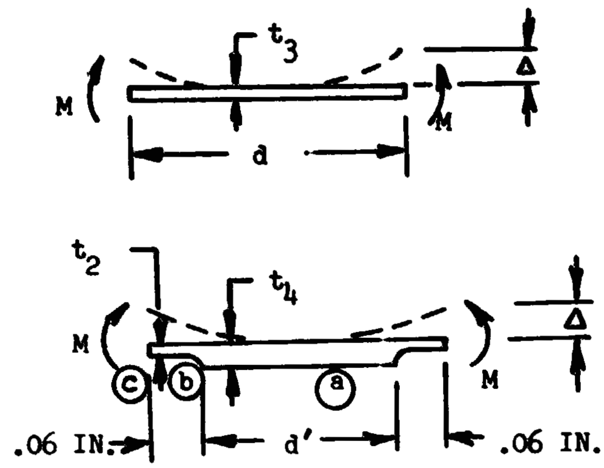

$$\Delta_2 = \Delta_{ba} + \theta_{ba}(.06) + \Delta_{cb}$$

$$\left.\begin{aligned} \Delta_{ba} &= \frac{M\left(\frac{d'}{2}\right)^2}{2EI} \\ \theta_{ba} &= \frac{M\left(\frac{d'}{2}\right)}{EI} \end{aligned}\right\} \quad I_{ba} = \frac{1}{12}(t_4)^3$$

$$\Delta_{cb} = \frac{M(.06)^2}{2\ EI} \qquad I_{cb} = \frac{1}{12}(t_2)^3$$

$$\Delta_2 = \frac{M}{E}\ \frac{1}{1/12}\left\{\frac{\left(\frac{d'}{2}\right)^2}{2t_4{}^3} + \frac{\left(\frac{d'}{2}\right)(.06)}{t_4{}^3} + \frac{(.06)^2}{2t_2{}^3}\right\}$$

$$= \left\{\frac{(d')^2}{8\ t_4{}^3} + \frac{.06}{2}\ \frac{d'}{t_4{}^3} + \frac{(.06)^2}{2} \cdot \frac{1}{t_2{}^3}\right\}\left(\frac{12M}{E}\right) \qquad (2)$$

Assume

$$\bar{d} - d' = 2(.06) \qquad (2a)$$

$$\alpha = \frac{d'}{\bar{d}} = \frac{d'}{d' + .12} \qquad (2b)$$

$$\therefore \left\{ \frac{1}{8} \frac{(\alpha\bar{d})^2}{t_4^3} + \frac{(\bar{d}-\alpha\bar{d})}{4} \cdot \frac{(\alpha\bar{d})}{t_4^3} + \frac{(d-\alpha d)^2}{8t_2^3} \right\} \left(\frac{12M}{E}\right)$$

which must be less than: $\frac{12M}{E}\left(\frac{d^2}{8t_3^3}\right)$

$$\bar{d}^2 \left| \frac{2\alpha-\alpha^2}{t_4^3} + \frac{(1-\alpha)^2}{t_2^3} \right| \leq \frac{d^2}{t_3^3} \qquad (3)$$

The left side of Eq. (3) is equivalent to a span of $\bar{d}$ with an equivalent thickness of $\bar{t}$, so that :

$$\frac{2\alpha-\alpha^2}{t_4^3} + \frac{(1-\alpha)^2}{t_2^3} \equiv \frac{1}{\bar{t}^3} \qquad (4)$$

For Local Buckling:

$$F_{crel} = K_{cr} E \left(\frac{t_3}{d}\right)^2 = K_{cr} E \left(\frac{\bar{t}}{\bar{d}}\right)^2 \qquad (5a)$$

$$\text{or} \qquad \bar{d} = \bar{t} \left(\frac{d}{t^3}\right) \qquad (5b)$$

Procedure

1. Assume d^1
2. Solve (1) for t_4
3. Solve (2b) for α
4. Solve (4) for $\bar{t}$
5. Solve (5b) for $\bar{d}$
6. Solve (2a) for d'

LOWER FLANGE (Cont'd)

7. Compare d' (Step 6) with d' (Step 1)

a. If $d_6' \neq d_1'$ use new d' and return to step 1.

b. If $d_6' \cong d_1'$ check (3) for validity

	Haynes 188	Rene' 41
d	.698 IN.	.439 IN.
t_3	.0129 IN.	.0122 IN.
t_2	.0055 IN.	.0071 IN.
d'	.566 IN.	.321 IN.
$\bar{d}$	.686 IN.	.441 IN.
t_4	.0147 IN.	.0140 IN.
EQ (4) Left	230170*	105860 IN.
EQ (4) Rt.	226960*	106130 IN.

*Approx. 1% too high - Acceptable

Since the bending moment for all conditions is a maximum at mid-span and varies to zero at the ends, the width of the chem-mill pad was varied to minimize weight.

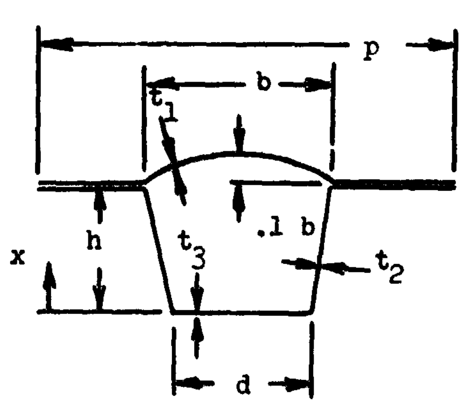

From Appendix A Page A-7

$$A = 1.02646\ bt_1 + (p-b)(t_1+t_2) + 2ht_2 + dt_3$$

$$Ax = 1.02646\ bt_1\ [h+b(.066493)] + (p-b)\ (t_1+ t_2)h + t_2h^2$$

$$A_x^{\ 2} = 1.02646\ bt_1\ [h+b(.066493)]^2 + (p-b)\ (t_1+t_2)h^2 + \frac{1}{2}\ t_1h^3$$

$$I_{oo} = \frac{1}{6}\ t_2h^3$$

$$\overline{X} = Ax/A$$

$$I_{NA} = A_x^{\ 2} + I_{oo} - A\overline{X}^{\ 2}$$

Let $dt_3 = A_5$

	Haynes 188	Rene' 41
p	1.50	1.50
b	.782	.782
t_1	.0051	.0073
h	.633	.435
t_2	.0055	.0071
d	.698	.439
t_3	.0129	.0122
A	$.01867 + A_5$	$.02237 + A_5$
A_x	.0098256	.0086947
$A_x^{\ 2}$	.0056679	.0036384
I_{oo}	.002325	.0000974

1368-070W

Lower Flange (Cont'd)

It can be seen that as A_5 decreases, $\bar{X}$ increases so that the lower flange is always more critical than the upper bead. Further, since as the width of the chem-mill pad is reduced, the local buckling allowable decreases. The creep allowable is always constant so that buckling under condition A is critical.

$$\text{Set} \quad f_b = \frac{M_{ALL}\bar{X}}{I_{NA}} = F_{ALL} = \frac{F_{CREL}}{1.4} = \frac{K_{CR}}{1.4} E\left(\frac{\bar{t}}{\bar{d}}\right)^2 \quad K_{CR} = 3.62 \text{ (GAC SM B5.11.11-1)} \tag{6}$$

$$E = 34.2 \times 10^6 \text{psi - Haynes 188}$$
$$= 31.6 \times 10^6 \text{psi - Rene' 41}$$

Procedure:

1. Assume d'
2. Calculate α from (2b)
3. Calculate $\bar{t}$ from (4)
4. Calculate F_{CREL} from (5a)
5. Calculate M_{ALL} from (6)
6. Calculate X from (7) below.

M_{ALL} is plotted against d' in Fig. B-1

The applied bending moment is given by:

$$W = \frac{P_R}{144} \cdot p = \frac{430}{144}(1.5) = 4.479 \text{ \#/IN.}$$

$$M = W\left[\frac{L^2}{8} - \frac{X^2}{2}\right] \tag{7}$$

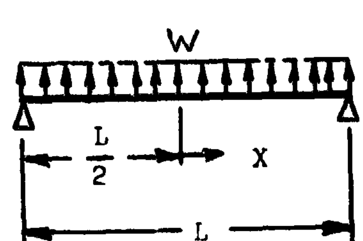

(L = 19.1 IN.)

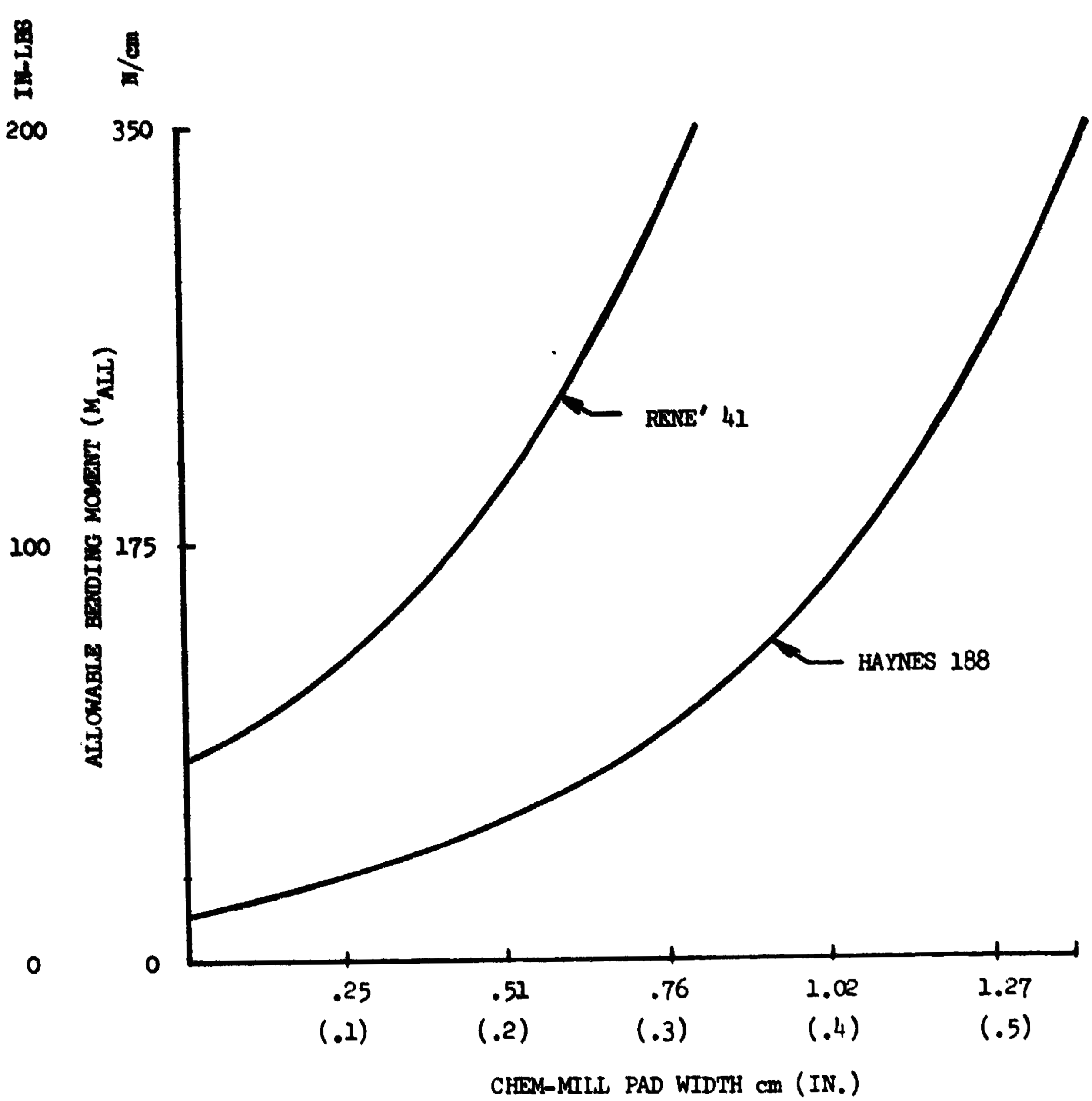

FIGURE B-1 ALLOWABLE BENDING MOMENT vs CHEM-MILL PAD WIDTH

TABLE B-1

DISTANCE X FROM MID-SPAN		CHEM MILL PAD WIDTH d′ (1)			
		HAYNES 188		RENE′ 41	
in	cm	in	cm	in	cm
0	0	.566	1.44	.321	.815
2	5.08	.560	1.42	.315	.800
4	10.16	.525	1.33	.283	.719
6	15.24	.460	1.17	.217	.551
7	17.78	-	-	.163	.414
8	20.32	.320	.813	.060	.152
8.33	21.16	-	-	.00	0
9.55	24.26	0.00	0.0	-	-
WT SAVED (CURVED PROFILING)		.168 kg/m^2 (.0344 lb/ft^2)		.092 kg/m^2 (.0188 lb/ft^2)	
WT SAVED (STRAIGHT PROFILING)		.145 kg/m^2 (.0299 lb/ft^2)		.080 kg/m^2 (.0163 lb/ft^2)	

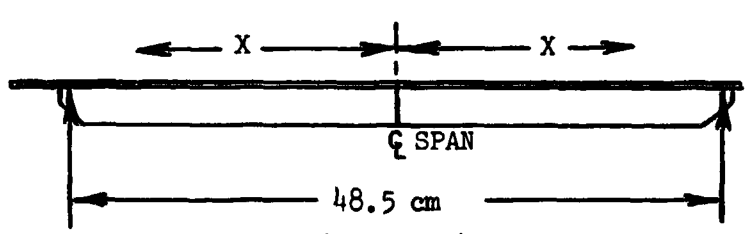

1368-026W

(1) The d′ shown are minimums required. Actual d′ will be slightly larger because straight line chem-milling will be used.

APPENDIX C

DETAIL STRESS ANALYSIS - HAYNES 188 TPS

The detail stress analysis of the Haynes 188 thermal protection system is given in the following pages. Included is the analysis for the surface panel to support rib attachments, the computer program developed for the support rib optimization, and the drag bracket detail analysis. The effect of panel spanwise thermal expansion on the support rib is also presented.

SURFACE PANEL/SUPPORT RIB ATTACHMENT ANALYSIS

MAXIMUM SHEAR LOAD, V

$$V = \frac{1}{2}\, pP_R\, \ell = \frac{1}{2}\,(1.5)\, P_R\,(20) = 15\, P_R \quad (P_R \text{ in psi})$$

Condition	P_R (lb/ft^2)	V (lb)
A	-430	-44.8 LIMIT
B	350	36.5 LIMIT
C	100	10.4 LIMIT
D	50	5.2 LIMIT

CORRUGATION SIDEWALL BUCKLING

Each wall carries $\frac{1}{2}V$ = 22.4 lb max

$$f_s = \frac{\frac{1}{2}V}{ht} = \frac{22.4}{.633\,(.0055)}$$

$= 6435$ psi

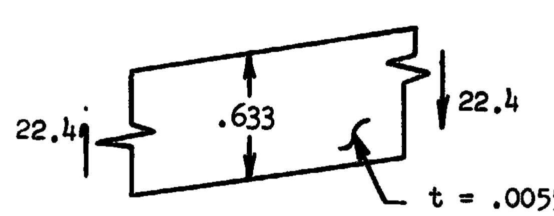

For a long plate S.S. all sides,

$$K_{cr} = 4.8$$

$$F_{crel} = K_{cr} E \left(\frac{t}{h}\right)^2 = 4.8(34.2\text{x } 10^6)\left(\frac{.0055}{.633}\right)^2 = 12390\text{psi}$$

$$\text{M.S.} = \frac{12390}{1.4(6435)} - 1 + .37$$

CORRUGATION SIDEWALL (Cont'd)

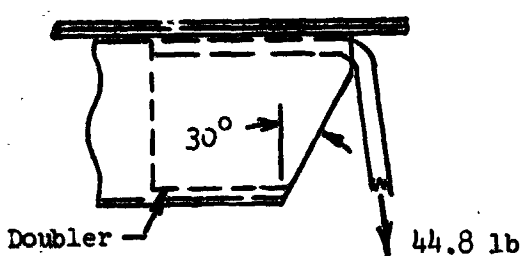

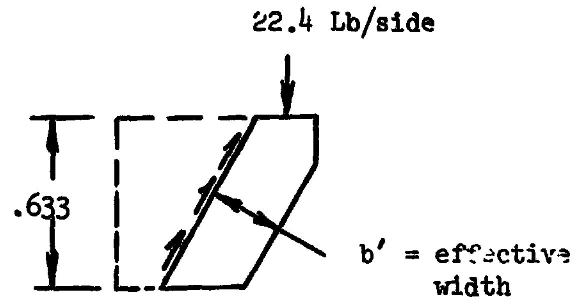

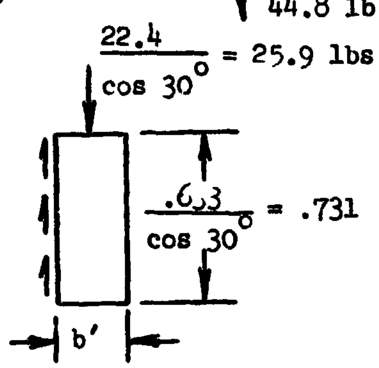

THICKNESS OF

Doubler = .015 in.

Sidewall = .0055 in.

.0205 in.

$$P_{cr} = \frac{\pi^2 EI}{M L^2}$$

For a pin-ended column with shear along the length, M = .53 (GAC S.M. B3.44.31-1)

$$E = 34.2 \times 10^6$$

$$P_{cr} = 1.4(25.9) = 36.3^{\#}.$$

$$\therefore I = \frac{P_{cr} M L^2}{\pi^2 E} = \frac{36.3(.53)(.731)^2}{\pi^2(34.2 \times 10^6)} = 3.05 \times 10^{-8} \text{ IN}^4$$

$$I = \frac{b' t_{TOTAL}^3}{12}$$ For $t_{TOTAL} = .0205$ IN, $b' = .042$ IN

M.S. = AMPLE

BENDING OF FLAT BETWEEN BEADS

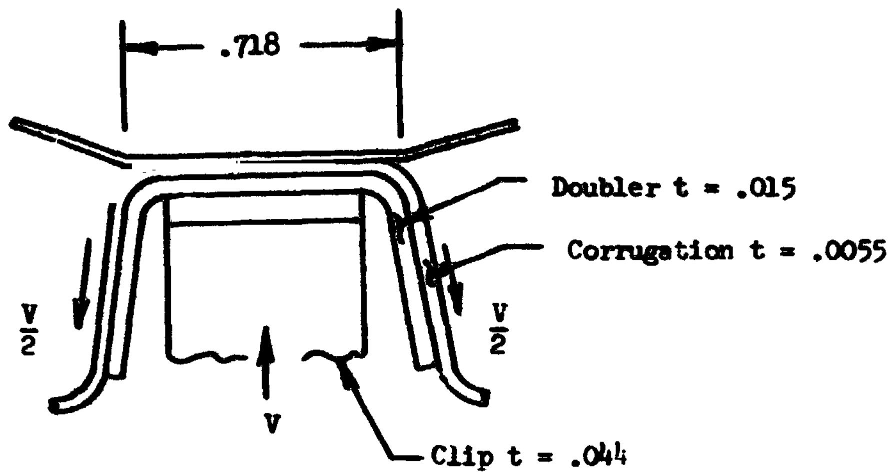

Condition A is critical, V = -44.8 lb. limit.

Treat layup as a beam of thickness of .0256 in.

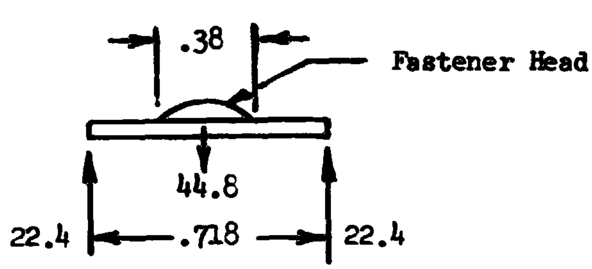

$$M = 22.4 \; \frac{.718 - .38}{2} = 3.786 \text{ in lb. limit}$$

Use 2 times the head dia. for the effective width.

$$\therefore f_b = \frac{6M}{bt^2} = \frac{6(3.786)}{2(.38)\,(.0256)^2} = 45{,}610 \text{ psi}$$

$F_{ty} = F_{cy} = 5$ [illegible] 0 psi

M. [illegible] $\frac{[illegible]}{(45610)} - 1 = .04$

FLEXIBLE RIB. (DWG AD1001-102)

DESIGN CONDITIONS

Condition	P_R (psf)	V(lb)
A	-430	-44.8
B	350	36.5
C	100	10.4
D	50	5.2
*		

* THERMAL EXPANSION:

$$\Delta = \alpha\Delta TL = 9.7 \times 10^{-6}\text{(1)}\ \text{IN/IN/}^{\circ}\text{F}\ (1800-70)\ ^{\circ}\text{F}\ (20-1.3)\ \text{IN}$$

$$= 0.314\ \text{IN}$$

(1) Ref 3-3

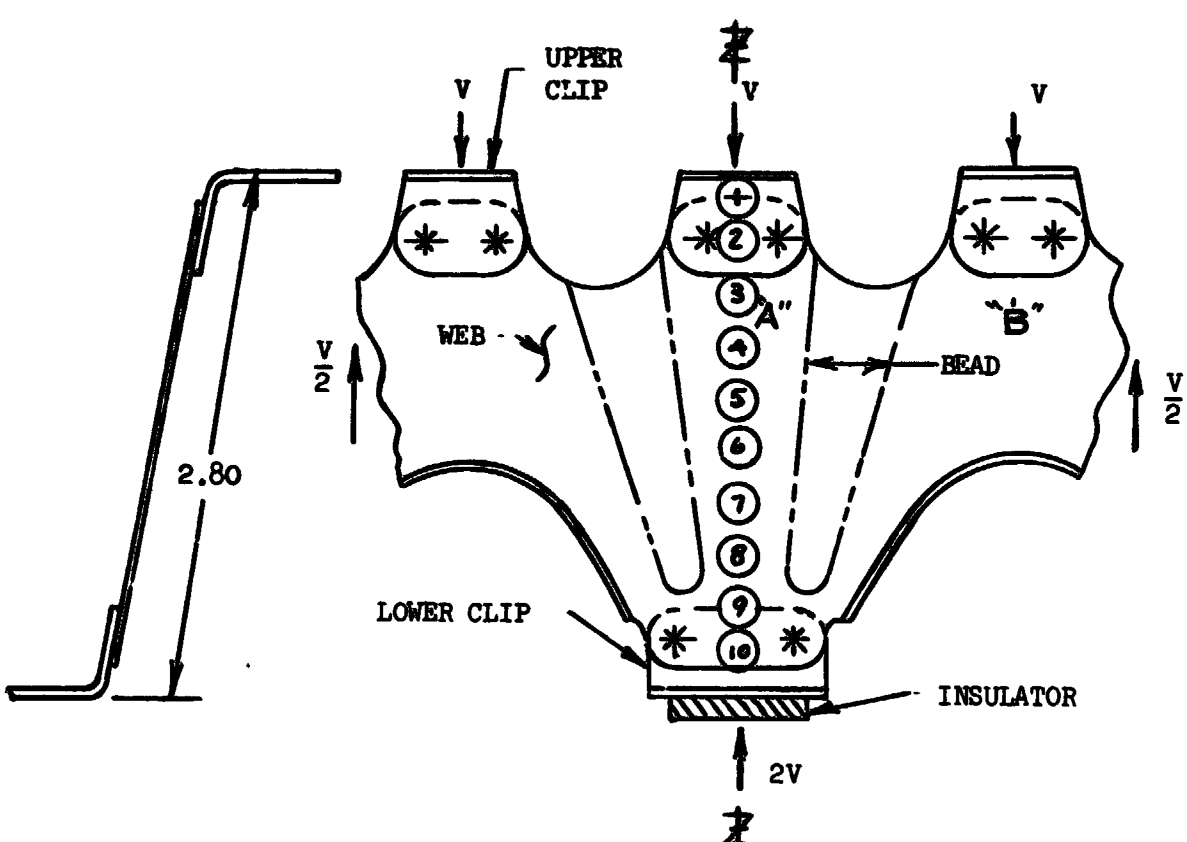

LATERAL THERMAL EXPANSION IN RIB

Between points A & B.

$$\Delta = \alpha\Delta TL = 9.7 \times 10^{-6}\,(1800-70)(1.5) = .0252 \text{ IN}$$

Using the method of Castigliano and neglecting secondary deflections:

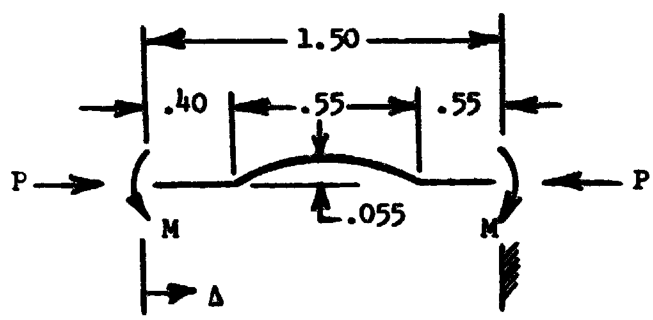

$$\Delta = \frac{1}{2EI}\,\{.35014M + .01513P\} \equiv .0252$$

$$\theta = \frac{1}{2EI}\,\{1.5M + .01926P\} \equiv 0.$$

$$P = 4.7414\ EI,\quad M = -.01284P$$

Maximum moment at top of bead, $\bar{M}$

$$\bar{M} = P(.055) + M = .19990\ EI$$

$$f_b = \frac{6\bar{M}}{bt^2} \qquad E = 13.7 \times 10^6 \text{ psi}$$

$$I = \frac{bt^3}{12(1-u^2)},\quad u = .29$$

$$= .09099bt^3$$

$$\therefore f_b = \frac{6(.19990)\,(13.7 \times 10^6)\,(.09099bt^3)}{bt^2}$$

$$= 1.495 \times 10^6\ t$$

LATERAL THERMAL EXPANSION (Cont'd)

It was shown that for:

$\varepsilon = .0034$ IN/IN, the yield stress was not exceeded, using a F.S. of 1.15.

$$F_{ALL} = \frac{\varepsilon E}{1.15} = \frac{.0034\ (13.7 \times 10^6)}{1.15} = 40{,}500 \text{ psi}$$

For $f_b = F_{ALL}$, $\quad t_{ALL} = .027$ IN.

$\therefore$ As long as the web is $\leq .027$ IN., thermal strain is not critical.

Web Buckling - Cond B (Ref Pg C-3)

$$V = 36.5^{\#}/\cos 11^{\circ} = 37.2^{\#} \text{ limit.}$$

Assume web is symmetric about Z-Z and work one side for section properties. Treat as a pin-ended column with varying inertia. Ref. Timoshenko, "Theory of Elastic Stability".

Half Section:

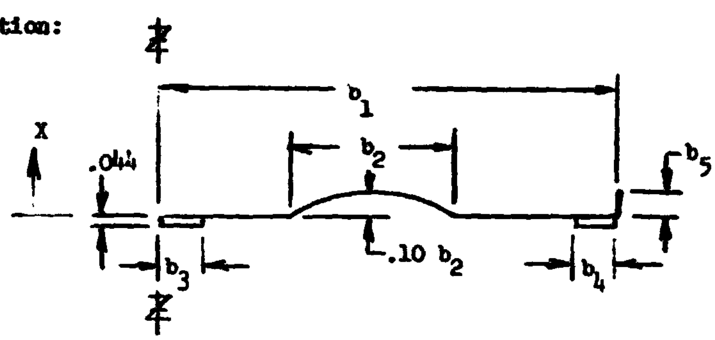

Section	b_1	b_2	b_3	b_4	b_5
1			.32	.32	
2	.80		.32	.32	
3	1.50	.55			
4	1.50	.48			
5	1.50	.41			
6	1.50	.34			
7	.97	.27			.15
8	.80	.20			.15
9	.62				.15
10			.48		

SECTION PROPERTIES

$$A = t\,[b_1 + .02645\, b_2 + (b_5-t)] + .044\,(b_3+b_4)$$

$$AX = t\left[.06825\, b_2^2 + .5(b_5-t)(b_5)\right] - .000968\,(b_3+b_4)$$

$$AX^2 = t\left[.004538\, b_2^3 + .25(b_5-t)(b_5)^2\right] + .0000213\,(b_3+b_4)$$

$$I_{oo} = (b_1-b_2)\frac{t^3}{12} + .0009158\, b_2^3\, t + (b_5-t)^3\frac{t}{12} + \frac{b_3+b_4}{12}\,(.044)^3$$

$$\bar{x} = AX/A, \quad I_{NA} = AX^2 + I_{oo} - A\bar{x}^2$$

Timoshenko's method involves assuming a deflected shape for the column and solving for the actual shape. The resultant shape is then used for the new assumption and the process repeated. When the assumed and calculated shapes are within some tolerance, say 0.1%, at all sections, the critical buckling load can be calculated.

Because of the iterative nature of the problem and the considerable number of arithmetic operations involved, a computer program, "Ribs" was written. This program is presented on pages C-19 and C-20.

Several thicknesses were assumed, and the resultant critical load curve is presented in Figure C-1.

The flexible rib has an equivalent applied load of 74.4 lb. limit (104.2 lb ultimate) for a 3 inch section of web during condition B. The required web thckness is less than 0.005 in (Ref. Fig. C-1). The minimum thickness was chosen as 0.008 in. due to handling and fabrication considerations.

$$M.S. = \frac{250}{104.2} - 1 = \text{AMPLE}$$

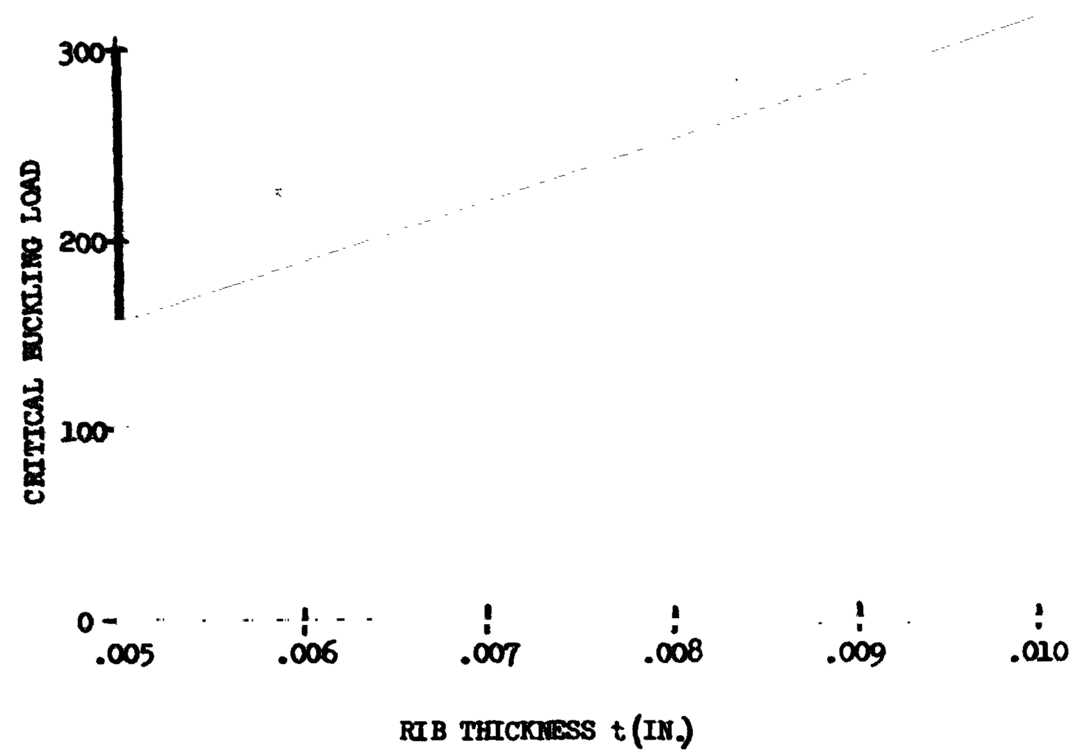

FIGURE C-1 CRITICAL BUCKLING LOAD VS RIB THICKNESS

WEB BUCKLING (Cont'd)

LOCAL BUCKLING -

(Over arches between beads.)

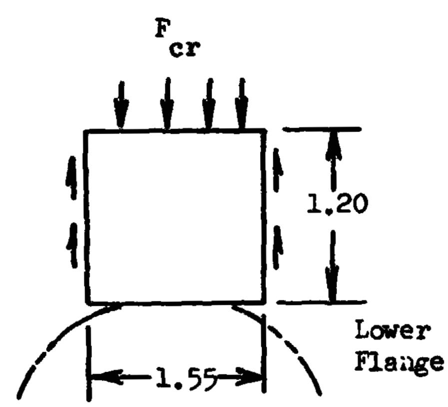

$\frac{b}{a} = \frac{1.2}{1.55} = .77$, $K_{cr} = 2.24$ GAC S.M. B5.11.11-2

$$F_{cr} = K_{cr}\, E \left(\frac{t}{b}\right)^2$$

$$= 2.24\ (34.2 \times 10^6) \left(\frac{.008}{1.2}\right)^2$$

$$= 3405 \text{ psi}$$

$P_{cr} = 3405\ (1.55)\ (.008) = 42.2$ lb.

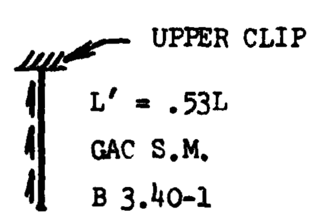

Consider equivalent length:

$$\therefore P'_{cr} = P_{cr}\left(\frac{L}{L'}\right)^2 = 42.2\left(\frac{1}{.53}\right)^2$$

$$= 150.2 \text{ lb.}$$

$$M.S. = \frac{150.2}{1.4(36.5)} - 1 = \text{AMPLE}$$

BUCKLING BETWEEN BEADS

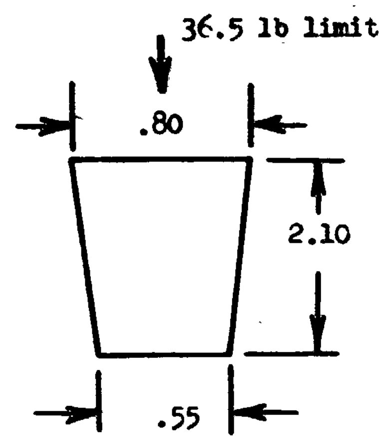

$$\frac{b_1}{b_2} = \frac{.55}{.80} = .77$$

$$\frac{a}{b_2} = \frac{2.1}{.80} = 2.63$$

$K_{cr} = 4.65$ (GAC SM B5.11.40-1)

$$F_{cr} = K_{cr} E \left(\frac{t}{b_2}\right)^2$$

$$= 4.65\,(34.2 \times 10^6)\left(\frac{.008}{.8}\right)^2 = 15900 \text{ psi}$$

$$P_{cr} = 15900\,(.8)\,(.008) = 101.8$$

$$M.S. = \frac{101.8}{1.4(36.5)} = 1 = .99$$

SPANWISE THERMAL EXPANSION

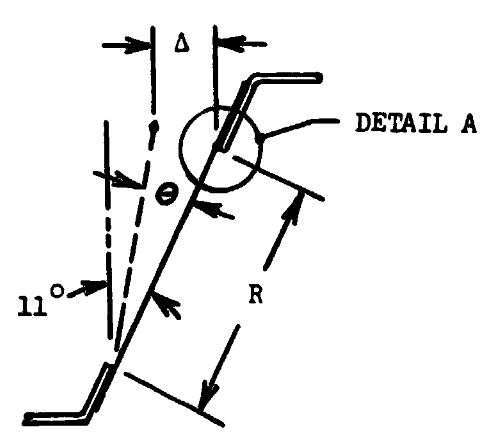

$\Delta = .314$ IN

$R = 1.88$ IN clear between clips

$R\sin 11^\circ - R\sin\theta = \Delta$

$$\theta = 9.6^\circ = .168 \text{ radians}$$

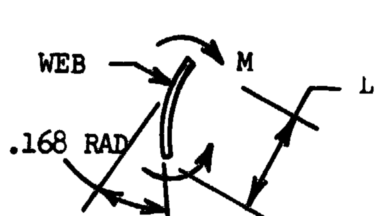

SPANWISE THERMAL EXPANSION (Cont'd)

Detail A

$$\theta = \frac{ML}{EI} \quad \text{and} \quad f_b = \frac{6M}{bt^2}$$

$$\therefore f_b = \frac{6EI\theta}{Lbt^2} \quad \text{and} \quad I = \frac{bt^3}{12}$$

$$f_b = \frac{Et\theta}{2L} \quad \text{and} \quad \epsilon = \frac{f_b}{E}$$

$$\epsilon = \frac{t\theta}{2L}$$

At 1800°F, the allowable strain at yield is 0.0034 in/in. Using a factor of safety of 1.15, the length, L is

$$L = \frac{t\theta}{2\frac{\epsilon}{1.15}} = \frac{.008\ (.168)}{2\ \frac{(.0034)}{1.15}} = .23 \text{ IN.}$$

This dimension is required at both the top and bottom web/clip interfaces. The accompanying sketch shows the extent of the 0.23 inch dimension from the edges of the clips. It can be seen that sufficient clearance exists, except at the bottom where it overlaps the beads "A". This latter situation is deemed to be acceptable since the beads are very shallow in this area.

The bending near "B" is across the bendline so that the stiffness of the bead is not a factor. Since a considerable amount of bending material is still available (non-cross hatched area) this analysis is considered to be quite conservative

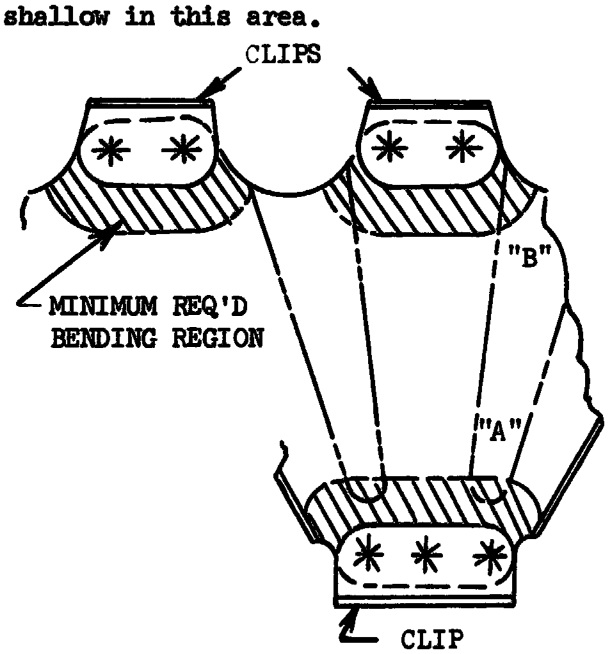

UPPER CLIP

$$M = 44.8\left(.34 - \frac{.31}{2}\right)$$

$$= 8.29 \text{ IN Lb}$$

$$f_b = \frac{6M}{bt^2}$$

$$= \frac{6(8.29)}{.54(.044)^2}$$

$$= 47580 \text{ psi}$$

$$f_{ty} = 55 \text{ ksi}$$

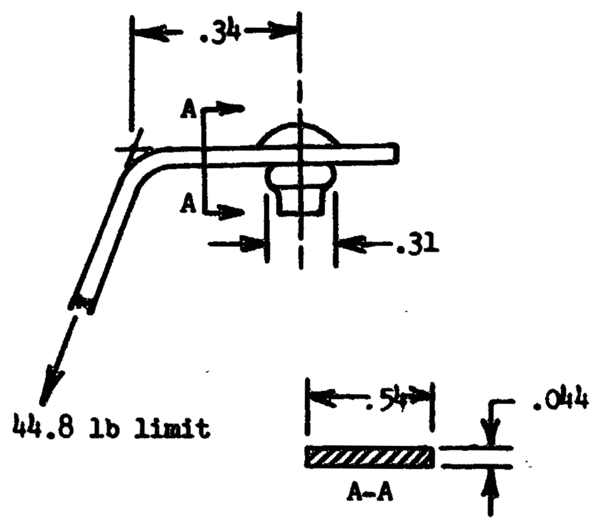

$$M.S. = \frac{55000}{1.15(47580)} - 1 = .00$$

LOWER CLIP

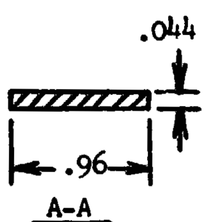

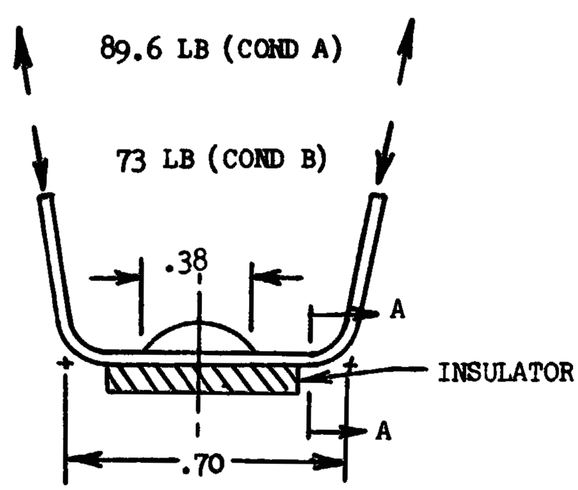

COND A

$$M = 89.6 \; \frac{.70-.38}{2} = 14.34 \text{ IN}^{\#}$$

$$f_b = \frac{6(14.34)}{.96(.044)^2} = 46{,}290 \text{ psi}$$

$$F_{ty} = 55 \text{ ksi}$$

$$M.S. = \frac{55000}{1.15(46290)} - 1 = .03$$

COND B

$M = 73\ (.085) = 6.21$ IN lb.

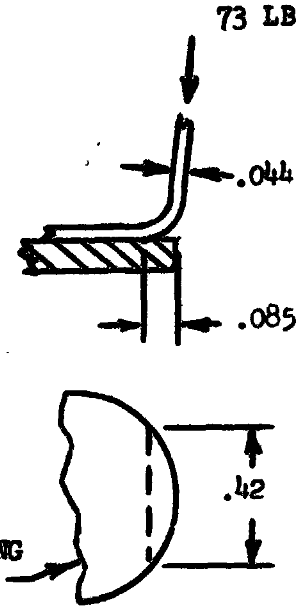

$$f_b = \frac{6(6.21)}{.42(.044)^2} = 45790 \text{ psi}$$

$F_{ty} = 55$ ksi

$$M.S. = \frac{55000}{1.15(45790)} - 1 = .04$$

FIXED RIB

DESIGN CONDITIONS

CONDITION	P_R(psf)	V(lb.)
A	-430	-89.6
B	350	73.0
C	100	20.8
D	50	10.4

LATERAL THERMAL EXPANSION

See flexible rib analysis,

$t_{ALL} \leq 0.027$ IN (Ref. Pg. C-6)

WEB BUCKLING

Equivalent applied load = 2V

$$2V = 2(73) = 146 \text{ lb. Limit}$$

$$= 204.4 \text{ lb ULT.}$$

For $t = .008$, $P_{cr} = 250$ lb (Ref. Fig. C-1)

$$M.S. = \frac{250}{204.4} - 1 = .22$$

Buckling over arches, $P_{cr} = 150.2$ lb (Ref. Pg. C-8)

$$M.S. = \frac{150.2}{1.4(73.0)} - 1 = .46$$

Buckling between beads

$$P_{cr} = 101.8 \text{ lb (Ref. Pg. C-8)}$$

$$M.S. = \frac{101.8}{1.4(73)} - 1 = .00$$

UPPER CLIPS:

COND. A. critical,

V = 89.6 lb limit

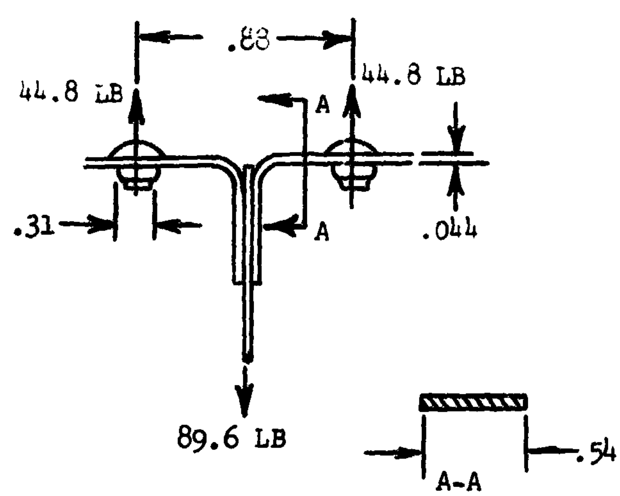

$L' = .88 - .31 = .57$ IN.

$$M = \frac{PL'}{8} = \frac{89.6\,(.57)}{8}$$

$$= 6.38 \text{ IN}^{\#}$$

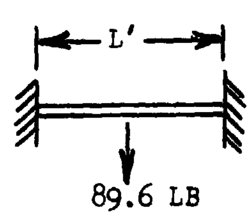

$$f_b = \frac{6M}{bt^2} = \frac{6(6.38)}{.54\,(.044)^2}$$

$$= 36,640 \text{ psi}$$

UPPER CLIPS: (Cont'd)

$F_{ty} = 55$ ksi

$$M.S. = \frac{55000}{1.15\ (36640)} - 1 = .30$$

(COND. B)

$M = 44.8(.132) = 5.91$ IN#

$$f_b = \frac{6M}{bt^2} = \frac{6(5.91)}{.54(.044)^2} = 33940 \text{ psi}$$

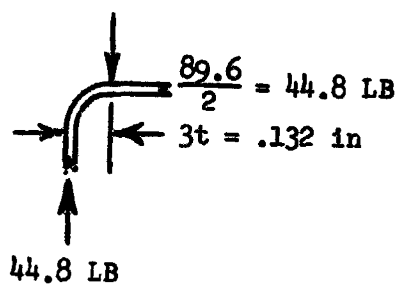

$F_{ty} = 55000$ psi

$$M.S. = \frac{55000}{1.15\ (33940)} - 1 = .40$$

LOWER CLIPS

(COND. A)

$L' = .74 - .31 = .43$

$$M = \frac{PL'}{8} = \frac{179.2(.43)}{8}$$

$= 9.63$ IN#

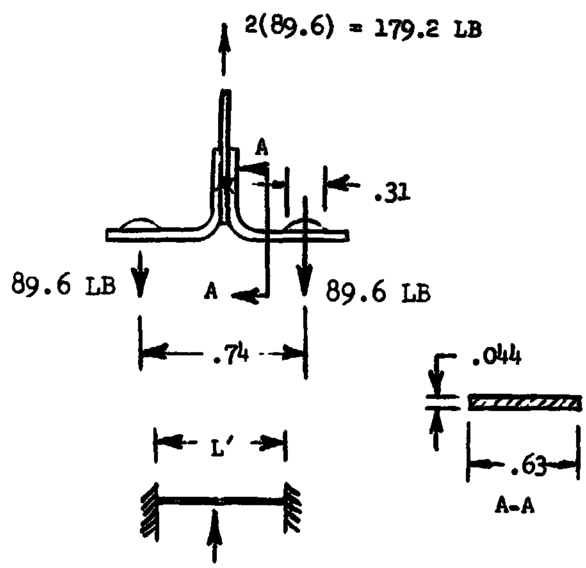

$$f_b = \frac{6M}{bt^2} = \frac{6(9.63)}{.63\ (.044)^2}$$

$= 47380$ psi

$$M.S. = \frac{55000}{1.15\ (47380)} - 1 = .00$$

$F_{ty} = 55$ ksi

(COND. B)

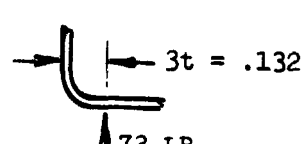

$M = 73(.132) = 9.64$ IN#

$$f_b = \frac{6(9.64)}{.63(.044)^2} = 47400$$

$$M.S. = \frac{55000}{1.15\ (47400)} - 1 = .00$$

DRAG BRACKET:

The load P is reversible and is caused by mechanically induced vibration:

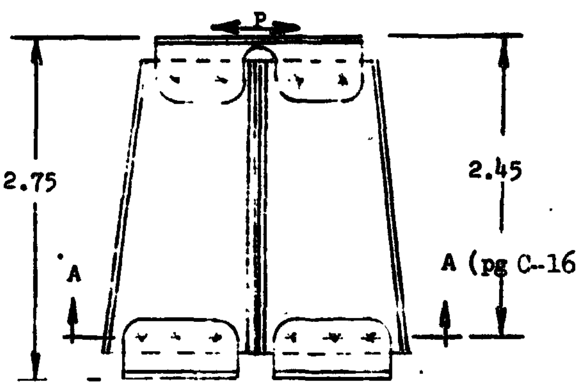

DESIGN "G" LEVEL:

Ref: MC 621-005, Rev. D, "Wing/Structure, Subsystems, Technical Requirements for", Paragraph 3.2.5.2 Flight Environment

K. Vibration

1. Random Vibration

ii. Orbiter Main Engine Burn

$$\left.\begin{aligned} f_o &= .15 \\ \omega &= 2000 \text{ Hz} \end{aligned}\right\} \text{Worst Case}$$

$$g = \sqrt{\frac{f_o \, \omega q}{4}}$$

q = magnification factor, taken as 10 (typical for secondary structure)

$$= \sqrt{\frac{.15(2000)\,(10)}{4}}$$

$$= 27.4 \longrightarrow \text{Use 30 g's}$$

STRUCTURE WEIGHT:

Panel plus upper clips

$$Wt = (.875 + .0440 + .0386) \text{ lb/ft}^2$$

$$= .9576 \text{ lb/ft}^2$$

Drag brackets are spaced every 40 inches streamwise and every 12 inches laterally

$$A = \frac{12(40)}{144} = 3\ 1/3\ ft^2$$

$$P = gW_tA = \pm\ 30\ (.9576)\ (3\ 1/2) = \pm\ 95.8\ \text{lb. limit.}$$

BRACKET

WEB SHEAR:

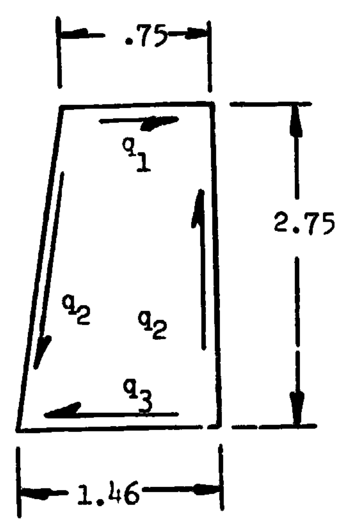

$$q_1 = \frac{\frac{1}{2}\ (95.8)}{.75} = 63.9^{\#}/IN$$

$$q_2 = \frac{\frac{1}{2}\ (94.8)(2.75)}{1.46(2.75)} = 32.8^{\#}/IN$$

$$q_3 = \frac{32.8\ (2.75)(.75)}{1.46\ (2.75)} = 16.9^{\#}/IN$$

$$f_{max} = \frac{63.9}{.015} = 4260\ psi$$

SHEAR BUCKLING.

Assume $\frac{a}{b} = \frac{1.46}{2.75} = .53$

$K_{cr} = 5.9$ (GAC SM. B5.11.12-1)

$$F_{crel} = K_{cr}\ E\ (\frac{t}{b})^2$$

$$= 5.9\ (34.2 \times 10^6) \left(\frac{.015}{1.46}\right)^2 = 21300\ psi$$

$$M.S. = \frac{21300}{1.4(4260)} - 1 = \text{AMPLE}$$

OVERALL BENDING.

$$I_{NA} = 2\,(.5)(.015)\left(\frac{2.78}{2}\right)^2 + \frac{1}{12}\,(.015)(2.78)^3$$

$$= .0558\ IN^4$$

$$M = 95.8(2.45) = 234.7\ IN^{\#}$$

$$f_b = \frac{Mc}{I} = \frac{234.7\ (\frac{2.78}{2})}{.0558} = 5850\ psi$$

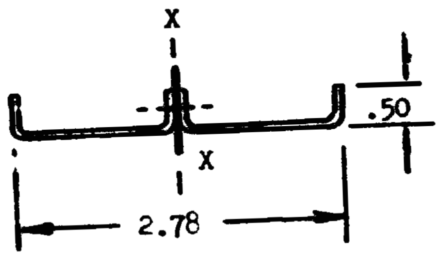

A-A (Pg C-14)

FLANGE BUCKLING:

$$F_{crel} = KE\left(\frac{t}{b}\right)^2 \qquad K = .384 \quad \text{GAC SM B5.11.11-1}$$

$$= .384\ (34.2 \times 10^6)\left(\frac{.015}{.5}\right)^2 =$$

$$= 11820\ psi$$

$$M.S. = \frac{11820}{1.4(5850)} - 1 = .44$$

<u>LOWER CLIP.</u>

$$M = 95.8\ (2.75) = 263.5\ IN^{\#}$$

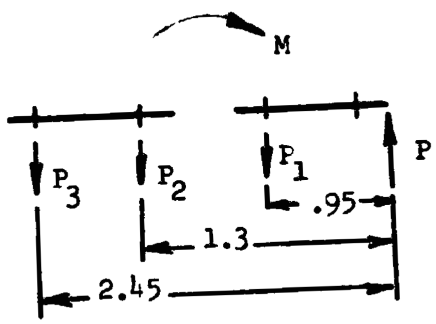

$$P_2 = P_1\left(\frac{1.3}{.95}\right)$$

$$P_3 = P_1\left(\frac{2.45}{.95}\right)$$

$$P_1(.95) + P_2(1.3) + P_3(2.45) = M$$

$$P_1 = 29.1^{\#}$$

$$P_2 = 39.9^{\#}$$

$$P_3 = 75.1^{\#}$$

$$P = 144.1^{\#}$$

BENDING THROUGH P_3

$M = 75.1\left(.25 - \frac{.31}{2}\right) = 7.1314\#$

EFFECTIVE WIDTH = .63 IN.

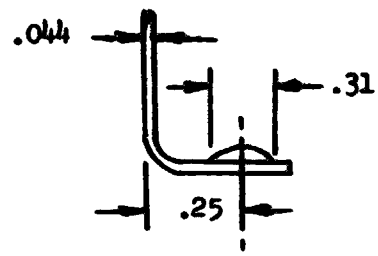

$f_b = \frac{6(\frac{M}{2})}{bt^2} = \frac{6\,(7.13)}{.63(.044)^2} = 35070$ psi

$F_{ty} = 55$ ksi

$M.S. = \frac{55000}{1.15\,(35070)} - 1 = .36$

BENDING AT P

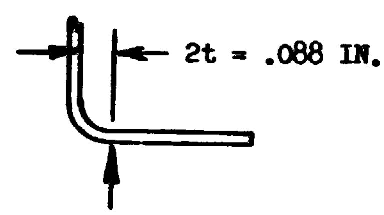

$M = 144.1(.088) = 12.68$ IN#

EFFECTIVE WIDTH = .85 IN.

$f_b = \frac{6\,M}{bt^2} = \frac{6(12.68)}{.85(.044)^2} = 46230$ psi

$F = 144.1^{\#}$

$F_{ty} = 55$ ksi

$M.S. = \frac{55000}{1.15\,(46230)} - 1 = .03$

UPPER CLIP

COND. A critical

$V = 44.8^{\#}$

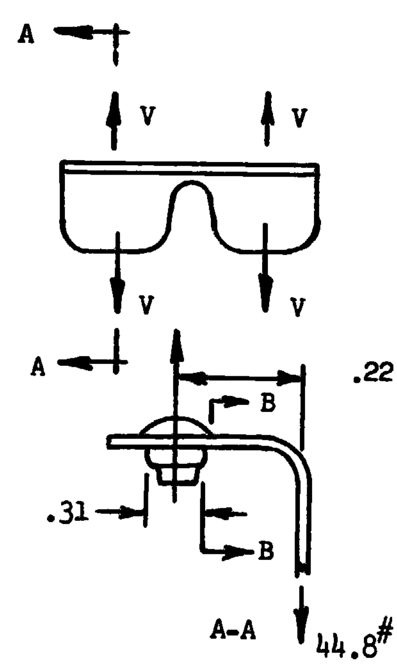

$M = 44.8\,(.22 - \frac{.31}{2}) = 2.91$ IN#

$f_b = \frac{6M}{bt^2} = \frac{6(2.91)}{.63(.044)^2}$

$= 14320$ psi

$F_{ty} = 55$ ksi

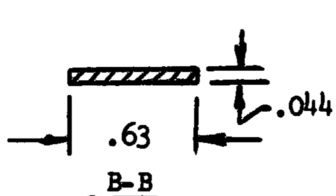

$M.S. = \frac{55000}{1.15(14320)} - 1 =$ AMPLE

```
      REAL LEN,INER(20),M(20)
      DIMENSION Y(2,20),B(20,5),V(20),TEMP1(20),X(20),F(20)
      PI = 3.14159
      E = 34.2*(1000.)**2
      READ(4,8) NP,LEN
      WRITE(6,3)
      WRITE(6,8) NP,LEN
      XNP = NP
      DO 10 J = 1,NP
      READ(4,1) F(J),(B(J,I),I=1,5)
      IF (J.EQ.1) F(J) = 1./2./XNP
      IF (J.NE.1) F(J) = F(J-1) + 1./XNP
      WRITE(6,1) F(J),(B(J,I),I=1,5)
   10 CONTINUE
   15 CONTINUE
      WRITE(6,4)
      READ(5,1) T
      IF (T.LE. 0.) GO TO 999
      WRITE(6,6)
    6 FORMAT(1H,/10X,'SECTION PROPERTIES, A,AX,AX2,XIN,INER(J)',/)
      DO 20 J = 1,NP
      A = T*(B(J,1)+.02645*B(J,2) + B(J,5) - T) + .044*(B(J,3) + B(J,4))
      AX = 1.02645*.00649*T*B(J,2)**2
     1     + (B(J,5)-T)*T*(B(J,5)/2.)
     2     - .044*(B(J,3) + B(J,4))*.022
      AX2 = 1.02645*B(J,2)*T*(.00649*B(J,2))**2
     1     + (B(J,5) - T)*T*(B(J,5)/2.)**2
     2     + .044*(B(J,3) + B(J,4))*(.022)**2
      XIN = (B(J,1) - B(J,2))/12.*T**3
     1     + .015514/1000.*B(J,2)**3*T
     2     + T*(B(J,5)-T)**3/12.
     3     + (B(J,3) + B(J,4))/12.*(.044)**3
      INER(J) = (AX2 + XIN - AX**2/A)*2.
C     WRITE(6,2) J,A,AX,AX2,XIN,INER(J)
      Y(1,J) = SIN(PI*F(J))
      X(J) = LEN*F(J)
   20 CONTINUE
   25 CONTINUE
      TOT1 = 0.
      TOT2 = 0.
      DO 30 J = 1,NP
      TEMP1(J) = Y(1,J)/INER(J)
      TOT1 = TOT1 + TEMP1(J)
      TOT2 = TOT2 + TEMP1(J)*F(J)
C     WRITE(6,2) J,TEMP1(J),TOT1,TOT2
   30 CONTINUE
      J = 1
      V(1) = TOT1 - TOT2
      M(1) = V(1)*X(1)
```

```
      DO 40 J = 2,NP
      V(J) = V(J-1) - TEMP1(J-1)
      M(J) = V(J)*(X(J)-X(J-1)) + M(J-1)
   40 CONTINUE
      CON = 0.
      DO 50 J = 1,NP
      IF(M(J) .GT. CON) CON = M(J)
   50 CONTINUE
      DO 60 J = 1,NP
      Y(2,J) = M(J)/CON
   60 CONTINUE
      DO 70 J = 1,NP
      IF(ABS(Y(1,J)/Y(2,J) - 1.) .GT. 0.001) GO TO 80
   70 CONTINUE
      GO TO 100
   80 CONTINUE
      DO 90 J = 1,NP
      Y(1,J) = Y(2,J)
   90 CONTINUE
      GO TO 25
  100 CONTINUE
      WRITE(6,9)
    9 FORMAT(2X,/10X,'J   INER(J)   TEMP1   V   M   Y1   Y2   PCRIT',/)
      DO 110 J = 1,NP
      XNP = NP
      P = Y(1,J)/M(J)*E/(LEN/XNP)
      WRITE(6,3) J,INER(J),TEMP1(J),V(J),M(J),Y(1,J),Y(2,J),P
  110 CONTINUE
      GO TO 15
    1 FORMAT(10F8.3)
    2 FORMAT(I8,6E14.6)
    3 FORMAT(I8,6E14.6,F10.2)
    4 FORMAT(2X,///,10X,'WHAT IS THICKNESS?',//)
    5 FORMAT(2X,///)
    6 FORMAT(I5,9F10.5)
  999 CALL EXIT
      END
EOF:
```

APPENDIX D

Detail Stress Analysis - Rene' 41 TPS

The detail stress analysis of the Rene' 41 thermal protection system is given in the following pages. Included is the analysis for the surface panel to rib/standoff upper and lower attachments, the rib/standoff design analysis, the drag bracket analysis, and the effect of panel spanwise thermal expansion.

SURFACE PANEL/RIB STANDOFF ATTACHMENT ANALYSIS

Maximum Shear Load, V

$$V = \frac{1}{2}p\ P_R \ell = \frac{1}{2}\ (1.5)\ P_R\ (20) = 15\ P_R$$

(P_R in psi)

CONDITION*	P_R (LB/FT^2)	V (LB.)
A	-430	-44.8 LIMIT
B	350	36.5 LIMIT
C	100	10.4 LIMIT
D	50	5.2 LIMIT

CORRUGATION SIDEWALL BUCKLING

Each wall carries $\frac{1}{2}$ V = 22.4 lb. max. (COND. A)

$$f_s = \frac{\frac{1}{2}V}{ht} = \frac{22.4}{.435\ (.0071)} = 7250 \text{ psi}$$

For a long plate S.S. all sides

$$K_{CR} = 4.8$$

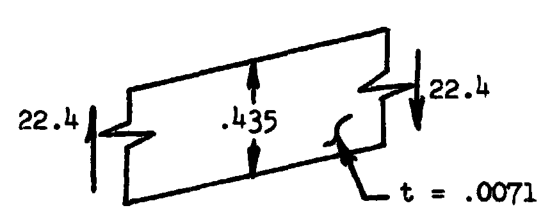

CORRUGATION SIDEWALL BUCKLING (Cont'd)

$$F_{CREL} = K_{cr}\,E\left(\frac{t}{h}\right)^2 = 4.8\,(31.6 \times 10^6)\left(\frac{.0071}{.435}\right)^2 = 40400 \text{ psi}$$

$$\text{M.S.} = \frac{40400}{1.4\,(7250)} - 1 = \text{AMPLE}$$

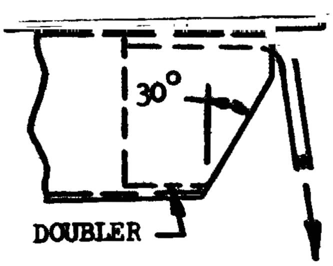

$$\frac{22.4}{\cos 30^\circ} = 25.9\#$$

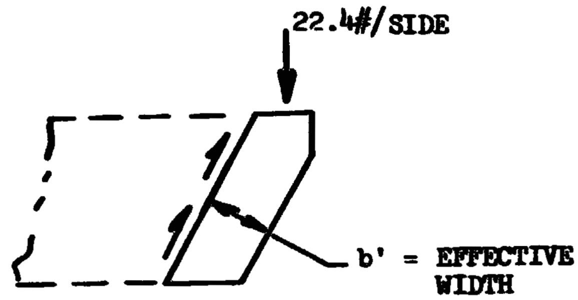

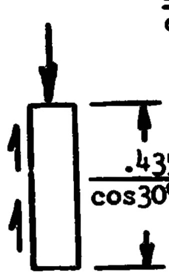

$$\frac{.435}{\cos 30^\circ} = .502$$

THICKNESS OF:

Sidewall	.0071
Doubler	.0073
	.0144

$P_{cr} = 1.4(25.9) = 36.6^{\#}$ required

$$P_{cr} = \frac{\pi^2 EI}{ML^2}$$

For a pin-ended column with shear along the length,

M = .53 (GAC SM B3.44. 31-1)

$E = 31.6 \times 10^6$ psi

$$I = \frac{P_{cr}\,ML^2}{\pi^2 E} = \frac{36.3\,(.53)(.502)^2}{\pi^2\,(31.6 \times 10^6)} = 15.545 \times 10^{-9}$$

$$I = \frac{b^1\,t_{TOT}^3}{12} \quad \text{for } t_{TOT} = .0144$$

$b' = .062$ IN

M.S. = AMPLE

BENDING OF FLAT BETWEEN BENDS.

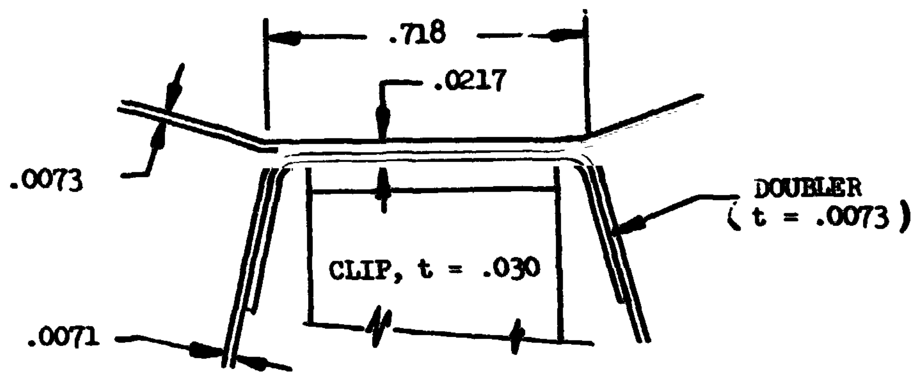

COND. A is critical, V = -44.8 lb limit

Treat layup as a beam of thickness = .0217 IN.

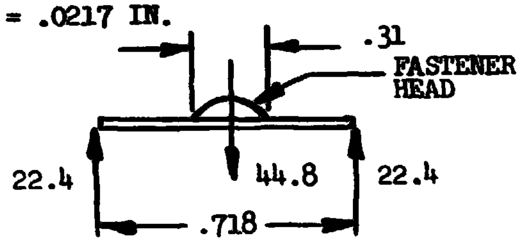

$$M = 22.4 \ \frac{.718-.31}{2}$$

$$= 4.57 \text{ IN LBS}$$

Use (2) times head diameter for the effective width.

$$\therefore f_b = \frac{6M}{bt^2} = \frac{6(4.57)}{2(.31)(.0217)^2} = 93900 \text{ psi}$$

$$F_{ty} = 127 \text{ KSI}$$

$$\text{M.S.} = \frac{127000}{1.15(93900)} - 1 = .17$$

FLEXIBLE RIB

DESIGN CONDITIONS (Ref. Pg. D-1)

COND.	P_R (psf)	V(lb)
A	-430	-44.8
B	350	36.5
C	100	10.4
D	50	5.2
*		

* THERMAL EXPANSION:

$$\Delta = \alpha \Delta TL = 8.5 \times 10^{-6(1)} (1600-70)(20-.88)$$

$$= .249 \text{ IN}$$

(1) REF 3-3

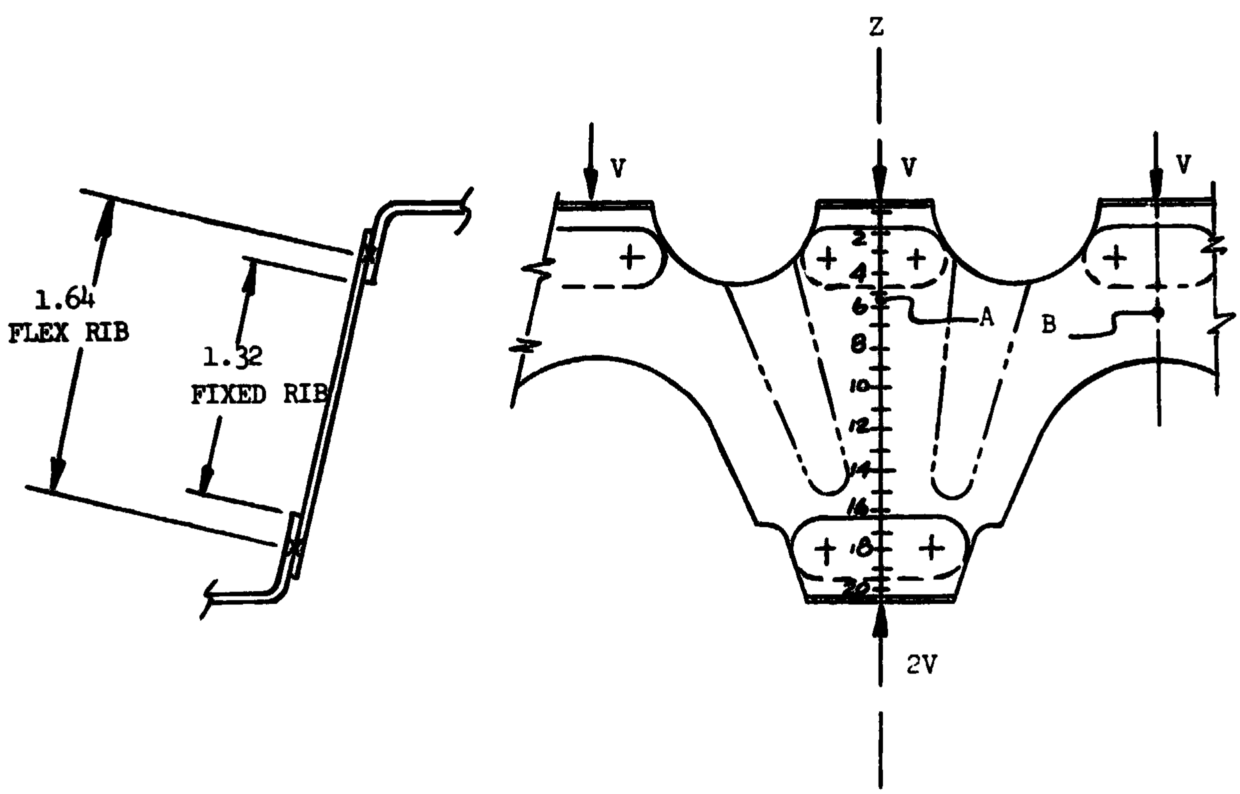

LATERAL THERMAL EXPANSION IN RIB

Between points A & B, $\Delta = \alpha \Delta T L$

$$= 8.6 \times 10^{-6} (1600-70)(1.5)$$

Conservative

$$= .0197 \text{ IN}$$

Using the same method as for the skin beads.

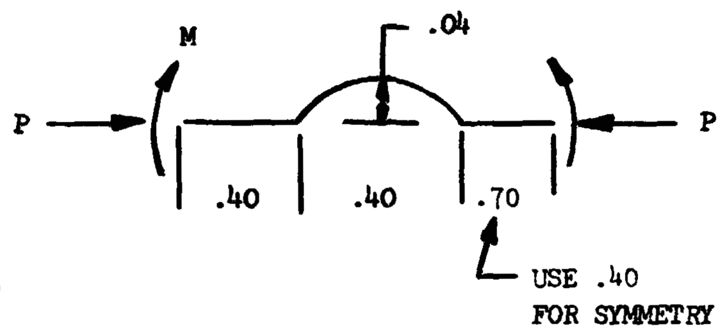

$\therefore$ p = 1.20, b = .40

$$P = EI\Delta\,(2374.863)$$

$$M = EI\Delta\,(35.778)$$

At top of bead, $\bar{M} = Pe - M$

$$= EI\Delta\,[2374.863(.04) - 35.778]$$

$$= EI\Delta\,(59.217)$$

$$E = 17.7 \times 10^6 \text{ psi} \quad @\ 1600^\circ F$$

$$I = \frac{bt^3}{12(1-\gamma^2)} \qquad \gamma = .31$$

$$\epsilon = \frac{f_b}{E} = \frac{6\bar{M}}{Ebt^2} = \frac{6\left[17.7 \times 10^6 \times \dfrac{bt^3}{12(1-.31^2)} \times .0197\right](59.217)}{(17.7 \times 10^6)\ bt^2}$$

$$= .6453t \qquad\qquad t = .0065 \text{ IN}$$

$$= .0042 \text{ IN/IN}$$

The 0.2% offset strain (yield stress) at 1600°F is: (σ_y = 58000 psi)

$$\epsilon = .002 + \frac{58000}{17.7 \times 10^6} = .0053 \text{ IN/IN}$$

The margin against exceeding the yield stress at 1600°F is:

$$\text{M.S.} = \frac{.0053}{1.15\ (.0042)} - 1 = .09$$

<u>WEB BUCKLING</u> - COND. B (Ref. Pg. D-4)

$$V = 36.5^{\#}/\cos 14^\circ = 37.6 \text{ lb limit (COND. B)}$$

<u>GENERAL INSTABILITY</u>

Assume web is symmetric about Z-Z and work one side for section properties. Treat as a pin-ended column with varying inertia. (Ref. Timoshenko, "Theory of Elastic Stability.")

HALF-SECTION:

NOTE: THIS BEAD
NEGLECTED FOR
GENERAL INSTABILITY

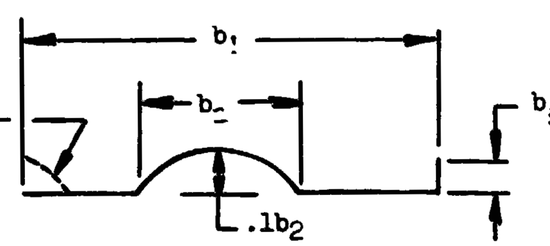

LOC (Pg D-4)	b_1	b_2	b_3	LOC	b_1	b_2	b_3
1				11	.98	.31	.15
2				12	.88	.28	.15
3	.83			13	.82	.26	.15
4	1.22			14	.77	.24	.11
5	1.5	.46		15	.73	.20	.07
6	1.5	.44		16	.68		
7	1.5	.41		17	.50		
8	1.5	.38		18	.48		
9	1.5	.36		19			
10	1.17	.34	.09	20			

SECTION PROPERTIES

$$A = t\left[b_1 + .02645\ b_2 + (b_3 - t)\right]$$

$$A_x = t\left[.06825\ b_2^2 + .5\ (b_3 - t)\ (b_3)\right]$$

$$A_x^2 = t\left[.004538\ b_2^3 + .25\ (b_3 - t)\ (b_3)^2\right]$$

$$I_{oo} = (b_1 - b_2)\ \frac{t^3}{12} + .0009158\ \ b_2^3 t + (b_3 - t)^3 \left(\frac{t}{12}\right)$$

$$\bar{x} = A_x/A;\ I_{NA} = A_x{}^2 + I_{oo} - A\bar{x}^2$$

Timoshenko's method involves assuming a deflected shape for the column and solving for the actual shape. The resultant shape is then used for new assumption and the process is repeated. When the assumed and actual shapes are within some tolerance, say 0.1%, at all sections, the critical buckling load can be calculated.

Because of the iterative nature of the problem and the considerable number of arithmetic operations involved, the "RIBS" computer program (Ref. Appendix C, pg C-19 & C-20) was modified to solve for the Rene' allowable loads. Several thicknesses were assumed, and the resulting critical load curves are presented in Figure D-1.

The flexible rib has an equivalent applied load of 75.2 lb limit (105.3 lb ultimate) for a 3 inch section of web during COND. B. The allowable load for t = .0065 IN is 222 Lb. (Fig. D-1)

$$\text{M.S.} = \frac{222}{105.3} - 1 = 1.10$$

LOCAL BUCKLING

Over arches between beads.

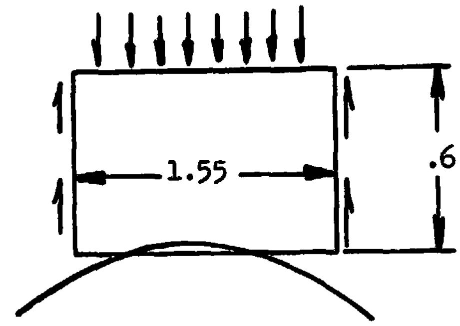

$$\frac{b}{a} = \frac{.6}{1.55} = .39,\ K_{c_r} = 1.15 \quad \text{GAC. S.M. B5.11.11-2}$$

$$F_{crel} = K_{cr}\ E\ \left(\frac{tN}{b}\right)^2$$

$$= 1.15\ (31.6 \times 10^6)\left(\frac{.0065}{.6}\right)^2$$

$$= 4260 \text{ psi}$$

$$P_{cr} = 4260\ (1.55)(.0065) = 43.0 \text{ lb}$$

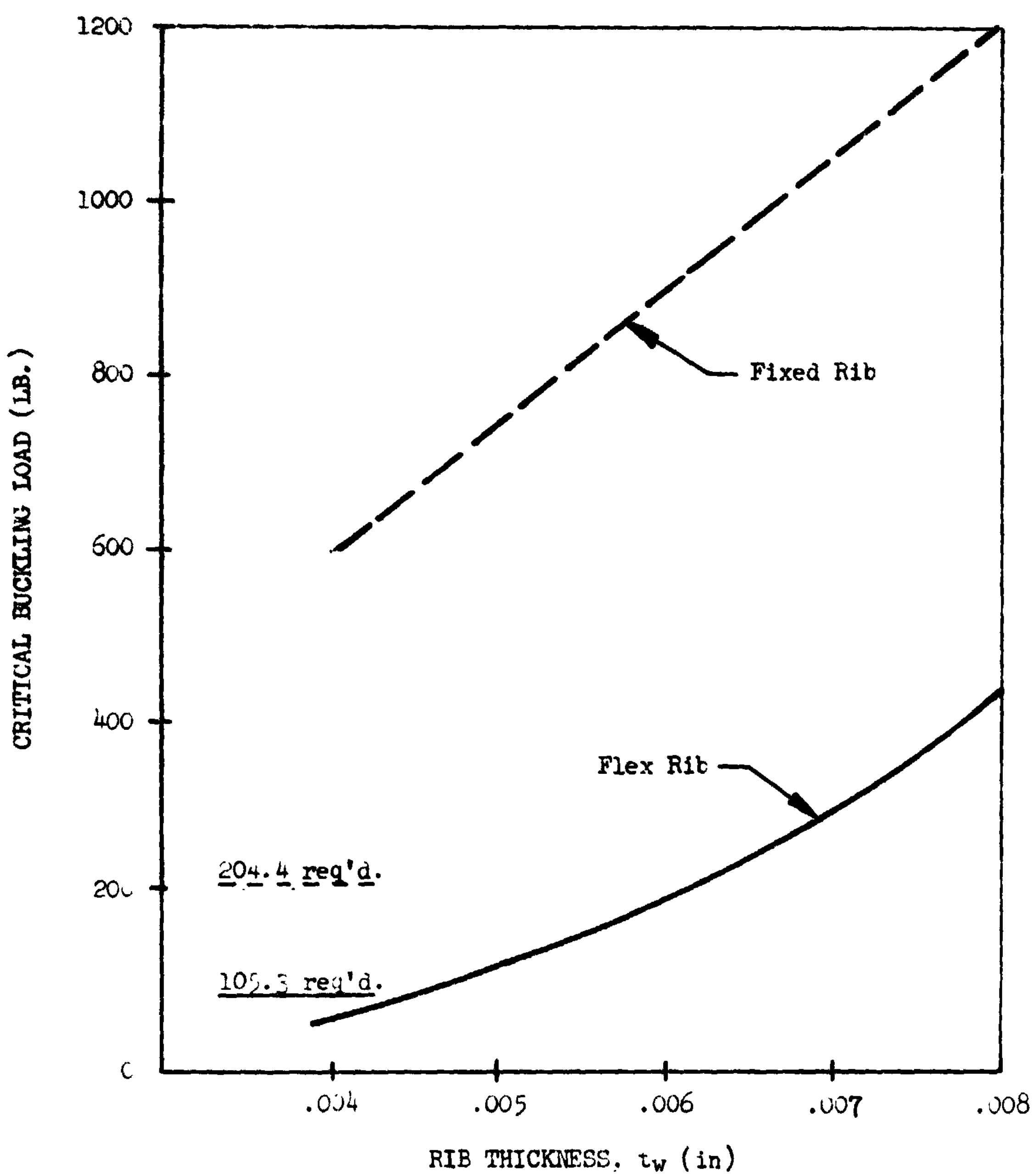

FIGURE D-1 - GENERAL INSTABILITY, CRITICAL LOAD VS. RIB THICKNESS

WEB BUCKLING (Continued)

Equivalent Length - Due to Shear:

L' = .53L
GACSM
B3.40-1

$$P_{cr}' \quad P_{cr}\left(\frac{L}{L'}\right)^2 = 153.0 \text{ lb.}$$

$$M.S. = \frac{153.0}{1.4(37.6)} - 1 = \text{AMPLE}$$

BUCKLING BETWEEN ARCHES.

(Small bead added, "B", to prevent Local Buckling)

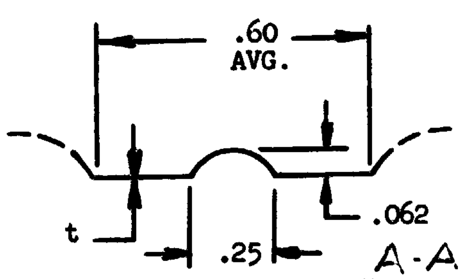

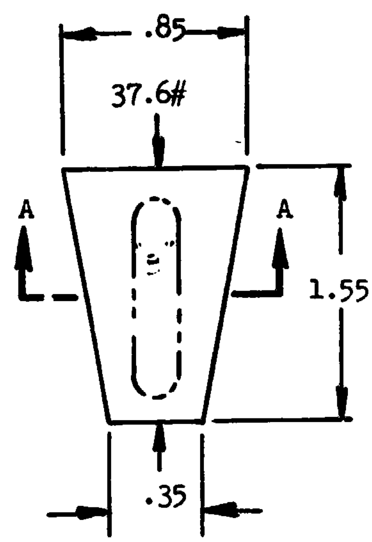

$$A = (.35 + .28932)t$$

$$A_x = (.28932t)\,(.040985)$$

$$A_x^{\,2} = (.28932t)\,(.040985)^2$$

$$I_{oo} \cong .00010226t$$

$$I_{NA} = I_{oo} + A_x^{\,2} - (A_x)^2/A$$

$$= .36832\text{x}10^{-3}t\ ,\ t = .0065,\ \therefore\ I = 2.394\text{x}10^{-6}\ \text{IN}^4$$

$$P_{CR} = \frac{\pi^2 EI}{L^2}$$ Neglecting any support along the long edges

$$P_{CR} = \frac{\pi^2(31.6\text{x}10^6)(2.394\text{x}10^{-6})}{(1.55)^2} = 311 \text{ lb.}$$

$$M.S. = \frac{311.}{1.4(37.6)} - 1 = \text{AMPLE}$$

SPANWISE THERMAL EXPANSION

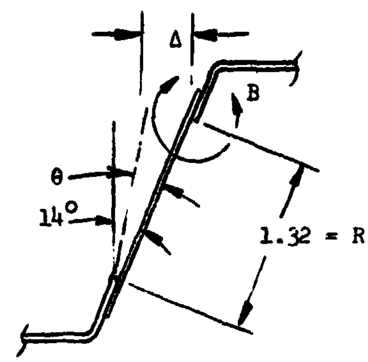

$\Delta = .249$ IN (Ref. Pg. D-4)

$R = 1.32$ IN between clips

$R\sin 14^{\circ} - R\sin(14-\theta)^{\circ} = .249$ IN

$\theta = 10.9^{\circ} = .191$ rad

$\theta = \frac{ML}{EI}$ & $f_b = \frac{6M}{bt^2}$

$\therefore f_b = \frac{6EI\theta}{Lbt^2}$ & $I = \frac{bt^3}{12}$

$f_b = \frac{Et\theta}{2L}$ & $\epsilon = \frac{f_b}{E}$

$\therefore \epsilon = \frac{t\theta}{2L}$

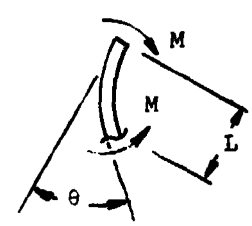

DETAIL B

THE ALLOWABLE STRAIN TO PREVENT YIELDING.

$$\text{At } 1600^{\circ}\text{F} = .002 + \frac{58000}{17.7 \times 10^{6}} = .0053 \leftarrow \text{CRIT.}$$

$$\text{At } 70^{\circ}\text{F} = .002 + \frac{127000}{31.6 \times 10^{6}} = .00[illegible]$$

$$\frac{.0053}{1.15} = \frac{.0065(.191)}{2L} \qquad L = .1[illegible]5 \text{ IN.}$$

This dimension (.135 IN.) is required at both the top and bottom web/clip interfaces, so that at least this much web is free to deflect and bend. A review of the assembly drawing shows that this criterion can be achieved

FLEXIBLE RIB-UPPER CLIP

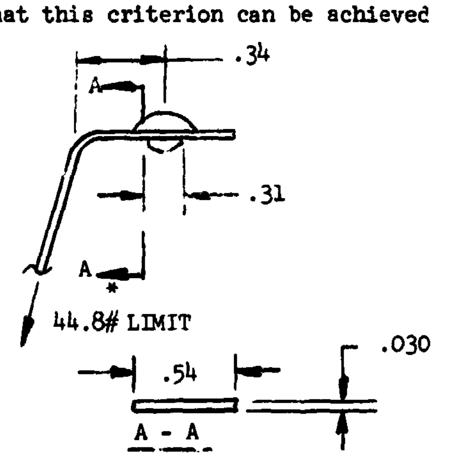

COND A Critical*

$M = 44.8\,(.34 - \frac{.31}{2})$

$= 8.29$ IN lb.

$f_b = \frac{6(8.29)}{.54(.03)^2}$

$= 102{,}300$ psi

FLEXIBLE RIB-UPPER CLIP (Continued)

Fty = 127 ksi

$$M.S. = \frac{127000}{1.15(102300)} - 1 = .08$$

FLEXIBLE RIB - LOWER CLIP

COND. A*

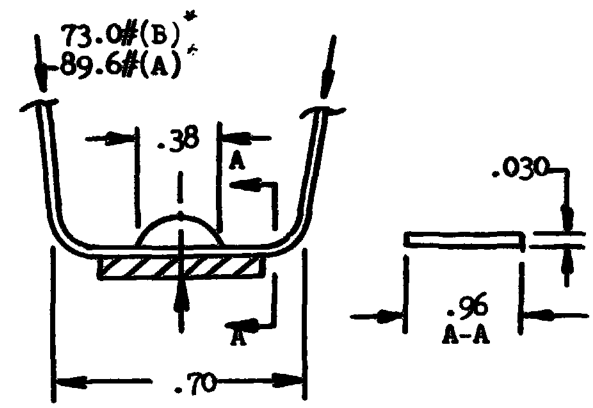

$$M = 89.6 \; \frac{.70-.38}{2} = 14.34 \text{ IN}^{\#}$$

$$f_b = \frac{6M}{bt^2} = \frac{6(14.34)}{.96(.030)^2}$$

$$= 99580 \text{ psi}$$

Fty = 127 ksi

$$M.S. = \frac{127000}{1.15(99580)} - 1 = .10$$

COND. B*

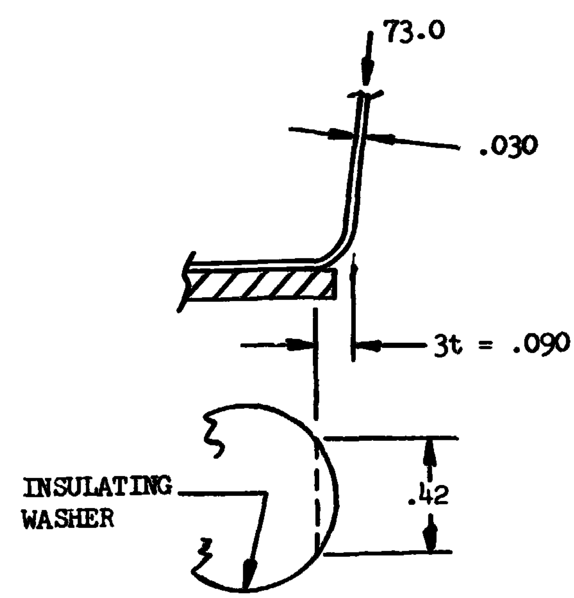

$$M = 73(.09) = 6.57 \text{ IN}^{\#}$$

$$f_b = \frac{6M}{bt^2} = \frac{6(6.57)}{.42(.03)^2}$$

$$= 104290 \text{ psi}$$

Fty = 127 ksi

$$M.S. = \frac{127000}{1.15\,(104290)} - 1 = .05$$

*Ref. Pg. D-4

FIXED RIB

DESIGN CONDITIONS*

CONDITION	P_R (psf)	V(lb.)
A	-430	-89.6
B	350	73.0
C	100	20.8
D	50	10.4

*Ref. Pg. D-4, Values of V are double flexible rib values.

LATERAL THERMAL EXPANSION

See Flexible Rib Analysis, page D-5

WEB BUCKLING - General Instability

Equivalent Applied Load = 2V for 3" width

$$2V = 2(73.0) = 146 \text{ lb. limit}$$
$$= 204.4 \text{ lb ult.}$$

For t = .0065, P_{CR} = 970 lb. (Ref. Fig. D-1)

$$M.S. = \frac{970}{204.4} - 1 = \text{AMPLE}$$

Buckling Over Arches; P_{CR} = 153.0 lb (Ref. Pg. D-8)

$$M.S. = \frac{153.0}{1.4(73.0)} - 1 = .49$$

Buckling Between Arches; P_{CR} = 311. lb (Ref. Pg. D-8)

$$M.S. = \frac{311}{1.4(73.0)} - 1 = \text{AMPLE}$$

FIXED RIB - UPPER CLIPS

CONDITION A Critical*

$V = 89.6$ lb limit*

$L' = .88 - .31 = .57$ IN.

$$M = \frac{PL'}{8} = \frac{89.6\ (.57)}{8}$$

$= 6.38$ IN#

$$f_b = \frac{6M}{bt^2} = \frac{6(6.38)}{.54(.030)^2}$$

$= 78810$ psi

$F_{ty} = 127$ ksi

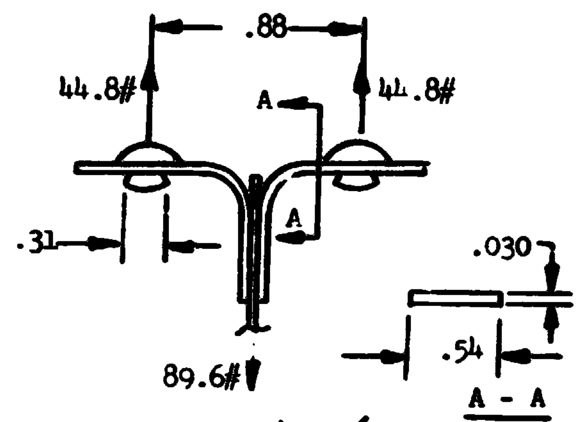

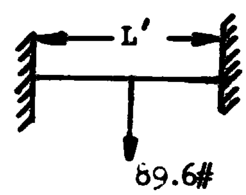

$$M.S. = \frac{127000}{1.15\ (78810)} - 1 = .40$$

CONDITION B, $V = 73.0$ lb.*

$M = 36.5(.09) = 3.29$ IN lb.

$$f_b = \frac{6M}{bt^2} = \frac{6(3.29)}{.54(.03)^2}$$

$= 40{,}560$ psi

$F_{ty} = 127$ ksi

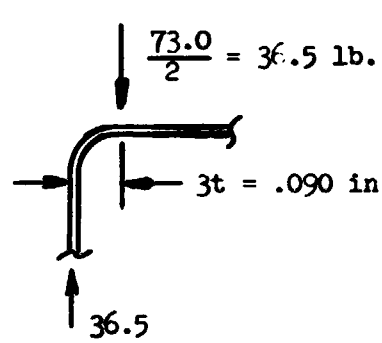

$$M.S. + \frac{127000}{1.15(40560)} - 1 = \text{AMPLE}$$

* Ref. Pg. D-12

FIXED RIB - LOWER CLIP

CONDITION A, $V = 2(89.6)^*$

$= 179.2$ lb.

$L' = .74 - .31 = .43$

$$M = \frac{PL'}{8} = \frac{179.2(.43)}{8}$$

$= 9.63$ IN#

$$f_b = \frac{6M}{bt^2} = \frac{6(9.63)}{.63(.030)^2}$$

$= 101900$ psi

FTY = 127 ksi

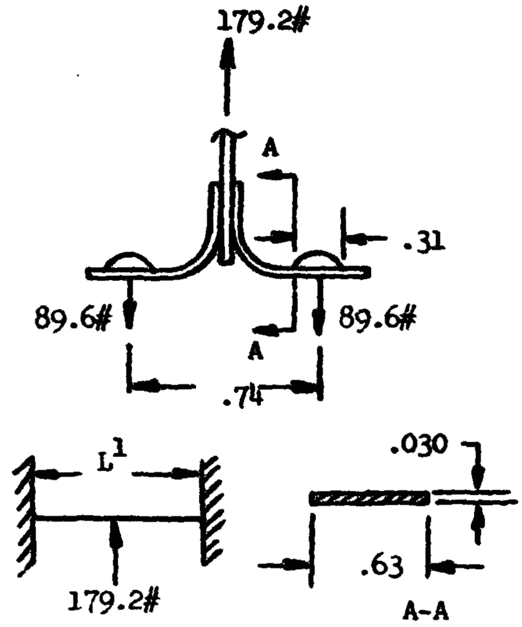

$$M.S. = \frac{127000}{1.15(101900)} - 1 = .08$$

CONDITION B, $V = 2(73.0) = 146$ lb.*

$M = 73.0(.09) = 6.57$ IN#

$$f_b = \frac{6M}{bt^2} = \frac{6(6.57)}{.63(.03)^2} = 69520 \text{ psi}$$

Fty = 127 ksi

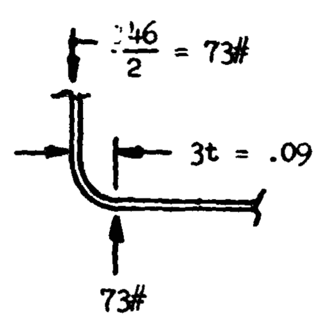

$$M.S. = \frac{127000}{1.15(69520)} - 1 = .58$$

*Ref. Pg. D-11

DRAG BRACKET

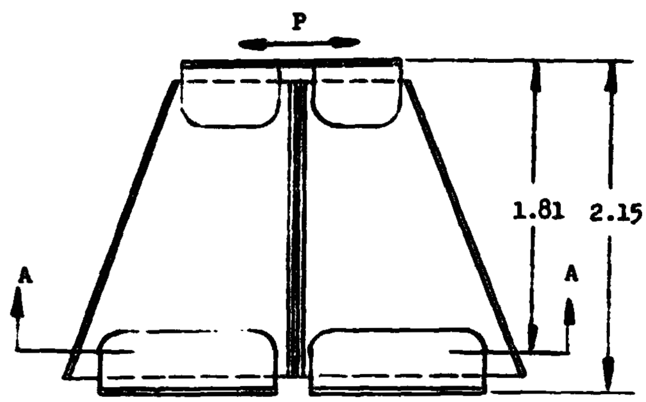

The load P is reversible and is caused by mechanically induced vibration:

"g" loading: 30 g's

(Ref. Appendix C pg. C-14)

Weight of panel plus

Upper Clips = .792 + .02618 + .02291

$= .84109 \text{ lb/FT}^2$

Drag brackets are spaced every 40 inches streamwise and every 12 inches laterally.

$$\therefore P = g\, W_T\, A = 30(.84109)\left(\frac{40 \times 12}{144}\right) = 84.1 \text{ lb.}$$

WEB SHEAR

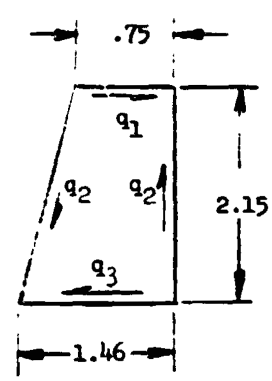

$$q_1 = \frac{\frac{1}{2}(84.1)}{.75} = 56.1 \text{ \#/IN}$$

$$q_2 = \frac{\frac{1}{2}(84.1)(2.15)}{2.15(1.46)} = 28.8 \text{ \#/IN}$$

$$q_3 = \frac{28.8\ (2.15)(.75)}{2.15(1.46)} = 14.8 \text{ \#/IN}$$

$$f_s = \frac{q_1}{t} = \frac{56.1}{.012} = 4680 \text{ psi}$$

BUCKLING OF WEB

Assume $\frac{a}{b} = \frac{1.46}{2.75} = .53$

$K_{cr} = 5.9$ GAC S.M. B5.11.12-1

$$F_{crel} = K_{cr}\, E\left(\frac{t}{b}\right)^2 = 5.9\ (31.6 \times 10^6)\left(\frac{.012}{1.46}\right)^2$$

$= 12590$ psi

$$M.S. = \frac{12590}{1.4\ (4680)} - 1 = .92$$

DRAG BRACKET (Continued)

OVERALL BENDING

$$I_{xx} = \frac{.012}{12}(2.68)^3 + 2\,(.5 \times .012)\left(\frac{2.68}{2}\right)^2$$

$$= .0408 \text{ IN}^4$$

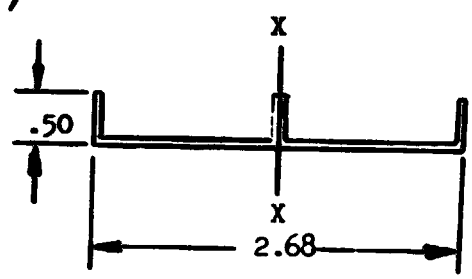

$$M = 84.1\,(1.81) = 152.2 \text{ IN.}^{\#}$$

$$f_b = \frac{Mc}{I} = \frac{152.2\left(\frac{2.68}{2}\right)}{.0408} = 5000 \text{ psi}$$

$$F_{crel} = K_{cr}\,E\left(\frac{t}{b}\right)^2$$

$K_{cr} = .384$ GAC Structures Manual B5.11.11-1

$$= .384\,(31.6 \times 10^6)\left(\frac{.012}{.5}\right)^2$$

$$= 6990 \text{ psi}$$

$$M.S. = \frac{1990}{1.4\,(5000)} - 1 = .00$$

LOWER CLIP

$$M = 84.1^{*}\,(2.15) = 180.8 \text{ IN}^{\#}$$

* Ref. Pg. D-14

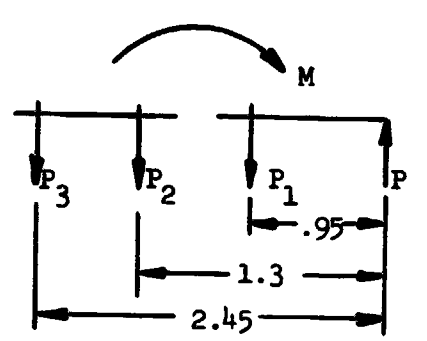

$$P_2 = P_1\left(\frac{1.3}{.95}\right)$$

$$P_3 = P_1\left(\frac{2.45}{.95}\right)$$

$$P_1(.95) + P_2\,(1.3) + P_3\,(2.45) = M$$

$P_1 = 20.0\#$

$P_2 = 27.3\#$ $\quad P = 98.8\#$

$P_3 = 51.5\#$

DRAG BRACKET (Continued)

LOWER CLIP (Continued)

BENDING THROUGH P_3

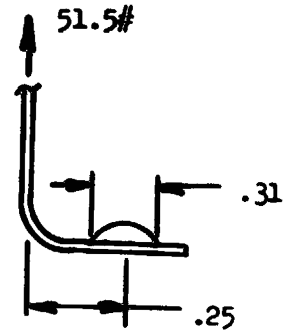

$$M = 51.5\left(.25 - \frac{.31}{2}\right) = 4.89 \text{ IN}^{\#}$$

Effective width = .63

$$f_b = \frac{6M}{bt^2} = \frac{6(4.89)}{.63\,(.03)^2} = 51750$$

Fty = 127 ksi

$$M.S. = \frac{127000}{1.15(51750)} - 1 = \text{AMPLE}$$

BENDING AT P.

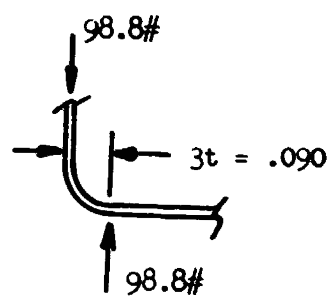

$$M = 98.8\,(.09) = 8.89 \text{ IN}^{\#}$$

$$f_b = \frac{6M}{bt^2} = \frac{6\,(8.89)}{.63\,(.03)^2} = 94070 \text{ psi}$$

$$M.S. = \frac{127000}{1.15\,(94070)} - 1 = .17$$

DRAG BRACKET (Continued)

UPPER CLIP

(Condition A Critical)

$V = \frac{89.6}{2} = 44.8$ (Ref. Pg. D-11).

$M = 44.8\ (.22 - \frac{.31}{2}) = 2.91$ IN

$f_b = \frac{6M}{bt^2} = \frac{6(2.91)}{.63(.03)^2}$

$= 30810$ psi

Fty = 127 ksi

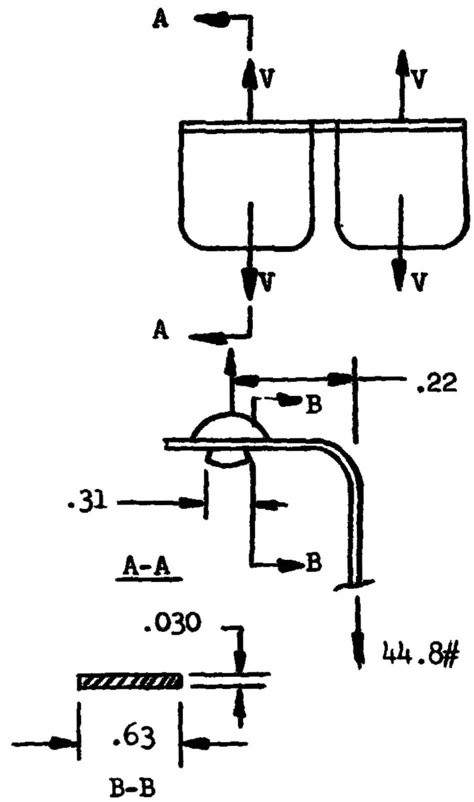

$M.S. = \frac{127000}{1.15\ (30810)} - 1 = \text{AMPLE}$

APPENDIX E

HAYNES 188 TPS PRODUCTION DRAWINGS

The Haymes 188 TPS test specimen production drawings are given, including:

AD1001-100	Test Specimen - Final Assembly
AD1001-101	Skin - Details and Assembly
AD1001-102	Support Ribs - Details and Assembly
AD1001-103	Insulation System - Details and Assembly
AD1001-104	Support Structure Assembly
AD1001-105	Insulation Spacer
AD1001-106	Fairings and End Seals - Details

FOLDOUT FRAME 1

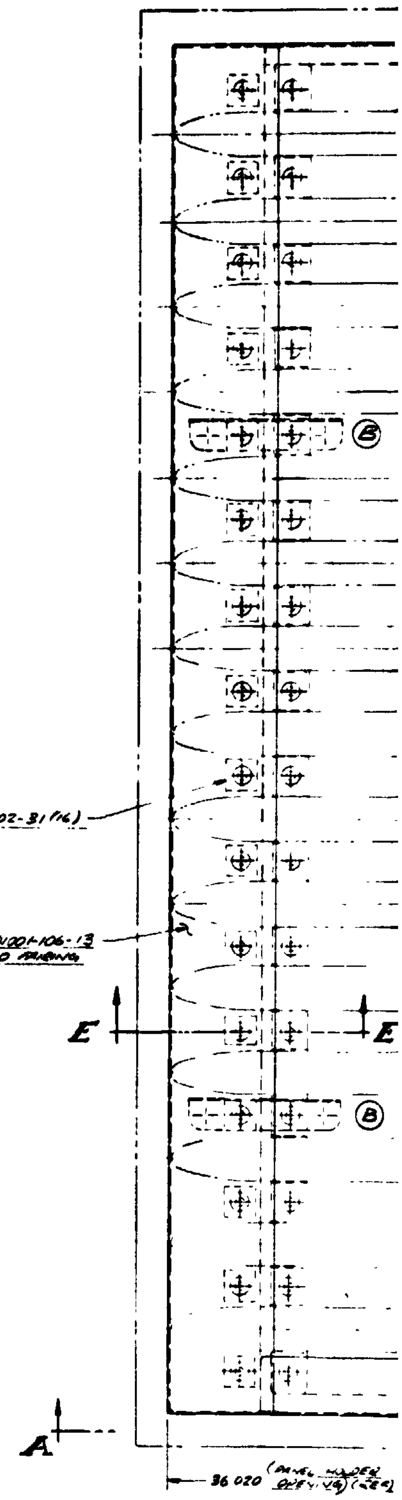

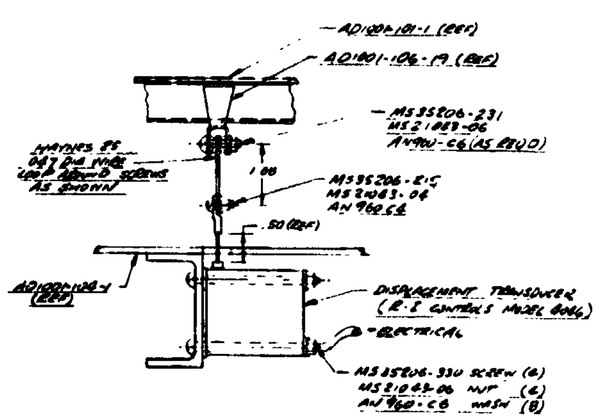

SECTION G-G
FULL SIZE

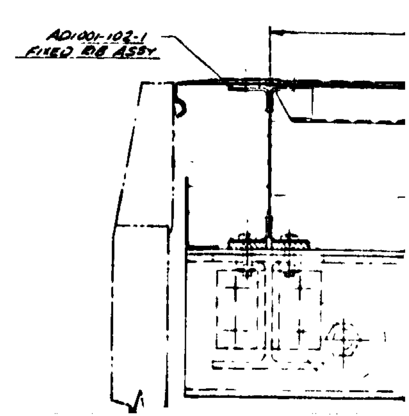

2217-102W

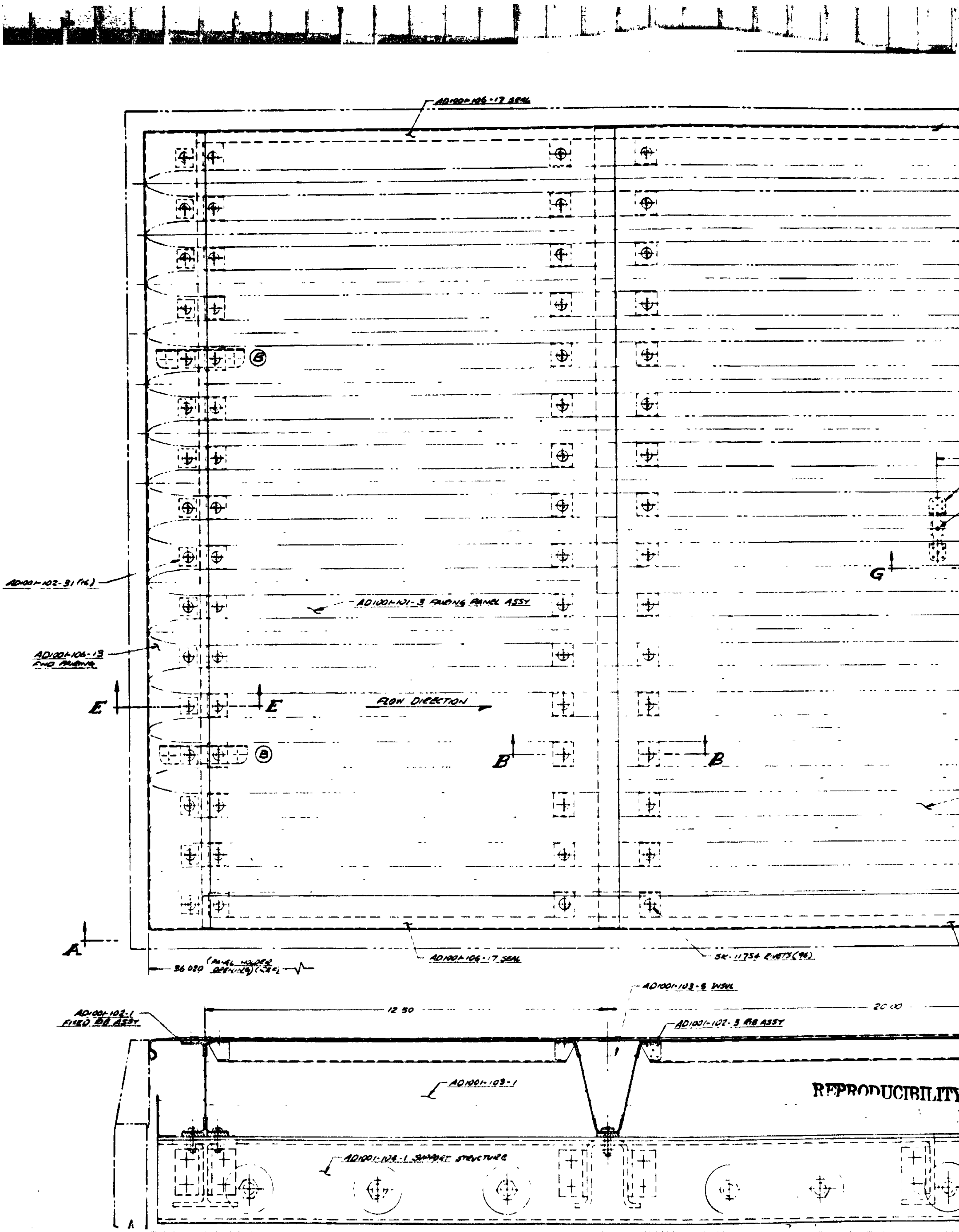
AD1001-106-17 SEAL
AD1001-102-31 (16)
AD1001-101-3 FAIRING PANEL ASSY
AD1001-106-13
END FAIRING
E
E
FLOW DIRECTION
B
B
G
A
AD1001-106-17 SEAL
SK-11754 RIVETS (96)
36.020 (PANEL HOLDER OPENING) (REF)
AD1001-102-1
FIXED RIB ASSY
12.50
AD1001-103-8 INSUL
20.00
AD1001-102-3 RIB ASSY
AD1001-103-1
AD1001-104-1 SUPPORT STRUCTURE

FOLDOUT FRAME 2

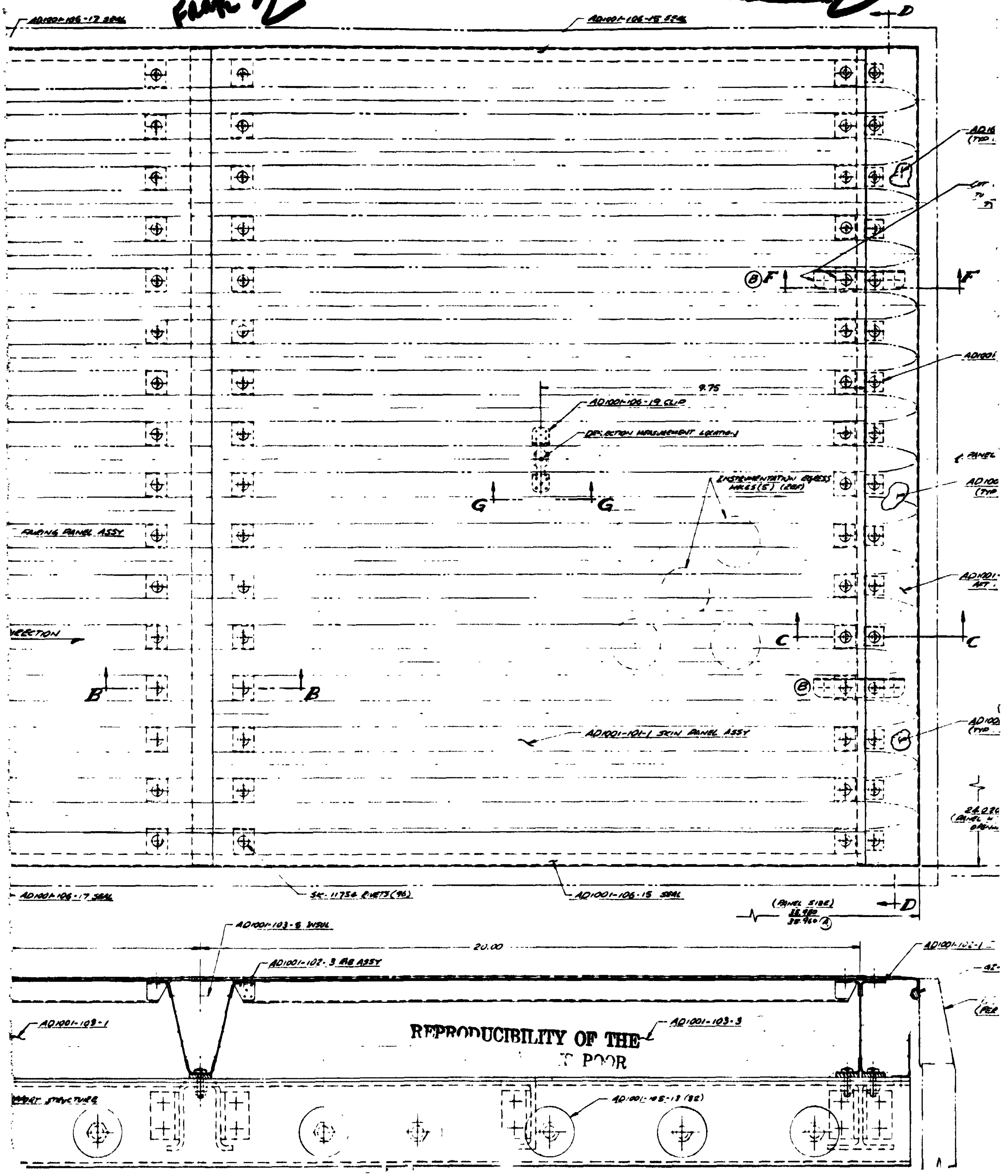

FOLDOUT FRAME 4

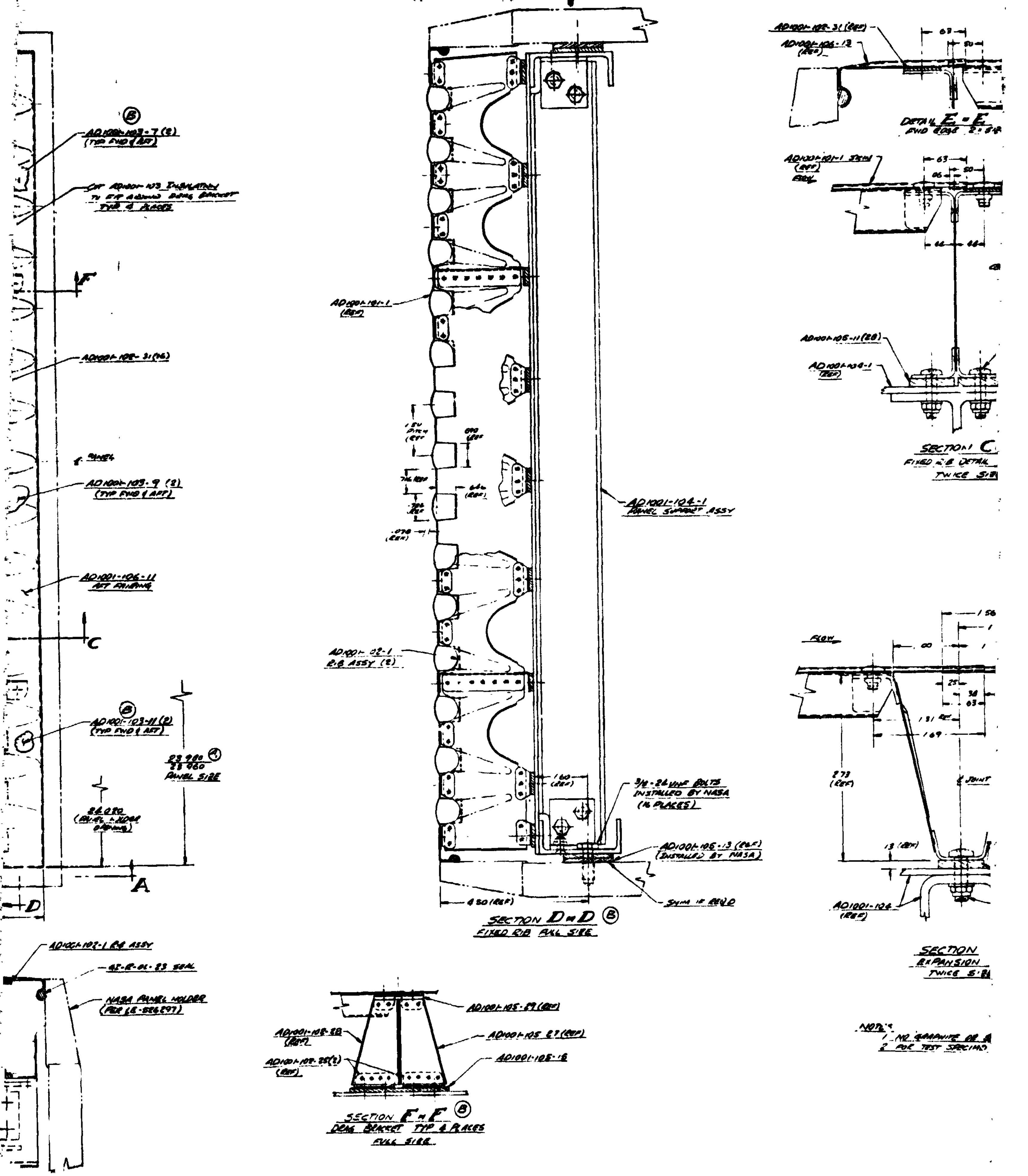

FOLDOUT FRAME 5

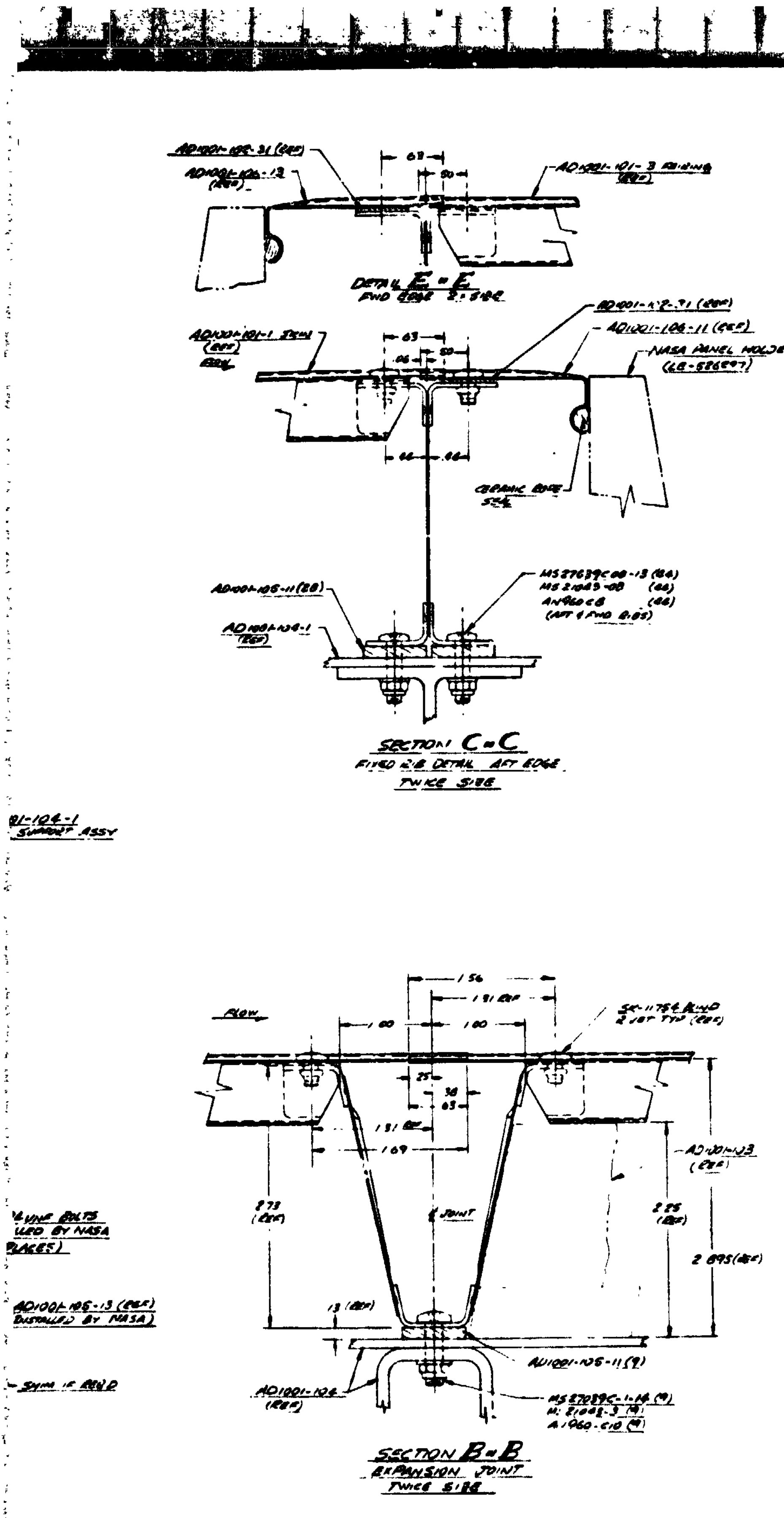

NOTES
1. NO GRAPHITE OR GREASE MARKS ALLOWED ON HAYNES PARTS.
2. FOR TEST SPECIMEN INSTRUMENTATION SEE AD1002

QTY	PART NO	DESCRIPTION	MATERIAL	GOVT SPEC	COML SPEC	STOCK SIZE
1	MODEL 6046	DSP TRANSDUCER				
4	MS35206-332	SCREW	STD PART			
1	MS35206-231					
1	MS35206-215					
9	MS27039C-1-14					
44	MS27039C08-13	SCREW				
9	MS21043-3	NUT				
44	MS21043-08					
12	MS21043-06					
1	MS21043-04	NUT				
9	AN960 C10	WASHER				
44	C8					
12	C6					
1	AN960 C4	WASHER	STD PART			
AR	GS-R-06-23	SEAL	CERAMIC EDGE	(AVL FROM GILBERTS INC)		
96	SK-11754	RIVET BLIND	HAYNES 188	(AVL FROM WHEEL MFG CO)		
1	AD1001-106-19	CLIP	SEE DWG			
2	-17	SIDE SEAL				
2	-15	SIDE SEAL				
1	-13	FAIRING FWD				
1	AD1001-106-11	FAIRING AFT				
4	AD1001-105-15	SPACER TUBE				
32	AD1001-105-3	SPACER INSUL				
37	AD1001-105-11	SPACER INSUL				
1	AD1001-104-1	SUPPORT STR				
2	AD1001-103-11	INSUL ASSY				
2	-9					
2	-7					
1	-5					
1	-3					
1	AD1001-103-1	INSUL ASSY				
32	AD1001-102-31	SPACER				
1	AD1001-102-3	RIB (FLEX)				
2	AD1001-102-1	RIB (FIXED)				
1	AD1001-101-3	FAIRING PANEL				
1	AD1001-101-1	SKIN PANEL	SEE DWG			
1	AD1001-100-1	TEST PANEL ASSY & INSTL				

AD1001-100. — Test specimen — final assembly.

FOLDOUT FRAME

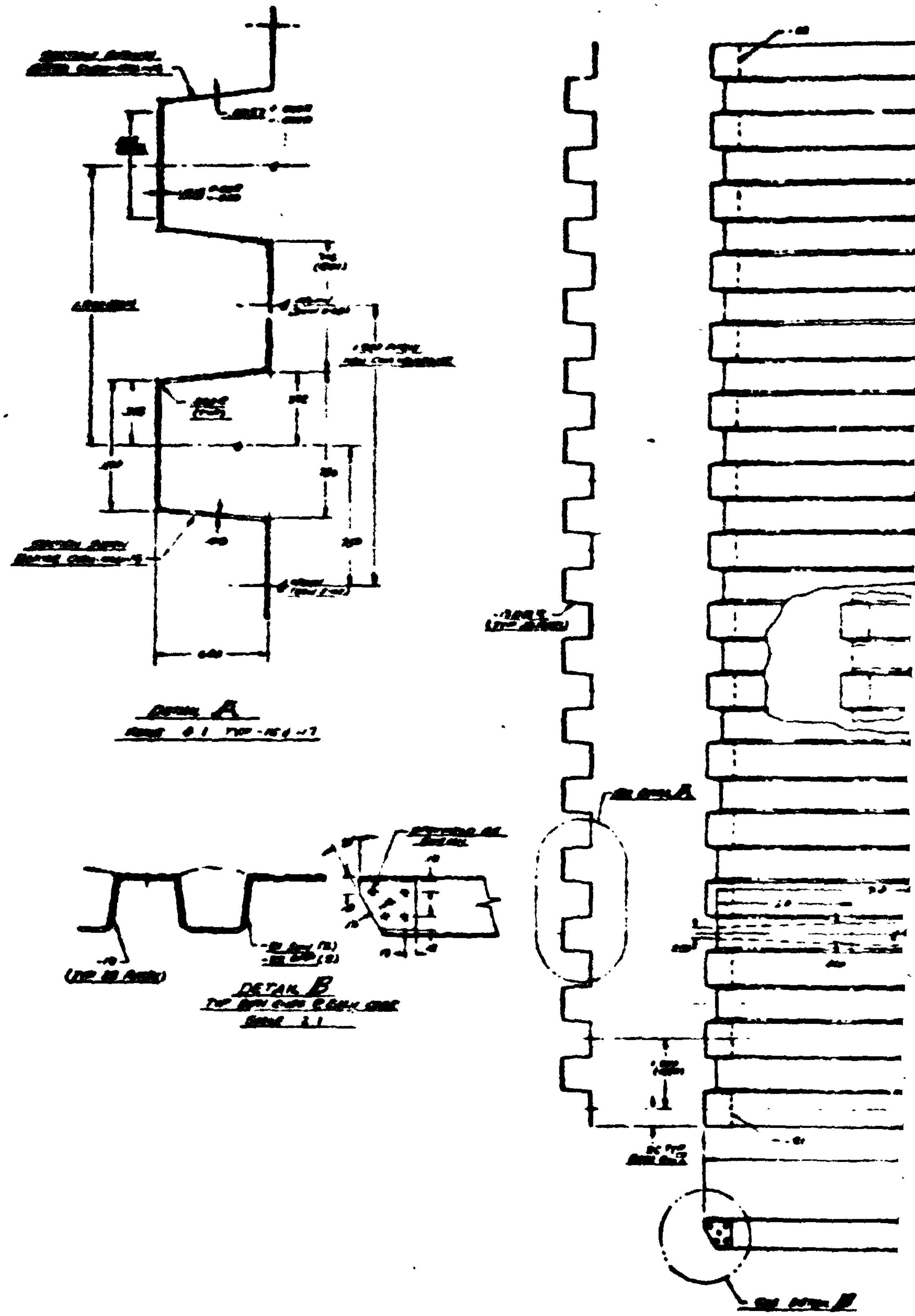

FOLDOUT FRAME

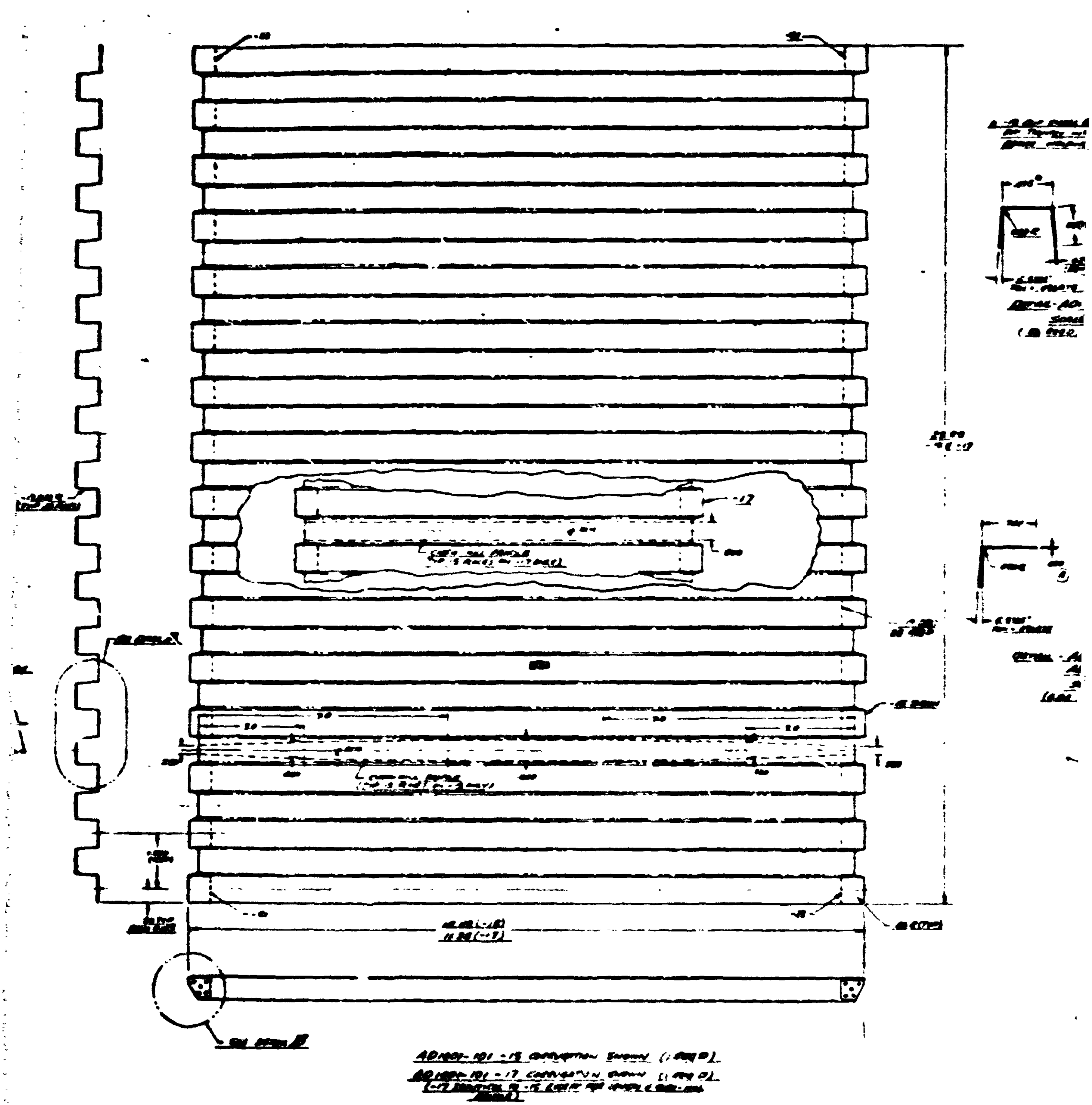

REPRODUCIBILITY OF THE ORIGINAL PAGE IS POOR

FOLDOUT FRAME 3

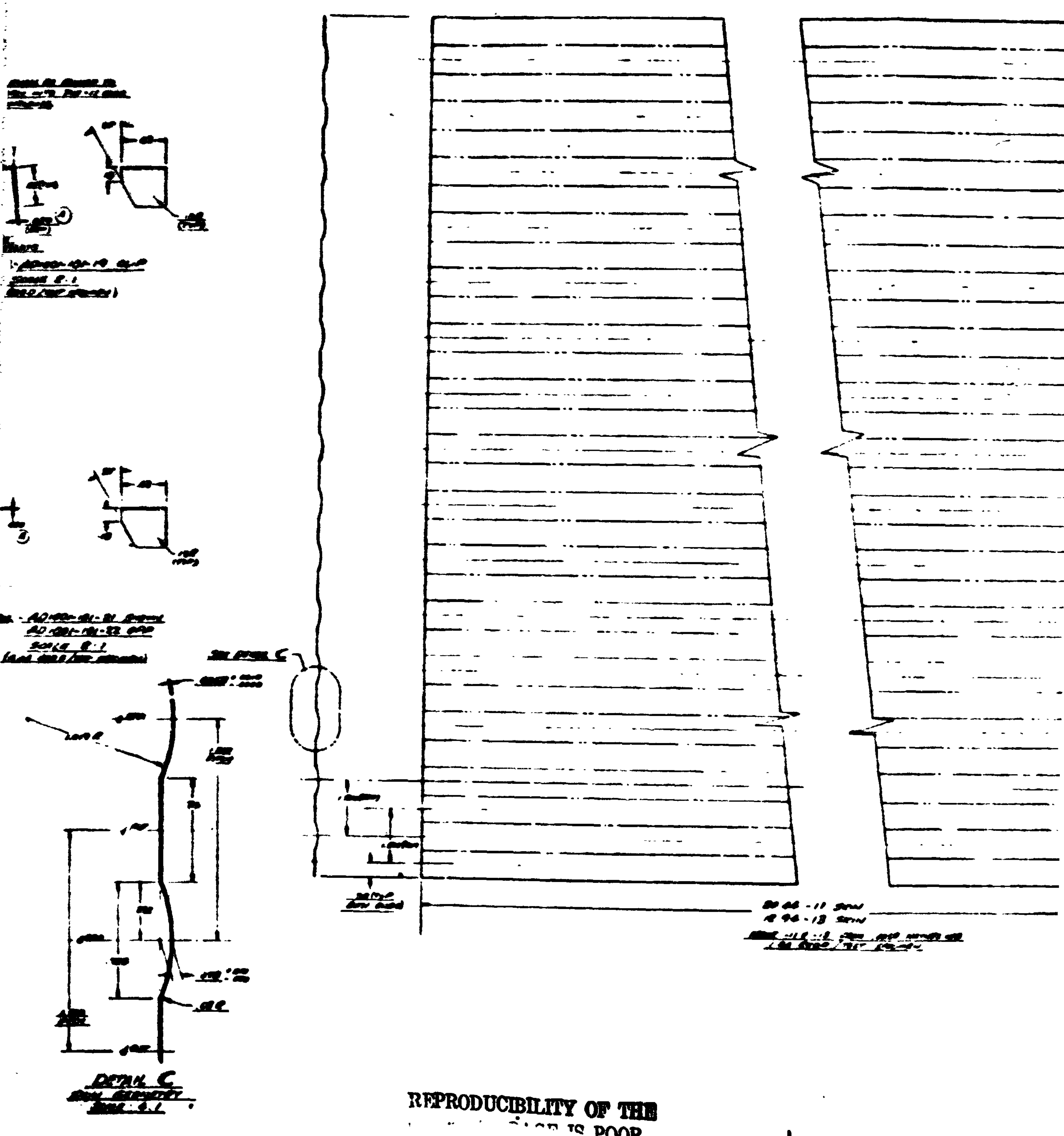

REPRODUCIBILITY OF THE
ORIGINAL PAGE IS POOR

FOLDOUT FRAME 4

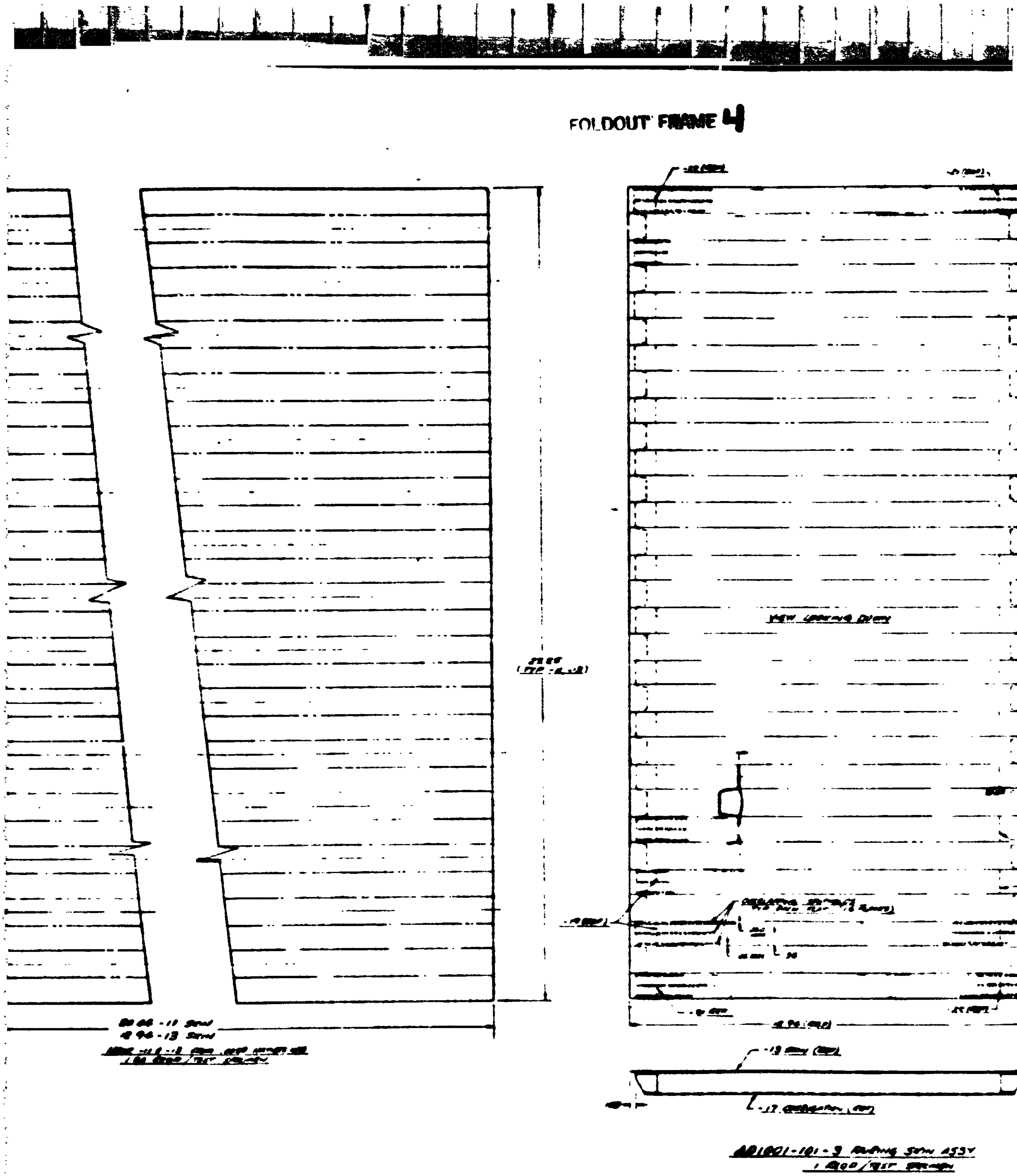

FOLDOUT FRAME 6

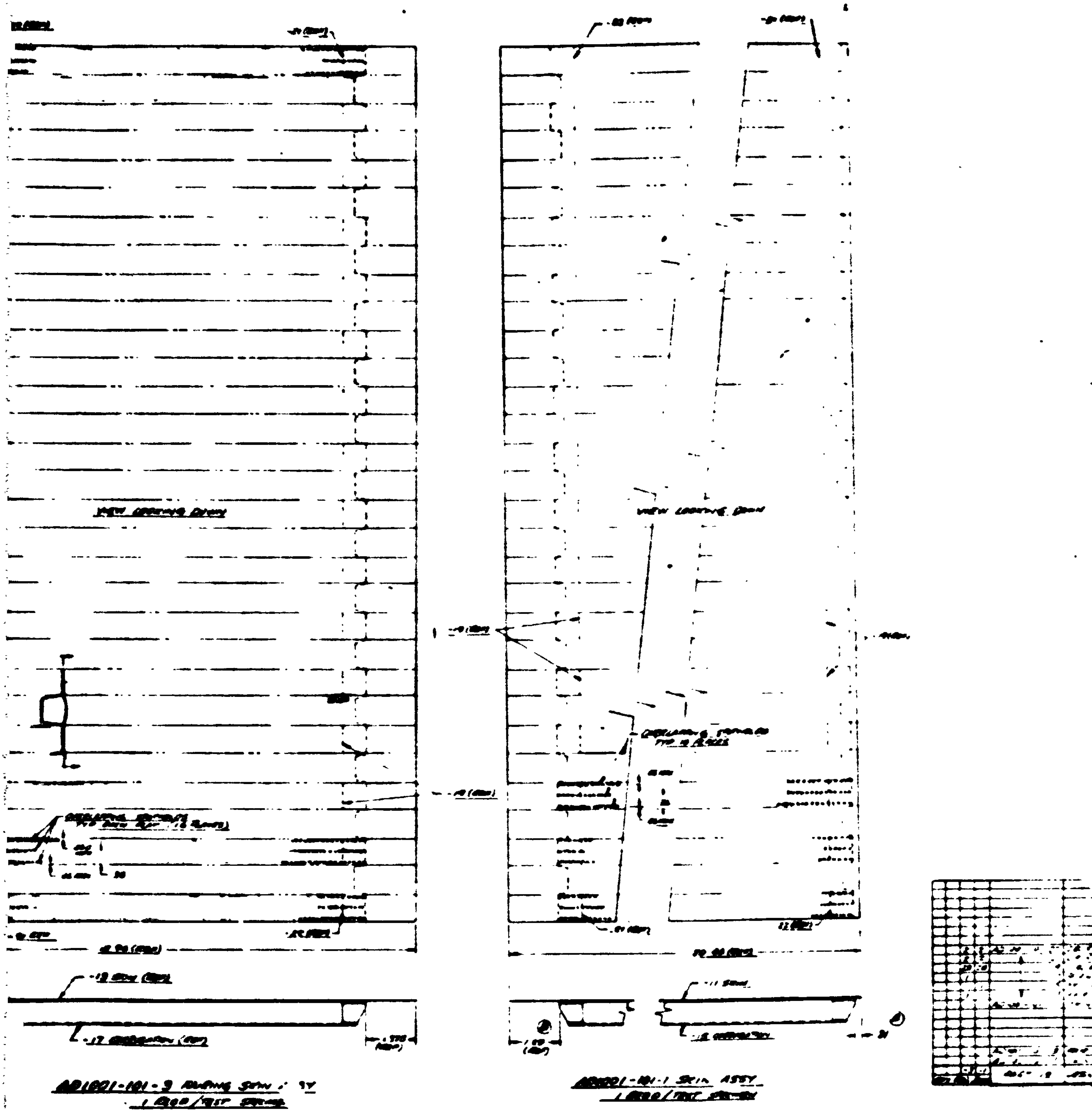

FOLDOUT FRAME 6

FOLDOUT FRAME 6

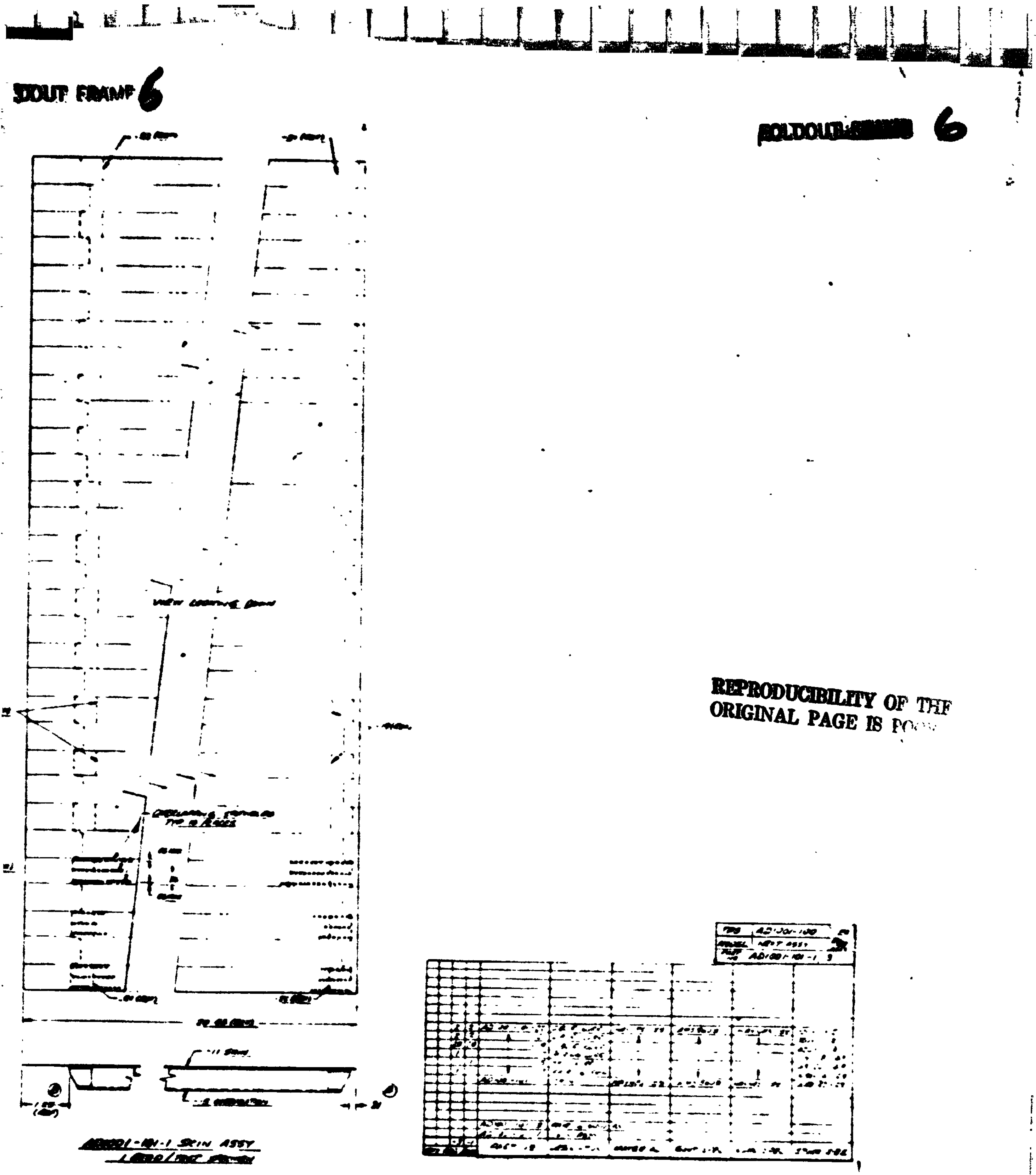

AD1001-101. – Skin – details and assembly.

FOLDOUT FRAME 1

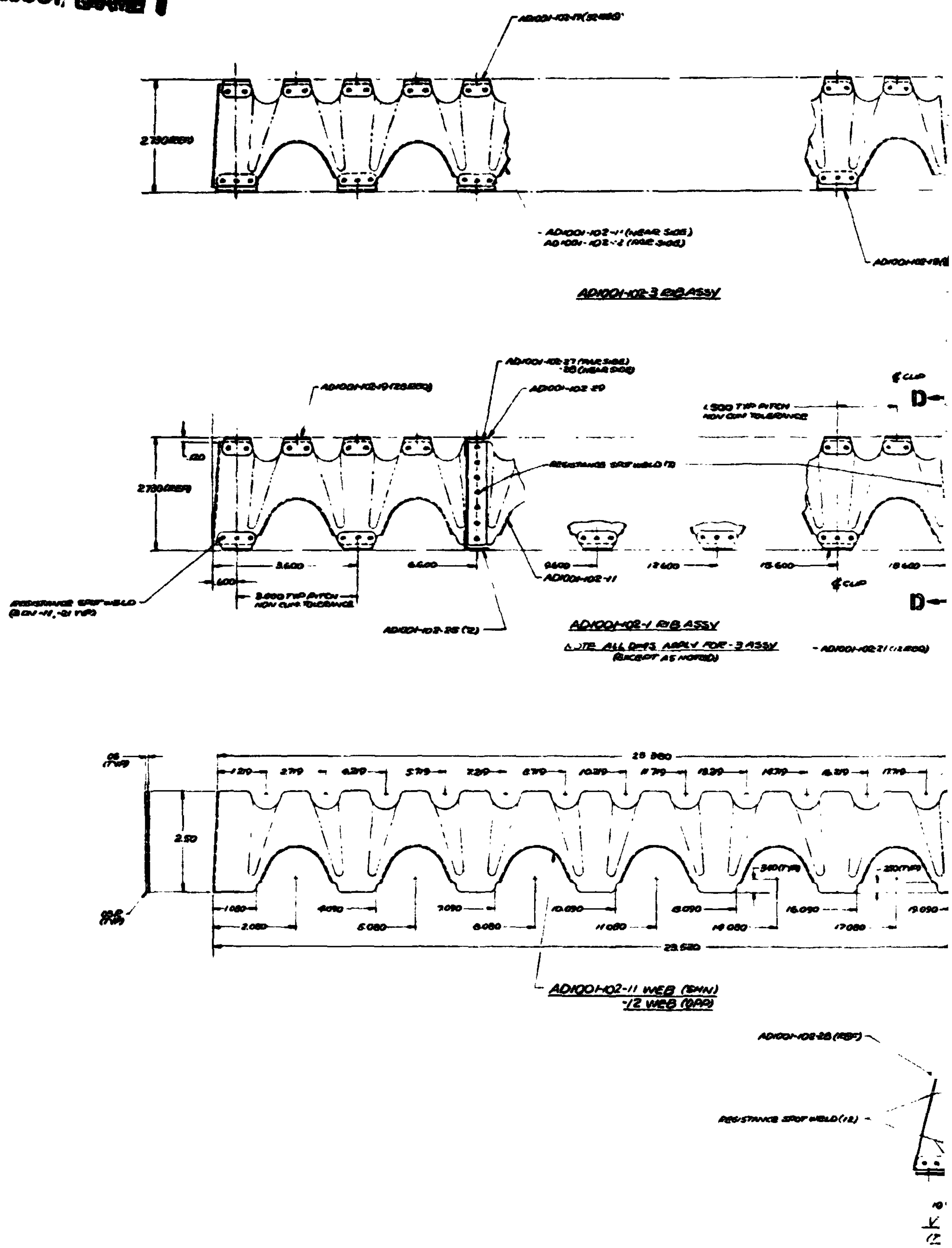

2217-104W

REPRODUCIBILITY OF THE ORIGINAL PAGE IS POOR

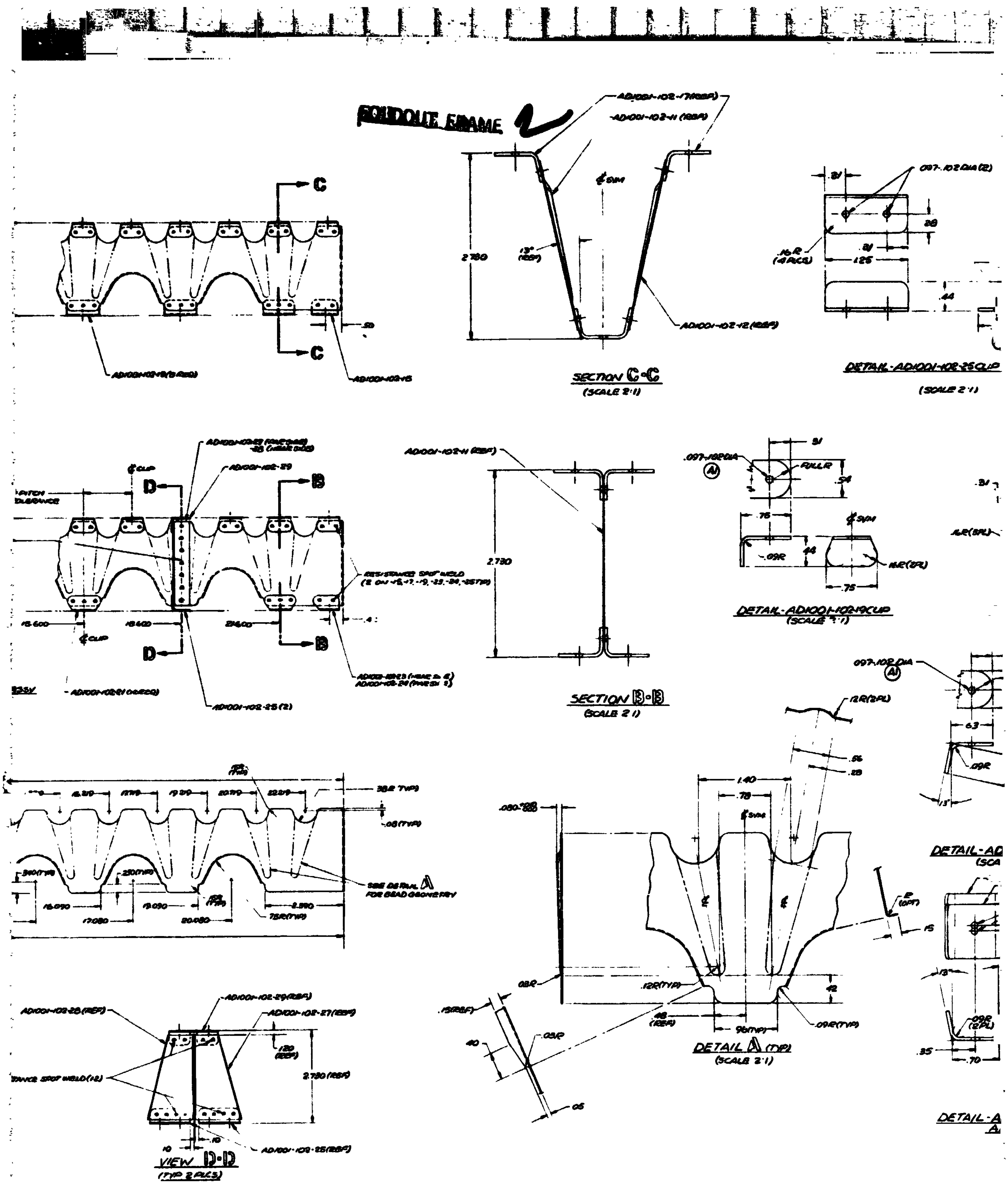

REPRODUCIBILITY OF THE
ORIGINAL PAGE IS POOR

FOLDOUT [redacted] 3

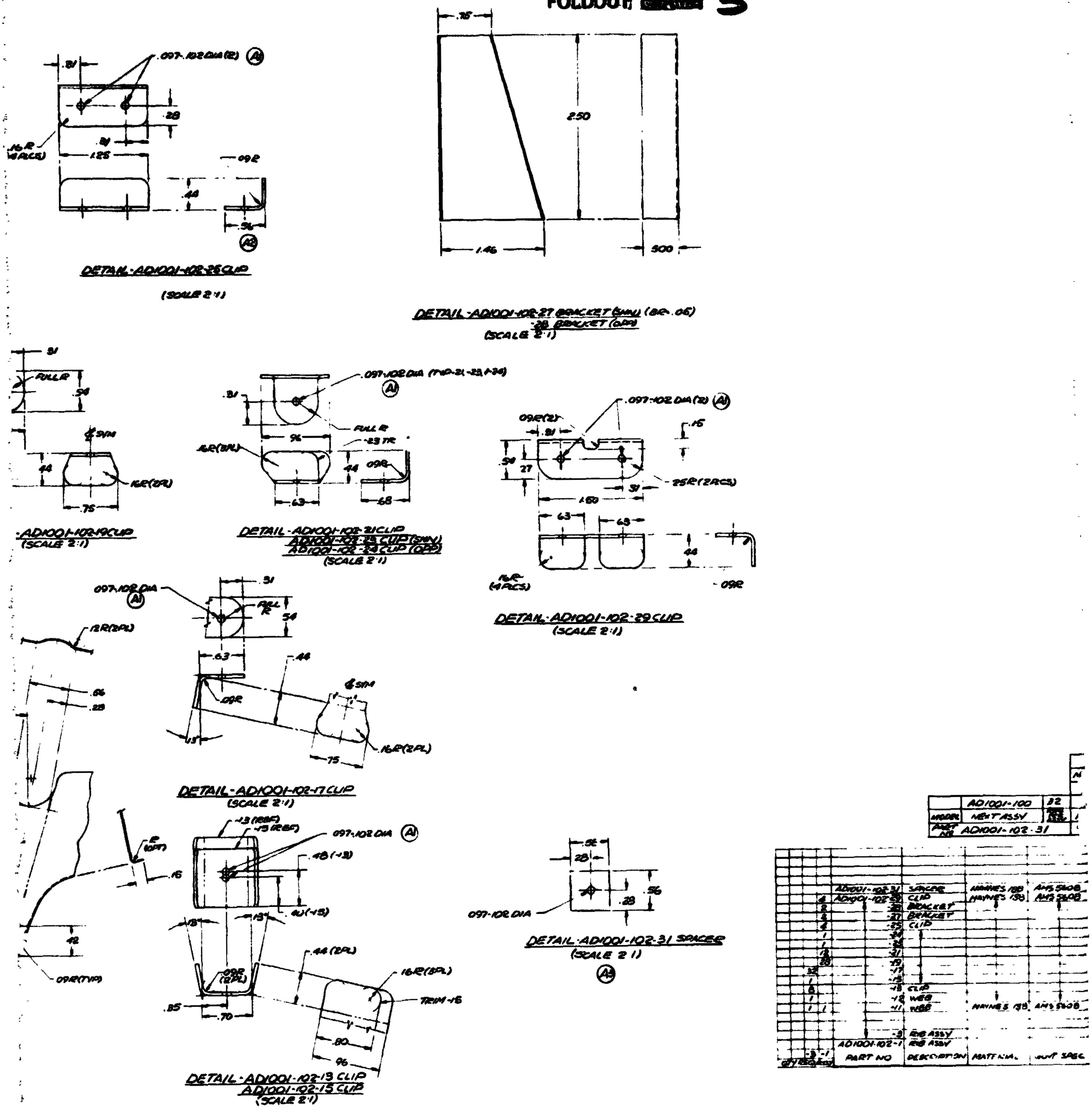

AD1001-102. – Support ribs – d

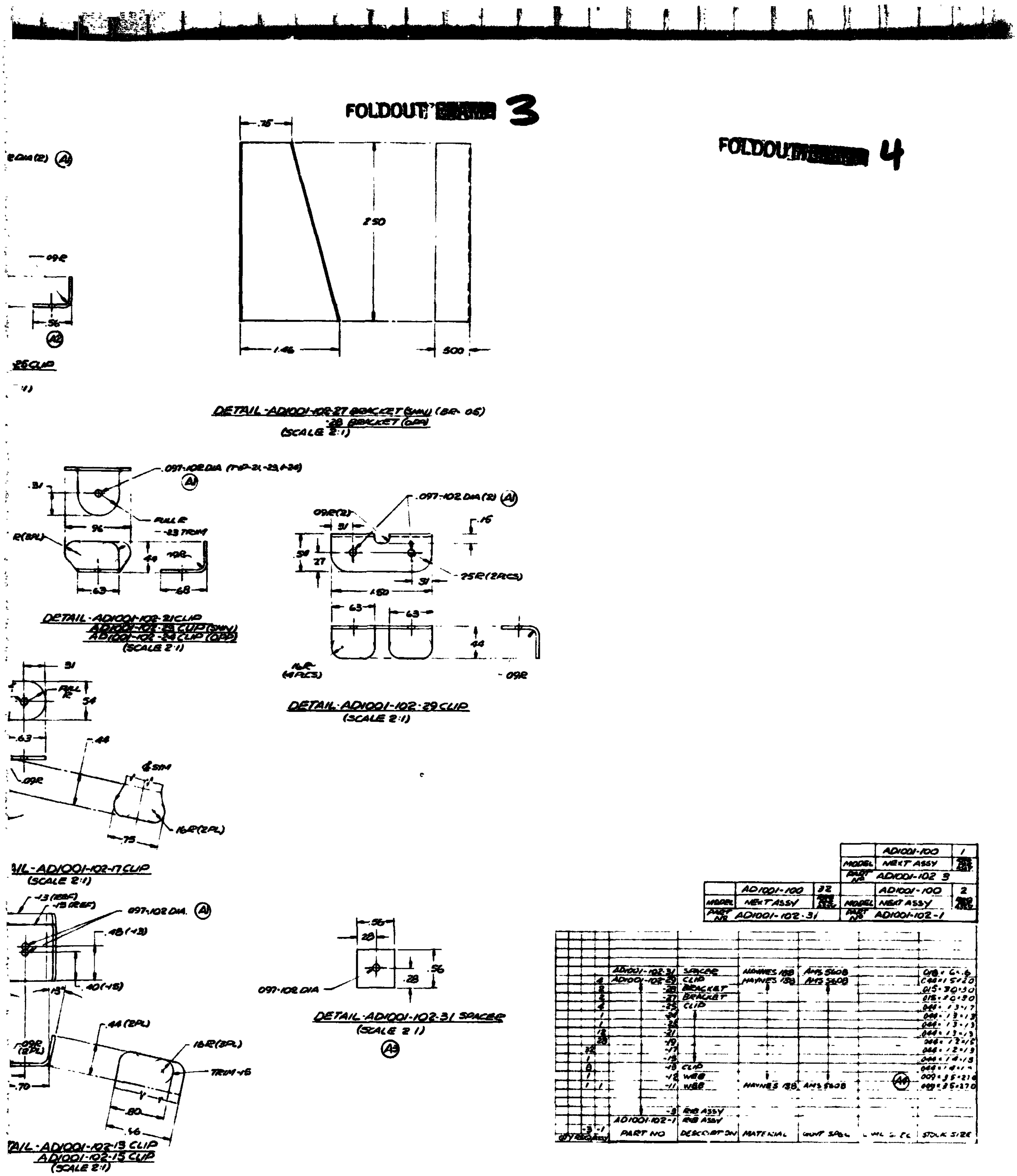

AD1001-102. – Support ribs – details and assembly.

FOLDOUT

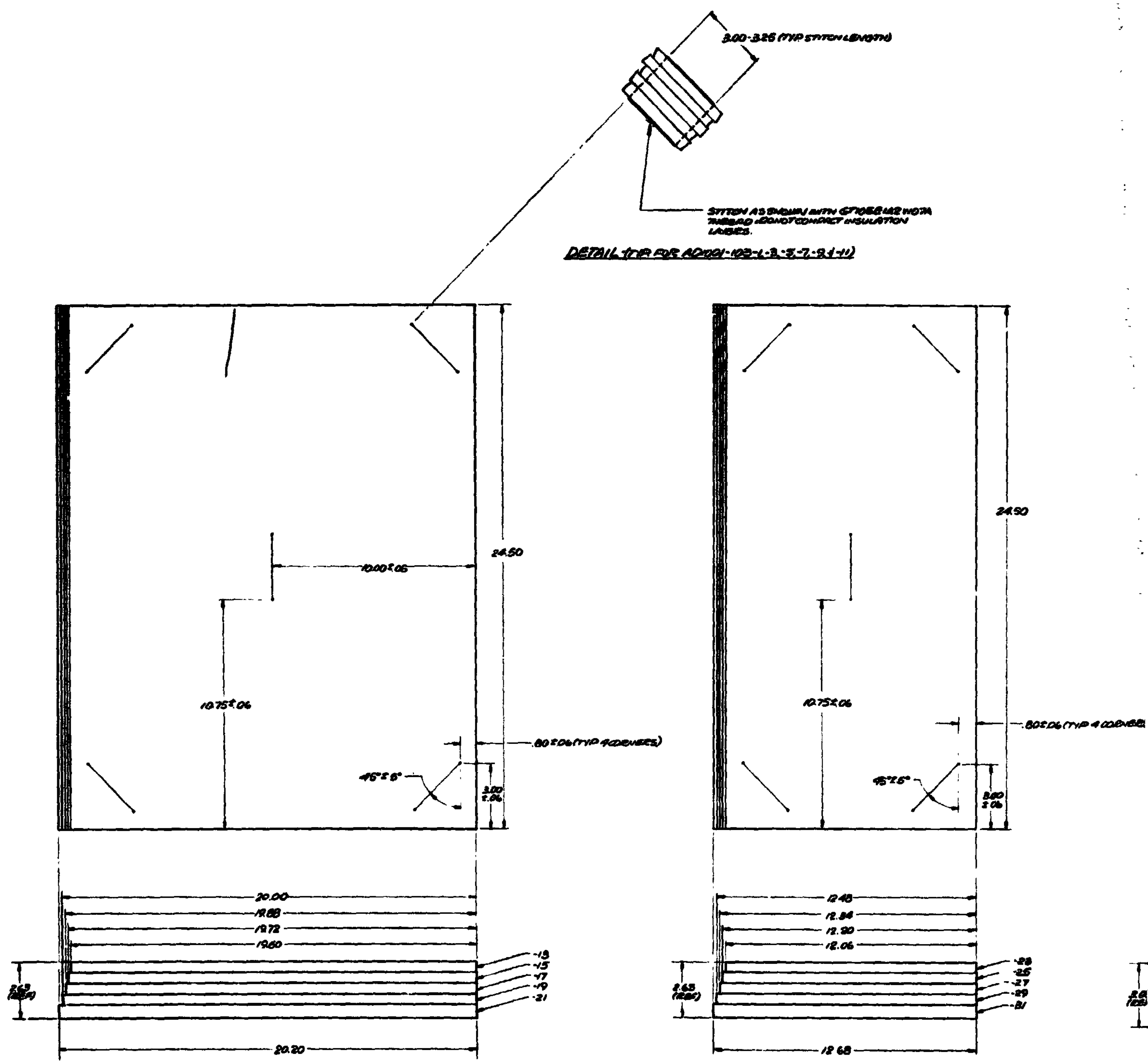

AD1001-103-1 INSULATION ASSY

AD1001-103-3 INSULATION ASSY

2217-105W

REPRODUCIBILITY OF THE

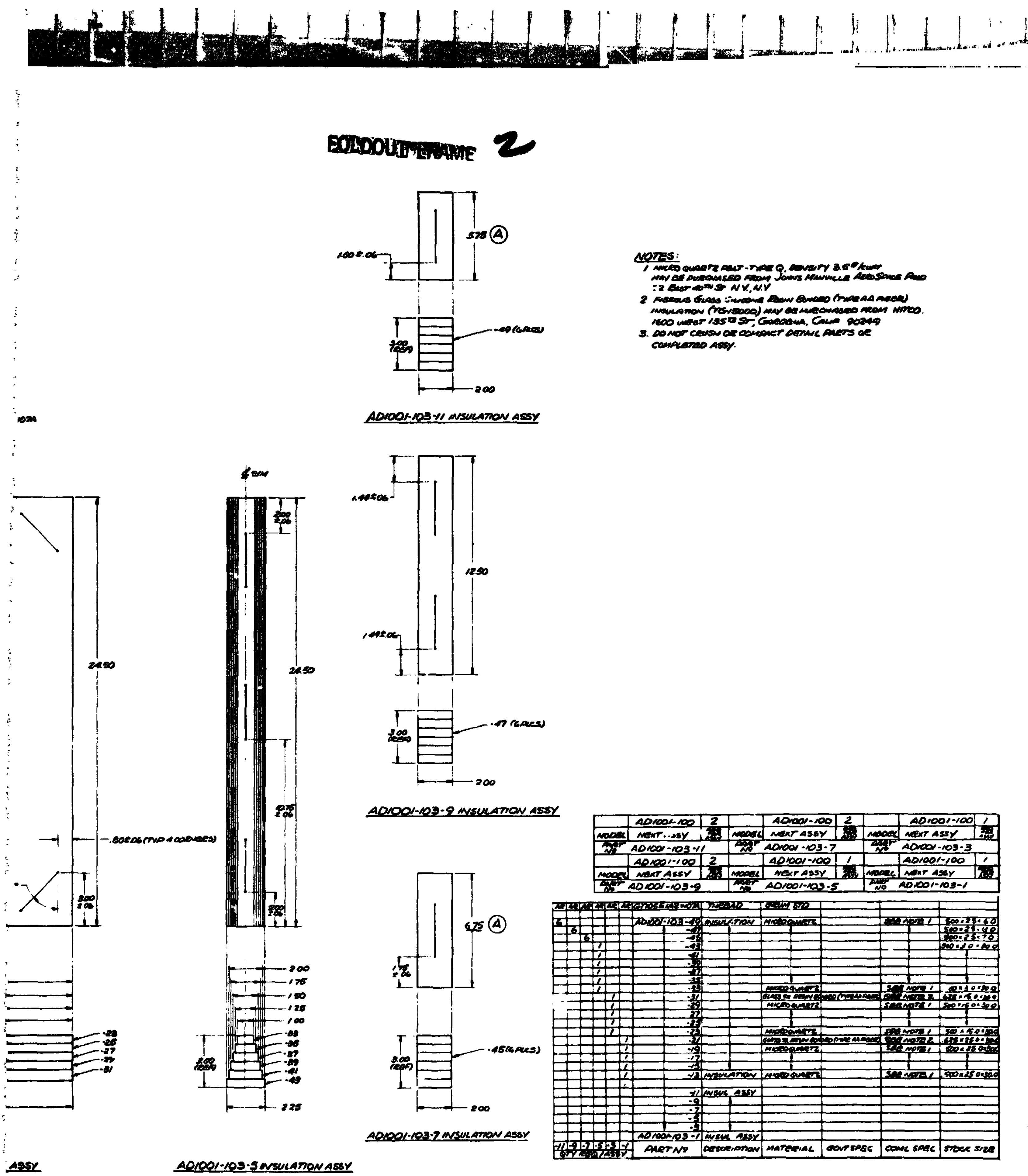

AD1001-103. – Insulation system – details and assembly.

FOLDOUT FRAME

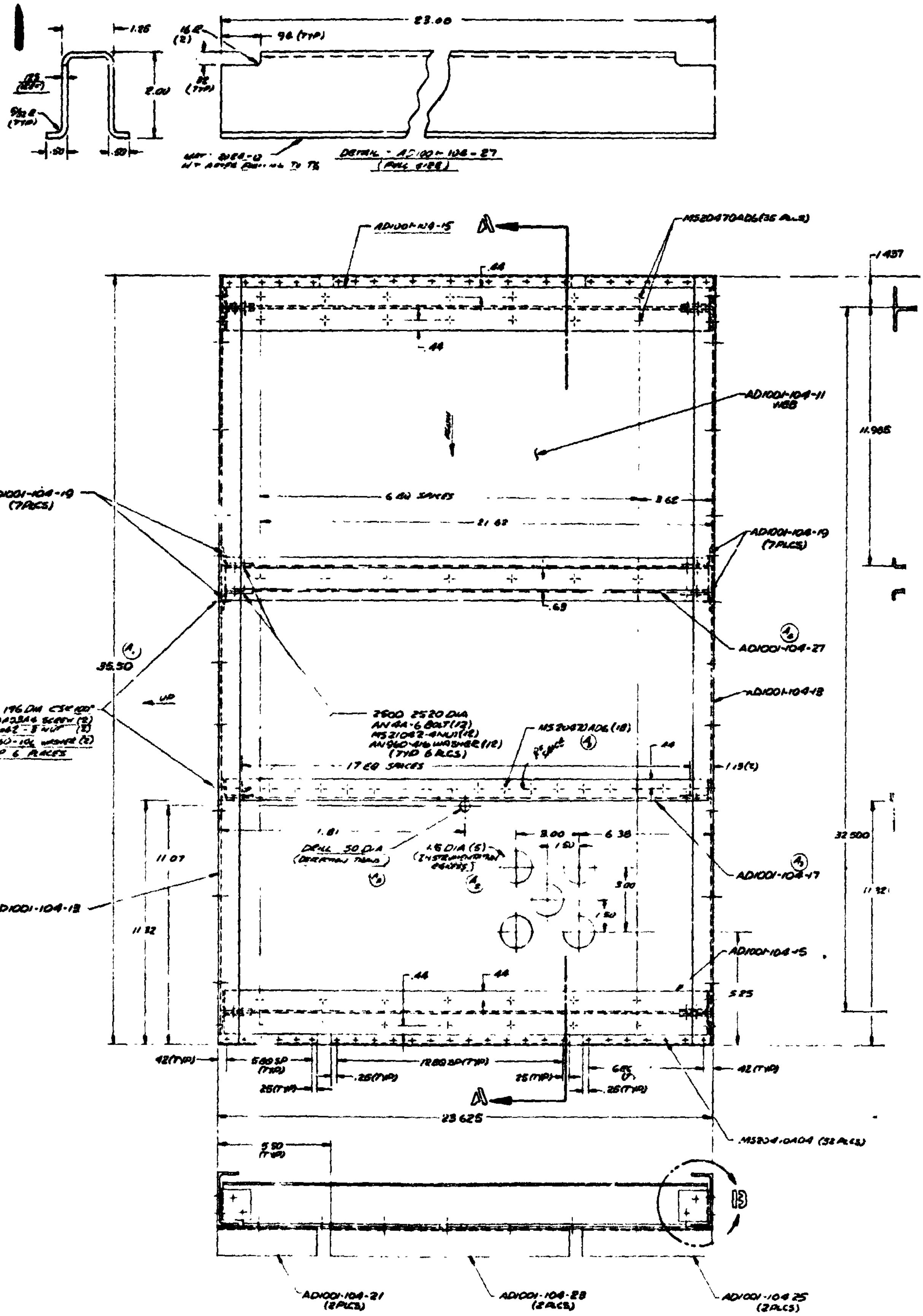

ADIOOI-104-1 SUPPORT STRUCTURE ASSY

(HALF SIZE)

2217-106W

FOLDOUT FRAME 2

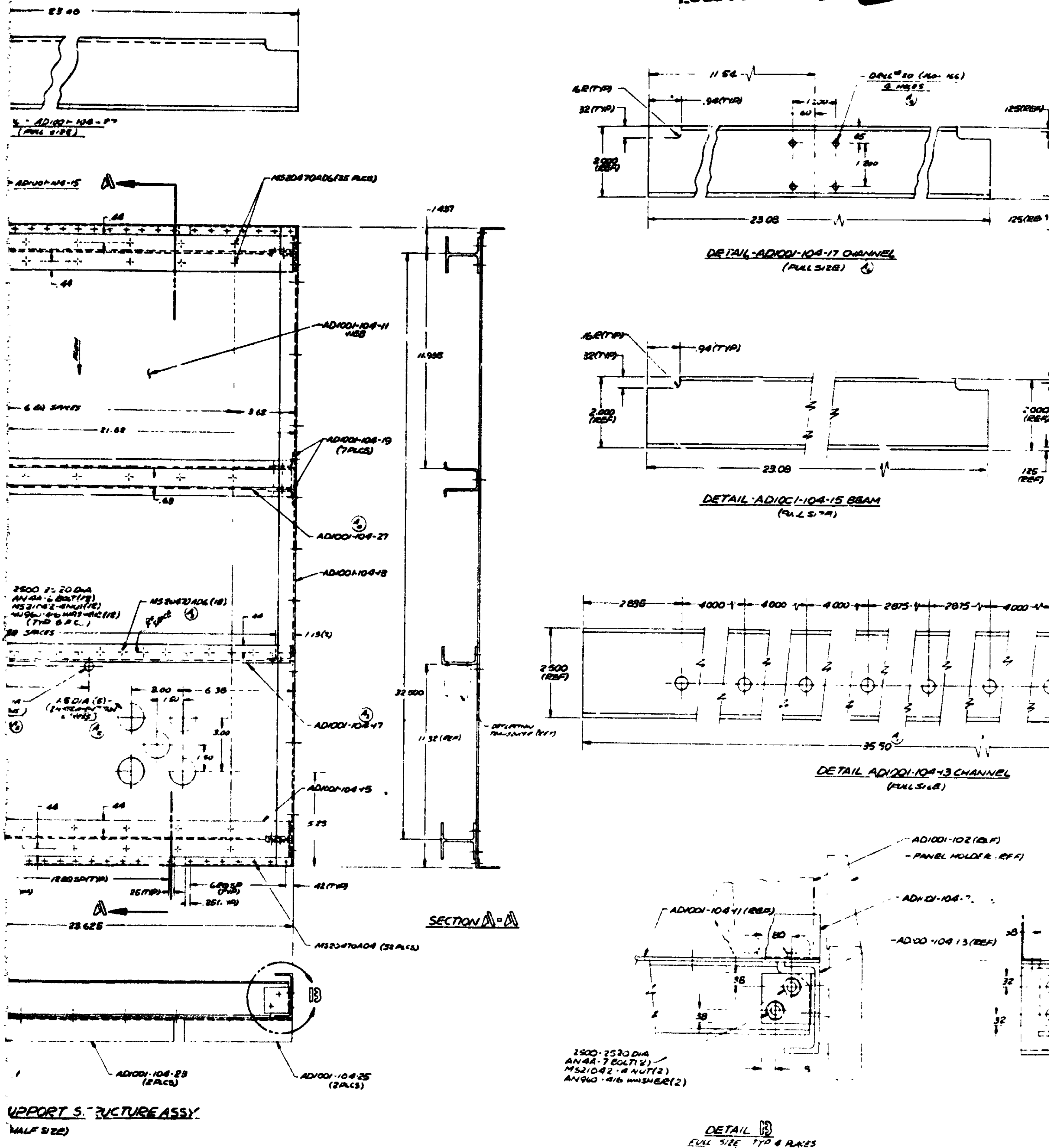

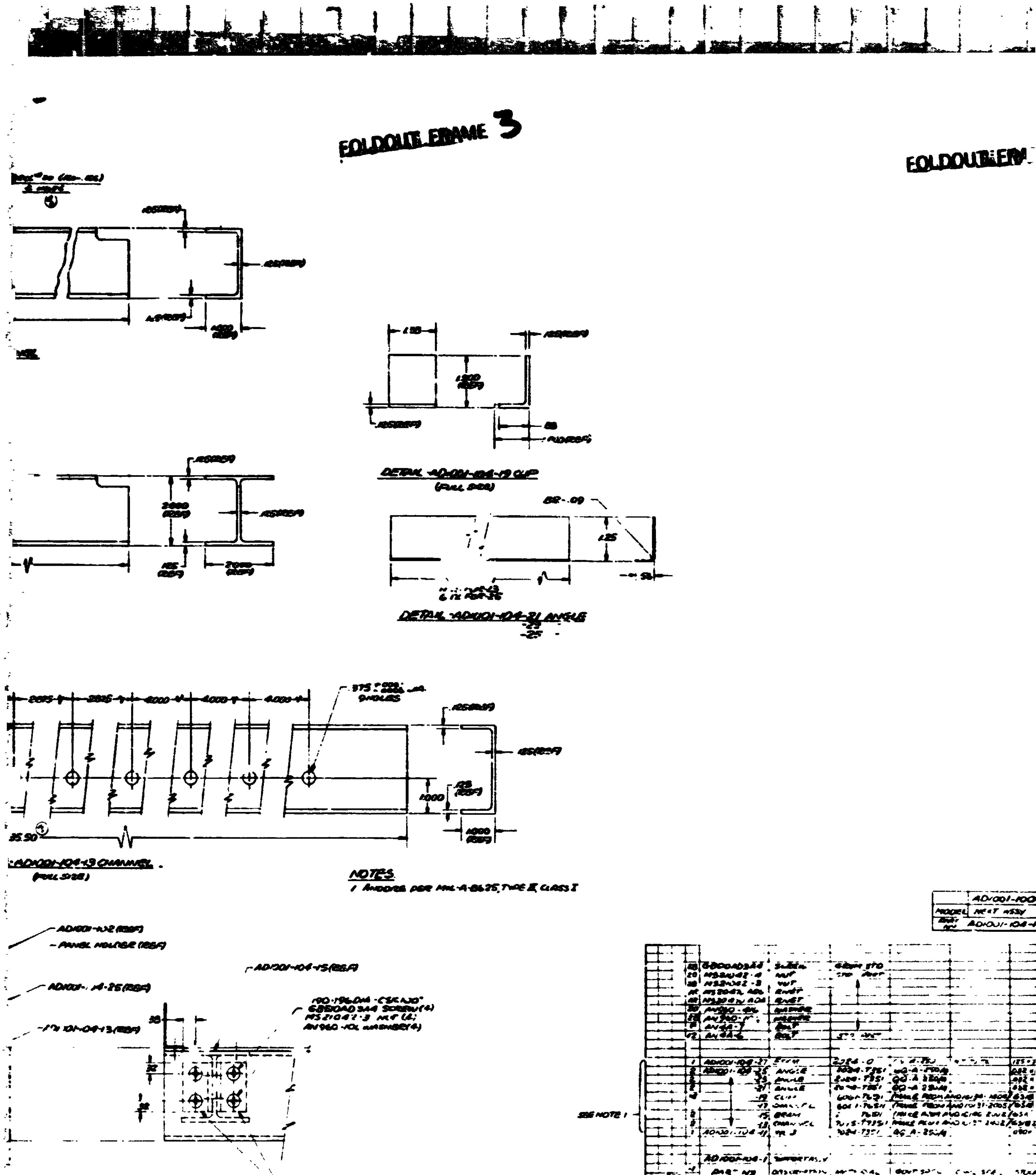

AD1001-104. – Support structure assembly.

FOLDOUT FRAME 3

FOLDOUT FRAME 4

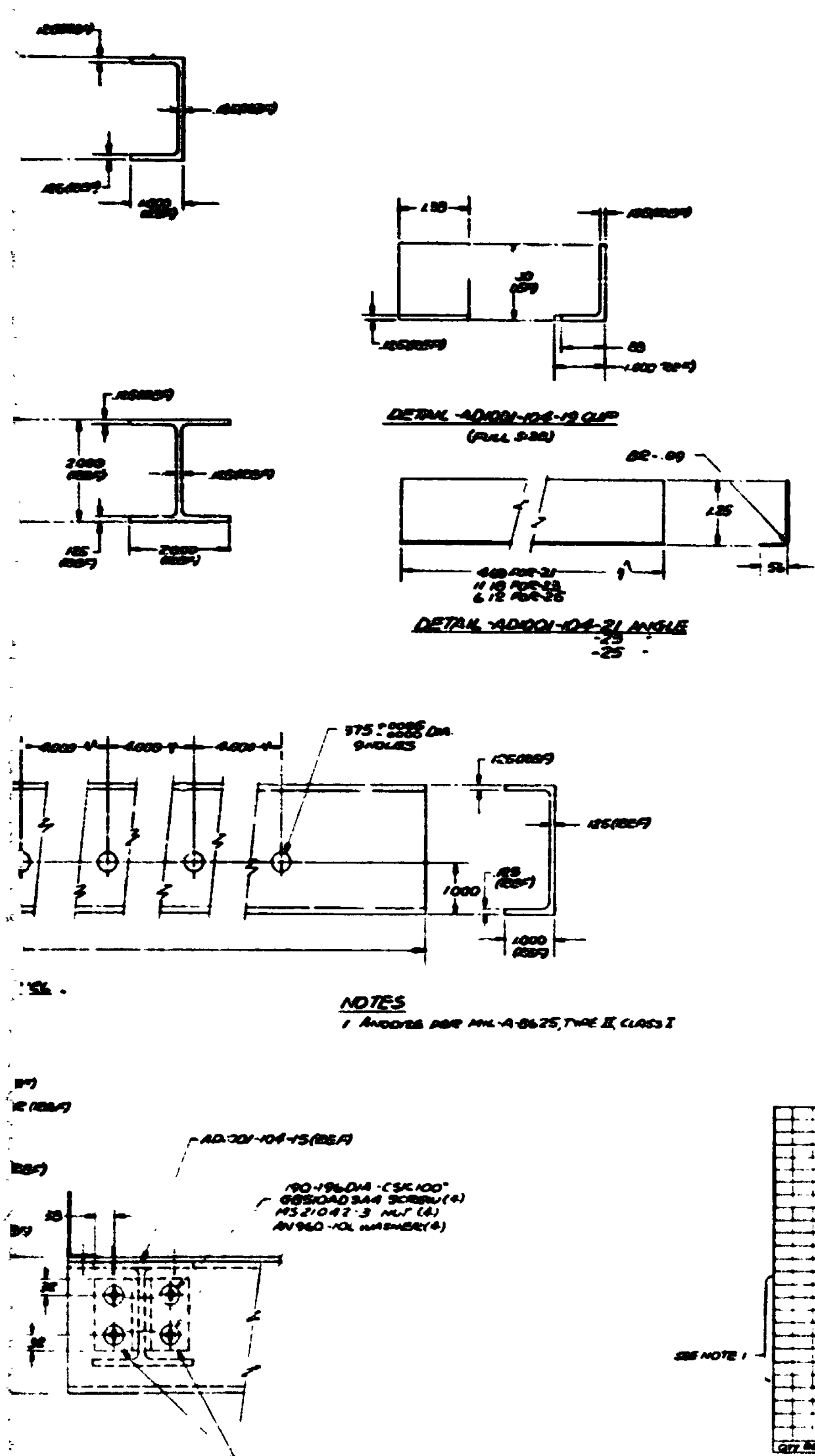

	AD1001-100	1
MODEL	NEXT ASSY	
SHEET NO	AD1001-104-1	

QTY REQD	PART NO	DESCRIPTION	MATL SPEC	GOVT SPEC	COML SPEC	STOCK SIZE
[illegible]	G8510AD3A4	SCREW	GRUM STD			
20	MS21042-4	NUT	STD PART			
[illegible]	MS21042-3	NUT				
[illegible]	MS20426AD6	RIVET				
[illegible]	MS20426AD4	RIVET				
[illegible]	AN960-616	WASHER				
[illegible]	AN960-10L	WASHER				
[illegible]	AN4A-7	BOLT				
12	AN4A-6	BOLT	STD PART			
1	AD1001-104-27	[illegible]	2024-0	[illegible]	[illegible]	[illegible]
2	AD1001-104-25	ANGLE	2024-T351	QQ-A-250/4		[illegible]
2	-23	ANGLE	2024-T351	QQ-A-250/4		[illegible]
2	-21	ANGLE	2024-T351	QQ-A-250/4		[illegible]
[illegible]	-19	CLIP	[illegible]	(MAKE FROM [illegible]		[illegible]
1	-17	CHANNEL	6061-T6511	(MAKE FROM [illegible]		[illegible]
2	-15	BEAM	[illegible]	(MAKE FROM [illegible]		[illegible]
2	-13	CHANNEL	7075-T73511	[illegible]		[illegible]
1	AD1001-104-11	WEB	2024-T351	QQ-A-250/4		[illegible]
	AD1001-104-1	SUPPORT ASSY				

AD1001-104. – Support structure assembly.

FOLDOUT

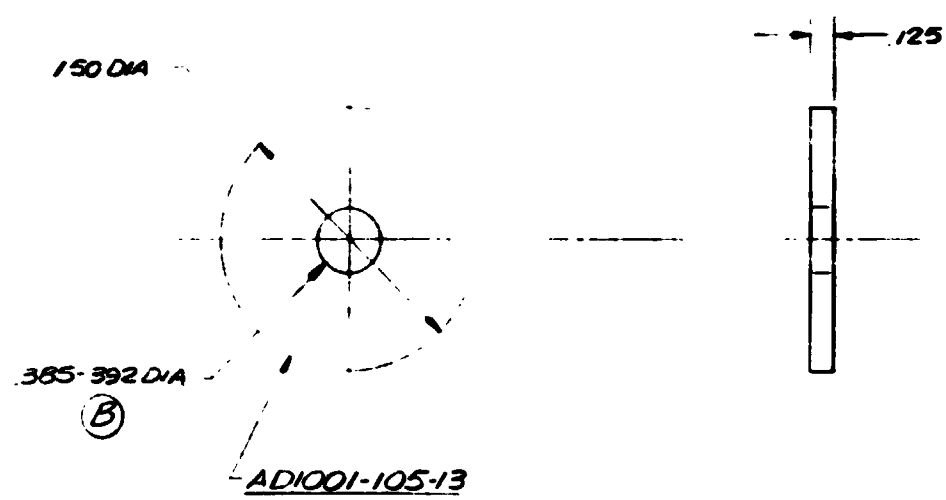

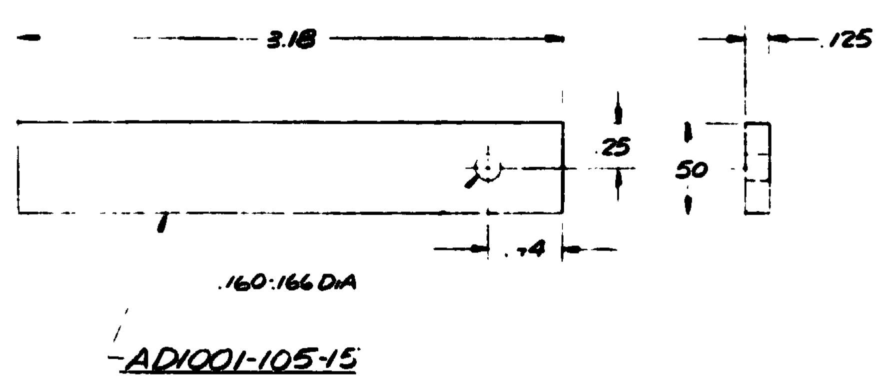

NOTE
1 FABRIC
a GLA
MFG
MAT
TO C
b. FOR
BE
AN
MINI
c NO
d WA
e. EX
TO

2217-107W

NOTES:

1. FABRICATION PROCESS FOR -11, -13, & -15 AS FOLLOWS
   a. GLASS REINFORCED SILICONE LAMINATE TO BE MFG'D IN ACCORDANCE WITH LSP-14-1104 USING MATERIAL IN ACCORDANCE WITH LSM-14-4082 AND TO CONFORM TO MIL-P-25518, TYPE I
   b. FOR -11, -13 & -15, THE 480°F STEP IN POST CURE SHALL BE HELD 20 HOURS MINIMUM AND THERE SHALL BE AN ADDITIONAL POST CURE CONDITIONING AT 750°F MINIMUM FOR 45 MINUTES MINIMUM.
   c. NO OF LAYERS 12 MINIMUM FOR .125 BUILDUP
   d. WARP DIRECTION OPTIONAL
   e. EXTERIOR SURFACE TO BE SUFFICIENTLY PIT FREE TO INSURE SATISFACTORY FINAL FINISH

.125

MODEL	NEXT ASSY	REQ PER ASSY
	AD1001-100 AD1001-300	36

PART NO AD1001-105-13

MODEL	NEXT ASSY	REQ PER ASSY
	AD1001-100 AD1001-300	4

PART NO AD1001-105-15

MODEL	NEXT ASSY	REQ PER ASSY
	AD1001-100 AD1001-300	37

PART NO AD1001-105-11

QTY REQ ASSY	PART NO	DESCRIPTION	MATERIAL	GOVT SPEC	COML SPEC	STOCK SIZE
	-15	SPACER	FIB SIL LAM			SEE NOTE 1
	-13	SPACER	FIB SIL LAM			SEE NOTE 1
	AD1001-105-11	SPACER	FIB SIL LAM			SEE NOTE 1

AD1001 105. – Insulation spacers.

FOLDOUT FRAME 1

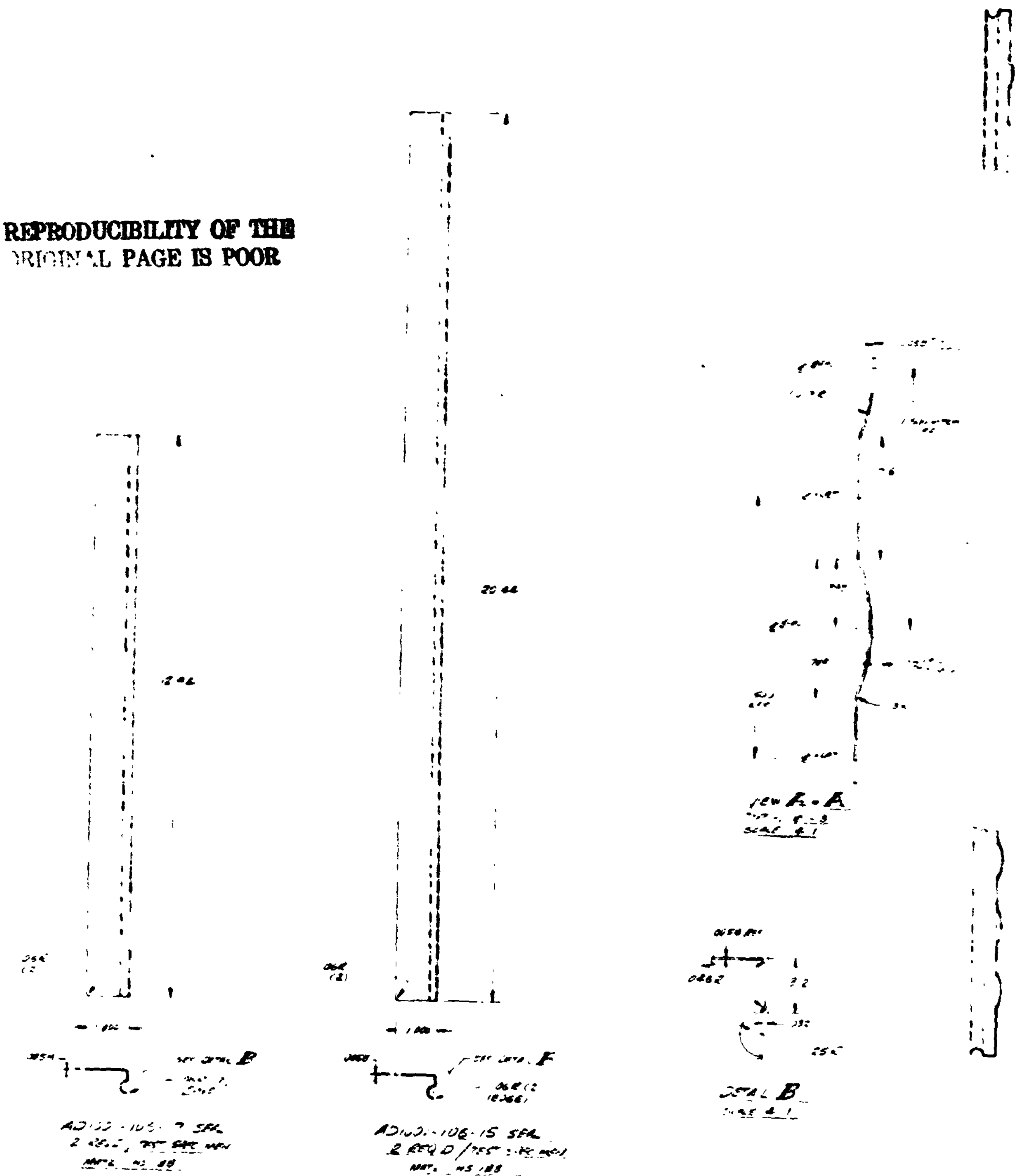

2217-108W

FOLDOUT FRAME 2

REPRODUCIBILITY OF THE ORIGINAL PAGE IS POOR

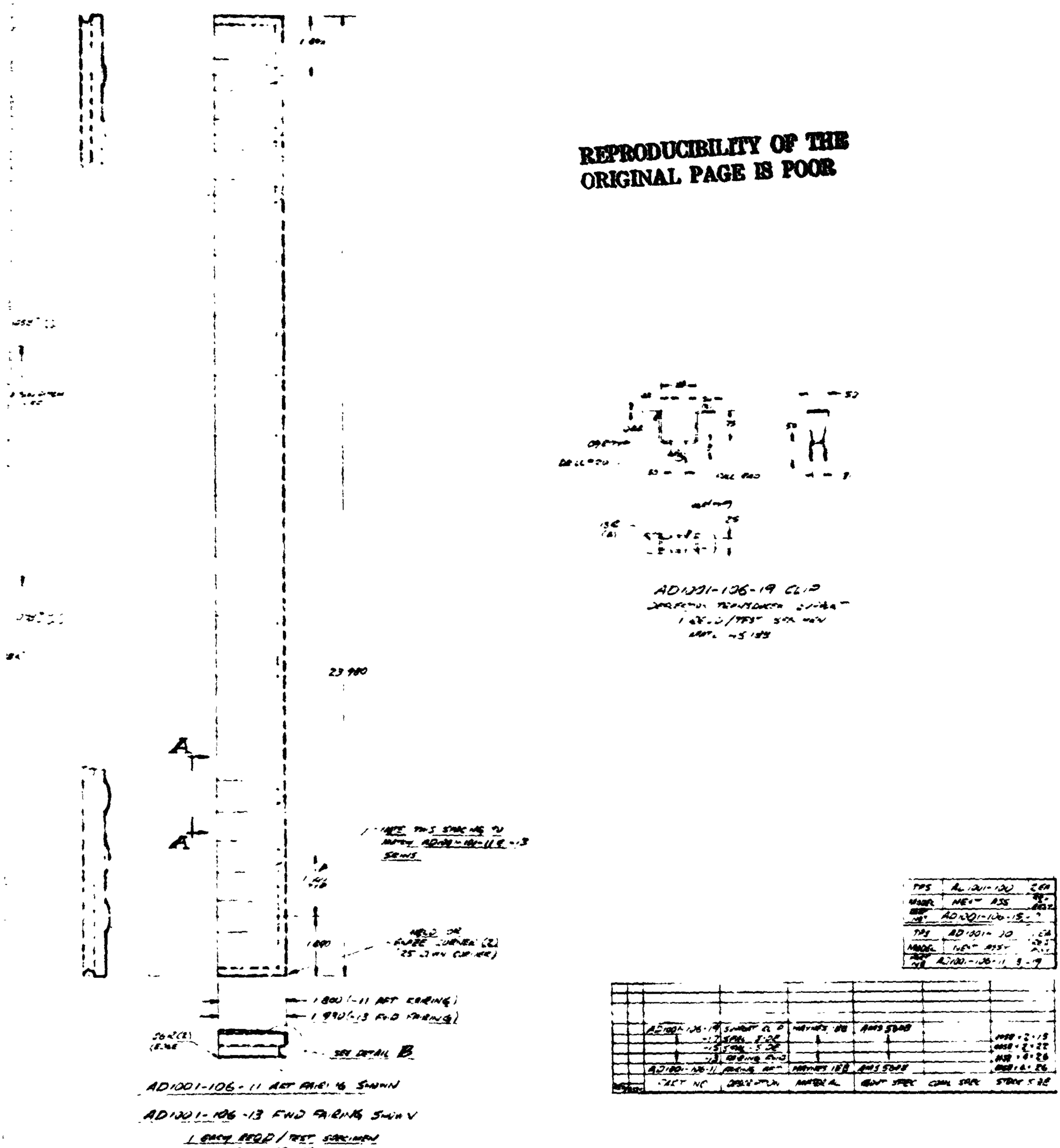

AD1001-106. – Fairing and end seals – details.

APPENDIX F

RENE' 41 TPS PRODUCTION DRAWINGS

The Rene' 41 TPS test specimen production drawings are given, including:

AD1001-300 Test Specimen Final Assembly
AD1001-301 Skin - Details and Assembly
AD1001-302 Support Ribs - Details and Assembly
AD1001-303 Insulation System Details and Assembly
AD1001-304 Support Structure Assembly
AD1001-306 Fairings and End Seal Details

FOLDOUT FRAME 1

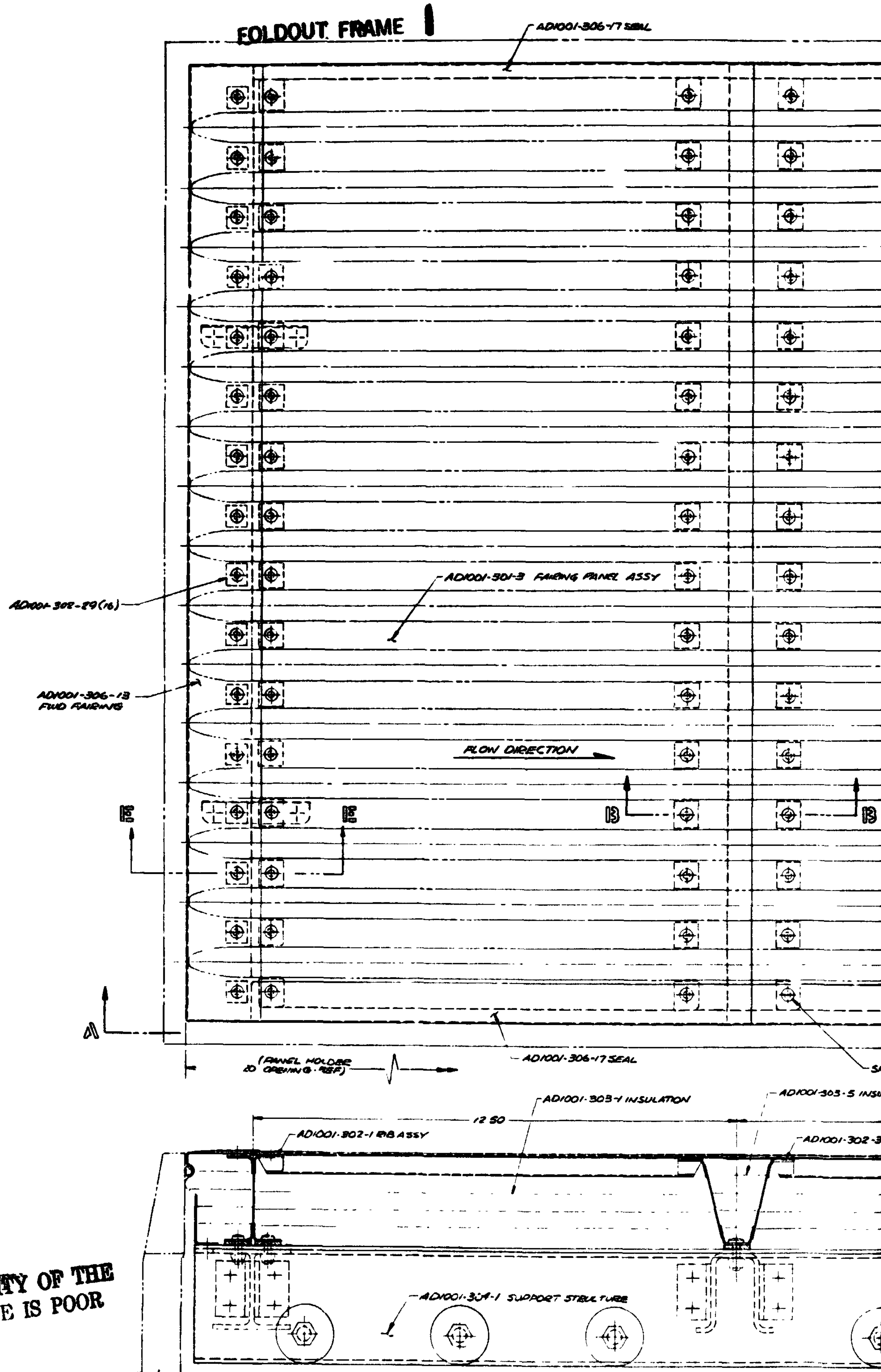

FOLDOUT FRAME 2

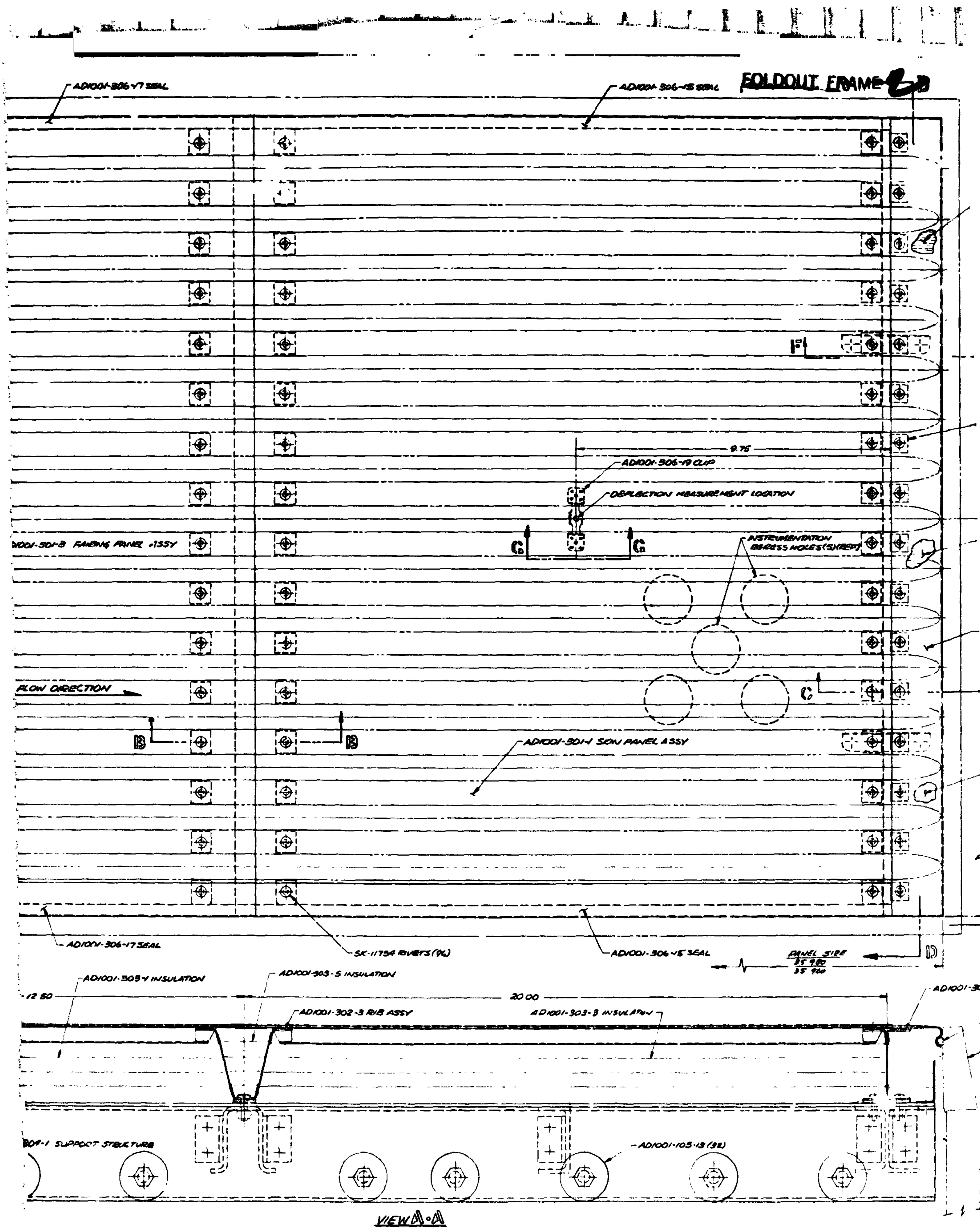

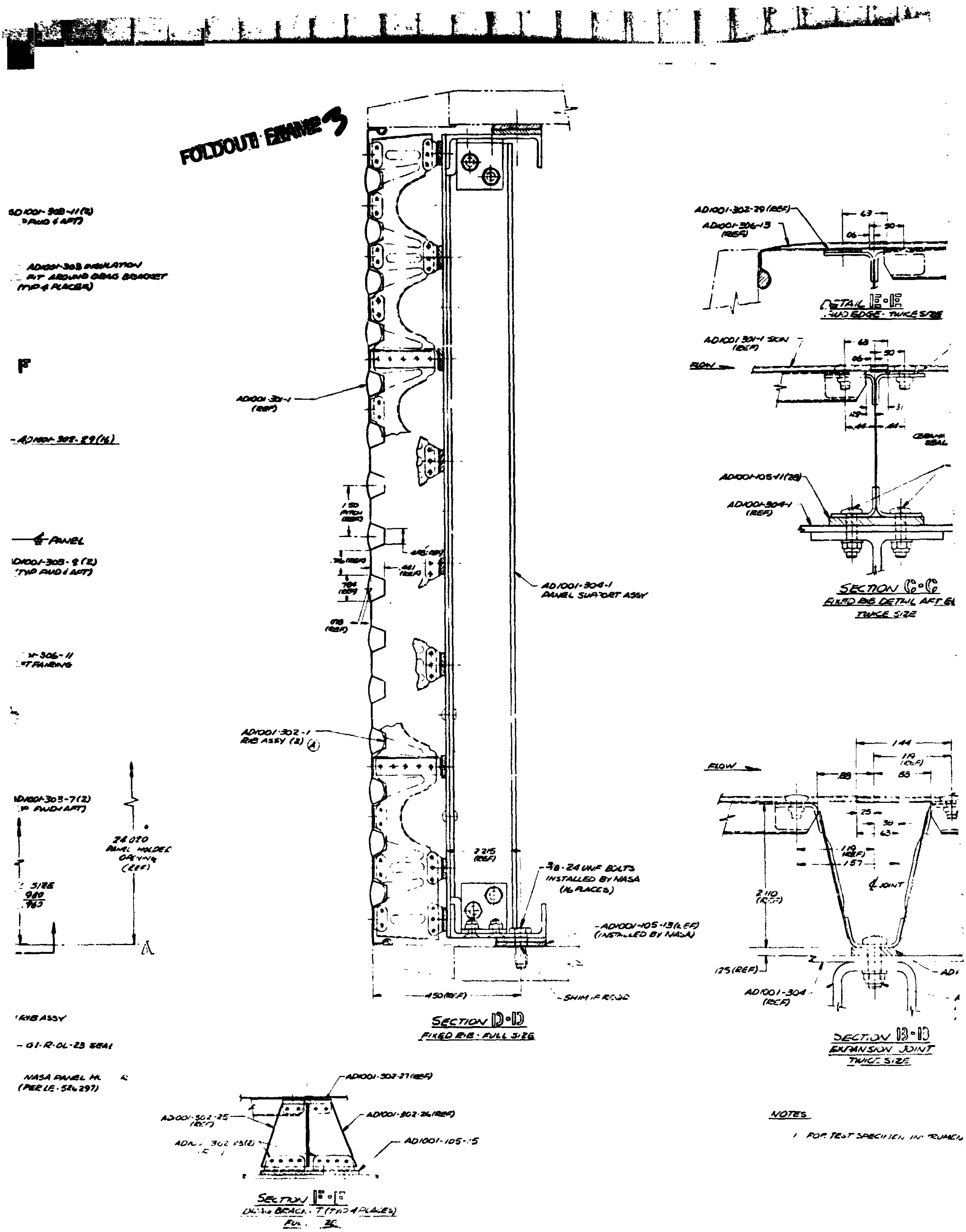

NOTES

1 FOR TEST SPECIMEN IN TRUMEN

FOLDOUT FRAME 4

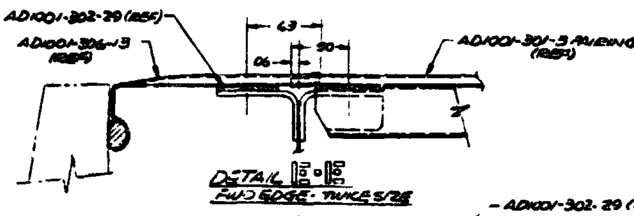

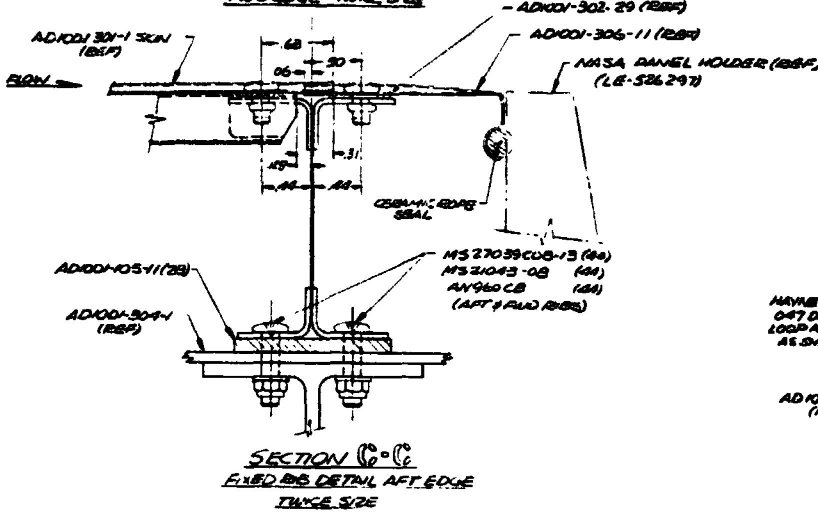

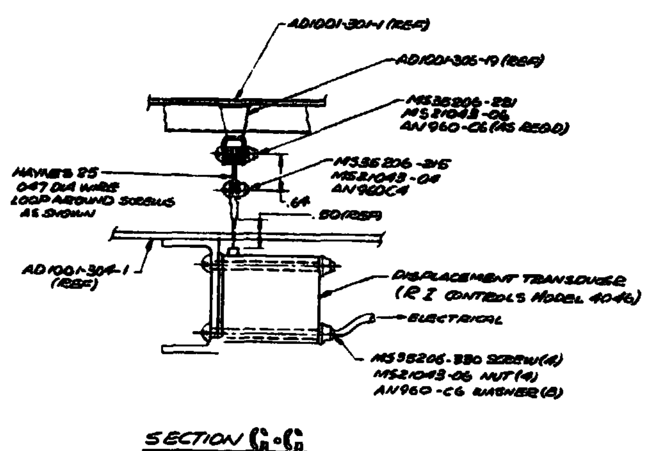

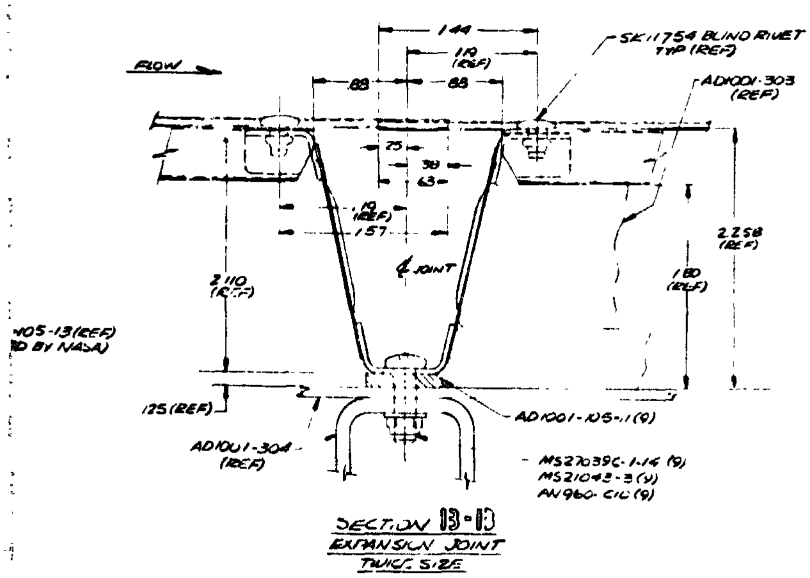

NOTES

1 FOR TEST SPECIMEN INSTRUMENTATION SEE AD1002

QTY REQD	PART NO	NOMENCLATURE	MATERIAL	GOVT SPEC	COML SPEC	STOCK SIZE
1	MODEL 4046	DSP TRANSDUCER				
4	MS35206-330	SCREW	STD PART			
1	MS35206-281					
1	MS35206-215					
9	MS27039-1-14					
44	MS27039C08-13	SCREW				
9	MS21043-3	NUT				
44	MS21043-08					
12	MS21043-06					
1	MS21043-04	NUT				
9	AN960 C10	WASHER				
44	C8					
12	C6					
1	AN960 C4	WASHER	STD PART			
AR	GIR OL-2E	SEAL	CERAMIC ROPE (PUR FROM GARRETT MFG. CO., INC.)			
96	SK-11754	RIVET, BLIND	HAYNES 188 (PUR FROM HUCK MFG CO.)			
1	AD1001-306-19	CLIP	SEE DWG			
2	-17	SIDE SEAL				
2	-15	SIDE SEAL				
1	-13	FAIRING FWD				
1	AD1001-306-11	FAIRING AFT				
4	AD1001-105-15	SPACER INSUL				
32	AD1001-105-13	SPACER INSUL				
37	AD1001-105-11	SPACER INSUL				
1	AD1001-304-1	SUPPORT STR				
2	AD1001-303-11	INSUL ASSY				
2	-9					
2	-7					
1	-5					
1	-3					
1	AD1001 303-1	INSUL ASSY				
37	AD1001-302-29	SPACER				
1	AD1001 302-3	RIB (FLEX)				
2	AD1001-302-1	RIB (FIXED)				
1	AD1001-301-3	FAIRING PANEL				
1	AD1001 301-1	SKIN PANEL	DWG			
	AD1001 300-1	TEST SPECIMEN ASSY & INSTL				
QTY REQD	PART NO	NOMENCLATURE	MATERIAL	GOVT SPEC	COML SPEC	STOCK SIZE

AD100'-300. – Test specimen final assembly.

FOLDOUT FRAME 1

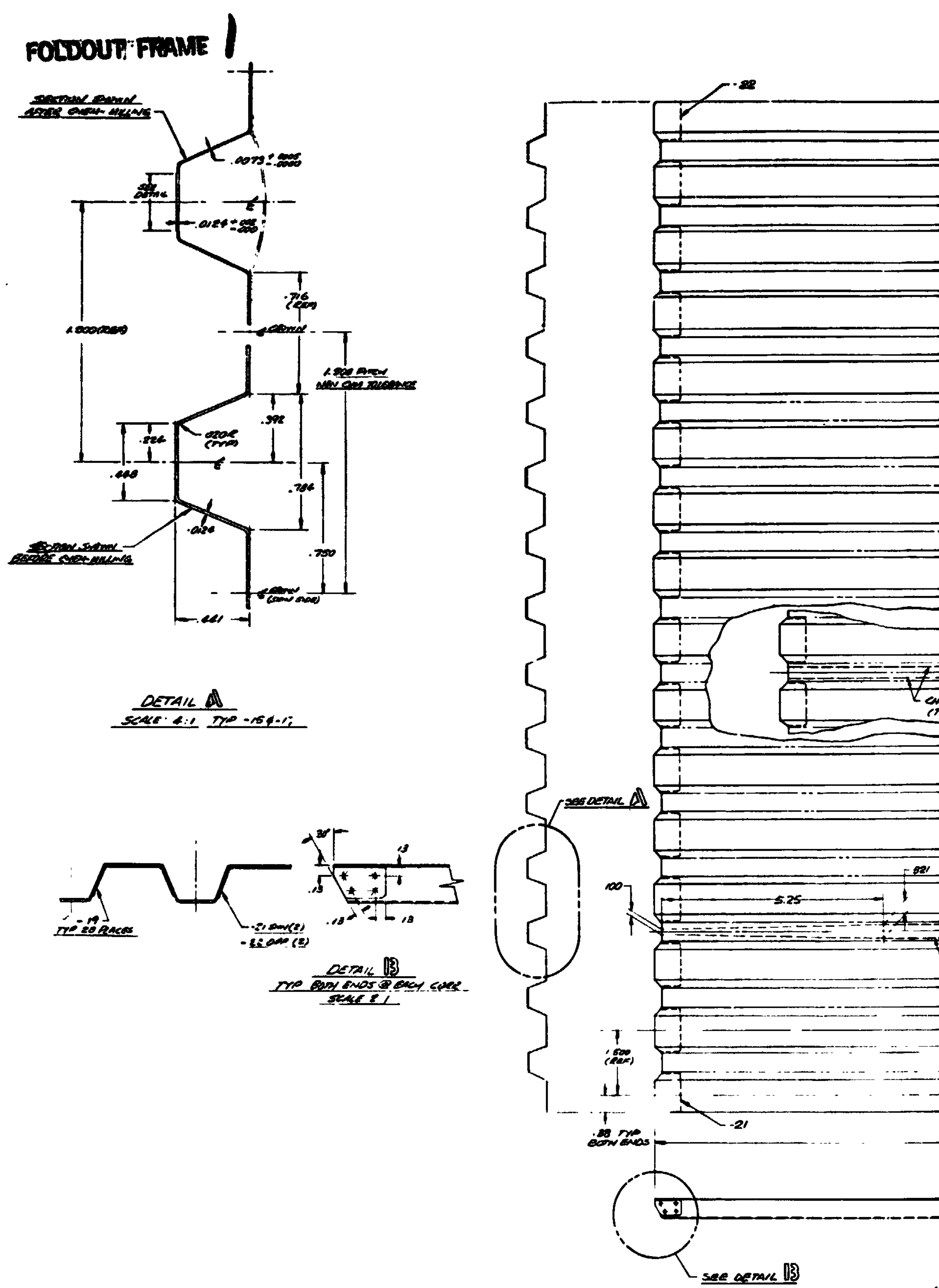

2217-110W

FOLDOUT FRAME 2

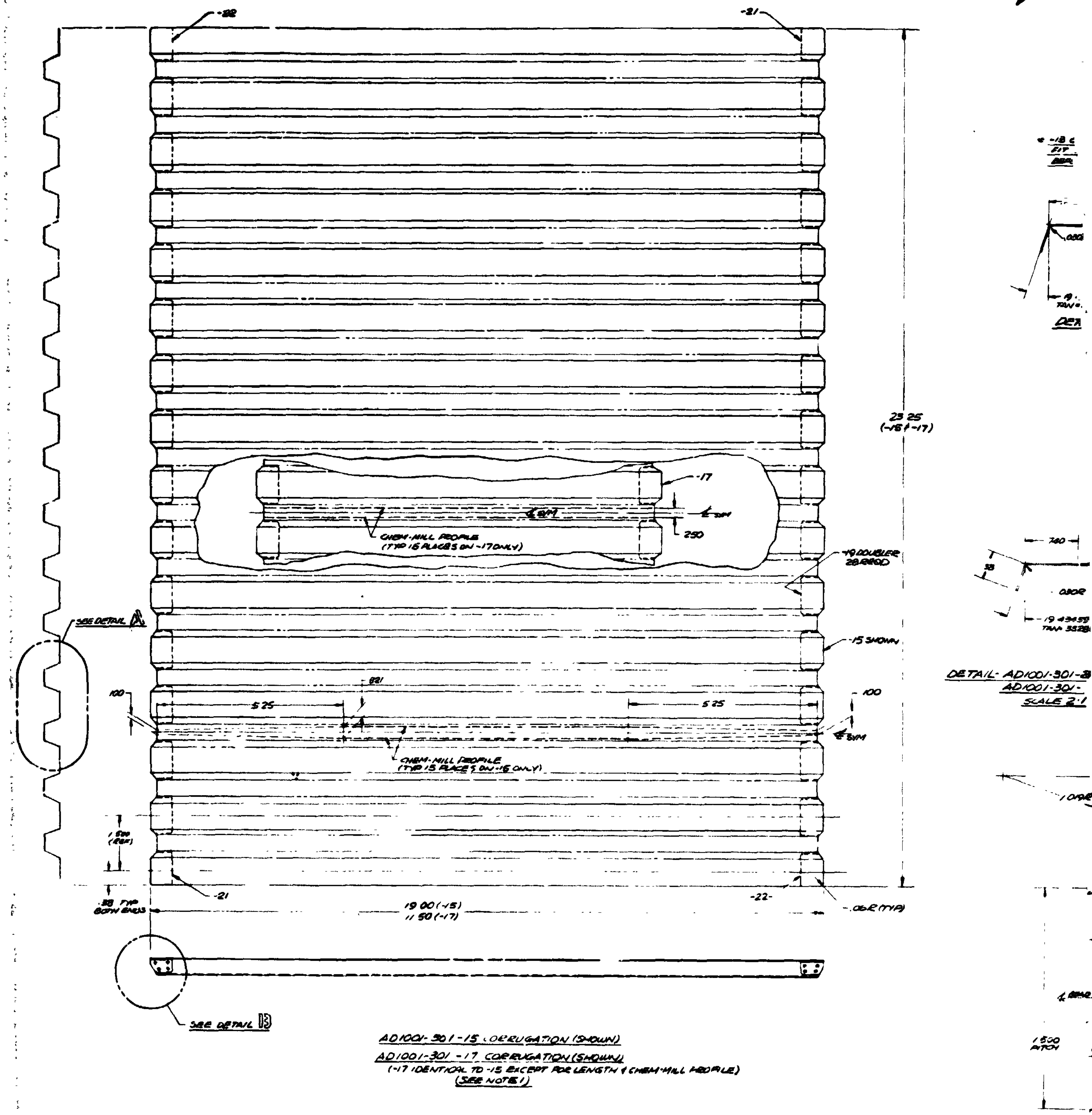

AD1001-301-15 CORRUGATION (SHOWN)

AD1001-301-17 CORRUGATION (SHOWN)
(-17 IDENTICAL TO -15 EXCEPT FOR LENGTH & CHEM-MILL PROFILE)
(SEE NOTE 1)

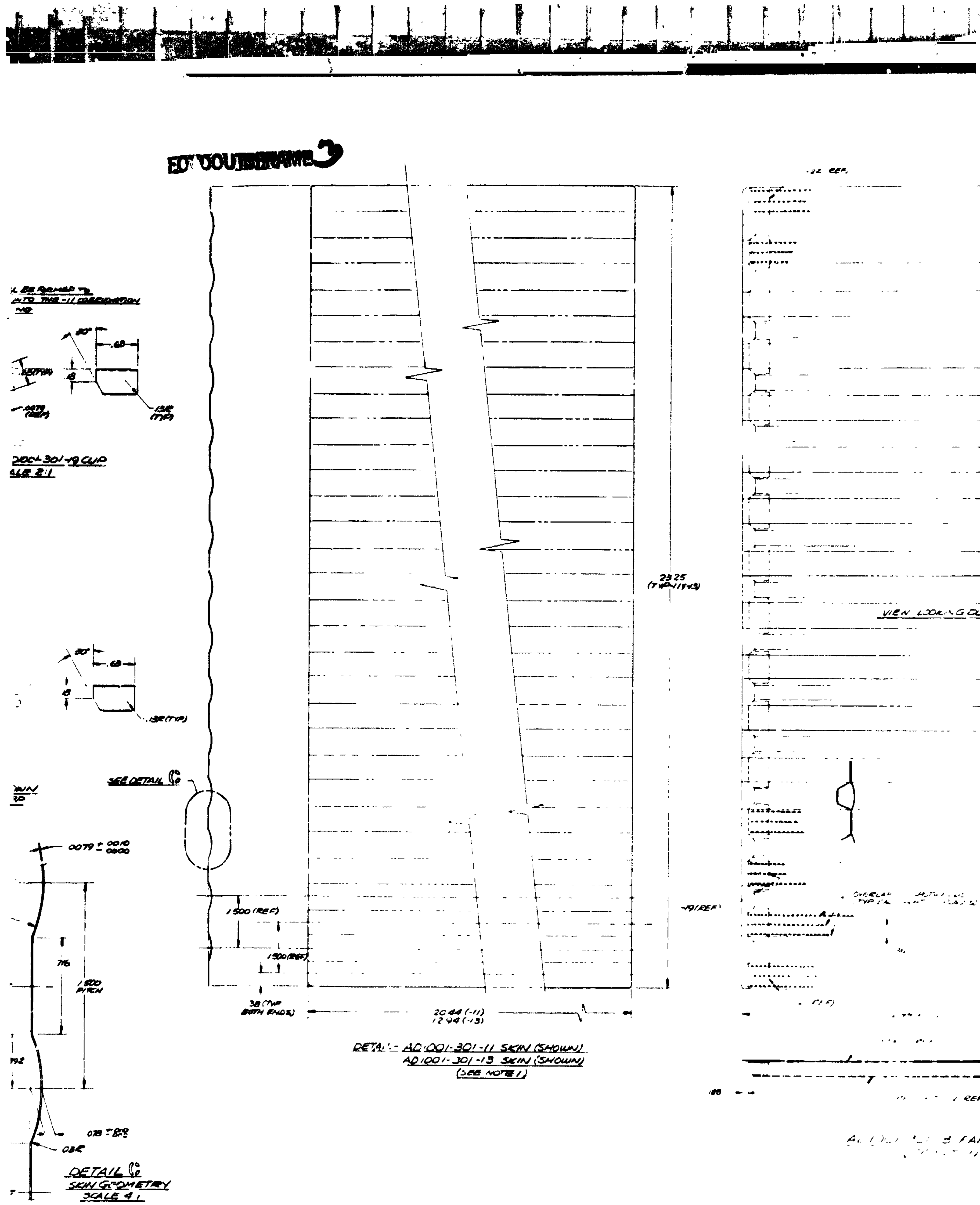

SEE DETAIL C
1.500 (REF)
1.500 (REF)
.38 (TYP BOTH ENDS)
1.500 PITCH
DETAIL - AD1001-301-11 SKIN (SHOWN)
AD1001-301-13 SKIN (SHOWN)
(SEE NOTE 1)
DETAIL C
SKIN GEOMETRY
SCALE 4:1

FOLDOUT FRAME 4

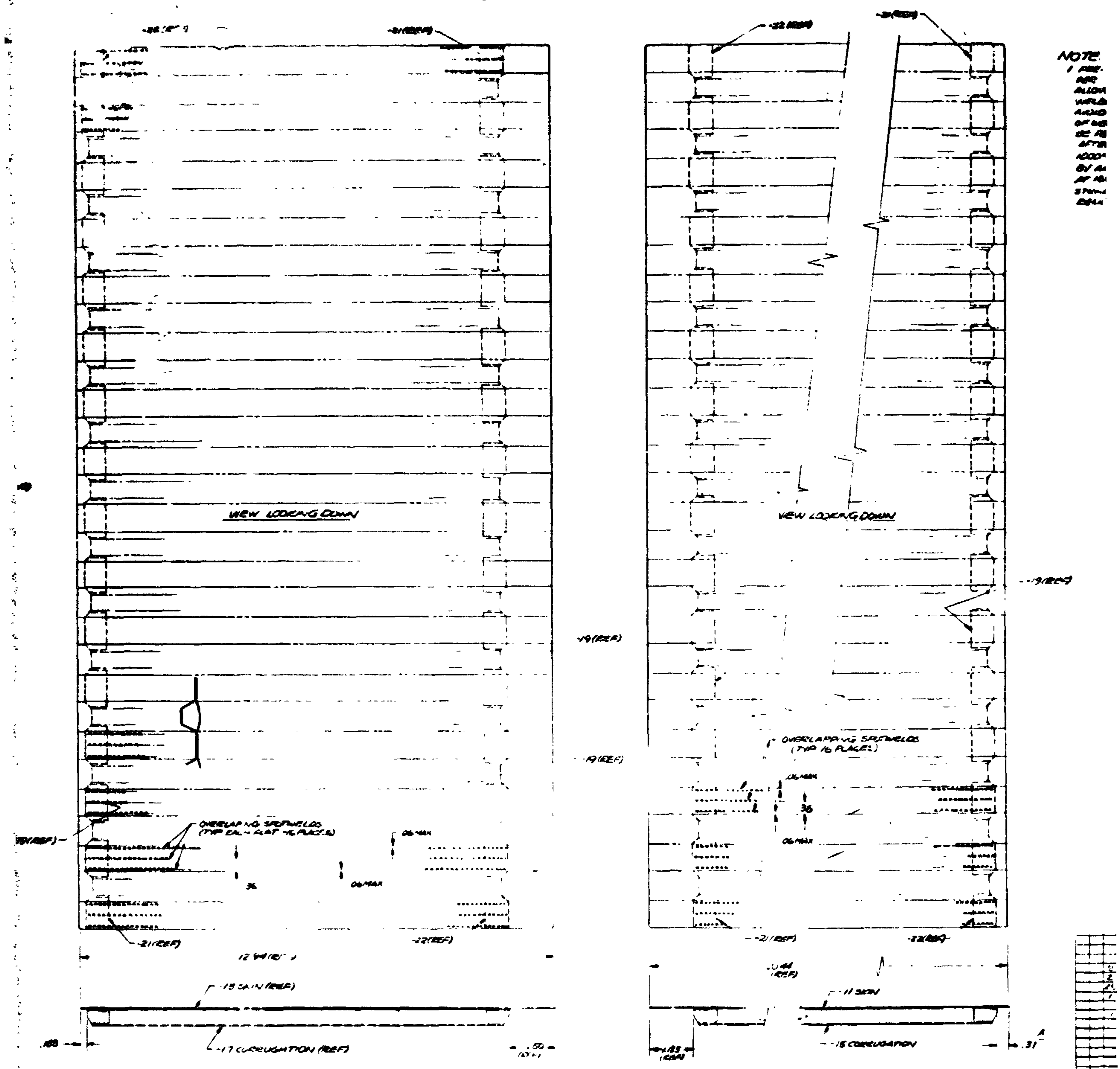

AD1001-301-3 FAIRING SKIN ASSY (SEE NOTE 1)

AD1001-301-1 SKIN ASSY (SEE NOTE 1)

FOLDOUT FRAME 3

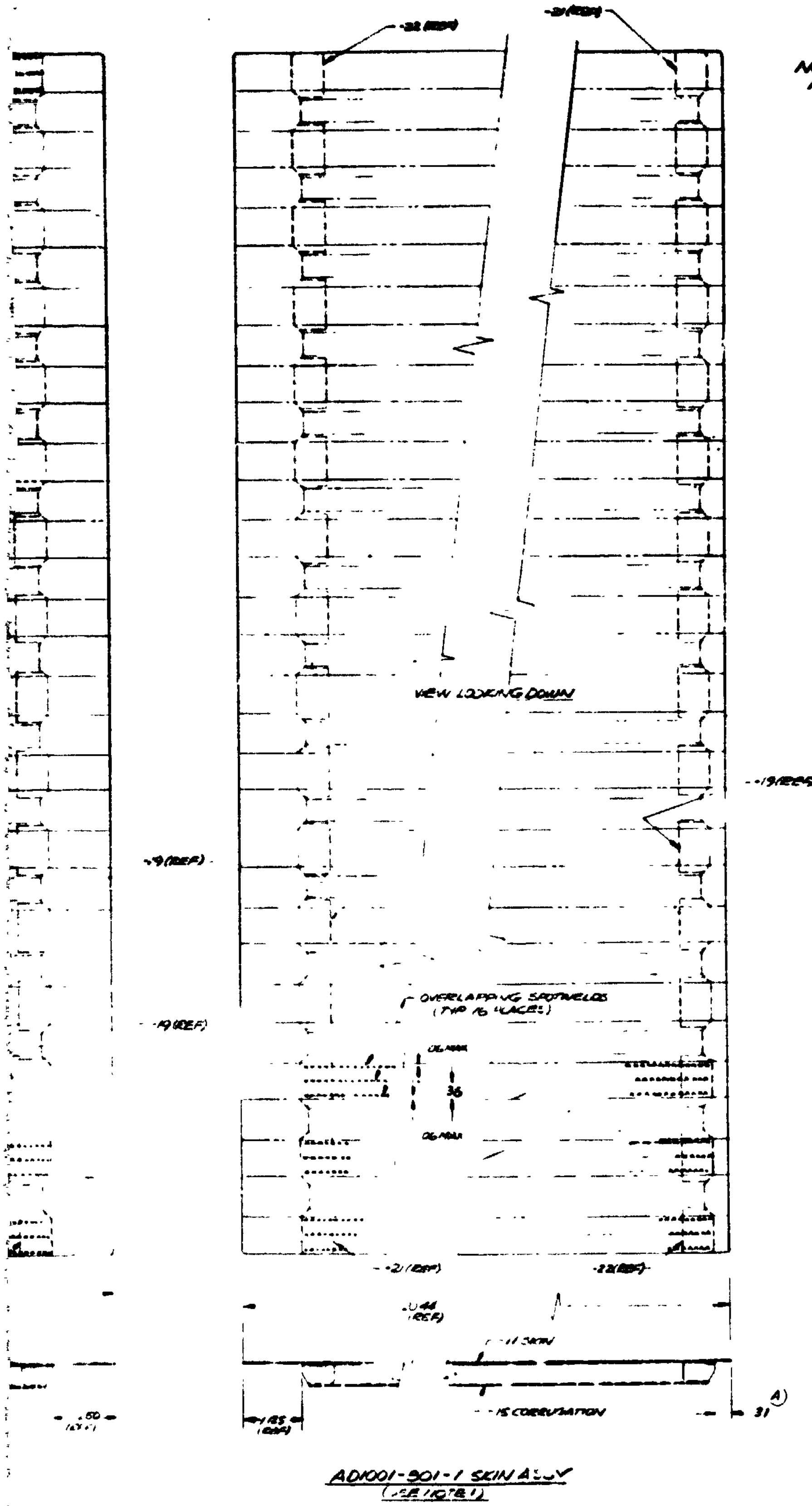

NOTES

1 PRE-WELD CLEANING SHOULD BE ACCOMPLISHED PER GSS 7021 ACID DESCALING AS USED FOR NICKEL ALLOYS. POST CLEANING HANDLING FOR RESISTANCE WELDING SHOULD BE A WHITE GLOVE OPERATION TO AVOID FINGER PRINT CONTAMINATION. SOLVENT CLEANING OF WELDED ASSY PRIOR TO STRESS RELIEF SHOULD BE PER GSS 7016
AFTER RESISTANCE WELDING, STRESS RELIEVE AT 1000°F FOR 5 HRS, FURNACE COOL TO 800°F, FOLLOWED BY AIR COOLING TO ROOM TEMPERATURE. AGE HARDEN AT 1650°F FOR 4 HRS. AND AIRCOOL IF REQUIRED. STRAIGHTENING MAY BE ACCOMPLISHED AFTER STRESS RELIEVE, & BEFORE AGE

REPRODUCIBILITY OF THE ORIGINAL PAGE IS POOR

TPS	AL XX-300	11-A
MODEL	NEXT ASSY	
PART NO	AD1001-301-1, -3	

QTY -3	QTY -1	ITEM	PART NO	DESCRIPTION	MATERIAL	GOVT SPEC	COML SPEC	STOCK SIZE
		8	AD1001-301-22	DBLR CORR	RENE 41	AMS 5545		[illegible]
2		2	-21	DBLR CORR				[illegible]
29		9	-19	DBLR CORR				[illegible]
1			-17	FAIRING CORR				[illegible]
		1	-15	SKIN CORR				[illegible]
1			-13	FAIRING SKIN				[illegible]
		1	AD1001-301-11	SKIN	RENE 41	AMS 5545		[illegible]
			AD1001-301-3	FAIRING SKIN ASSY				
			AD1001-301-1	SKIN ASSY				

AD1001-301. – Skin – details and assembly.

FOLDOUT

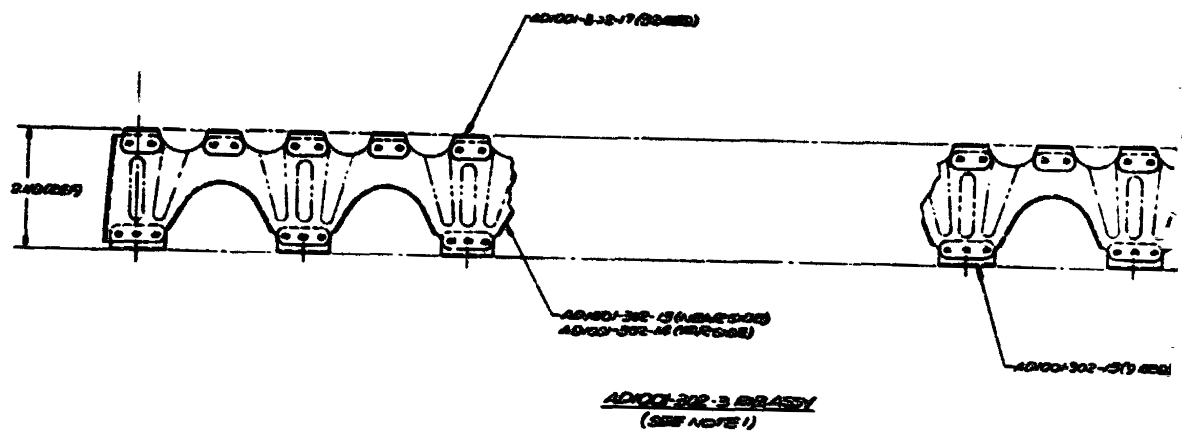
AD1001-302-3 RIB ASSY
(SEE NOTE 1)

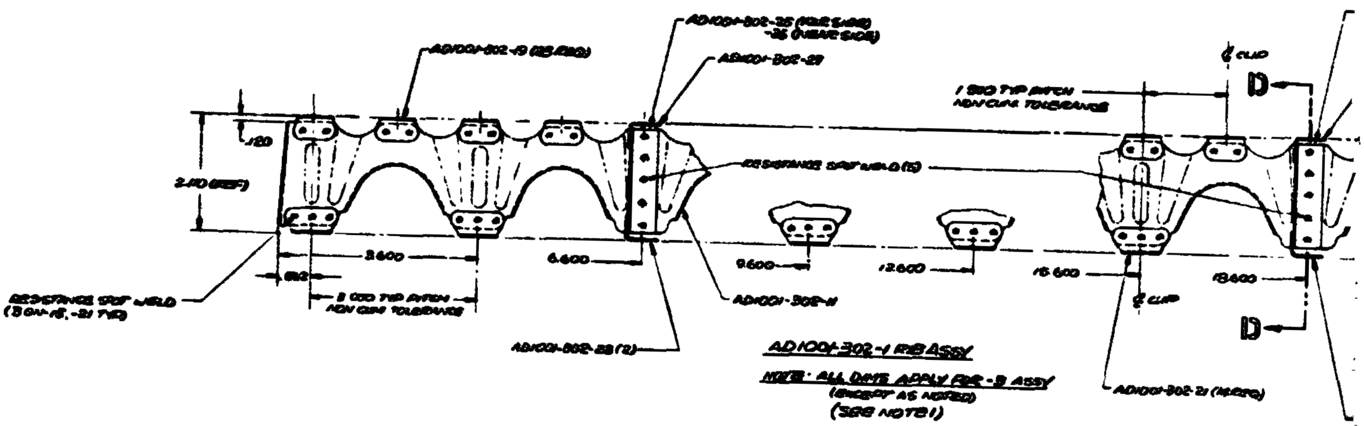
RESISTANCE SPOT WELD
AD1001-302-1 RIB ASSY
(SEE NOTE 1)

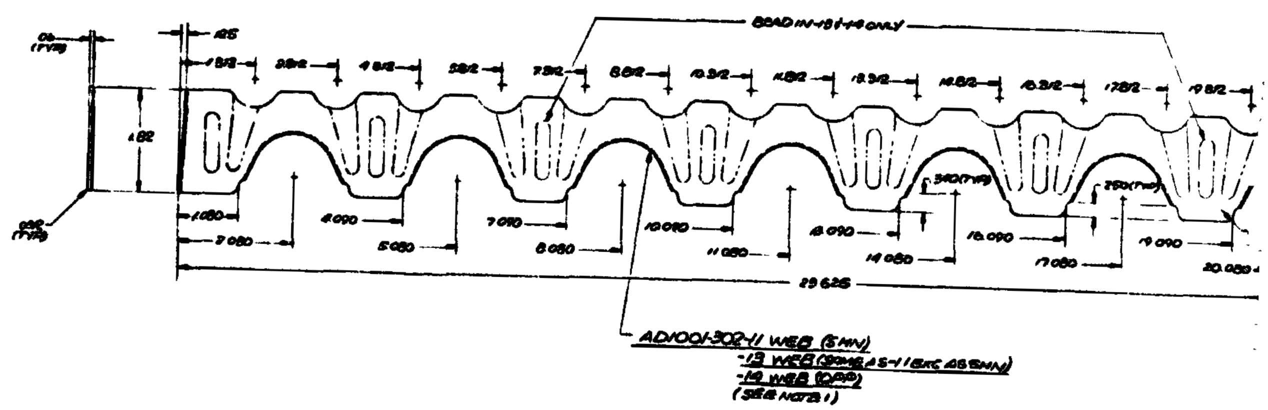
29.626
(SEE NOTE 1)

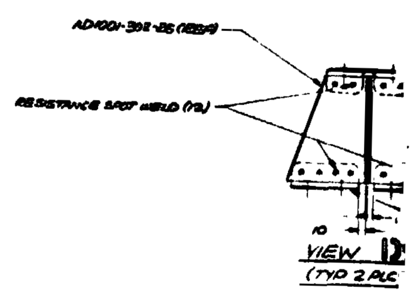
RESISTANCE SPOT WELD
VIEW
(TYP 2 PLC)

FOLDOUT FRAME 1

FOLDOUT FRAME 2

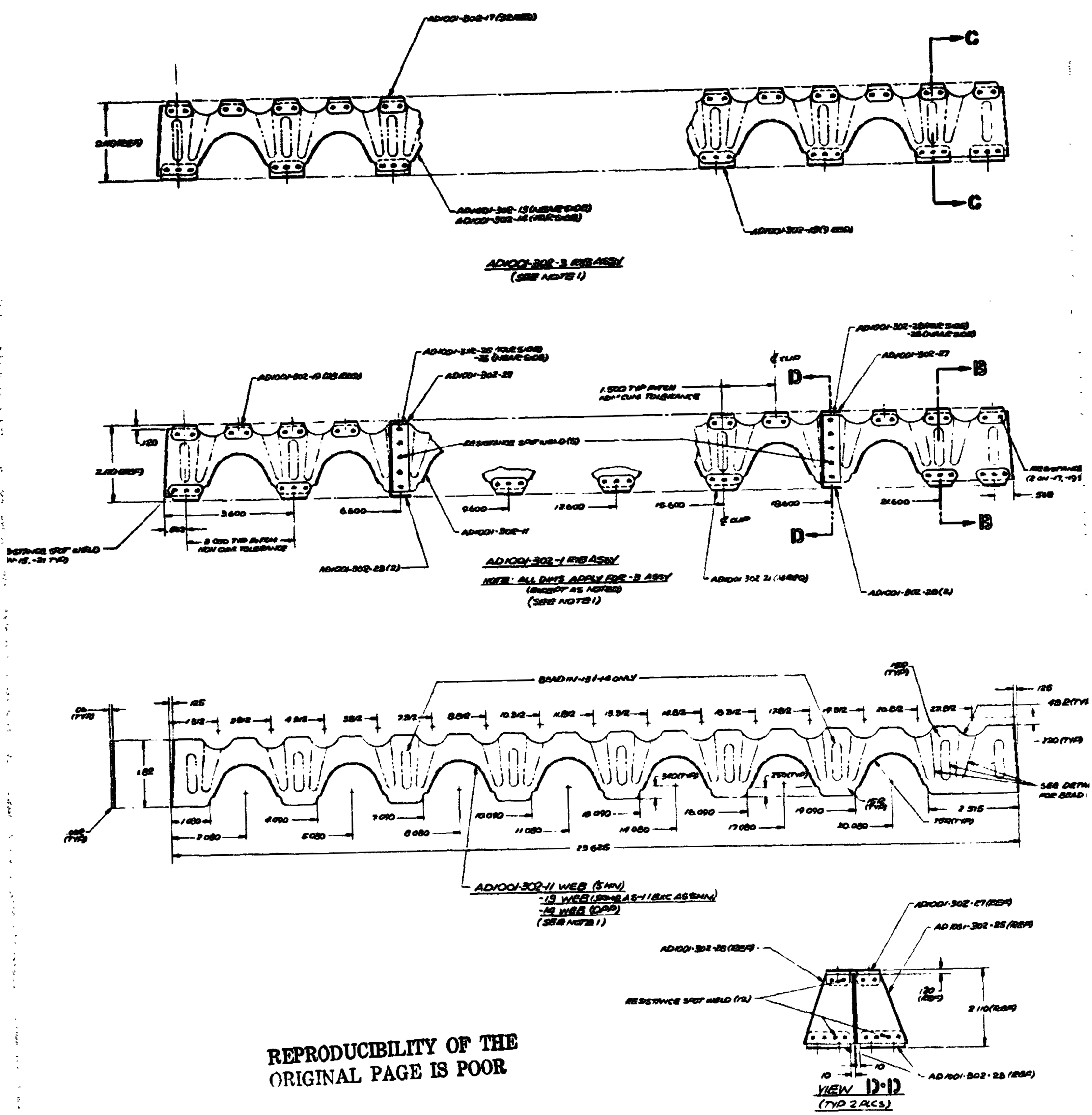

111W

FOLDOUT FRAME 3

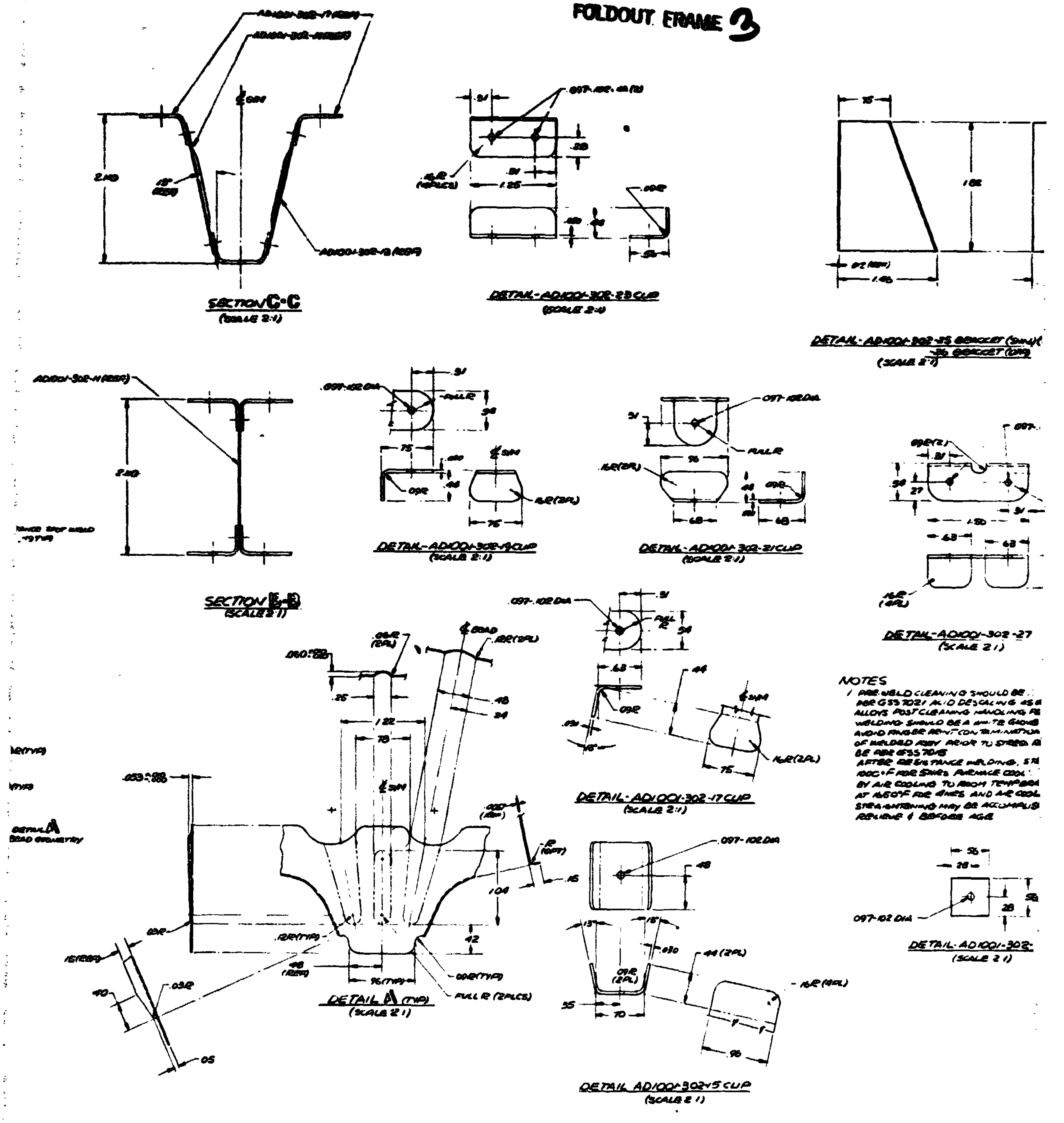

3

FOLDOUT FRAME 4

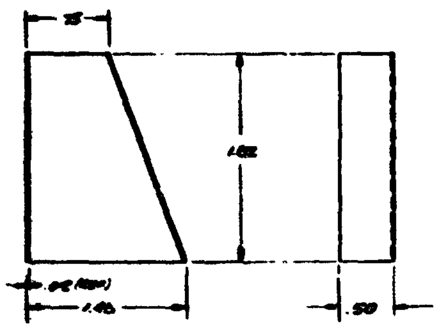

DETAIL - AD1001-302-25 BRACKET (SHOWN)(BR .06)
-26 BRACKET (OPP)
(SCALE 2:1)

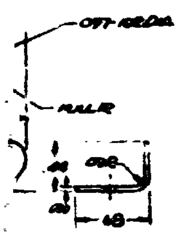

..-302-21 CLIP
(2:1)

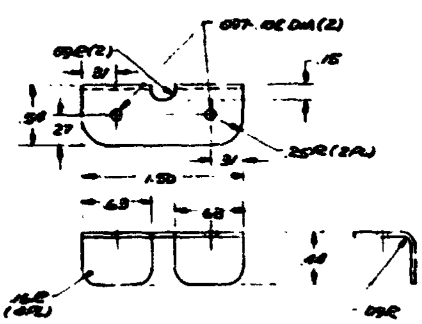

DETAIL - AD1001-302-27 CLIP
(SCALE 2:1)

NOTES

1 PRE-WELD CLEANING SHOULD BE ACCOMPLISHED PER GSS 7021 ACID DESCALING AS USED FOR INCONEL ALLOYS. POST CLEANING HANDLING FOR RESISTANCE WELDING SHOULD BE A WHITE GLOVE OPERATION TO AVOID FINGER PRINT CONTAMINATION. SOLVENT CLEANING OF WELDED ASSY PRIOR TO STRESS RELIEF SHOULD BE PER GSS 7045
AFTER RESISTANCE WELDING, STRESS RELIEVE AT 1900°F FOR 5 HRS, FURNACE COOL TO 800°F, FOLLOWED BY AIR COOLING TO ROOM TEMPERATURE. AGE HARDEN AT 1650°F FOR 4 HRS AND AIR COOL. IF REQUIRED, STRAIGHTENING MAY BE ACCOMPLISHED AFTER STRESS RELIEVE & BEFORE AGE

..-17 CLIP

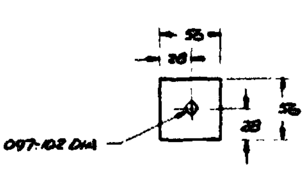

DETAIL - AD1001-302-29 SPACER
(SCALE 2:1)

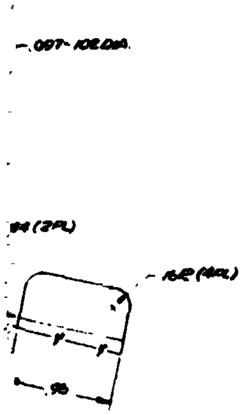

..CLIP

	AD1001-300	32	
MODEL	NEXT ASSY		
PART NO	AD1001-302-29		

	AD1001-300	1	
MODEL	NEXT ASSY		
PART NO	AD1001-302-3		
	AD1001-300	2	
MODEL	NEXT ASSY		
PART NO	AD1001-302-1		

QTY REQ'D -3	QTY REQ'D -1	PART NO	DESCRIPTION	MATERIAL	GOVT SPEC	CIVIL SPEC	SIZE
		AD1001-302-29	SPACER	RENE 41	AMS 5545		.012 × .6 × .6
	4	-27	CLIP				[illegible]
	2	-26	BRACKET				[illegible]
	2	-25	BRACKET				[illegible]
	4	-23	CLIP				[illegible]
	14	-21					[illegible]
	28	-19					[illegible]
32		-17					[illegible]
9		-15	CLIP				[illegible]
1		-13	WEB				[illegible]
1		-13	WEB				[illegible]
	1	-11	WEB	RENE 41	AMS 5545		[illegible]
		-3	RIB ASSY				
		AD1001-302-1	RIB ASSY				

SCALE 2:1

AD1001-302. – Support ribs – details and assembly.

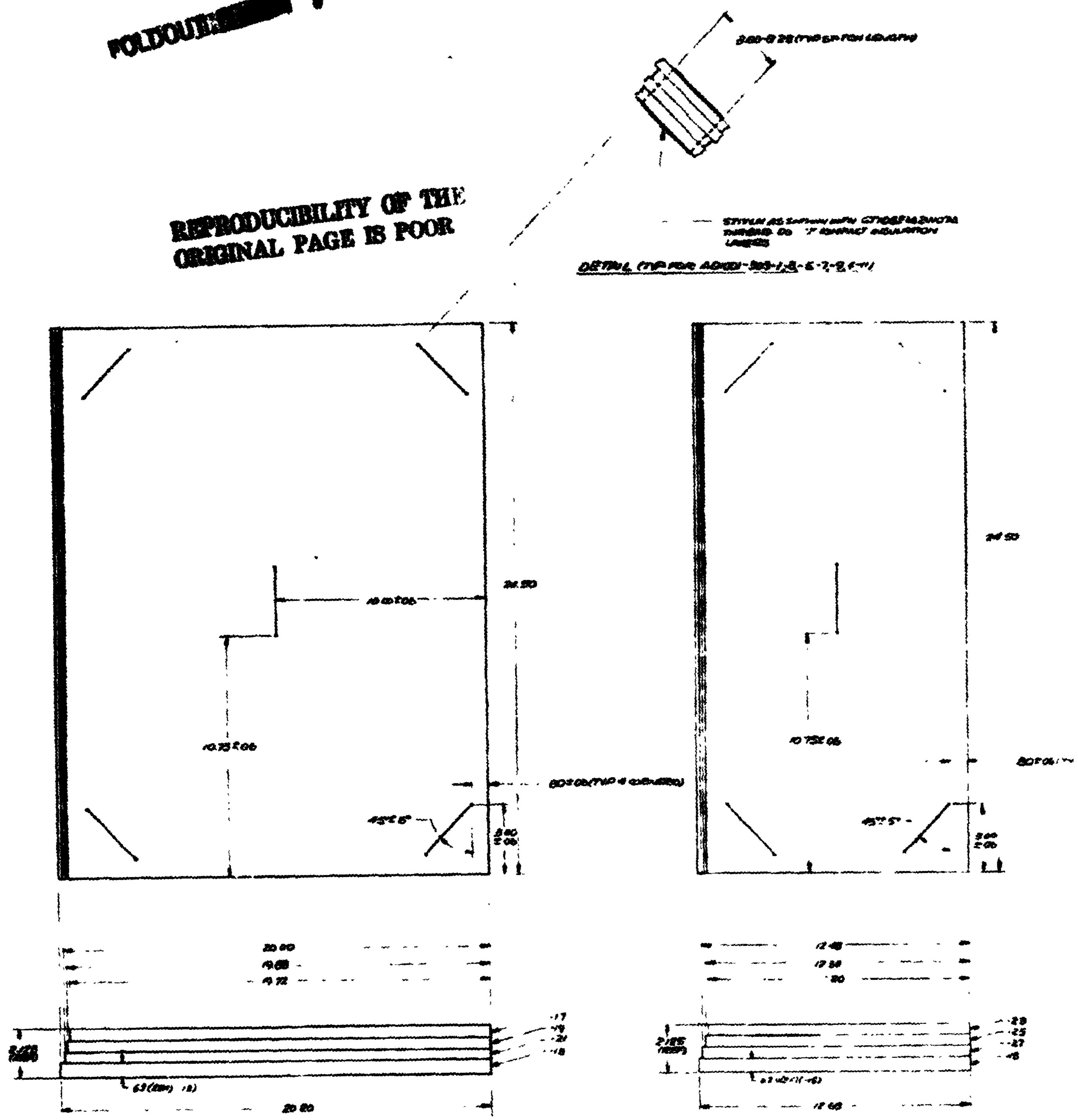

AD1001-303-1 INSULATION ASSY

AD1001-303-3 INSULATION ASSY

2217-112W

FOLDOUT FRAME 2

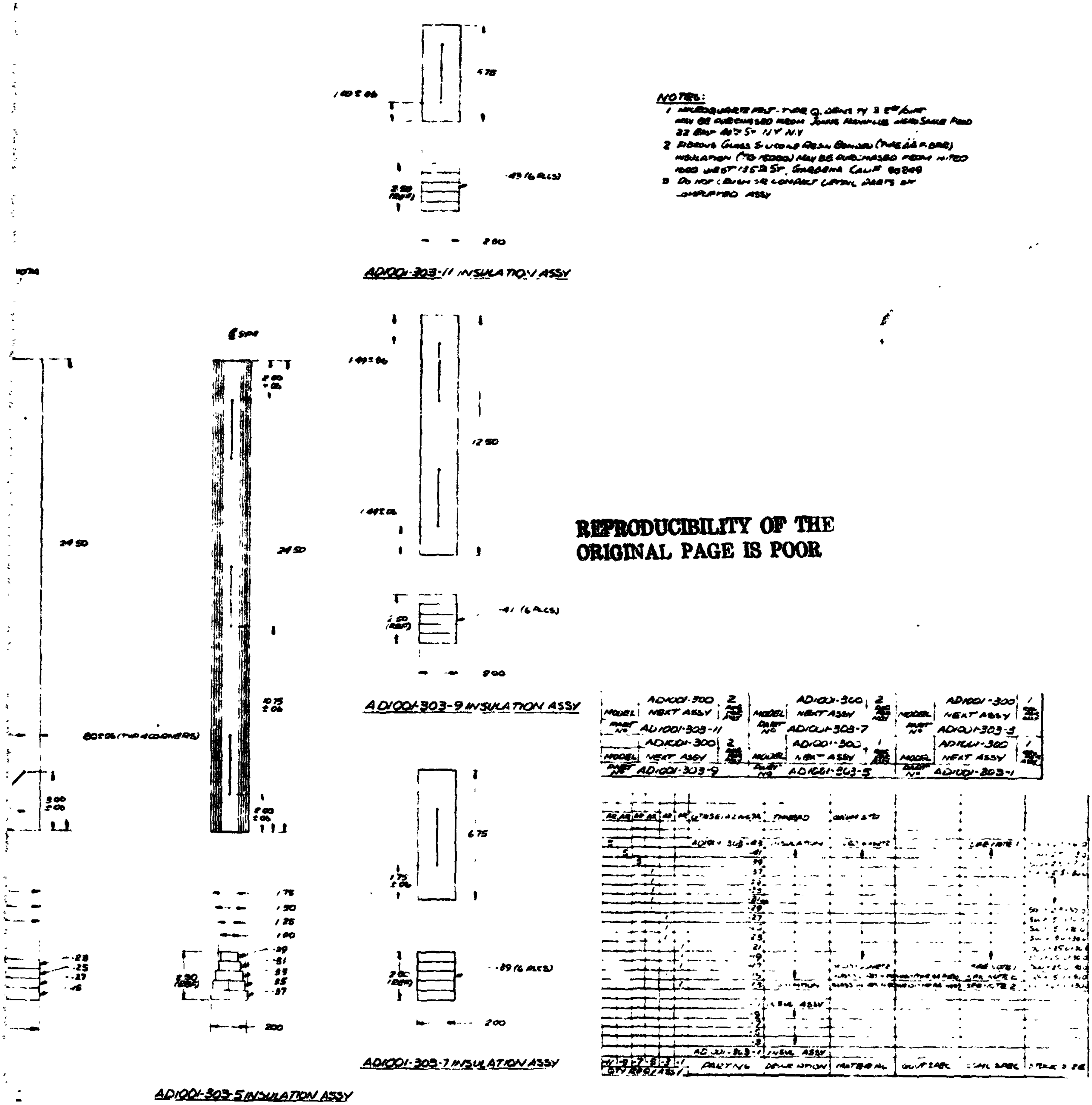

AD1001-303. – Insulation system details and assembly.

FOLDOUT FRAME

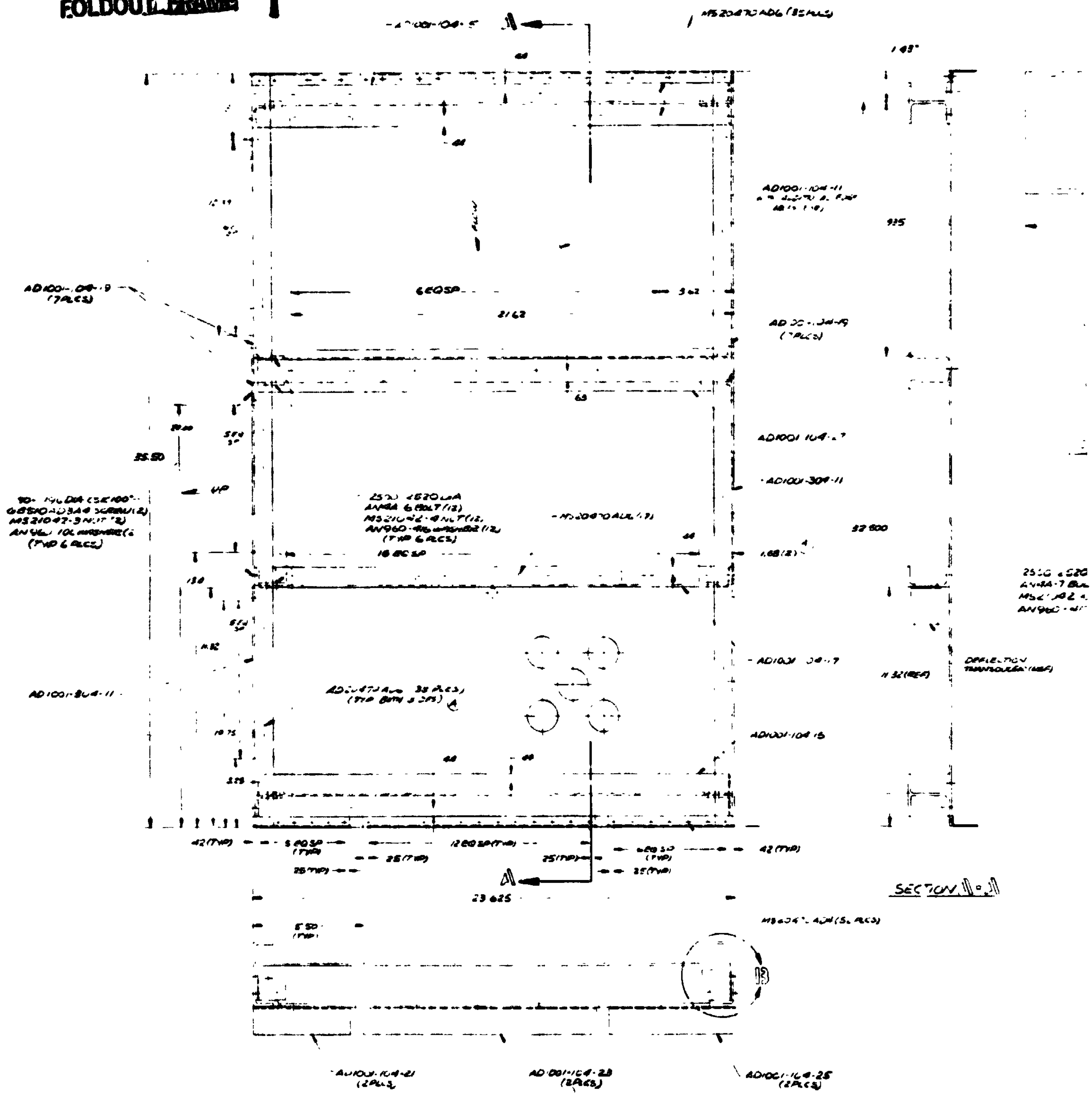

AD1001-304-1 SUPPORT STRUCTURE ASSY

(HALF SIZE)

2217-113W

FOLDOUT [redacted]

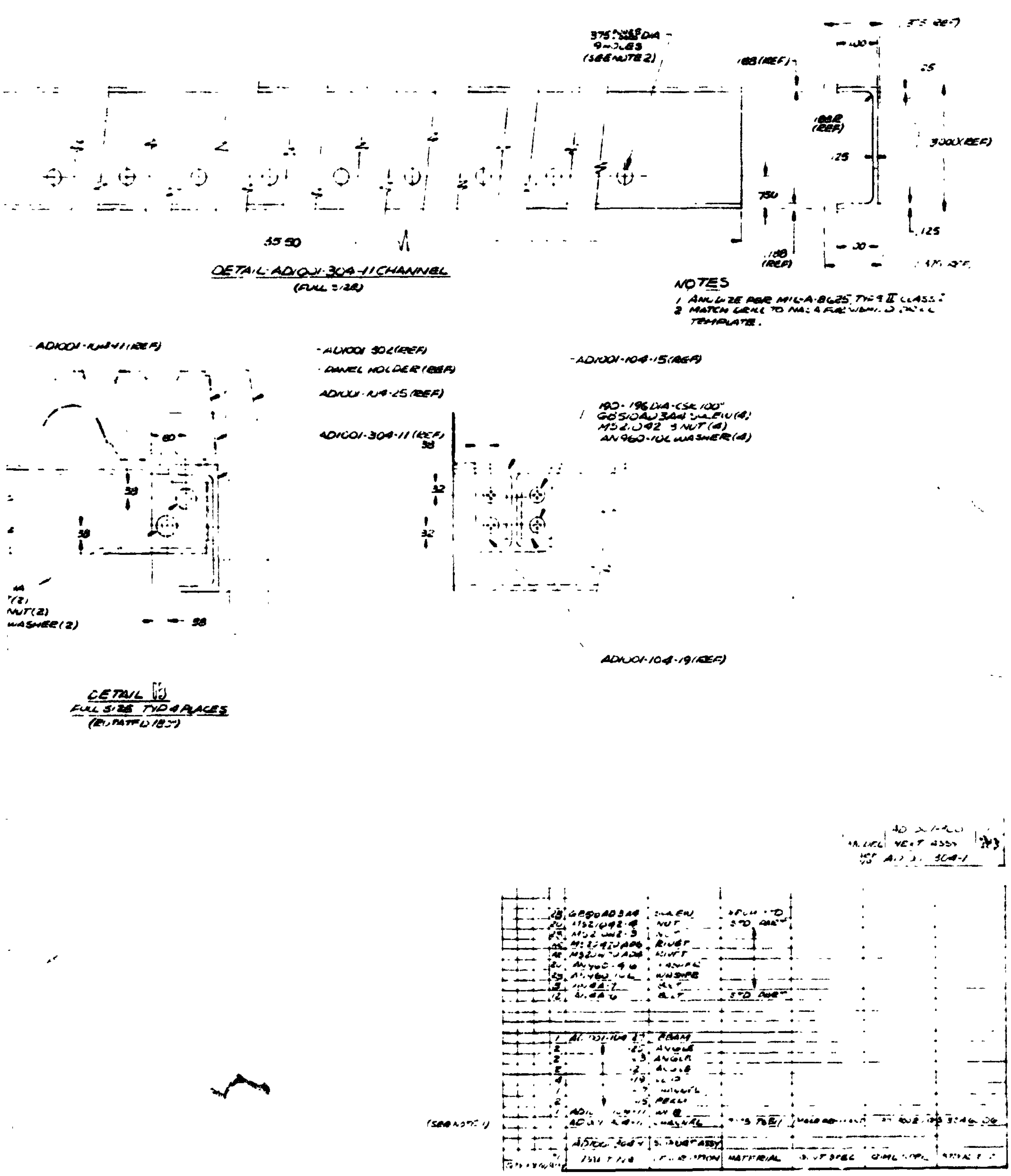

AD1001-304. – Support structure assembly.

FOLDOUT FRAME 1

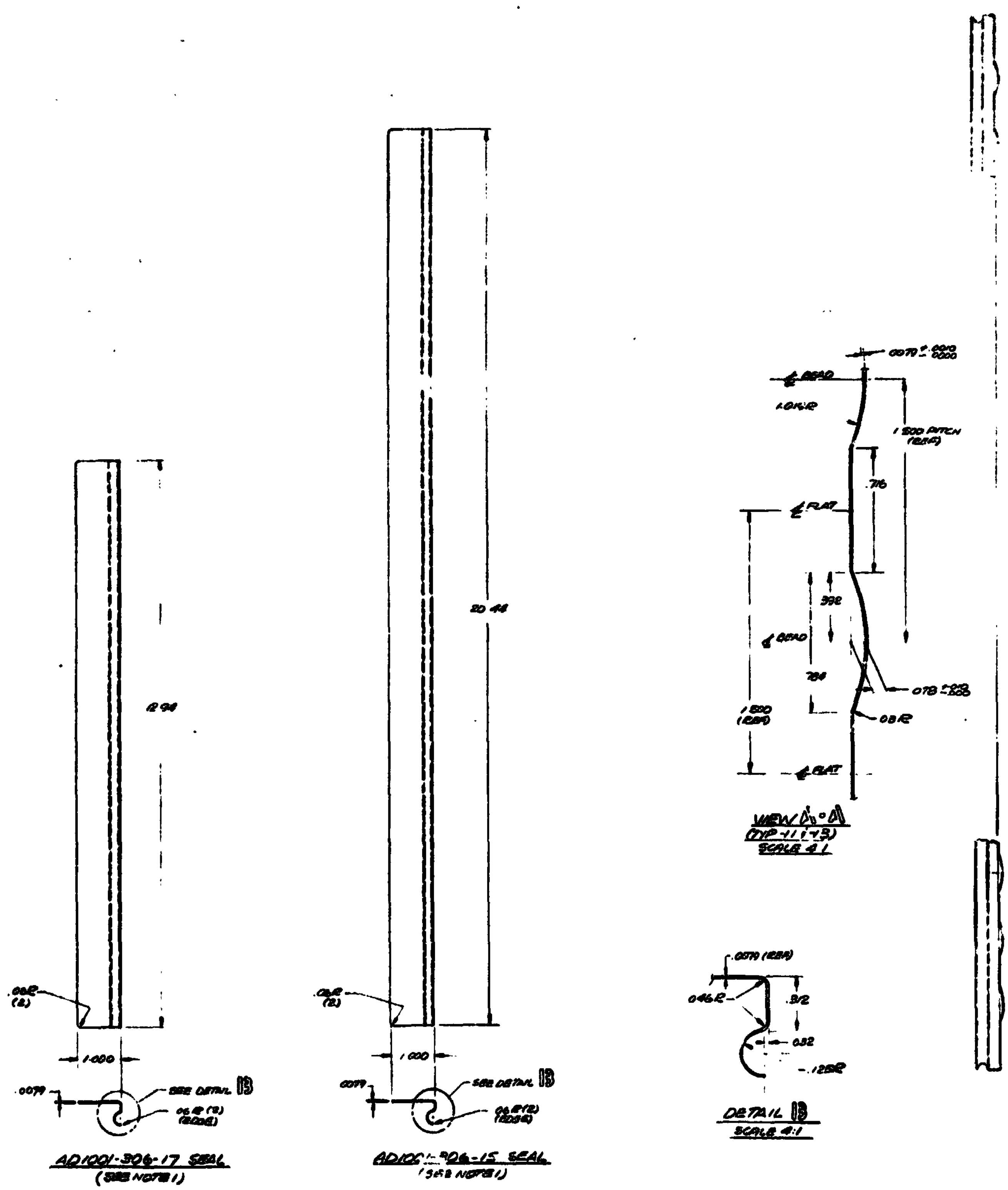

1368-031W

FOLDOUT FRAME 2

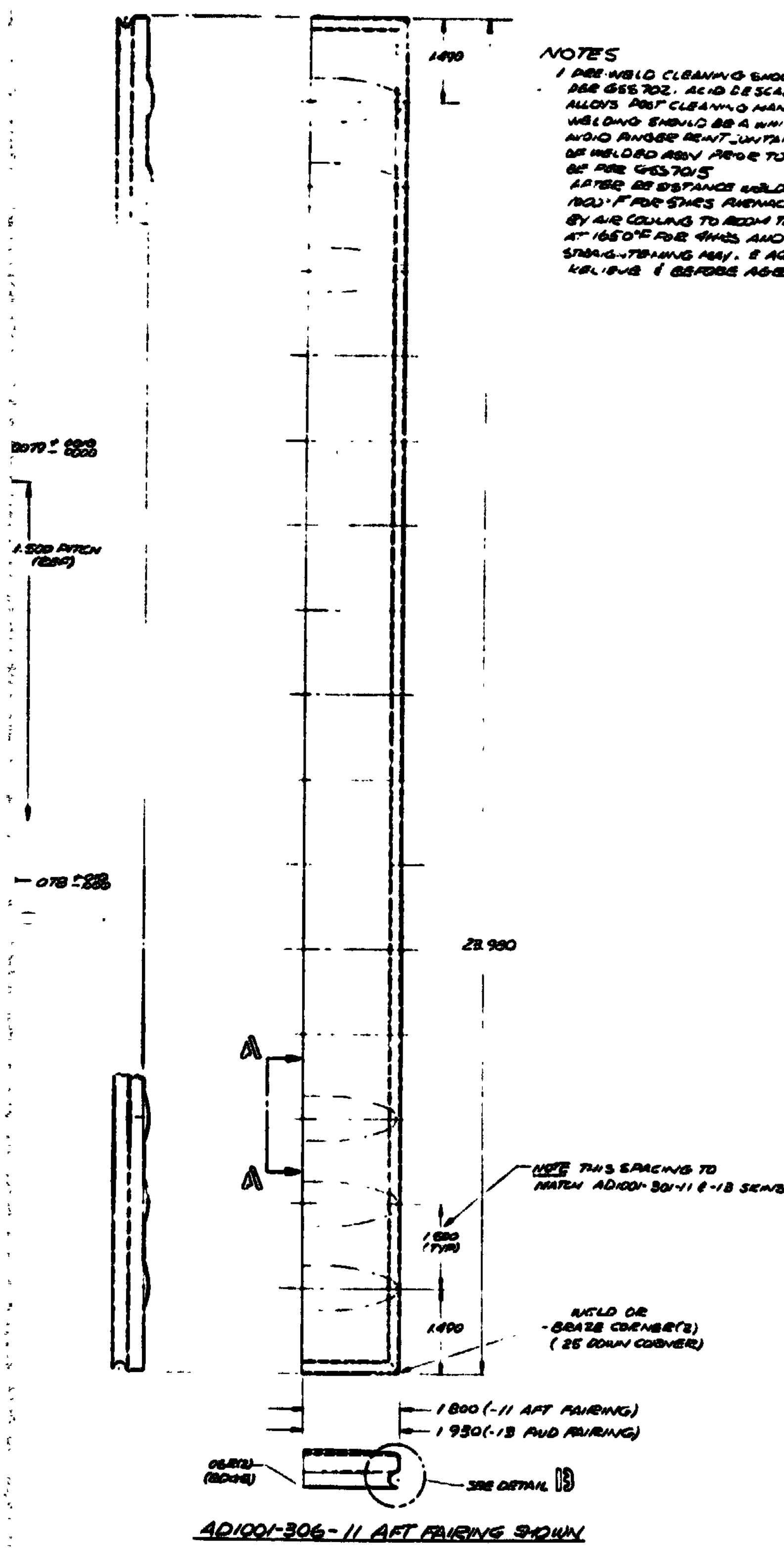

AD1001-306-11 AFT FAIRING SHOWN

AD1001-306-13 FWD FAIRING SHOWN

(SEE NOTE 1)

NOTES

1 PRE-WELD CLEANING SHOULD BE ACCOMPLISHED DER GSS702. ACID DESCALING AS USED FOR INCONEL ALLOYS. POST CLEANING HANDLING FOR RESISTANCE WELDING SHOULD BE A WHITE GLOVE OPERATION TO AVOID FINGER PRINT CONTAMINATION. SOLVENT CLEANING OF WELDED ASSY PRIOR TO STRESS RELIEVE SHOULD BE PER GSS7015

AFTER RESISTANCE WELDING STRESS RELIEVE AT 1600°F FOR 5 HRS. FURNACE COOL TO 500°F FOLLOWED BY AIR COOLING TO ROOM TEMPERATURE. AGE HARDEN AT 1650°F FOR 4 HRS AND AIR COOL. IF REQUIRED STRAIGHTENING MAY BE ACCOMPLISHED AFTER STRESS RELIEVE & BEFORE AGE

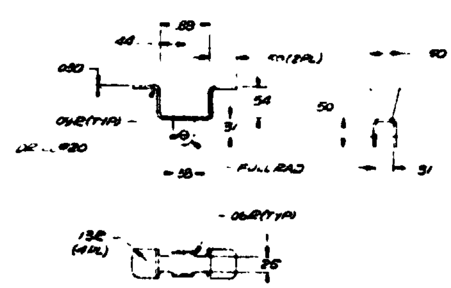

AD1001-306-19 CLIP

DEFLECTION TRANSDUCER SUPPORT

TPS	AD1001-300	2 EA REQ ASSY
MODEL	NEXT ASSY	
USED ON	AD1001-306-15, -17	
TPS	AD1001-300	1 EA REQ ASSY
MODEL	NEXT ASSY	
USED ON	AD1001-306-11, -13, -19	

PART NO	DESCRIPTION	MATERIAL	GOVT SPEC	COML SPEC	STOCK SIZE
AD1001-306-19	SUPPORTCLIP	RENE 41	AMS 5545		050 × 1 × 3
-17	SEAL - SIDE				[illegible]
-15	SEAL - SIDE				[illegible]
-13	FAIRING FWD				[illegible]
AD1001-306-11	FAIRING AFT	RENE 41	AMS 5545		[illegible]

AD1001-306. – Fairings and end seal details.

APPENDIX G

Insulation System - Radiation Barriers

Analysis

The use of metal foil radiation barriers was considered to increase the insulation system efficiency by reducing heat transmission by radiation. The analytical evaluation is presented on the following pages.

An evaluation of the manner in which heat is transmitted through low density fibrous insulations indicates that at temperatures above 811K (1000°F) the majority of the heat transmission is by radiation. The two points in Fig. 4 of Ref. 4-7 illustrates this effect vividly. The radiation component is a function of the cube of the absolute temperature. Therefore it appears attractive to attempt to reduce the radiation component to affect a reduction of the apparent thermal conductivity of the insulation at elevated temperatures. Various methods have been proposed to accomplish this, such as increasing the back scattering cross section by reducing fiber diameter, addind pacifiers, and modifying the emissivity of the fibers. These methods were out of the scope of this program The approach investigated here involves the use of metal foils to block radiation transfer such as has been successfully done in multiple foil cryogenic insulations.

The evaluation was entirely analytical. To determine the effect of the foil the three main components of heat transnission through the insulation are assumed to act independently of each other. These components are; solid particle conduction, gaseous conduction, and internal radiation. For low density $\rho < 64$ kg/m^3 (4.0 lbm/ft^3) insulations at high temperatures the solid conduction component is very small compared to the gaseous and radiation components. The solid conduction component can be determined by subtracting the gaseous and radiation component from existing measured data which contains all three components. The gaseous component can be evaluated by methods presented in Ref. G-1 and G-2.

The gaseous conductivity is

$$k_{gas} = A\rho C_v V_a L_q \left(\frac{d}{d + L_q} \right) \qquad \text{Equa. (1)}$$

where
- A = constant depending on gas
- ρ = density of gas
- C_v = specific heat at constant volume
- V_a = one molecular velocity
- L_q = mean free path of gas molecule
- d = distance between fibers

$$d = \frac{\pi R \rho_s}{2 \rho_i} \qquad \text{Equa. (2)}$$

where
- R = fiber diameter
- ρ_i = insulation density
- ρ_s = fiber material density

These equations basically state that the gaseous conduction component is dependent on gas pressure and fiber size for low density insulation.

The radiation component is determined by methods presented in Ref. 4-7 and is given by the approximate equation

$$k_r = \frac{4\sigma T_M^3}{N} \qquad \text{Equa. (3)}$$

where
- σ = Stephan Bolzman constant
- T_M = mean absolute temperature
- N = back scattering cross section

Values for N, the back scattering cross section, are given in Ref. 4-7 and are shown in Fig. G-1. Examination of the equation for the radiation component suggests that N is the inverse of the overall effective emissivity (ϵ_{EFF}) through the insulation from the hot face to the cold face. That is,

$$k_r = 4\epsilon_{EFF}\,\sigma T_M^3 \qquad \text{Equa. (4)}$$

From the radiation transmission standpoint the insulation can be thought of as a series of surfaces analogous to a multiple foil system. The ϵ_{EFF} for a series of layers is

$$\epsilon_{EFF} = \frac{\epsilon}{(2-\epsilon)(m-1)} \qquad \text{Equa. (5)}$$

where m = number of layers per unit thickness

ϵ = emissivity of layer

By assuming that the addition of metal radiation foils is analogous to merely adding more surface to those already existing in the insulation a new effective emissivity ϵ'_{EFF} can be computed to determine the reduction in the radiation component when metal foils are added. From equa. (5).

$$m = \frac{\epsilon}{(2-\epsilon)\,\epsilon_{EFF}} + 1 \qquad \text{Equa. (6)}$$

Assume n = number of metal foils per unit thickness

$$\epsilon'_{EFF} = \frac{\epsilon}{(2-\epsilon)\,(n + m-1)} \qquad \text{Equa. (7)}$$

Combining equations (6) and (7) and assuming that it is computed on the basis of the emissivity of the metal foils.

$$\epsilon'_{EFF} = \frac{1}{\frac{1}{\epsilon_{EFF}} + \frac{n\,(2-\epsilon)}{\epsilon}} = \frac{1}{N + \text{[illegible]} -\epsilon)}$$

Therefore the radiation component with n metal foils per unit thickness can be expressed as

$$k_r = 4\,\epsilon'_{EFF}\,\sigma T_M^{\,3}$$

REFERENCES

G-1 Strong, H.M.; Bundy, F.P.; and Bovenkerk, H.P.: Flat Panel Vacuum Thermal Insulation. Journal of Applied Physics, Vol. 31, No. 1, 39-50, January 1960.

G-2 Stephenson, M.E., Jr.; and Mark, M.: The Effect of Apparent Density and Gas-Cell Size on the Thermal Conductivity of Cellular Materials. ASME 59-A-254.

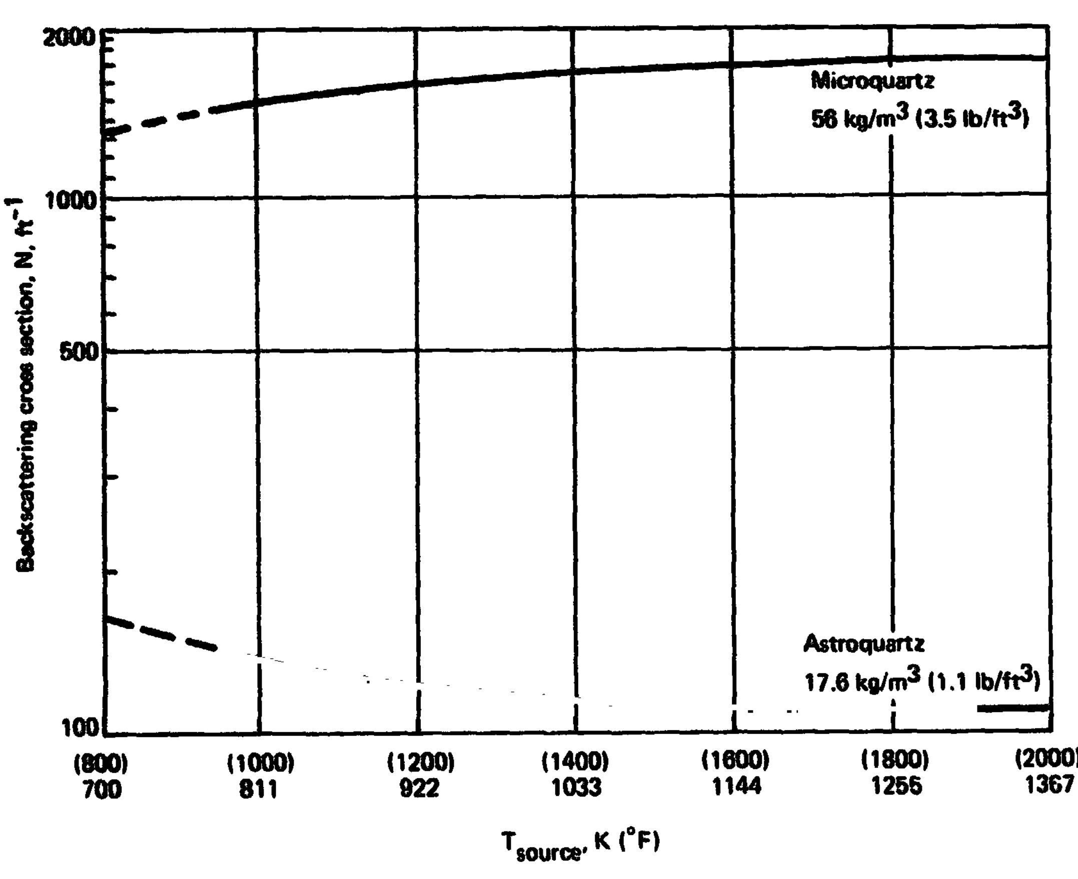

Figure G-1. – Backscattering cross section vs temperature for fibrous insulation (ref. 4-7)

APPENDIX H

THERMOCOUPLE NUMBER AND LOCATION

A correlation of thermocouple number and location is given. Table H-1 lists the number and location. Figure H-1 gives the coding system employed.

Table H-1. – Thermocouple location

Thermocouple ID no.	Row-col	Location (Fig. H-1)	Type
1	3-1	Edge seal – fairing panel	Ceramo
2	3-2	Skin – fairing panel	Ceramo
3	3-2	Clip – fairing panel	Ceramo
4	3-2	Standoff web fairing panel	Ceramo
5	3-2	Heat sink – fairing panel	Fiberglass
6	2-3	Skin – fairing panel	Ceramo
7	3-3	Skin – fairing panel	Ceramo
8	4-3	Skin – fairing panel	Ceramo
9	3-4	Clip – fairing panel	Ceramo
10	3-4	Standoff web – fairing panel	Ceramo
11	3-4	Heat sink – fairing panel	Fiberglass
12	2-5	Skin – fairing panel	Ceramo
13	3-5	Skin – fairing panel	Ceramo
14	4-5	Skin – fairing panel	Ceramo
15	4-5	Clip – fairing panel	Ceramo
16	4-5	Standoff web – fairing panel	Ceramo
17	4-5	Heat sink – fairing panel	Fiberglass
18	2-6	Skin – test panel	Ceramo
19	3-6	Skin – test panel	Ceramo
20	4-6	Skin – test panel	Ceramo
21	2-7	Skin – test panel	Ceramo
22	2-7	Clip – test panel	Ceramo
23	2-7	Standoff web – test panel	Ceramo
24	2-7	Heat sink – test panel	Fiberglass
25	3-7	Skin – test panel	Ceramo
26	4-7	Skin – test panel	Ceramo
27	3-8	Insulation at 2" – test panel	Ceramo
28	3-8	Insulation at 1½" – test panel	Ceramo
29	3-8	Insulation at 1" – test panel	Ceramo
30	3-8	Insulation at ½" – test panel	Ceramo
31	3-8	Heat sink – test panel	Fiberglass
32	3-9	Skin – test panel	Ceramo
33	3-9	Corrugation bottom – test panel	Ceramo
34	1-10	Edge seal – test panel	Ceramo
35	2-10	Skin – test panel	Ceramo
36	3-10	Skin – test panel	Ceramo
37	3-10	Corrugation bottom – test panel	Ceramo
38	3-10	Insulation at 2" – test panel	Ceramo
39	3-10	Insulation at 1½" – test panel	Ceramo
40	3-10	Insulation at 1" – test panel	Ceramo
41	3-10	Insulation at ½" – test panel	Ceramo
42	3-10	Heat sink – test panel	Fiberglass
43	4-10	Skin – test panel	Ceramo
44	4-10	Corrugation bottom – test panel	Ceramo
45	4-10	Heat sink – test panel	Fiberglass
46	5-10	Edge seal – test panel	Ceramo
47	3-11	Skin – test panel	Ceramo
48	3-11	Corrugation bottom – test panel	Ceramo
49	3-12	Skin – test panel	Ceramo
50	3-12	Clip – test panel	Ceramo
51	3-12	Standoff web – test panel	Ceramo
52	3-12	Heat sink – test panel	Fiberglass
53	3-13	Edge seal – test panel	Ceramo

2217-69W

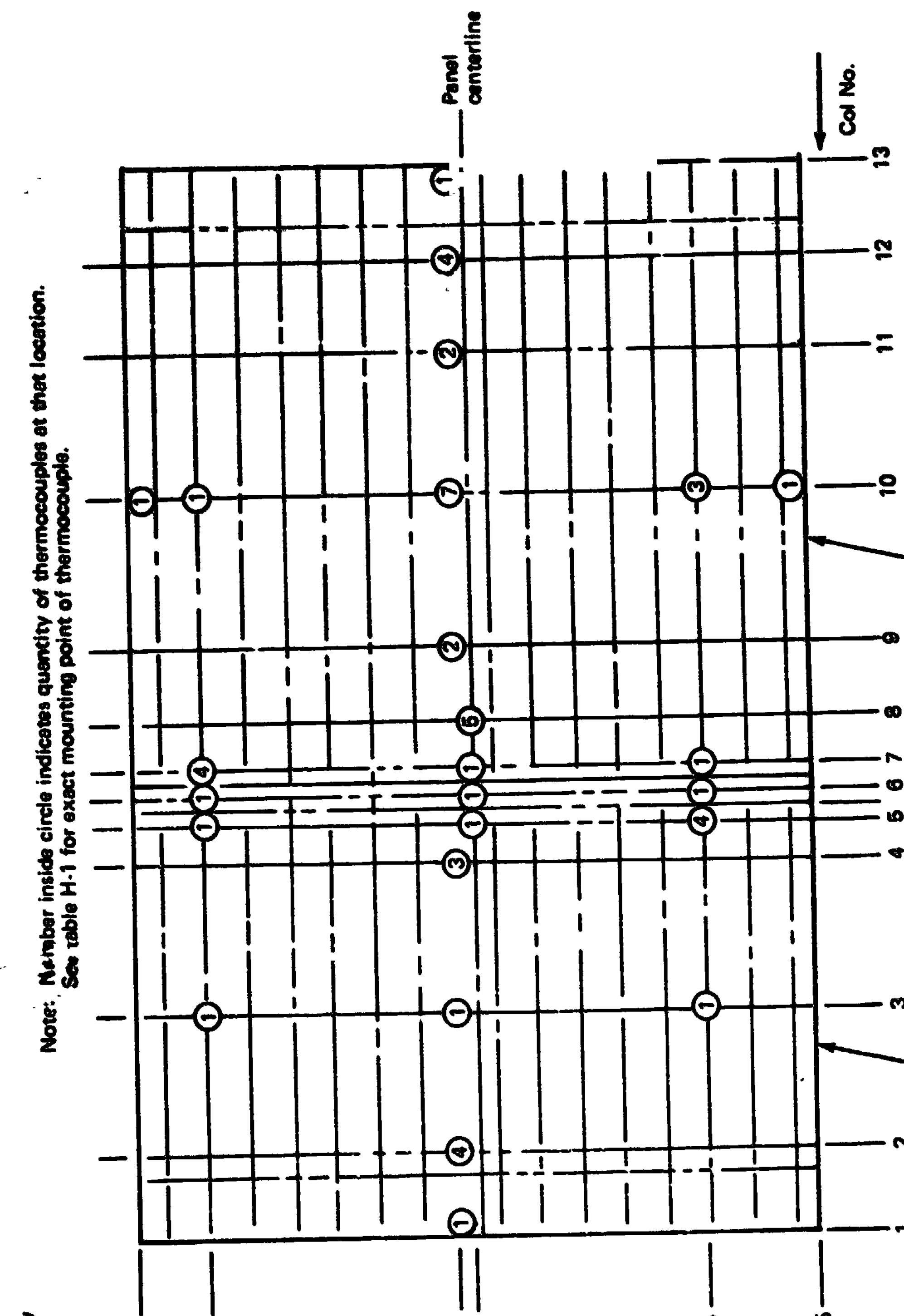

2217-70W

Figure H.1. — Thermocouple code system

APPENDIX I

SUPPORT STRUCTURAL - DETAIL STRESS ANALYSIS

The TPS test article support structure detail stress analysis is presented on the following pages. The support structure for the Haynes 188 and Rene' 41 test specimens are identical.

SUPPORT STRUCTURE (DWG. AD1001-104)

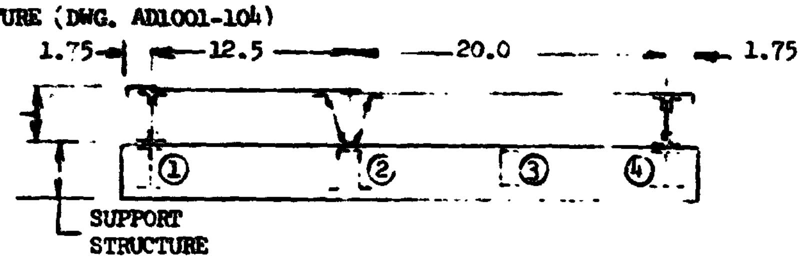

SIDE VIEW

Beam ② is critical

(PART AD1001-104-27)

(2024-T6 MAT'L)

F_{tu} = 64 ksi

F_{ty} = 50 ksi

E_T = 10.7 x 10^6 psi

E_c = 10.9 x 10^6 psi

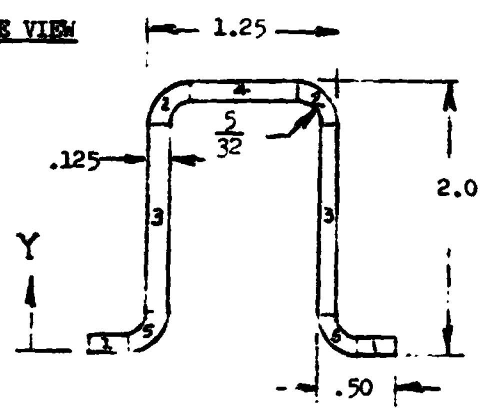

ITEM	b	h	A	Y	AY	AY^2	I_{oo}
1	2(.21875	.125	.054688	.0625	.003418	.000214	.000071
2	–	–	.099709	1.85444	.184904	.342894	.000660
3	2(.125)	1.4375	.359375	1.00	.359375	.359475	.061885
4	.6875	.125	.085938	1.9275	.166504	.322601	.000112
5	–	–	.099709	.14556	.014514	.002113	.000660
Σ			.699419		.728715	1.027197	.063388

$$\bar{X} = \frac{\Sigma AY}{\Sigma A} = 1.04189 \text{ IN}$$

$$I_{NA} = \Sigma A_x^2 + \Sigma I_{oo} - \Sigma A \cdot \bar{x}^2 = .33134 \text{ IN}^4$$

SUPPORT STRUCTURE (Continued)

Beam (2) (Continued)

$$W = \frac{P_R}{144}\left[\frac{12.5 + 20.0}{2}\right]$$

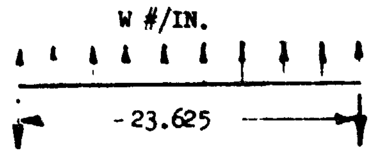

P_R = 350 psf (LIMIT)*

W = 30.5 #/IN

$$M = \frac{WL^2}{8} = \frac{39.5\,(23.625)^2}{8} = 2755 \text{ IN}^{\#} \text{ at mid-span}$$

$$f_b = \frac{M\bar{x}}{I_{NA}} = \frac{2755\,(1.04189)}{.33134} = 8660 \text{ psi}$$

F_{ty} = 50 ksi

F.S. = 1.15

$$M.S. = \frac{50000}{1.15(8660)} - 1 = \text{AMPLE}$$

DEFLECTION AT MID-SPAN

$$\Delta = \frac{5WL^3}{384EI} = \frac{5(39.5)(23.625)^3}{384\,(10.7 \times 10^6)(.33134)} = .002 \text{ IN}$$

Beam (3) sees no load

Beams (1) & (4) are the same, with beam (4) being more highly loaded.

$$I_{NA} = \frac{1}{12}\left[2.(2)^3 - 1.875(1.74)^3\right]$$

$$= .4959 \text{ IN}^4$$

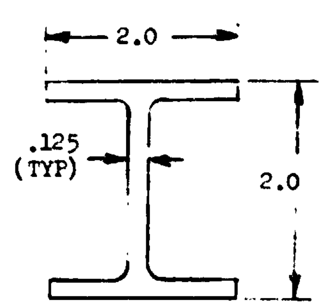

$$W = \frac{P_R}{144}\left[\frac{20.0}{2} + 1.75\right]$$

P_R = 350 psf

W = 28.6 LBS/IN

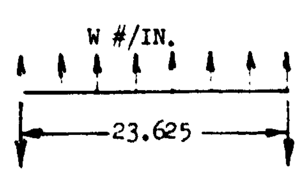

*Maximum positive airload. The maximum pressure in the TPSTF is .025 atmospheres or 52.9 psf

SUPPORT STRUCTURE (Continued)

$$M = \frac{WL^2}{8} = \frac{28.6(23.625)^2}{8} = 1990 \text{ IN LBS (Mid-Span)}$$

$$f_b = \frac{M\bar{x}}{I_{NA}} = \frac{1990\ (1.0)}{.4959} = 4020 \text{ psi}$$

$$\text{M.S. } \frac{50000}{1.15(4020)} -1 = \text{AMPLE}$$

SHEAR CLIPS (DWG AD1001-104-19)

Max. shear occurs on beam 2

$$V = \frac{WL}{2} = \frac{39.5\ (23.625)}{2} = 466.6 \text{ LBS per end}$$

V/2 = 233.3 LBS per clip.

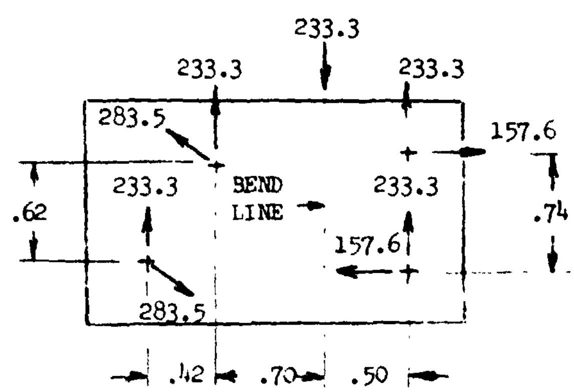

Upper left fastener has highest load

Resultant = 457.2 lb.

Fastener Shear Allowable:

4420 lb. min (Ref. 16)

$$\text{M.S.} = \frac{78000}{1.4(457.2)} = -1 = \text{AMPLE}$$

Bearing: $$f_b = \frac{457.2}{.125(.190)} = 19250 \text{ psi}$$

F_{bru} = 78 ksi (Ref 16) $$\text{M.S.} = \frac{78000}{1.15\ (19250)} -1 = \text{AMPLE}$$